Targeting microtubules in the distal neuromuscular circuitry to improve outcomes in Amyotrophic Lateral Sclerosis

By

Jayden Andrew Clark, BMedRes (Hons)

Submitted in fulfilment of the
requirement for the Degree of
Doctor of Philosophy

Menzies Institute for Medical Research
University of Tasmania (December, 2016)

DECLARATION OF ORIGINALITY

This thesis contains no material which has been accepted for a degree or diploma by the University or any other institution, except by way of background information and duly acknowledged in the thesis, and to the best of my knowledge and belief no material previously published or written by another person except where due acknowledgement is made in the text of the thesis, nor does the thesis contain any material that infringes copyright.

Jayden Andrew Clark

Date: 03/07/17

STATEMENT OF AUTHORITY OF ACCESS

This thesis may be made available for loan and limited copying in accordance with the *Copyright Act 1968*.

Jayden Andrew Clark

Date: 03/07/17

STATEMENT OF CO-AUTHORSHIP

The following people and institutions contributed to the publication of work undertaken as part of this thesis:

Jayden A Clark, Menzies Institute for Medical Research = **Candidate**
Katherine J Southam, Menzies Institute for Medical Research = **Author 1**
Catherine A Blizzard, Menzies Institute for Medical Research = **Author 2**
Anna E King, Wicking Dementia Research and Education Centre = **Author 3**
Elise J Yeaman, Menzies Institute for Medical Research = **Author 4**
Jyoti A Chuckowree, Menzies Institute for Medical Research = **Author 5**
Tracey C Dickson, Menzies Institute for Medical Research = **Author 6**

Paper 1, 'Axonal degeneration, distal collateral branching and neuromuscular junction architecture alterations occur prior to symptom onset in the SOD1G93A mouse model of amyotrophic lateral sclerosis'.
Located in Chapter 3
Candidate was equal first author with author 1. Author 2, author 3 and author 6 contributed to the idea, its formalisation and development.

Paper 2, 'A Case for Microtubule Vulnerability in Amyotrophic Lateral Sclerosis: Altered Dynamics During Disease'.
Located in Chapter 1
Candidate was the primary author. Author 2, author 4, author 5 and author 6 contributed to the idea, its formalisation and development. Author 4 assisted in refinement and revision.

We, the undersigned agree with the above stated "proportion of work undertaken" for each of the above published (or submitted) peer-reviewed manuscripts contributing to this thesis:

Signed:

Assoc. Prof. Tracey Dickson
Supervisor
Menzies Institute for Medical Research
University of Tasmania

Prof. Alison Venn
Head of Department
Menzies Institute for Medical Research
University of Tasmania

This thesis contains work either published or submitted for publication as follows;

1. Clark, J., Southam, K., Blizzard, C., King, A. and Dickson, T. Axonal degeneration, distal collateral branching and neuromuscular junction architecture alterations occur prior to symptom onset in the SOD1G93A mouse model of amyotrophic lateral sclerosis. *J. Chem. Neuroanat.* 1–13 (2016). *Equal first author*
2. Clark, J., Yeaman, E., Blizzard, C., Chuckowree, J., and Dickson, T. (2016). A Case for Microtubule Vulnerability in Amyotrophic Lateral Sclerosis: Altered Dynamics During Disease. *Frontiers in Cellular Neuroscience* 10.

This thesis contained work presented at the following conferences;

1. Clark, J., Yeaman, E., Blizzard, C., Chuckowree, J., and Dickson, T. Targeting microtubules to improve outcomes in ALS. *Australasian Society for Neuroscience*, Hobart, 2016, oral presentation.
2. Clark, J., Blizzard, C., Chuckowree, J., and Dickson, T. Targeting microtubules to improve outcomes in ALS. *26th International Symposium on ALS/MND*, Orlando, 2015, Poster
3. Clark, J., Blizzard, C., Chuckowree, J., and Dickson, T. Targeting microtubules to improve outcomes in ALS. ISN/ANS, Cairns, 2015, Poster.
4. Clark, J., Blizzard, C., Southam, K., Chuckowree, J., and Dickson, T. Characterizing distal dysfunction and degeneration in ALS: The potential for axon protection? *International symposium on ALS/MND*, Milan, 2013, Poster.

Work in preparation;

1. Clark, J., Yeaman, E., Breslin, M., Blizzard, L., Blizzard, C., Chuckowree, J., and Dickson, T. The microtubule stabilizing compound Epothilone D modifies disease progression in the $SOD1^{G93A}$ mouse model of ALS [*manuscript in preparation*]

SUMMARY

Amyotrophic lateral sclerosis (ALS), the most common form of motor neuron disease, is a disease that is characterised by the degeneration of motor neurons, their axons and synapses. The distal neuromuscular circuitry, consisting of the spinal alpha motor neuron, distal axon, and the specialised synapse called the neuromuscular junction (NMJ), is a unique and vulnerable circuit, as it resides both in the central and peripheral nervous systems. Denervation of this circuitry leads to the ALS phenotype of progressive paralysis and muscle atrophy. Currently, no cure exists to combat ALS, with the only disease-modifying drug, Riluzole, showing modest improvements in a subset of patients. The lack of therapeutics highlights the need to identify the pathological mechanisms that drive the development and progression of this disease. The involvement of microtubules in the pathogenesis of ALS is becoming increasingly appreciated, with microtubules implicated in axon degeneration, and causing axonal transport dysfunction due to a pathogenic increase in the dynamics of the microtubule network. Pharmacological targeting of microtubules in neurodegenerative diseases with similar cellular pathology has suggested the possible benefit of a microtubule targeting approach in ALS. To this end, the current thesis is based upon the hypothesis that stabilising microtubules in the distal neuromuscular circuitry will improve outcomes in ALS.

This thesis investigated the sequence of degenerative events that occur to the distal axon and NMJ in the $SOD1^{G93A}$ mouse model of ALS. This was with the intent of identifying the earliest distal pathology to develop a targeted therapy regime. The microtubule-targeting compound Epothilone D (EpoD) was used with the aim of preserving the integrity and function of the distal neuromuscular circuitry by stabilising microtubules. It investigated the behavioural, histological and molecular outcomes of targeting microtubules in ALS as a potential therapy. Furthermore, using a primary culture *in vitro* approach, it investigated the dose-dependant effect of stabilising microtubules on normal neuronal functioning.

It was determined that degenerative morphology of the axonal compartment in the neuromuscular circuitry is an early pathological event in the hindlimb muscles of the $SOD1^{G93A}$ mouse model of ALS. Additionally, a decline in the colocalisation of pre- and post-synaptic markers of the NMJ occurs over the disease time course, coupled with aberrant alterations to the levels of synaptic proteins in diseased mice. Interestingly, forelimb pathology progresses slower than hindlimb pathology, suggesting gross anatomical differences in disease progression of the distal

neuromuscular circuitry in this model. Results from this thesis indicate that targeting the distal axon with stabilising agents such as EpoD may improve axonal pathology and thus outcomes in ALS.

The efficacy of EpoD treatment in ALS was subsequently investigated using the $SOD1^{G93A}$ mouse model. EpoD was found to stabilise microtubules in spinal motor neurons, protecting the soma and axon of the distal neuromuscular circuitry early in the disease, coupled with modest improvements to motor function. However, EpoD was subsequently identified to be detrimental to motor behaviour, neurological outcomes and survival in the later stages of the disease. Furthermore, EpoD treatment was found to cause increased motor neuron death at end stage. *In vitro* investigations examined the impact of EpoD on normal neuronal functioning. Parameters investigated included neuronal viability, initial neurite growth and complexity, microtubule protein levels and mitochondrial transport.

Collectively, these studies address the need for therapeutic development for the treatment of ALS. This thesis provides evidence that distal pathology is an early and progressive degenerative event in the pathogenesis of ALS, with axonal pathology offering a novel target to preserve the function of neuromuscular circuitry. This thesis provides evidence in support of the use of EpoD to improve pathology early in the disease. Furthermore, it suggests that EpoD affects aspects of the microtubule network in a dose-dependant manner, suggesting that the intended target and outcome are both vitally important considerations when utilising microtubule stabilising compounds in a neurological setting. These results highlight the heterogeneity of ALS pathology, and suggest that a combination of therapies with varied doses and timing are most likely needed to positively modify or alleviate the disease phenotype.

ACKNOWLEDGMENTS

First and foremost I would like to thank my supervisors Associate Professor Tracey Dickson, Dr Catherine Blizzard and Dr Jyoti Chuckowree. Your guidance and support during my PhD has been instrumental in the completion of this thesis, and coupled with your friendship, has made my days at work dynamic and enjoyable.

I would like to thank all of my colleagues in the Dickson research group, with particular mention of Rosie Clark, my unofficial twin and the person who has been with me on our university journey from the first day as a student, up until the last. Special mention to past members Dr Stan Mitew, Dr Edgar Dawkins and Dr Kate Lewis for their help and friendship. I would also like to thank my friends and colleagues from the Menzies Institute for Medical Research for their support, coffee trips and social events. I would also like to thank Dr Katherine Southam with her input into the study described in Chapter 3.

I would like to thank our collaborators Associate Professor Leigh blizzard and Dr Monique Breslin, whose invaluable expertise and knowledge of advanced statistical methods used in Chapter 4 have made interpreting and developing behavioural data both enjoyable but also informative.

Finally, I would like to thank my family, particularly my parents Sharon and Andrew Clark, for their constant support. I would also like to thank my partner Clare Hawkes, who has always been there for me whenever I needed her and has never stopped encouraging me.

TABLE OF CONTENTS

ABBREVIATIONS

°C	degrees Celsius
Ach	acetylcholine
AChRs	acetylcholine receptors
a-MN	alpha motor neuron
AD	Alzheimer's disease
ALS	amyotrophic lateral sclerosis
ALS2	alsin
ANOVA	analysis of variance
BDNF	brain derived neurotrophic factor
CNS	central nervous system
CNTF	ciliary neurotrophic factor
CO_2	carbon dioxide
DIV	days *in vitro*
EB	end binding protein
EB3	end binding protein 3
EpoD	Epothilone D
fALS	familial amyotrophic lateral sclerosis
FTD	fronto-temporal dementia
FUS	fused in sarcoma
g	gram
GDNF	glial derived neurotrophic factor
GDP	guanine diphosphate
GEF	guanine nucleotide exchange factor
GFAP	glial fibrillary acidic protein
GFP	green fluorescent protein
GTP	guanine triphosphate
HDAC6	histone deacetylase 6
IgG	immunoglobulin G
kDa	kilo Dalton
kgf	kilograms of force
L	Litre

LRP-4	low-density lipoprotein receptor related protein 4
M	Molar
MAP	microtubule associated protein
MAP2	microtubule associated protein 2
mg	milli gram
ml	milli litre
mM	milli molar
mm	milli mitre
MN	motor neuron
MND	motor neuron disease
MuSK	muscle specific kinase
NEK	nima related kinase
NFM	neurofilament M
nM	nano molar
PAGE	polyacrylamide gel electrophoresis
PBS	phosphate buffered saline
PD	Parkinson's disease
PFA	paraformaldehyde
PIX	pixels
PNS	peripheral nervous system
PSCs	perisynaptic schwann cells
ROS	reactive oxygen species
s	seconds
sALS	sporadic amyotrophic lateral sclerosis
SD	standard deviation
SDS	sodium dodecyl sulphate
SEM	standard error of the mean
SOD1	superoxide dismutase 1
TBI	traumatic brain injury
TBS	tris buffered saline
TBS-T	tris buffered saline solution with tween
TDP43	transactive response DNA binding protein 43

TIP	microtubule plus end tracking protein
UPS	ubiquitin proteosome system
YFP	yellow fluorescent protein
α-BTx	alpha bungarotoxin
μL	micro litre
μm	micro metre
μM	micro molar

Chapter 1

1 Introduction

Amyotrophic Lateral Sclerosis (ALS) is a late onset and ultimately fatal neurodegenerative disease, classified primarily by the loss of upper motor neurons (MNs) in the motor cortex and brainstem, and lower alpha motor neurons (a-MN) in the spinal cord. The incidence of ALS is approximately 2 in every 100,000 individuals, with a mean onset age range of 55 – 60 years (Logroscino et al., 2010; Ferraiuolo et al., 2011; Ragonese et al., 2012). The disease can be separated into phenotypically distinct classes based on the area of onset: upper 'bulbar' onset involving cortical and brain stem (hypoglossal nuclei) MN loss, and lower 'lumbar' onset spinal a-MN loss (Figure 1.1). This is due to the locality of neuronal loss, which leads to these specific clinical manifestations. Bulbar onset initially presents as difficulty speaking and swallowing, as well as muscle spasticity. Lumbar onset patients initially present with limb muscle weakness and reduction in fine motor ability, as well as the pronounced asymmetrical weakness and wasting associated with ALS (Mulder et al., 1986). However, in patients with either bulbar or lumbar onset, the progressive loss of muscle innervation due to degeneration of firstly the connections (synapses), nerves (axons) and finally MN cell bodies, culminates in respiratory failure approximately 2-5 years after onset of symptoms. ALS is also considered a spectrum disorder, where patients can suffer from cognitive dysfunction (particularly behaviour/mood, personality, language disturbances) in frontotemporal dementia (FTD); a pure motor phenotype in classical ALS; or a combination of both cognitive and motor dysfunction (Ling et al., 2013). Perplexingly, a number of MN populations are spared in the disease course, such as the occulomotor neurons, which control eye movement, and the Onufs nucleus, which facilitates bladder control (Bruijn et al., 2004). Similarly, higher order cortical functioning is generally spared in both FTD and ALS, with dysfunctions in memory, problem solving ability and spatial orientation either not occurring, or occurring in the later stages of the disease. There is currently no cure for ALS. A patient's life expectancy is approximately 3-5 years after initial diagnosis, and the current treatment, Riluzole, only extends life for 3-6 months (Wood-Allum and Shaw, 2010).

Approximately 10% of ALS cases are inherited (familial ALS, fALS), whereas the vast majority, 90%, have no inheritable link and are termed sporadic ALS (sALS) (Ticozzi et al., 2011). Both the clinical phenotype and neuropathology of ALS are quite similar between fALS and sALS

FIGURE 1.1. Clinical phenotypes of ALS. Onset of disease is determined by the signs and symptoms associated with both site of onset (limb or bulbar) and also the MN type affected (upper/cortical or lower/spinal). In most cases, patients will experience both limb and bulbar clinical signs over the disease course. It is estimated that up to half of ALS patients will suffer from symptoms associated with Fronto-temporal dementia.

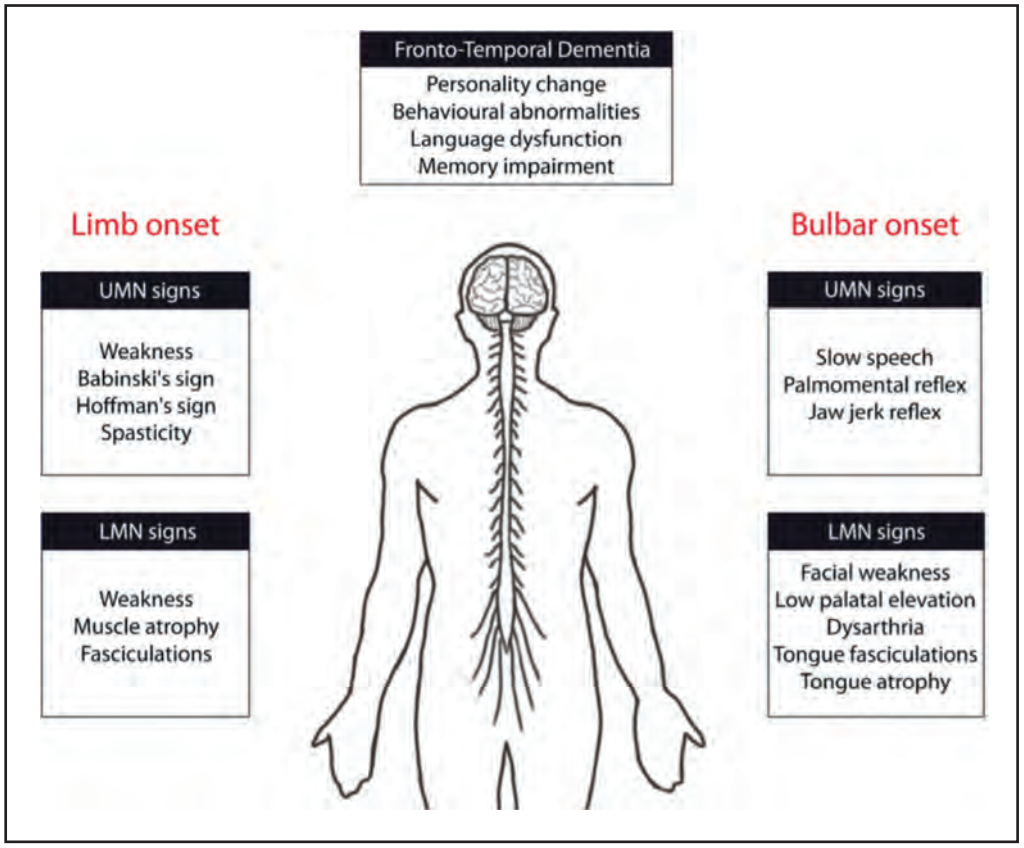

Adapted from Picher-Martel et al., 2016

cases, suggesting that there may be a large variety of mechanisms and initial insults that ultimately lead to a similar disease phenotype and the primary damage to MNs (Ticozzi et al., 2011; Al-Chalabi et al., 2012; Marangi and Traynor, 2015). However, a number of clinical differences are observed between fALS and sALS. fALS has an equal male to female sex ratio, an earlier disease onset and extended disease duration. Contrastingly, sALS is characterised by males being 2.5 times more likely to develop ALS, coupled with a later onset and shorter disease duration (Bruijn et al., 2004). The development of ALS has also been attributed to a growing number of risk factors, other than genetic susceptibility. These include high physical activity, certain toxins, electromagnetic fields, occupation and past neuromuscular injuries (Ingre et al., 2015).

Neuropathy in ALS results in atrophy of cortical structures represented as shrinkage of the cortex and nerves (Mezzapesa et al., 2013). However, the fundamental gross anatomical changes in ALS can be seen as muscle wastage; a result of degeneration to neuromuscular circuitry that facilitate voluntary movement (Rizzuto et al., 2015). Many possible disease mechanisms have been proposed in the development and progression of ALS (reviewed previously (Peters et al., 2015)) however the underlying primary mechanism of the disease is yet to be elucidated. Indeed the key factor behind the pathological vulnerability of MNs in ALS is still unknown. Contributing factors that may result in the selective vulnerability of MNs include their large cell size, polarity, their excitable nature as well as their interaction with neighbouring non-neuronal cells (Robberecht and Philips, 2013). This vulnerability is further emphasised by higher levels of protein aggregate deposition and cellular degeneration in the spinal cord MNs than other populations of neurons inside the central nervous system (CNS) (Bruijn et al., 2004). Pathogenic mechanisms implicated in ALS pathogenesis include excitotoxicity (Van Damme et al., 2005), oxidative stress (Filezac de L'Etang et al., 2015), neuroinflammation (Henkel et al., 2004), dysregulated RNA signalling (Cookson, 2016), mitochondrial dysfunction (Park et al., 2013), protein aggregation (Leigh et al., 1988) and impaired cytoskeletal functioning including microtubule dynamics (Fanara et al., 2007) and axonal transport (Bilsland et al., 2010) (Figure 1.2).

Whilst the cortex is increasingly implicated in the initial development and maintenance of the disease (Vucic et al., 2008; Menon et al., 2015), this literature review will focus on the defining hallmarks of ALS spinal cord pathology, particularly of a-MNs, a-MN axons and neuromuscular junctions. The impact ALS mutations have on muscle pathology will also be discussed.

FIGURE 1.2. Mechanisms hypothesised to underlie the dysfunction and degeneration of MNs in ALS. Many of the proposed mechanisms have been derived from studies utilising mouse models expressing various mutant forms of SOD1. Neurodegeneration in ALS may be an accumulation of multiple insults that culminate in the eventual death of the cell. These insults include excitotoxicity, oxidative stress, mitochondrial dysfunction and axonal transport disruption. Mutations in genes such as *SOD1*, *TARDBP* and *FUS* and *C9ORF72* repeat expansion is thought to either directly cause such insults, or predispose vulnerable cells, thus increasing their risk of dysfunction and degeneration.

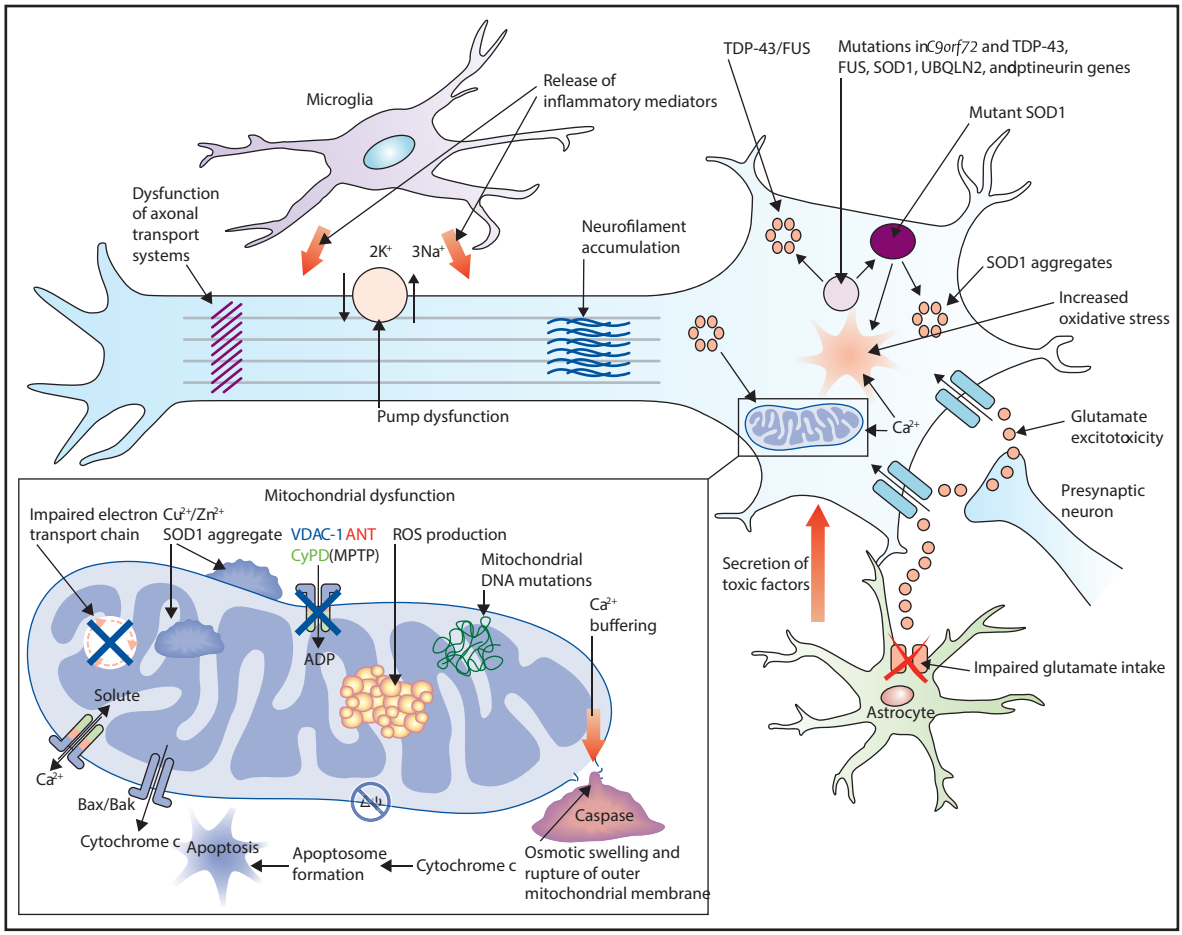

Adapted from Turner et al, 2013

Mechanisms behind the degeneration of a-MNs will also be reviewed, with a particular focus on the involvement of the cytoskeletal organelle, microtubules. Lastly, therapeutic strategies focusing on ameliorating microtubule pathologies will be examined, particularly in relation to the increasing use of microtubule stabilising drugs in the treatment of neurodegenerative disorders.

1.1 ALS genetics

For over a century it has been appreciated that the neuromuscular circuitry is particularly vulnerable to dysfunction, which can generate clinical symptoms associated with MN loss. ALS was first characterised by the French neurologist Jean-Martin Charcot in 1869, although two decades earlier in 1850, Aran described a lower MN disease he termed progressive muscle atrophy (PMA) (Charcot and Joffroy, 1869). These two pioneering neurologists suggested that diseases effecting the neuromuscular circuitry, and thus MNs, are heritable. Indeed, approximately 10% of cases are fALS, due to familial inheritance of mutated genes that increase the risk of developing ALS (for extensive review see (Marangi and Traynor, 2015)). However, the majority of cases (90%) are sALS cases, suggesting there exists some innate property of MNs that makes them susceptible to ALS without a genetic cause. These can also include random mutations to susceptible genes without any familial inheritance. A breakthrough in the understanding of familial ALS occurred in 1993, when mutations to the gene encoding the protein superoxide dismutase 1 (*SOD1*) were first discovered (Rosen et al 1993). As time and technology progresses, the detection of disease causing mutations and the prevalence of each fALS mutation in the population has expanded, as shown in (Figure 1.3).

The gene *SOD1* codes for the superoxide dismutase 1, an enzyme localised to the cytoplasm. This specialised enzyme is responsible for superoxide radical ($O2^-$) catabolism; breaking superoxides down into hydrogen peroxide (H_2O_2) and molecular oxygen (O_2) (McCord and Fridovich, 1969). Superoxide is a reactive oxygen species (ROS) that has the capacity to damage the cytoskeleton, organelles, membranes and transcript components of a cell (Rosen et al., 1993; Ferraiuolo et al., 2011). The enzyme is a 35 kDa metal binding protein that is able to bind zinc and copper. The *SOD1* gene itself spans 9.3kb on chromosome 21q, consisting of five exons (Getzoff et al., 1989; Ticozzi et al., 2011). More than 160 different mutations to the gene encoding for *SOD1* have been reported (Rosen et al., 1993; Al-Chalabi et al., 2012), accounting for approximately 20% of all familial forms of ALS (Andersen and Al-Chalabi, 2011; Robberecht and Philips, 2013). Not only was *SOD1* the first gene to be linked to ALS development, the glycine to alanine

FIGURE 1.3. Timeline and representation of disease causing mutations in familial ALS (fALS). The first identified ALS causing mutation was in superoxide dismutase 1 (*SOD1*), representing approximately 15% of all fALS cases. The other mutations with high representation are mutations to *TARDBP* (gene coding for TDP-43), and Fused in Sarcoma (*FUS*), with 4% each. The hexanucleotide repeat expansion in *C9ORF72* represents approximately 40% of all mutations in fALS cases. Increasing in frequency is the discovery of disease causing rare variant mutations, such as in *TUBA4A*.

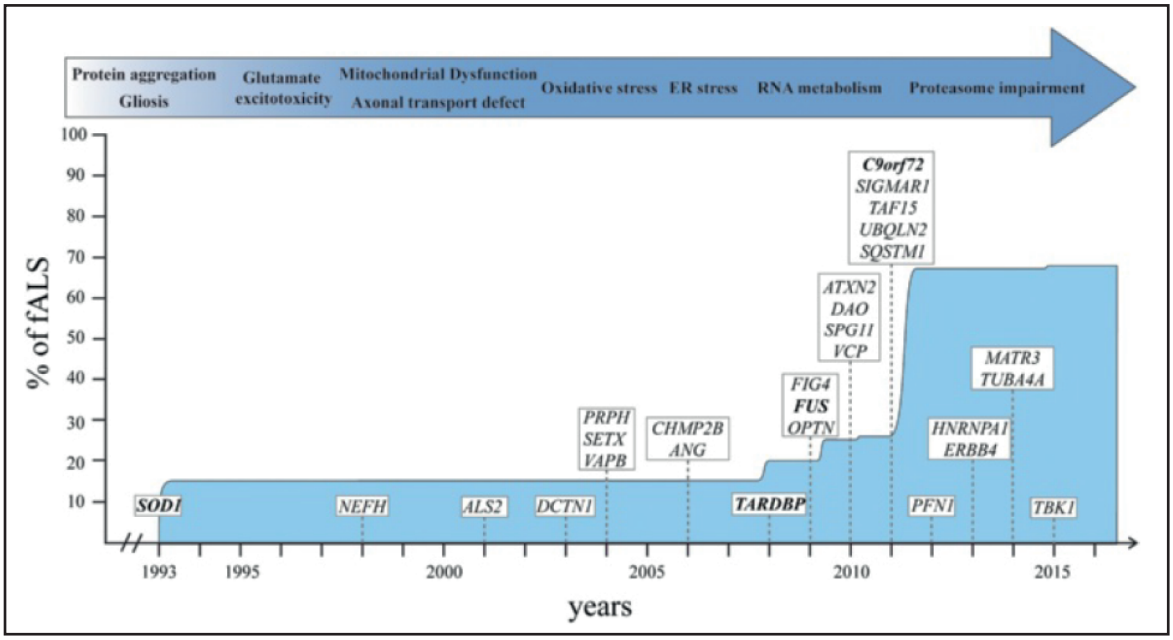

Adapted from Picher-Martel et al., 2016

substitution at amino acid 93 SOD1 mutant variant ($SOD1^{G93A}$) was also the first ALS causing mutation to be used to generate the first animal model of the disease (Gurney et al., 1994).

To date, there is no clear explanation for how SOD1 mutations relate to cortical and a-MNs loss in ALS. Initially it was hypothesised that impaired enzyme activity would lead to increased levels of cellular ROS creating oxidative stress and eventually cell death (Deng et al., 1993). Indeed, SOD1 knockout mice show pathological features similar to those described in the ALS patients and the mutant $SOD1^{G93A}$ mouse model of ALS, leading to impaired neurotransmitter release and decreased NMJ stability (Shi et al., 2014). However, studies have shown that some mutants still have catalytic ability, and there appears to be no correlation between lingering enzyme activity, disease phenotype and its clinical progression (Radunovic et al., 1997; Ticozzi et al., 2011). Several studies have shown that in MNs, SOD1 aggregates into cytoplasmic inclusions, with a skein-like morphology (Shibata et al., 1996; Deng et al., 2010). Moreover, it has long been established that SOD1 mutations, particularly the most widely studied $SOD1^{G93A}$ mutation, causes dysfunction of axonal transport, suggesting an aberrant interaction with the microtubule system (Warita et al., 1999; Ligon et al., 2005; Bilsland et al., 2010; Ikenaka et al., 2012). This has been reported to be occurring as early as embryonic day 13 in the $SOD1^{G93A}$ mutant mouse (Kieran et al., 2005), but is still poorly understood. Recently, mutations in genes coding for DNA/RNA binding proteins have been linked to fALS cases. Moreover, a number of the proteins involved in fALS related mutations are associated with sALS as well.

Discoveries of mutations in DNA/RNA processing proteins such as TDP-43 (*TARDBP*) and fused in sarcoma (*FUS*) were both identified as a cause of familial ALS and FTD (Kabashi et al., 2008; Sreedharan et al., 2008; Kwiatkowski et al., 2009; Vance et al., 2009), and subsequently used to generate further models of ALS, which have been reviewed elsewhere (Liu et al., 2013; Philips and Rothstein, 2015; Nolan et al., 2016). TDP-43 is a 43-kDa protein that is localised to the cell nucleus in unaffected neurons (Buratti and Baralle, 2008). The specific function of TDP-43 remains unclear, but it is associated with transcription repression (Ou et al., 1995), the regulation of slice variants (Buratti and Baralle, 2001), mRNA stability and/or transport (Tollervey et al., 2011) and is a member of the heterogeneous nuclear ribonucleoprotein (hnRNP) family of proteins (Pesiridis et al., 2009). The c-terminal glycine-rich region is thought to modulate RNA transcription and metabolism through interactions with other hnRNPs, such as hnRNP A2/B1 (Buratti and Baralle, 2001).

TDP-43 also interacts with microtubules in the microtubule dependant transport of mRNP granules (Kanai et al., 2004; Alami et al., 2014). Approximately 30 TDP-43 mutations have been reported, all of which involve a missense substitution, and make up 4% of fALS cases and a small percentage of sALS (Ticozzi et al., 2010). The majority of TDP-43 mutations are located in the glycine rich c-terminal domain, suggesting that this may impact hnRNP interactions and thus promote aberrant RNA metabolism and processing (Sofola et al., 2007; He et al., 2014). There is no current clear genotype-phenotype relationship, however, the A382T variant mutation has been shown to lead predominantly to a lower MN disease (Corrado et al., 2009). Mutated TDP-43 in fALS, as well as native and mutated TDP-43 in sporadic cases, mislocalises from the nucleus to the cytoplasm and forms cytoplasmic inclusions (Neumann et al., 2006). Aggregated TDP-43 found in inclusion bodies is abnormally phosphorylated (Hasegawa et al., 2008), and are found in the cortex of the majority of ALS/FTD patients (Ito and Suzuki, 2011). Two main theories regarding the role TDP-43 plays in ALS pathogenesis have been put forward. Either the change in distribution of TDP-43 from the nucleus, to cytosolic aggregates, is impeding its normal nuclear function and/or that TDP-43 aggregates develop a toxic gain-of-function that is independent of the proteins normal physiological activities (Lagier-Tourenne et al., 2010; Strong, 2010; Ticozzi et al., 2010).

Mutations to the gene encoding fused in sarcoma (*FUS*) on chromosome 16p12.1-q21, have also been linked to the development of familial ALS. Pathology includes cytoplasmic inclusions in the cortex and spinal cord with neuronal cell loss (Kwiatkowski et al., 2009; Vance et al., 2009). The *FUS* gene encodes for a DNA/RNA binding protein which was originally isolated in cancer-associated fusion genes, described by Crozat et al. 2003, in their study of mesenchymal tumours (Crozat et al., 1993). Studies of ALS cohorts show a disease distribution of approximately 4% of fALS cases and 1% of sALS cases, which display a mutated *FUS* genotype (Belzil et al., 2009; Baumer et al., 2010; Yan et al., 2010). The majority of *FUS* mutations in ALS are missense mutations, and the rest being non-sense or frame shift mutations (Ticozzi et al., 2011).

Similar to TDP-43, FUS is localised to the nucleus where it acts to regulate gene expression, with implications for gene transcription, splicing and mRNA transport (Kwiatkowski et al., 2009; Vance et al., 2009; Dormann et al., 2010). Furthermore, FUS is mislocalised to cytoplasmic inclusions due to a loss of nuclear import signalling (Morohoshi et al., 1998; Zakaryan and

Gehring, 2006; Dormann et al., 2010). FUS nuclear import disruption appears to promote disease progression, as the extent of the blockage of nuclear import can be correlated to the disease severity; severe disruption results in an earlier disease onset and faster progression (Dormann and Haass, 2011). However, *FUS* mutations do not seem to be detrimental to its normal physiological function, as it can still bind its RNA targets (Kwiatkowski et al 2009). It is hypothesised that FUS positive cytoplasmic inclusions, the loss of nuclear FUS and thus its ability to participate in its normal nuclear functions, may contribute to ALS related pathogenesis (Ticozzi et al., 2011).

As methods of analysis and new technologies progress into the molecular world, an increased number of ALS associated mutations in vastly different genes have been identified. In 2011, three independent studies identified the hexanucleotide repeat expansion (G_4C_2) of the non-coding region of reading frame 72 on chromosome 9 (*C9ORF72*); a mutation that occurs in both sporadic and familial ALS/FTD, at greater frequency than other previously known mutations (DeJesus-Hernandez et al., 2011; Renton et al., 2011; Gijselinck et al., 2012). Initially it was postulated that this abnormal mRNA transcript was cytotoxic, however the exact mechanism of pathogenesis remains unclear (DeJesus-Hernandez et al., 2011). More recently it has been proposed that the presence of the repeat expansion results in 'unconventional translation' generating intranuclear RNA foci (Ash et al., 2013; Todd and Petrucelli, 2016). This leads to G_4C_2 hexanucleotide repeat proteins, which accumulate in neurons, and are neurotoxic (Lee et al., 2013b; Mori et al., 2013). Indeed, C9ORF72 transcripts show striking homology to signalling molecules called guanosine nucleotide exchange factors (GEFs) that can impact a vast number of intracellular signalling cascades (Levine et al., 2013; Droppelmann et al., 2014). Interestingly, C9ORF72 has been shown to intact in the TDP-43/hnRNP A2/B1 RNA processing pathway, without direct interaction with TDP-43 (He et al., 2014). It was shown that mutations in *UBQLN2*, which codes for ubiquilin 2 (regulator of degradation of ubiquinated proteins), cause dominant X-linked ALS/Dementia pathology (Deng et al., 2011). This was hypothesised by Deng, et al (2011) to lead to impairment in protein degradation, abnormal protein aggregation and neurodegeneration. As these genetic abnormalities have only recently been discovered, their function and pathogenesis in ALS is yet to be determined.

Whilst the majority of fALS follows a dominant pattern of inheritance, mutations to alsin (ALS2) have been found to exhibit a recessive pattern of inheritance (Hadano et al., 2001). Mutations in

the ALS2 gene have been associated with the development of juvenile onset ALS, as well as a range of other conditions such as primary lateral sclerosis and hereditary spastic paraplegia (HSP) (Eymard-Pierre et al., 2002; Panzeri et al., 2006), with 12 different mutations identified to contribute to the development of such conditions (Chandran et al., 2007). Many of these mutations result in a premature stop codon, rendering the ALS2 protein non-functional (Yamanaka et al., 2006). ALS2 is a guanine nucleotide exchange factor, which promotes guanosine diphosphate (GDP) release and guanosine triphosphate (GTP) binding onto target proteins, as well as the stimulation certain signalling cascades (Tudor et al., 2005). ALS2 mutations have been suggested to contribute to the pathogenicity of ALS through the disruptions of Rab5-dependent exocytosis, endosome trafficking and also glutamate associated excitotoxicity, which is considered a hallmark of ALS pathology (Devon et al., 2006; Hadano et al., 2006; Lai et al., 2006).

Although this chapter has discussed the major ALS causing mutations, it is appreciated that there are many mutations that occur at lower frequency, but are still vitally important in understanding disease pathogenesis (as shown in Figure 1.3). Indeed, it is becoming increasingly apparent that mutations to proteins that are associated with key structural and functional processes can act as a primary driver of pathology in ALS. Familial mutations to proteins associated with microtubules, a cytoskeletal element, have been recently identified as the cause of an increasing number of fALS cases (Munch et al., 2004; Munch et al., 2005; Levy et al., 2006; Laird et al., 2008; Smith et al., 2014). The downstream effects of such mutations will be discussed in later sections of this introductory thesis chapter.

1.2 Motor neurons and non-cell autonomous processes in ALS

A relatively new concept of selective MN cell death is the involvement of non-cell-autonomous processes (Ilieva et al., 2009; Peters et al., 2015). Expressing mutant SOD1 in MNs alone does not usually lead to ALS like neuropathy; in some cases it extends the duration of disease progression (Clement et al., 2003; Bruijn et al., 2004). This suggests that ALS is not a cell autonomous disorder, meaning that damage to the MNs alone does not suffice to produce the disease phenotype (Figure 1.4) (Ilieva et al., 2009). Whilst other neuronal populations, such as interneurons (Clark et al., 2015), are increasingly being implicated in the pathogenesis of ALS, this thesis will focus on spinal neuromuscular circuitry associated cell types, for which there are select cellular populations implicated in disease.

FIGURE 1.4. ALS is recognised as a non-cell autonomous disease. Although motor neurons are the cell type whose demise facilitates the clinical phenotype of ALS, astrocytes, microglia, myelinating oligodendrocytes and schwann cells, endothelial cells and skeletal muscle all play a role in the development and progression of the disease. These findings have generally been determined by selectively removing mutant SOD1 from these key cell types and evaluating changes to the phenotype of the ALS model, typically in the $SOD1^{G93A}$ mouse.

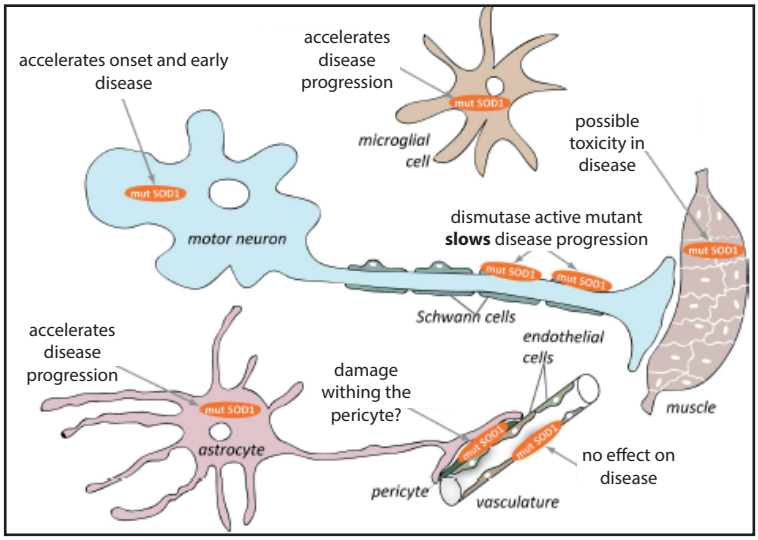

Adapted from Ilieva et al., 2009

1.2.1 Glia play an active role in the pathogenesis of ALS

Glia have been found to have a key role in the pathogenesis in ALS, particularly through investigations utilising the $SOD1^{G93A}$ mouse model (Radford et al., 2015). Glia are the non-neuronal cells of the CNS and are responsible for providing growth factors, a supportive framework, monitoring of the CNS environment and the formation and selective transport of the blood brain barrier. In 2003 Clement and colleagues reported that mice expressing mSOD1 in selective populations of glia developed ALS pathology in the MNs that were surrounded by these affected glia (Clement et al., 2003). It was shown that it is not sufficient for MNs, which were engineered to be the only cell type to carry mSOD1 through a Cre recombinase system, to develop ALS pathology. These results suggest ALS may not be a cell autonomous disorder, relying on dysfunctions in non-neuronal cells to produce a disease phenotype. Interestingly, the development of axonal swellings and the resulting dysfunction in axonal transport has also been attributed to defective neuron-glia crosstalk (King et al., 2011). Moreover, the phenomenon of 'reactive gliosis' occurs in ALS, involving astrocyte activation and microglial proliferation, which is localised to areas of neuronal and axonal degeneration (Brettschneider et al., 2012; Radford et al., 2015).

Astrocytes are a supporting glial cell with a plethora of functions, with a role in MN upkeep and homeostasis. Astrocytes play a crucial role in preventing MN over stimulation by excitatory neurotransmission (Howland et al., 2002; Ilieva et al., 2009; Yang et al., 2009). Indeed, astrocytes can directly impact MN receptor expression; for example, they promote the expression of Ca^{2+} permeable glutamate receptors in neighbouring MNs (Van Damme et al., 2007). Activated astrocytes are also found surrounding degenerating MNs (Zagami et al., 2009) and astrocytes isolated from fALS and sALS patients are toxic to control MNs *in vitro* (Haidet-Phillips et al., 2011), suggesting astrocytes form a degenerative environment for MNs in ALS. This toxicity was subsequently established to be driven by the secretion of neurotoxic factors from astrocytes of ALS patients, which activated necroptotic pathways in human MNs, leading to selective MN demise (Re et al., 2014). Further supporting that astrocyte toxicity can drive ALS pathology, Meyer and Colleagues (2014) showed that C9ORF72 and SOD1 mutant containing induced pluripotent stem cells (iPSCs) derived from fALS and sALS patients are also toxic to human MNs (Meyer et al., 2014). Conversely, transplantation of astrocytes lacking ALS mutations improves MN survival in a SOD1 mouse model of ALS (Kondo et al., 2014). Indeed, mice with selective SOD1 removal from astrocytes show a slower disease progression

(Yamanaka et al., 2008). These studies highlight that MNs are vulnerable to mutant ALS astrocytes, and that astrocyte expression of mutant proteins is sufficient to cause an ALS phenotype (Tong et al., 2013; Radford et al., 2015).

Microglia are typically thought of as the resident immune cells of the CNS (Schafer et al., 2012), however, they also play a role in synaptic pruning, axonal upkeep and debris clearance (Paolicelli et al., 2011; Schafer and Stevens, 2013; Davis et al., 2014). They are involved in the neuropathology of ALS, with microglia activation occurring before MN loss (Henkel et al., 2004) and reviewed in (Brites and Vaz, 2014). However, it is unclear whether their activation (microgliosis) is a direct cause of the disease, or if it is a result of the disease (Boillee et al., 2006a; Gowing et al., 2008). Mice with selective elimination of mutant SOD1 from microglia have a slower disease progression (Boillee et al., 2006b). Moreover, slowing of disease progression is produced in mice treated with the tetracycline derivative compound minocycline (Yrjanheikki et al., 1999). The attributed main factor of minocycline treatment is its ability to reduce macrophage activation (Kriz et al., 2002). However, whilst minocycline is a microglia deactivator, is also induces anti apoptotic effects in neurons, therefore it is difficult to determine the true effect of microglia on disease progression in ALS (Zhu et al., 2002). More recently, a mutant variant in the gene *TREM2* was a risk factor for sALS (Thrash et al., 2009). *TREM2* codes for the TREM2 protein, which is a constituent of the microglial specific signalling complex involved in generating the 'neuroprotective' microglial phenotype (Takahashi et al., 2005). The hypothesised loss of TREM2 function is suggested to aberrantly alter the inflammatory response in ALS, resulting in a decrease in phagocytosis and cytokine signalling (Kleinberger et al., 2014). Dysfunctional microglial phagocytosis has also been implicated in mutant progranilin (*GRN*) - linked FTD (Petkau and Leavitt, 2014), and loss of function mutations to profiling 1 (*PFN1*) in associated fALS cases (Wu et al., 2012). This suggests that microglial dysfunction can drive ALS pathophysiology, with a variety of ALS mutations effecting normal microglia function.

Oligodendrocytes and Schwann cells are responsible for the myelination of axons in both the CNS and PNS, respectively. They play a role in the pathogenesis of ALS, with studies indicating abnormal myelination of axons in both ALS patients (Hayashi et al., 2001) and also in $SOD1^{G93A}$ transgenic rat models (Niebroj-Dobosz et al., 2007). Indeed, TDP-43 and FUS aggregates have been described in the cytoplasm of oligodendrocytes from both fALS and sALS cases (Zhang et al., 2008b; Seilhean et al., 2009; Nonneman et al., 2014). Recently, it has been identified that the

whilst oligodendrocyte loss is an early event in ALS pathogenesis, the inability of precursor cells to mature and remyelinate motor axons may compound the effects of oligodendrocyte dysfunction in ALS (Kang et al., 2013). In 2009, Keller and colleagues developed a GFAP-luc/SOD^{G93A} mouse model; through which GFAP up regulation in Schwann cells could be visualised *in vivo* utilising live imaging techniques (Keller et al., 2009). Schwann cells associated with distal axons of a-MNs show increased levels of GFAP, growth-associated protein-43, low-affinity nerve growth factor (NGF), the p75 receptor and nestin throughout disease progression, suggesting a link between peripheral axon pathology/degeneration and Schwann cell stress (Keller et al., 2009; Arbour et al., 2017). Interestingly terminal schwann cells associated with denervated NMJs have been shown to extend processes to innervated NMJs, forming 'bridges' and promoting nerve terminal sprouts (O'Malley et al., 1999; Tallon et al., 2016). Further, terminal schwann cells require pre-synaptic acetylcholine release to stimulate repair and maintenance of NMJs; a process that is impaired in ALS due to nerve terminal retraction and denervation (Arbour et al., 2017). Schwann cell involvement at the NMJ is summarised further in section 1.3.4 of this thesis.

An further interesting avenue of research could follow on from a study by Court and Colleagues (2008), who described the role of capping cells (kranocytes) in the formation and upkeep of NMJs (Court et al., 2008). Their role in ALS pathogenesis has not yet been investigated, and as NMJ loss is a pathological hallmark of ALS, it would be prudent to investigate this further. The close link of a-MNs and their processes with their surrounding cellular environment, particularly neuron-glia interactions and the possible mechanisms at play between the two could result in disease development (King et al., 2011).

1.2.2 Skeletal muscle as an instigator and bystander of disease

The guidance of developing a-MNs and subsequent innervation of skeletal muscle relies on a combination of intrinsic neuronal electrochemical cues (Kastanenka and Landmesser, 2010), and extrinsic cues such as ephrin mediated motor axon patterning on muscles (Feng et al., 2000a), and tropic factors which induce nerve-muscle branching (Sakuma and Yamaguchi, 2011). Muscle development results in functional syncytia of myoblasts (myotubes), which histologically appear as large cells with multiple nuclei. Each muscle fibre has one connection (through a NMJ), with a single a-MN being able to innervate multiple muscle fibres, creating a functional motor unit. These motor units can contract together, creating a directionally orientated and controlled

contractile force, which is dependent on the fibre type and the number of fibres presents (Gillingwater and Ribchester, 2003). The NMJ, signalling events that lead to muscle contraction and description of the pre and post-synaptic apparatus will be discussed shortly.

Muscle weakness, followed by subsequent muscle atrophy, is the first symptomatic signs of ALS (Ngo et al., 2012; Lee et al., 2017a). Loss of muscle mass does not always correlate fully with the loss of NMJs and distal portions of axons in ALS, suggesting a possible compensatory event occurring (Gonzalez de Aguilar et al., 2008). There are currently two hypotheses surrounding a-MN and skeletal muscle involvement in ALS neuropathy. The first is that ALS begins in the skeletal muscle; with a-MN and NMJ degeneration due to the loss of skeletal muscle mass and activity. Evidence to support this was presented by Teng and Tang (2008), who described increased expression levels of the neurite growth inhibitor Nogo-A, with increased levels of disease severity, suggesting skeletal muscle may initiate or regulate neuronal degeneration as seen in ALS (Teng and Tang, 2008). Moreover, a study by Wong and colleagues expressed mutant human SOD1 selectively in the muscle of mice, which lead to lower a-MN loss, and a motor phenotype similar to models where SOD1 is expressed ubiquitously (Wong and Martin, 2010). However, others showed that depleting SOD1 synthesis in muscle alone does not alter any facet of disease progression or pathology (Towne et al., 2008), suggesting that the impact of muscle on disease pathogenesis is significantly less than the CNS, but is still sufficient to cause degeneration when expressed in muscle alone (Dobrowolny et al., 2008; Wong and Martin, 2010). Regardless, it is appreciated that mutant SOD1 causes muscle pathology, however the sequence of these events remains poorly understood. Others have highlighted that factors released from muscle can impact on both the denervation and reinnervation potential of the distal neuromuscular circuitry, particularly surrounding the promotion of collateral branching (Williams et al., 2009; Taetzsch et al., 2017). Interestingly, in the $SOD1^{G93A}$ mouse model of ALS the muscle-specific microRNA miR-206 it unregulated, which promotes compensatory regeneration of the neuromuscular circuitry through histone deacetylase 4 and fibroblast growth factor signalling pathways (Williams et al., 2009). Conversely, the expression of fibroblast growth factor binding protein 1 (FGFBP1) decreases at the NMJ prior to denervation in $SOD1^{G93A}$ mice. These studies emphasise the importance of muscle dependant signalling in ALS pathogenesis.

Conversely, others believe that motor neuropathy is the initial driving force behind ALS, resulting in muscle atrophy due to a loss of neuronal innervation (Miller et al., 2006). A-MNs in the $SOD1^{G93A}$ mouse model are hyper active, resulting in an increased release of Ach at their respective NMJs (Rocha et al., 2013). Indeed, Ach and other AchR agonists increase AchR endocytosis (St John and Gordon, 2001); a process that is inhibited by pre-synaptic release of neuronal agrin (Misgeld et al., 2005). This suggests that over activation of the NMJ may mediate receptor dispersal (Morsch et al., 2013) and decrease synaptic strength (Zhu et al., 2011), leading to NMJ degeneration.

It has also been identified that NMJs are plastic; meaning they can regulate and change the fibres they innervate, the muscle fibre type and also increase and decrease the size of the motor unit (Frey et al., 2000; Santos and Caroni, 2003; Pun et al., 2006). This is suggestive of an innate compensatory mechanism available to skeletal muscle. It also poses the problem of determining the pathological relevance of NMJ alterations during disease progression, with correlations between NMJ pathology and ALS neuropathy being skewed by this ability to re-innervate skeletal muscle. Indeed, the sequence of pathological events that transpires in both the pre and post synapse in ALS, particularly in comparison to each other remain elusive. It is yet to be determined whether pathology in the NMJ presynaptic compartment (of the a-MN) occurs prior to that of the postsynaptic muscle, and whether alterations, if any, occur prior to that of disease onset. Investigations into this problem will highlight early pathology of the distal synapse and cellular components, and hopefully elucidate therapeutic targets to improve pathological outcomes.

1.3 Vulnerability and pathology of motor neurons in ALS

The vulnerability of select, individual populations of neurons is a key feature in many neurodegenerative diseases. Indeed, the aforementioned mutations that occur in ALS highlight that MNs are selectively vulnerable to multiple insults, with the end result being MN dysfunction and degeneration. However, the inherent vulnerability of MNs to mutations found in ubiquitous proteins such as SOD1 and TDP-43 and their aggregation is not fully understood. Contributing factors which may result in this selective vulnerability of affected MNs in ALS can include their large cell size (energy dependency), intracellular transport, their excitable nature coupled with a lack of buffering capacity, their intimate relationship with neighbouring non-neuronal cells as well as mRNA trafficking and distribution for localised protein production (Ilieva et al., 2009;

Ferraiuolo et al., 2011). Indeed, the narrow margin for MN cellular homeostasis may increase their vulnerability to the numerous ALS associated mutations, such as to *SOD1*, *TARDBP*, *FUS* and *Alsin*. Many proteins associated with ALS pathogenesis converge on mechanisms and targets in MNs that either regulate or effected signalling cascades and normal neuronal function. This can occur as a result of the proteins normal role in various signalling cascades, or through mutation dependant gain of function. This will be discussed in subsequent sections regarding the microtubule cytoskeleton.

1.3.1 Somatic intracellular inclusions as a hallmark of ALS pathology

A key theme in the pathology of ALS is the deposition of ubiquinated intracellular inclusions (or aggregates) in MNs (Leigh et al., 1988). Indeed, historically ALS was classified as a neurological proteinopathy. Intracellular inclusions occur as the direct result of protein mutations, or as the downstream effect of particular pathological mechanisms, which drive wild-type proteins to deposit in the cell due to abnormal cleavage or posttranslational modifications such as aberrant ubiquitination or hyper phosphorylation (Peters et al., 2015). As mentioned previously, misfolded SOD1 forms inclusions in a-MNs of both fALS patients harbouring *SOD1* mutations, but also in many sALS patients (Shibata et al., 1994; Forsberg et al., 2010; Grad et al., 2014). It has also been established that oligomeric misfolded SOD1 is more cytotoxic than larger inclusions (Redler et al., 2014), with increasing evidence that misfolded SOD1 can be directly transmitted between cells in a 'prion-like' mechanisms of propagation throughout the CNS (Grad et al., 2014).

TDP-43 also forms intracellular inclusions that are both ubiquitinated and hyperphosphorylated in most cases of fALS, sALS and FTD, with TDP-43 mislocalising from the nucleus to the cytoplasm (Neumann et al., 2006). Increasing evidence suggests that TDP-43 mislocalisation may drive the aggregation of these proteins, as mutations to the c-terminus of the protein results in increases protein-protein interactions, thus increased aggregation (Pesiridis et al., 2009; Mutihac et al., 2015). Whilst it is still yet to be determined whether TDP-43 is a gain of function due to aberrant cleavage and aggregation of the protein, or a loss of its normal function, it is widely appreciated that pathological TDP-43 plays a distinct role in the pathogenesis of ALS (Pokrishevsky et al., 2012). Similar to misfolded SOD1, pathogenic TDP-43 has been described as a 'prion-like' protein, with the ability to propagate through the CNS circuitry, causing further

TDP-43 pathology in unaffected cells (Zhang et al., 2009; Budini et al., 2012; Feiler et al., 2015). Mutant FUS, similar to TDP-43 and SOD1, has been identified in intracellular inclusions of both the cortex and spinal cord of fALS, sALS and FTD patients (Kwiatkowski et al., 2009; Vance et al., 2009), but not in patients with *SOD1* mutations (Deng et al., 2010).

As described in previous sections, the *C9ORF72* G_4C_2 expansion produces repeat peptides, which have the capacity to generate inclusions. However, C9ORF72 inclusions in MNs due to aberrant translation of the dipeptide repeat are rare in patients with the G_4C_2 repeat expansion; these patients show robust TDP-43 aggregation (Gomez-Deza et al., 2015). The role inclusions play in MN dysfunction and degeneration is still poorly understood. However, a number of mechanisms of aggregate-mediated toxicity have been proposed. These include aggregates having an innate ability to inhibit proteosome function and protein degradation, decreased chaperone activity and disruption to global organelle function (Rothstein, 2009; Ferraiuolo et al., 2011). Indeed, cytoplasmic inclusions have also been implicated in causing axonal transport dysfunction, which has ramifications for axonal, and ultimately MN, survival (Bosco et al., 2010).

1.3.2 Axonal inclusions in ALS

A pathological hallmark of ALS is the formation of neurofilament inclusions or 'swellings' in the axons of a-MNs, a pathology that is though to physically hinder axonal transport (Hirano et al., 1984; Bilsland et al., 2010). Neurofilamentous swellings have been described in the axons wild-type and mutant *SOD1* neurons *in vitro* and have been demonstrated to induce cytoskeletal changes (King et al., 2011). Axonal swellings are also immunoreactive for neurofilament triplet proteins and peripherin (Wong et al., 2000), neurofilament-L, neurofilament-M, neurofilament-H, α-internexin and in some inclusions, ubiquitin (King et al., 2011). Converse to the pathological functions of neurofilament swellings, others have hypothesised that axonal neurofilament inclusions may in fact be neuroprotective, acting as a phosphorylation 'sink', thus reducing aberrant phosphorylation of other more vulnerable intracellular targets (Nguyen et al., 2001). Regardless of pathological significance of neurofilaments, axons are a primary site of degeneration in ALS, and may be an early event with a large capacity for therapeutic intervention.

1.3.3 Axonal degeneration in ALS

There are several described methods of axon degeneration, including axon die-back, Wallerian degeneration and axonal pruning. Wallerian degeneration is the mechanism that occurs as a result

of a transection or crushing injury to the distal portion of an axon (Gillingwater and Ribchester, 2003). Dying-back of the axon, starting at its most distal region and spreading towards the cell body, is a common theme in neurodegenerative diseases (Coleman, 2005). In ALS, axonal die-back is typical of NMJ and distal axon pathology, leading to a loss of motor units and atrophy of the denervated muscle (Pun et al., 2006; Fischer and Glass, 2007). Evidence from both patients and ALS disease models suggest that ALS is a dying-back axonopathy; an active and controlled process (Fischer et al., 2004; Pun et al., 2006; Vickers et al., 2009; Clark et al., 2016b). This is thought to occur independently of the cell soma (Coleman, 2005; Saxena and Caroni, 2007).

Interestingly, similarities exist between axonal degeneration seen in neurodegenerative diseases and normal phasic pruning of neuronal processes in normal circuitry growth and maintenance (Yaron and Schuldiner, 2016). For example, the Ubiquitin Proteosome System (UPS), the intracellular system responsible for protein metabolism and recycling, is used to degrade and alter the proteinacious axonal structure prior to membrane disintegration; similar processes occur in ALS during axon degeneration (Watts et al., 2003). However, axonal degeneration initiated by Wallerian mechanisms is thought to begin with a loss of axonal survival factors, either by physical blockage of the axon or by a decrease in axonal transport (Pun et al., 2006; Wang et al., 2012). Although still not fully understood, this loss of survival factors, including trophic signalling (Taetzsch et al., 2017), mRNA, and energy depletion due to decrease mitochondria recycling, lead to a localised increase in intracellular calcium in the axon (Coleman, 2005). Cytoskeletal disintegration is one of the first identified signs of Wallerian degeneration, particularly the neurofilament and microtubules networks (Griffin et al., 1995; Watts et al., 2003; Zhai et al., 2003). However, the precise timeline of these events in ALS are unknown. Indeed, over a decade after these initial observations, our understanding of the process of cytoskeletal disintegration in axonal degeneration remains limited. Nevertheless, it is appreciated that a sharp rise in intracellular calcium in the axon activates caspases and calpain enzymatic pathways, leading to protein degradation and cytoskeletal abnormalities (as both neurofilaments and microtubule proteins are caspase/calpain substrates), and has been reviewed previously (Watts et al., 2003; Wang et al., 2012; Ma, 2013).

The first clinical sign of ALS is muscle weakness, which is attributed to the loss of muscle innervation by MNs as a result of axon degeneration (Boillee et al., 2006a). Axonal degeneration by Wallerian mechanisms starts with axonal beading, a result of cytoskeletal proteins being

dismantled. The axon then fragments, with surrounding glia removing the axonal debris (reviewed in (Coleman, 2005)). The initial insult that results in axonal degeneration can be due to metabolic stress, axonal transport dysfunction, ischemia and neuroinflammation, as stated previously. However, it is increasingly being appreciated that compensatory responses to axonal and synaptic degeneration occur in ALS. The reinnervation of recently denervated synapses to maintain muscle function has been shown to occur in ALS (Schaefer et al., 2005; Pun et al., 2006; Clark et al., 2016b), thus illuminating the extended asymptomatic stage of the disease that may begin decades before symptoms are apparent. Axon pruning is a intrinsic form of functional remodelling and rearrangement of neuronal processes in the developing central nervous system through the destruction of redundant or excessive amounts of synapses (Katz and Shatz, 1996; Luo and O'Leary, 2005). Indeed, axons in ALS show plasticity via their ability to collaterally branch, forming new axonal offshoots and innervating recently denervated endplates; a characteristic of ALS pathology (Pun et al., 2006; Ketschek et al., 2015b; Clark et al., 2016b). This ability of the neuromuscular circuitry to maintain this plastic, reinnervative state is thought to lose its efficiency, leading to an environment where neuromuscular loss exposes a clinical phenotype.

1.3.4 NMJs and ALS

As mentioned previously, NMJs are the anatomical connections between the nervous system and muscle, and are located at the terminus of motor axons, ending on a motor unit. They are a part of a two-way interface of communication that includes orthograde depolarisation events that initiate muscle contraction; and retrograde transmission, which is involved in neurotrophic signalling, leading to regulation and functional adjustments to the a-MN (Northcutt, 1989). Contraction of the muscle is firstly initiated by the a-MN (presynaptic compartment), which stimulates the NMJ to release the neurotransmitter acetylcholine (ACh) into the synaptic cleft (Figure 1.5). ACh binds to cholinergic receptors, a specifically nicotinic receptor subtype, on the muscle cell surface. Upon receptor activation, Na^+ is diffused across the receptor, which in itself is a voltage gated ion channel, leading to a depolarisation event in the muscle (Martyn et al., 2009). This event is called an excitatory post-synaptic potential (EPSP), or more specifically to the muscle fibre, an endplate potential. If the EPSP is large enough, a postsynaptic action potential in the muscle will occur, leading to the release of internal calcium stores and contraction of the muscle fibre through contractile protein (actin and myosin) activation (Bear and Connors, 2007; Martyn et al., 2009).

FIGURE 1.5. The NMJ consists of the pre-synaptic motor neuron end terminal, basal lamina, synaptic cleft, and the post-synaptic myocyte. It is made up of a plethora of pre- and post-synaptic proteins that are involved in the development, maintenance and stability of the synapse. Many trans-membrane and cytosolic post-synaptic proteins are involved in initial NMJ formation through signalling, such as the Agrin-LRP4-MuSK signalling complex, as well as structural support through proteins such as rapsyn and nestin.

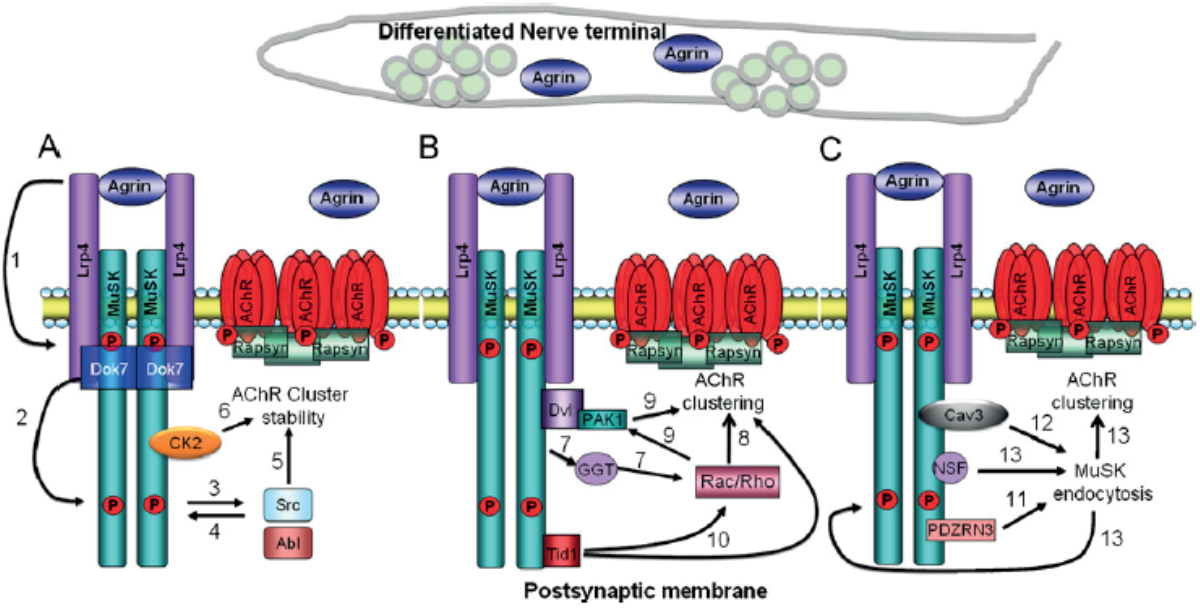

Adapted from Ghazanfari et al, 2011

The development and maturation of the NMJ is a complex process. A pioneering study by Sanes and Colleagues (1978) showed that reinnervating frog motor nerve terminals, in specimens that have had their associated muscle removed, form new active zones on the basal lamina at original synaptic sites (Sanes et al., 1978). This suggested that the synaptic basal lamina contains the components that play a pivotal role in NMJ differentiation. Subsequent studies have identified that this process involves tri-directional cross talk between the presynaptic a-MN, the postsynaptic muscle fibre and perisynaptic schwann cells (PSCs) (Shi et al., 2012; Darabid et al., 2014). Guidance of the terminal a-MN axons are controlled primarily by molecular 'cues' that occur along the path of the axon (Tessier-Lavigne and Goodman, 1996). Muscle fibres destined to be innervated by approaching axons already show basal levels of postsynaptic maturation, with expression, and in many cases clustering (pre-patterning) of AChRs on the cell surface (Lin et al., 2001; Yang et al., 2001). Once contacted with muscle, axons will innervate the muscle fiber, with multiple axons being able to innervate one NMJ (polyinnervation) (Wyatt and Balice-Gordon, 2003). Following this, maturation of the synapse ensues, with alterations to the presynaptic and postsynaptic compartments, as well as controlled synaptic elimination to obtain mature NMJs innervated by a single axon. Presynaptic maturation, whilst being the least understood process of NMJ development, involves the contribution of structural and signalling molecular in the synaptic end terminal and lamina. For example, the laminin family of glycoproteins have many isoforms and subunits involved in NMJ maintenance and stability. Laminin laminin-beta2 is the laminin isoform involved in the enhancement and clustering of P/Q voltage gated calcium channel 'active zones' at the NMJ (Knight et al., 2003; Nishimune et al., 2004; Chand et al., 2015). A decline in laminin-alpha4 expression results in both the pre- and post-synaptic function and stability (Chand et al., 2017), and its absence accelerates NMJ aging and fragmentation (Lee et al., 2017b). Further roles of laminins are the orchestration of synaptic vesicle clustering, prevent PSC invasion (Knight et al., 2003), and the physical alignment of the synapse (Patton et al., 2001).

Indeed, similar mechanisms of presynaptic maturation are also regulated by type IV collagen (Miner and Sanes, 1994), and type XIII (Latvanlehto et al., 2010). Synaptic vesicle clustering in the pre-synaptic terminal can also be regulated by signal regulatory protein-α, suggesting that multiple presynaptic lamina proteins are necessary for presynaptic maturation (Umemori and Sanes, 2008). The involvement of extracellularly active growth factors has also been implicated

in NMJ maturation. For example, fibroblast growth factors (FGFs), which are produced primarily by muscle, promotes presynaptic vesicle clustering and synaptic varicosities (Fox et al., 2007). Similarly, glial-derived neurotropic factor (GDNF), produced by both muscle and Schwann cells, promotes a-MN survival by retrograde signalling (Henderson et al., 1994). Interestingly, brain-derived neurotropic factor (BDNF), which is found in precursor (Pro-BDNF) and mature (mBDNF) form, shows vastly different effects dependant on processing. Pro-BDNF promotes synaptic elimination, whereas mBDNF favour synaptic maturation and survival (Je et al., 2013).

Postsynaptic maturation of the NMJ involves dynamic alterations to receptors and architectural proteins in relation to synaptic activity and various signalling mechanisms. For example, synaptic activity, driven by Ach concentration at both the terminal, can alter the expression and clustering of AChRs on the postsynaptic membrane (Misgeld et al., 2005). Indeed, as discussed in Section 1.2.2 of this thesis, activity at the NMJ promotes its maturation, whereas hyper-activity of AchRs can promote their dispersal; a process that is countered by the activation of the agrin-LRP4-MuSK signalling complex, the main pathway of postsynaptic maturation (St John and Gordon, 2001; Misgeld et al., 2005). Agrin, a proteoglycan released from a-MN synaptic terminals, muscle and schwann cells (neuronal agrin is more potent), is a ligand for the low-density lipoprotein receptor-related protein 4 (LRP4) (Bowen et al., 1996; Burgess et al., 1999). Signalling through LRP-4, agrin causes muscle-specific tyrosine kinase (MuSK) autophosphorylation (DeChiara et al., 1996), which induce the clustering of AChRs. Interestingly, LRP-4 has also been implicated in MuSK independent retrograde signalling in concurrent presynaptic maturation (Yumoto et al., 2012). Postsynaptically, LRP-4 interaction with MuSK without the precedence of agrin can induce MuSK activation, synonymous with both LRP-4 and MuSKs role in the pre-patterning and surface recruitment of AChRs prior to presynaptic involvement (Kim et al., 2008; Darabid et al., 2014). MuSK activation also recruits scaffolding proteins such as rapsyn, which is responsible for maintaining the clustering of AchRs (Gautam et al., 1995; Gervasio and Phillips, 2005), and other important proteins, such as those in the dystroglycan complex (Darabid et al., 2014). Furthermore, maturation of the postsynapse apparatus corresponds with an increase in the expression of AChRs, rapsyn and MuSK (Jo et al., 1995; Sandrock et al., 1997; Rimer et al., 1998). Of note is the involvement of laminins (mentioned previously as being involved in presynaptic maturation), in the stabilisation of AChRs in the membrane and in regulating aspects of ACh transmission (Jacobson et al., 2001; Arikawa-Hirasawa et al., 2002).

Although involved in the development and maintenance of NMJs, a number of the aforementioned proteins have been implicated in the generation of neuromuscular disorders. Autoantibodies that target AChRs, MuSK and LRP-4, as well as mutations to particular postsynaptic architectural proteins, have been implicated in the development of myasthenia gravis and various congenital neuromuscular diseases (Ohno et al., 2002; Li et al., 2010; Pilgram et al., 2010; Pevzner et al., 2012; Ohkawara et al., 2014). This highlights that the NMJ is a site of pathological vulnerability. In ALS the denervation of NMJs results in the clinical phenotypes associated with the disease, particularly progressive paralysis and muscle wastage. According to the distal 'die-back' hypothesis of the neuromuscular circuitry in ALS, NMJ and distal axon degeneration occurs prior to that of the a-MN cell body, with degeneration progressing in a distal-to-proximal direction; see extensive review (Moloney et al., 2014). Loss of motor units have been shown to occur in SOD1 transgenic mouse model (Maselli et al., 1993; Frey et al., 2000; Clark et al., 2016b) and more recently has been shown that loss of synaptic terminals occurs via retraction of presynaptic components (McCann et al., 2007).

Further, the neuromuscular circuitry shows vulnerability depending on the fibre type of the synapse, as well as the capacity for plasticity that synapse has (a fibre type is a neuromuscular unit, made up of a a-MN, NMJ and corresponding type specific muscle fibre). For example, fast-fatigue synapses (corresponding to fast-fatigue a-MNs/NMJs and fast-fatigue muscle fibres), are the most vulnerable fibre type, and are lost early in the disease (Frey et al., 2000). Fast-fatigue resistant and slow fibre type NMJs are more resistant to degeneration, with a high capacity for remodelling in disease, reinnervating recently denervated synapses (Fischer et al., 2004; Pun et al., 2006). However, the capacity for firstly fatigue resistant, then later in disease slow fibre types to compensate for denervation wanes, resulting in a significant motor unit loss that unmasks the clinical phenotype of ALS (Hegedus et al., 2008). However, our understanding of NMJ degeneration is still not fully appreciated. For example, identification of early alterations to the presynaptic compartment of the NMJ is still incomplete; this information may allow for the development of novel therapeutics to target this structure. Further, the identification of pathological events that occur to the NMJs post-synaptic architecture is an area of research that has not been fully explored. Much of the research to date has focused on MuSK, with the importance of such architectural proteins highlighted by the significant improvement of SOD1 mice when MuSK expression is increased, resulting in synaptic stabilisation (Perez-Garcia and

Burden, 2012). However, the attention given to MuSK has not been shown to other proteins of the post-synapse, specifically to those that stabilise and maintain NMJ integrity, such as rapsyn, dystrophin and nestin. Indeed, this highlights that NMJ architectural proteins require further research into their role in ALS pathogenesis, as they play a key a role in the demise of the NMJ in various neuromuscular disorders, and also possibly in ALS (Clark et al., 2016b).

1.4 Microtubule involvement in ALS

Neurons are highly refined communicating cells that receive, process and relay information to their target cells, with MNs being particularly vulnerable to ALS associated pathology. As discussed previously, factors contributing to the selective vulnerability of MNs in ALS include their large cell size and therefore energy dependency, their excitable nature coupled with a lack of buffering capacity, and their intimate relationship with neighbouring non-neuronal cells. Although many disease mechanisms have been described (reviewed in (Peters et al., 2015)), the impairment of the axonal transport system highlights the significance of the intracellular cytoskeleton, particularly the microtubules, in the neurodegenerative process. The role of this cytoskeletal system in ALS will be a focus of this thesis.

1.4.1 Microtubules are integral to neuronal function

Microtubules are structural cytoskeletal elements expressed in all eukaryotic cells. Their composition and general function is conserved between different cell types and organisms, and is essential for cell division and motility. Microtubules are of particular importance to neurons and are involved in a great number of additional functions including the development of neuronal cell polarity, the generation of neuronal compartments, growth cone mechanics, neurite remodelling and intracellular transport (Chen et al., 2006; Baas and Lin, 2011; Sakakibara et al., 2013). Within neurons, microtubules form protofilaments from heterodimerised tubulin. These cylindrical structures are vitally important for the function of long extending axons, which have a high demand for intracellular transport of organelles, proteins and RNA granules. Therefore, it can be said microtubules are essential to both the development and maintenance of the neuronal circuitry.

Microtubule protofilaments are comprised of dimers of α and β-tubulin, which through lateral interactions, form the characteristic microtubule structure (Desai and Mitchison, 1997). Microtubules undergo bouts of assembly and disassembly from their ends, a process termed dynamic instability (Mitchison and Kirschner, 1984) (Figure 1.6 and 1.7 A). A slow growing α-

FIGURE 1.6. Microtubules are dynamic hollow polymers. (A) Microtubules are protofibrils comprised of polymerised α- and β-tubulin. They consist of a slow growing minus (-) end, and a fast growing plus (+) end. When not bound to the microtubule lattice, α- and β-tubulin exist together as heterodimers. (B) Microtubules undergo the phenomenon of dynamic instability, with a fast growing phase, a stable 'paused' phase, and a shrinking depolymerisation phase.

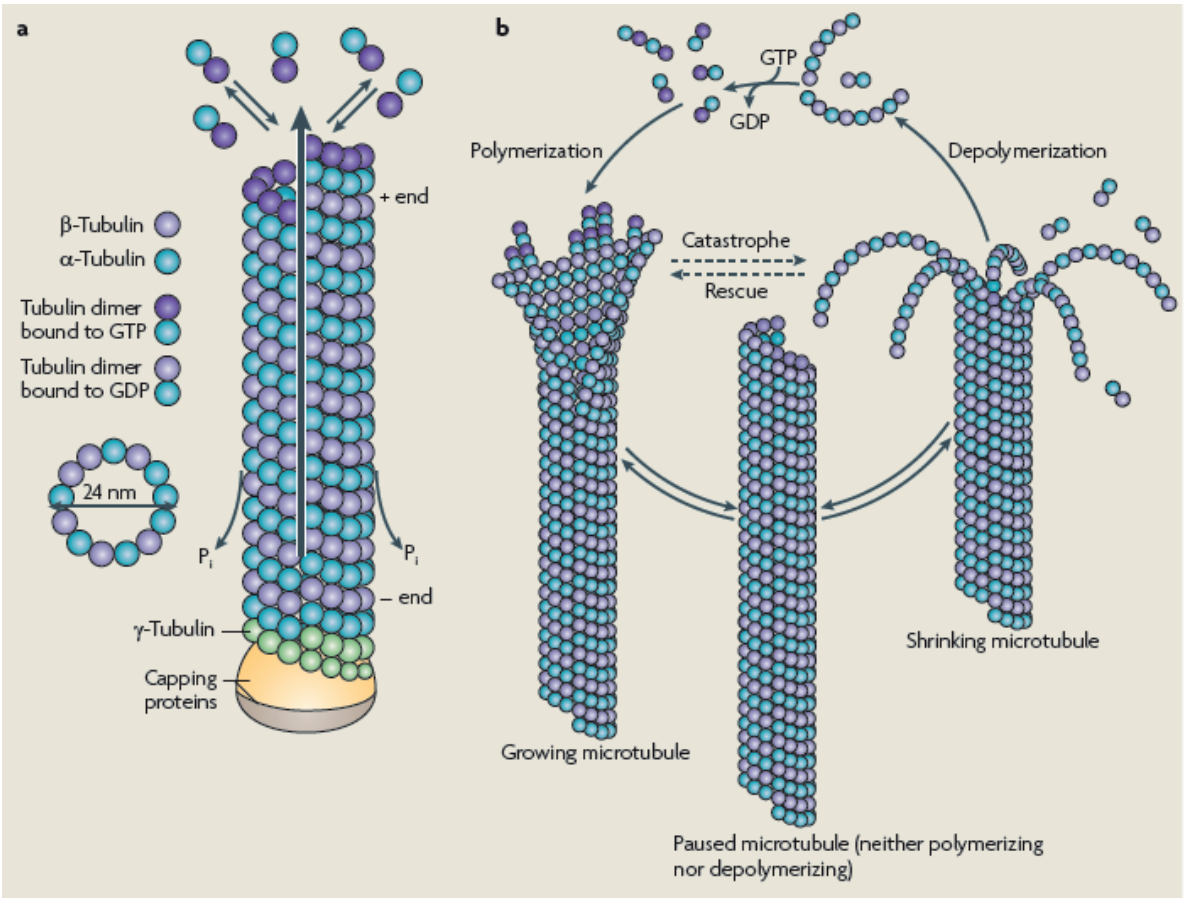

Adapted from Conde and Caceres, 2009

FIGURE 1.7. Modifications to neuronal microtubules in ALS. A) Normal microtubule +TIP dynamics and kinesin/dynein transport, mRNA granule transport and chemical modifications. B) Mutant SOD1 expression leading to microtubule hyperdynamics, increased +TIP protein density, decreased transport, increased acetylation, phosphorylation of MAPs and accumulation of microtubule protein containing aggregates. A global increase in HDAC activity is also present. C) Mutant TDP-43 expression causes dysfunction in mRNA granule transport. Decreased local translation of MAP mRNA is also implicated in TDP-43 mutants. D) Mutant TUBA4A expression alters microtubule dynamics and network stability, with unknown impact on +TIP proteins, transport or chemical modifications. Select mutations are incorporated into intracellular aggregates. E) Energy depletion and calcium dysregulation generates increased microtubule depolymerisation, tubulin GTP cap hydrolysis, and increased MAP phosphorylation. F) Neuronal oxidative stress leads to tubulin glutathionylation, increased microtubule depolymerisation, decreased axonal transport and alterations to MAPs, with unknown impact on classical chemical modifications or +TIP proteins.

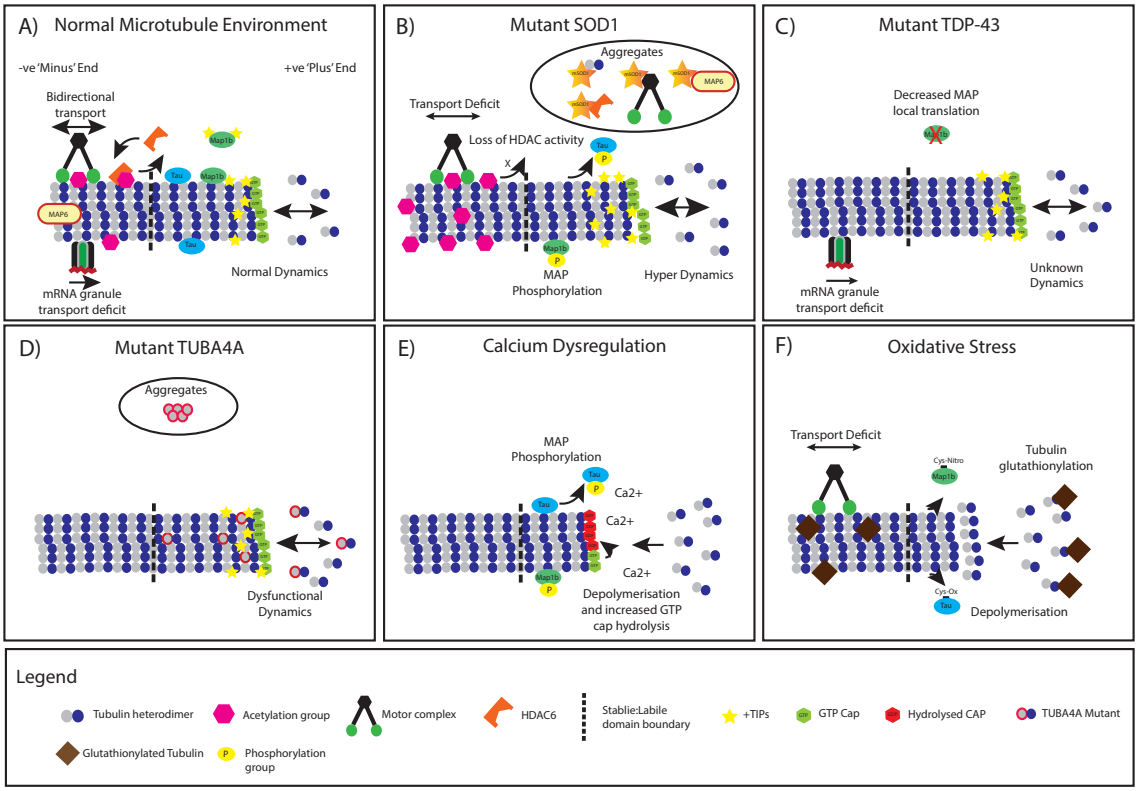

Adapted from Clark et al, 2016

tubulin ‘minus-end’ and fast growing β-tubulin ‘plus-end’ (Allen and Borisy, 1974; van Beuningen et al., 2015; Yau et al., 2016) can be accounted for by the GTP cap model. GTP bound to β-tubulin confers plus end stability, and upon hydrolysis, leads to microtubule depolymerisation (Desai and Mitchison, 1997; Nogales and Wang, 2006). This directionality in microtubule structure allows the formation of neuronal compartments and therefore confers neuronal polarity. The axonal compartment has exclusively distal facing positive polarity, or ‘plus-end out’ orientating microtubules (Heidemann et al., 1981). Contrastingly, the somatodendritic compartment contains a mixed orientation of microtubule directions, with equal quantities of plus and minus-end facing microtubules (Yau et al., 2016).

Neurons, being relatively long-lived and stable cells, require a stable cytoskeleton. Neuronal microtubules can be separated into two domains: labile and stable (Baas and Black, 1990; Baas, 2013). Whilst mature neurons have a microtubule network consisting of both domains, the majority of the microtubules are stable (Ferreira and Caceres, 1989; Lim et al., 1989). These domains cannot be fully explained by the myriad of tubulin isoforms available in the genome (Tischfield and Engle, 2010). This functional diversity has instead been associated with domain specific chemical modification to tubulin subunits, which aid in increasing the functionality of microtubules, and in some cases, can impact upon their stability (Baas, 2013; Janke, 2014). These modifications to neuronal microtubules include, but are not limited to, tubulin tyrosination, acetylation, polyamination, glutathyonilation, glutamylation and glycylation (reviewed previously in (Janke and Kneussel, 2010; Janke, 2014)). These post-translational modifications may confer stability to microtubule structure and alter binding affinity of microtubule associated proteins, thereby altering their function. Whilst not being fully understood, these chemical modifications can also be utilised as molecular markers of microtubule network stability, and alterations to chemical modifications are thought to be an attractive therapeutic target for neurodegenerative disorders (d'Ydewalle et al., 2011; Taes et al., 2013).

Perturbations in microtubule and microtubule associated protein (MAP) function have been implicated in a range of neurodegenerative diseases (Dubey et al., 2015), including Alzheimer’s disease (AD) (Matsuyama and Jarvik, 1989), Parkinson’s disease (PD) (Ren et al., 2003; Cartelli et al., 2010), Huntington’s disease (HD), various congenital developmental disorders (Tischfield and Engle, 2010), schizophrenia (Morris et al., 2003; Andrieux et al., 2006), as well as ALS (Baird and Bennett, 2013; Smith et al., 2014). Of note the microtubule stabiliser, Tau (Drubin and

Kirschner, 1986), is involved in the pathophysiology of AD (reviewed in (McMurray, 2000; Hanger et al., 2014; Stancu et al., 2014)) as well as other neurodegenerative diseases (collectively tauopathies) such as supranuclear palsy, corticobasal degeneration and Picks disease, (reviewed in (Cairns et al., 2004)). Alterations to proteins involved in microtubule stability, dynamics and microtubule turnover also occur in PD (Alim et al., 2004; Yang et al., 2005; Gillardon, 2009). Similarly, microtubule involvement has also been established through 1-methyl-4-phenylpiridinium (MPP+) (Cappelletti et al., 2005) and Rotenone (Ren et al., 2005) mediated PD in *in vitro* models, with these found to destabilise the microtubule network. Furthermore, it has been highlighted that perturbations to microtubule dynamics also leads to microtubule dependent transport impairment in a model of PD (Cartelli et al., 2010). The gene disrupted-in-schizophrenia-1 (DISC-1), whose mutations are associated with familial forms of schizophrenia, has been suggested to associate and interact with microtubule components (Morris et al., 2003; Callicott et al., 2005), further implicating microtubule alterations as a causal factor in multiple neurodegenerative disorders. Conversely, mutations to tubulin genes generally leads to disorders associated with dysregulated neurogenesis, due to abnormalities in neuronal migration, cellular division of progenitor cells, neuronal differentiation and induction of cell polarity. These disorders include lissencephaly, polymicrogyria, mirocephaly, cerebellar dysplasia and some occulomotor disorders (Francis et al., 2006; Guerrini et al., 2008; Tischfield et al., 2011).

In ALS the consequence of microtubule dysfunction has classically been hypothesised as being due to the physical length of the axon in affected MNs, with alterations to microtubules being thought to impact on axonal transport (De Vos et al., 2007; Millecamps and Julien, 2013). However, evidence for microtubule dysfunction having a primary role in ALS has significantly increased over the last 15 years. The recent identification of tubulin rare variants and their impact on microtubule function, specific interactions with mutant and pathological proteins as well as altered function of microtubule associated proteins and signalling pathways which affect microtubule dynamics, have all been implicated in ALS pathogenesis.

1.4.2 The genetic inheritance of ALS: recent insights into microtubule function

As the familial genetics of ALS become increasingly understood, microtubules and their functions are being identified as a site of pathological convergence for various ALS mutations. For example, it has long been established that *SOD1* mutations can cause axonal transport dysfunction, thus suggesting an interaction with the microtubule network (Warita et al., 1999; Ligon et al., 2005; Bilsland et al., 2010; Ikenaka et al., 2012). This has been reported to occur as

early as embryonic day 13 in the $SOD1^{G93A}$ mutant mouse (Kieran et al., 2005). Recently, evidence has been published supporting the hypothesis that alterations to microtubule dynamics is driving MN dysfunction in these mice (Fanara et al., 2007; Kleele et al., 2014) (Figure 1.7 B). Indeed, mutant SOD1 has been implicated in the alteration of signalling cascades that may affect proper microtubule functioning, however, this process is still poorly understood (Evans et al., 2000; Nguyen et al., 2001; Vadlamudi et al., 2005; Lopez-Fanarraga et al., 2007; Ikeda et al., 2011; Zyss et al., 2011; Bunton-Stasyshyn et al., 2015).

TDP-43 interacts with microtubules in the microtubule dependant transport of mRNP granules (Kanai et al., 2004; Alami et al., 2014) (Figure 1.7 C). This transport is particularly important due to TDP-43's role in local mRNA translation of proteins in dendrites, axons, and synapses, such as the neuromuscular junction (NMJ) (Kanai et al., 2004; Belly et al., 2005; Fallini et al., 2012). Indeed, TDP-43 is present at the pre-synaptic motor terminal endings, and has been shown to bind to several pre-synaptic proteins that are involved in regulating neurotransmitter release (Narayanan et al., 2013; Alami et al., 2014). Similarly, TDP-43 interacts directly with proteins involved in RNA transport (Freibaum et al., 2010). Mutated TDP-43 has recently been identified to impair axonal transport of mRNA *in vivo*, as well as in induced pluripotent stem cell (iPSC) derived MNs of patients with TDP-43 mutations (Alami et al., 2014). mRNP granule transport defects were independent of other transport reporter defects such as mitochondrial transport. It was hypothesised that diminished transport of mRNA to compartments such as the axon and NMJ may lead to a decrease in proteins particularly important for NMJ maintenance and survival (Polymenidou et al., 2011; Lagier-Tourenne et al., 2012).

Similarly, the association of C9ORF72 dipeptide repeats and aberrant interactions on the microtubule network may also exist; however this is still unproven. Although the function of this repeat expansion is still under investigation, Droppelmann and colleagues (2014) have highlighted that possible interaction with microtubules may exist, due to the C9ORF72 homology to a guanine nucleotide exchange factor (GEF) that signals Rab-GTPases. Rab-GTPases are involved in membrane trafficking of proteins (Levine et al., 2013; Droppelmann et al., 2014) and hence, may be dependent upon microtubules. As mentioned previously, mutations to Alsin (ALS2), another GEF, is implicated in juvenile onset ALS and other various motor disorders (Eymard-Pierre et al., 2002; Panzeri et al., 2006). Interestingly ALS2 acts through signalling cascades that impact microtubules, and whose loss of function may generate microtubule

dysfunction; a process that requires further research (Tudor et al., 2005).

Vascular endothelial growth factor (VEGF) is a polymorphic risk factor for ALS, and its expression is reduced in patients (Brockington et al., 2006; Brockington et al., 2010). A mouse model that produces decreased levels of VEGF develops a motor neurodegenerative phenotype, with behavioural deficits and cellular loss (Oosthuyse et al., 2001). VEGF mice show decreased expression of the MAPS tau, MAP1b and MAP6, which has implications for stability of both the stable and labile domains of microtubules in ALS (Brockington et al., 2010). Furthermore, genes relating to transport and dynein complex cargo loading are also down regulated. This occurs well before MN loss, but at the time of motor behaviour phenotype generation. This may highlight a link between dysfunction of microtubules and other identified genes, leading to MN dysfunction, followed by cellular demise (Brockington et al., 2010).

Recently, and with great excitement in the ALS research community was the discovery of loss of function NEK1 rare variant mutants as a risk factor in ALS patients (Kenna et al., 2016). Interestingly, NEKs (NIMA related kinases) are involved in regulation and formation of non-motile primary cilium (Shalom et al., 2008), a process that involved regulating microtubule dynamics, growth and organisation (Chang et al., 2009; Cohen et al., 2013). Indeed patient derived fibroblasts with truncation variants of NEK1 show microtubule abnormalities (Lee, 2013), suggesting a link between NEK1 loss of function and the generation of a pathological microtubule environment; however, this is yet to be investigated in mature neuronal microtubules, particularly in vulnerable MNs in ALS. However, it does suggest that microtubule dynamics may be a common denominator of ALS pathogenesis.

1.4.3 Microtubule protein mutations: a primary cause of ALS

Various studies have suggested that mutations to microtubules can also initiate adult onset MN dysfunction, suggesting that microtubules may be a primary driver for ALS pathophysiology (Al-Chalabi et al., 1999; Puls et al., 2003; Gros-Louis et al., 2004; Wu et al., 2012; Smith et al., 2014). Smith and Colleagues (2014) found dominant negative mutated variants in the *TUBA4A* gene on chromosome 2 in fALS patients. These mutations were reported to cause classical lumbar onset ALS, with upper and lower MN loss, and in some cases, FTD-like symptoms (Smith et al., 2014). The mutated region normally interacts with β-tubulin and the motor domain of kinesins and other MAPs (Liu et al., 2012; Howes et al., 2014). These variants were further

shown to ineffectively form tubulin dimers and displayed a decreased incorporation into protofibrils, inhibiting microtubule network stability (Figure 1.7 D). Similarly, other mutations affecting the conformation of tubulin proteins may subsequently alter the assembly of tubulin, resulting in an unstable microtubule structure (Tischfield et al., 2011).

TUBA4A is ubiquitously expressed in all cell types, but at high levels in the nervous system (Rustici et al., 2013; Smith et al., 2014). The expression of TUBA4A also increases over time, possibly illuminating why mutations in these genes cause later age disease phenotypes, unlike congenital tubulin mutations, which generate developmental disorders (Tischfield et al., 2011; Hersheson et al., 2013). Further supporting this, and as highlighted by Smith and Colleagues (2014), expression of the β-tubulin subunit, TUBB4A, whose mutations cause adult onset disease Torsion Dystonia Type 4, increases over time, similar to the expression pattern of α-tubulin TUBA4A (Hersheson et al., 2013). Further impacts of tubulin alterations in ALS can be seen in sALS patients, where there is a down regulation of α-tubulin subunit genes (Jiang et al., 2005). However, how microtubule dynamics and transport are impacted as a result of TUBA4A mutations are still not clear. Future development of animal models with TUBA4A mutations will allow for the identification of its role in pathogenesis, particularly focusing on its age-dependant expression pattern.

Collectively, disease-causing mutations have shed light on an integral role for microtubules in ALS. However, with the majority of ALS cases still seemingly sporadic, it remains unclear if altered microtubule function is the cause, or consequence, of upstream initiating pathogenic mechanisms.

1.4.4 Pathogenic ALS mechanisms impact on microtubule structure and function

Many mechanisms and molecular pathways involved in both the initiation and maintenance of ALS have been identified (Van Damme et al., 2005; Ferraiuolo et al., 2011; Peters et al., 2015). These include, but are not limited to, mitochondrial dependant energy depletion, excitotoxicity and calcium dysregulation and cellular oxidative stress. The interplay between these disease mechanisms and insults to microtubules are not well understood, however, it is becoming increasingly appreciated that microtubules may act as a site for mechanistic convergence, as they are impacted by various pathogenic molecular mechanisms associated with ALS.

One such pathological mechanism is mitochondria dependant energy depletion. A study conducted by Park et al. (2013) highlighted that energy depletion itself could be a cause of microtubule depolymerisation, which may in turn further facilitate energy depletion through the inability of the microtubules to facilitate movement of mitochondria (Park et al., 2013) (Figure 1.7 E). Interestingly, microtubule pathology was identified prior to alterations to mitochondrial swellings, suggesting it may be a primary event in energy depletion and axon degeneration. This inability to recycle mitochondria may contribute to the abnormal accumulations of these organelles as observed in mutant SOD1 transgenic mice (Sotelo-Silveira et al., 2009). However, aberrant calcium dysregulation as a result of mitochondrial energy depletion, an identified toxic mechanism in ALS, does not seem to directly a cause microtubule dysfunction, suggesting other, as yet unidentified mechanism may be at play (Park et al., 2013).

Similarly, excitotoxicity has also been identified as a primary mechanism in the initiation and maintenance of ALS (Van Damme et al., 2005; Blizzard et al., 2015). Excessive influx and concentrations of intracellular Ca^{2+}, whether from damaged mitochondria (Jaiswal, 2014), glutamatergic over stimulation, lack of glutamate clearance or a loss of Ca^{2+} buffering capacity, can lead to MN death (Heath and Shaw, 2002). Ca^{2+} concentrations also have an effect on microtubule based transport of mitochondria through inhibition of attachment of kinesins to microtubules (Wang and Schwarz, 2009). Indeed, excessive intracellular Ca^{2+} can lead to aberrant cyclin dependent kinase 5 (CDK5) activity, which is particularly prominent in the SOD1 mouse model of ALS (Patzke and Tsai, 2002). Moreover, Ca^{2+} can interact directly with microtubules, altering their dynamics (O'Brien et al., 1997) (Figure 1.7 E). Interestingly, heightened Ca^{2+} concentrations are sufficient to cause MAP containing microtubule preparations to depolymerise, due to an increase in β-tubulin GTP cap hydrolysis. Furthermore, Ca^{2+} can cause MAP2 loss and microtubule depolymerisation in dendrites treated with NMDA, through calpain proteolysis of MAP2, however, it remains unclear if microtubule destabilisation occurs prior to MAP2 loss (Hoskison et al., 2007). Excitotoxicity has also been shown to impact on retrograde transport machinery (Fujiwara and Morimoto, 2012). Indeed, this insult leads to caspase activation and subsequent cleavage and disintegration of the cytoskeleton, reported to be downstream of microtubule events (King et al., 2013). However, investigation of low dose, long lasting, chronic excitotoxic effects on both microtubule dynamics and transport are yet to be completed, as recognised ALS insults are chronic or accumulative in their nature. Investigations such as these will identify whether biologically relevant levels of neuronal excitotoxicity alter

microtubule dynamics and transport first, or contrastingly activate the CDK5-p25 and caspase pathways, which lead to cellular pathology.

Comparably, oxidative stress occurs due to the build-up of oxidative species, which whilst being a process of general aging of an organism, can cause uncontrollable oxidation on proteins or molecules, leading to cellular dysfunction. Therefore, homeostatic control of reactive oxygen species (ROS) is required for proper cell function. Uncontrollable ROS production and cellular oxidation leads to a number of neurodegenerative diseases (Andersen, 2004). Relevant to ALS, and in addition to Ca^{2+} toxicity, dysfunctional mitochondria can also drive uncontrollable ROS production (Tahara et al., 2009). While ROS are required for cytoskeletal remodelling and during axonal growth (Munnamalai and Suter, 2009; Wilson and Gonzalez-Billault, 2015), aberrant ROS and increases oxidative environment can lead to deleterious impacts on microtubules, particularly oxidation of tubulin and selected MAPs (Landino et al., 2004). Although still poorly understood in neurons, increasing ROS in myocytes increase microtubule depolymerisation (Drum et al., 2016). Both α- and β-tubulin contain Cys residues that have the capacity to oxidize (Landino et al., 2007; Wilson and Gonzalez-Billault, 2015). Oxidative species added to purified tubulin preparations can cause a reduction in polymerisation, and increase microtubule depolymerisation, similar to that of increased Ca^{2+} levels (Landino et al., 2007) (Figure 1.7 F). Moreover, it has been established that oxidative stress affects microtubule integrity; this is evidenced by the presence of methionine sulphaoxides in the β-III tubulin in the brain of AD patients (Boutte et al., 2006). Furthermore, glutathionylation of tubulin, particularly in MNs, occurs during oxidative phases, altering microtubule dynamics and structure (Carletti et al., 2011). Indeed, the MAPs tau and MAP2 contain Cys residues, which when oxidize, impede MAP function, thus causing microtubule stability issues (Landino et al., 2004). Others have identified that recapitulating neuronal oxidative stress through the addition of hydrogen peroxide inhibits axonal transport, prior to mitochondrial dysfunction or axonal degeneration (Fang et al., 2012).

1.4.5 Altered regulation of microtubule dynamics has been associated with ALS

Changes to microtubule dynamics in ALS have also been reported, particularly increases to microtubule dynamic instability. Fanara et al. (2007) identified that hyperdynamic microtubules were present in the $SOD1^{G93A}$ mouse model of ALS, and modulation of microtubule dynamics can ameliorate disease progression (Fanara et al., 2007). A subsequent study found that microtubules are indeed more dynamic, with an increase in end binding-protein 3 (EB3) +TIP

comets on sciatic nerve axonal microtubules in the $SOD1^{G93A}$ mouse, in comparison to unmutated individuals (Kleele et al., 2014). End binding (EB) proteins are +TIP MAPs that bind to the growing phase of the labile domain of microtubules, aiding in both dynamics and microtubule interactions with other intracellular objects. Increases in +TIP comets signify that the microtubule network is hyperdynamic. It was found that increased microtubule dynamics consequently slowed axonal transport, occurring presymptomatically (Fanara et al., 2007; Bilsland et al., 2010). Axonal transport dysfunction is then followed by an increase in neuronal pathology and subsequent mortality (Collard et al., 1995; Sasaki and Iwata, 1996; Williamson and Cleveland, 1999; Sasaki et al., 2004). Pharmacological amelioration of microtubule hyperdynamics not only reverses axonal transport deficits, but also improves clinical symptoms and survival (Fanara et al., 2007). This hints that hyperdynamics can indeed drive transport deficits, followed by cell demise; however, this process is still poorly understood. A possible mechanism through which SOD1 mice develop microtubule hyperdynamics may be through the interaction of mutant SOD1 and tubulin (Kabuta et al., 2009). Interestingly mutant SOD1/tubulin interactions do not diminish the free tubulin pool; however, it generates a destabilising effect on the microtubule network.

Kabuta and colleagues (2009) suggest that homology exists between the site of mutant SOD1 binding to tubulin and the binding site of microtubule destabilising agents such as colchicine and nocodazole (Kabuta et al., 2009). This may indicate that mutant SOD1 interacts in a similar manner to microtubule destabilising agents, increasing the dynamic instability of microtubule labile domains, leading to a reactive, hyperdynamic phenotype. A phenomenon less often considered in ALS research is the impact that intracellular aggregates, consisting of proteins such as misfolded SOD1 and neurofilaments, (as discussed in section 1.3.2), may have on microtubule dynamics. Indeed, these aberrant structures have the propensity to incorporate many different cytosolic proteins into the aggregate mass, with microtubule proteins being particularly prone in aggregate localisation. This may be an interesting avenue of research as a recent study showed that decreasing the neurofilaments in a *pmn* mice improves aberrant microtubule dynamics and instability that is associated with this model (Yadav et al., 2016).

An increasing and popular notion is that alterations to transport proteins, tubulin, other MAPs, or the dysregulation of microtubule dynamics can result in aberrant microtubule structure and function, leading to either developmental disorders or degenerative phenotypes, such as in ALS (Dubey et al., 2015). Indeed, MAPs, which facilitate microtubule functions such as cytoskeletal

interactions, intracellular signalling and modification of microtubule dynamics and stability, are thought to 'tune' microtubule dynamics through both direct and indirect interactions (Tortosa et al., 2013; Sayas et al., 2015). Indeed, MAP function, whether through direct protein modification or signalling becomes dysfunctional, leading to microtubules becoming aberrantly affected in ALS. Mechanisms driving these alterations in microtubule dynamics are not well understood, nor are the hypothesised subsequent transport dysfunctions. Identification of whether dysfunction of microtubule dynamics is a common pathology between familial mutations and sporadic disease is paramount to understanding disease onset, its maintenance and possible therapeutic approaches.

1.4.6 Motor protein dysfunction and axonal transport deficits in ALS.

Intracellular transport is a major function of neuronal microtubules, with alterations in transport associated with a number of neurodegenerative diseases (reviewed in (Millecamps and Julien, 2013)). A-MNs are thought to be particularly vulnerable to transport dysfunction, due to their axonal length. It is becoming increasingly appreciated that alterations to microtubule dynamics precede, and thus may aberrantly affect, axonal transport, and that the resultant transport defect can have deleterious effects on neuronal function (Hurd and Saxton, 1996; Fanara et al., 2007; Bilsland et al., 2010; Cartelli et al., 2010; Dubey et al., 2015). The transport MAPs, kinesin and dynein, act as carriers for organelles, proteins and other cellular cargo in a directionally dependant manner. Kinesin motor proteins transport cell cargo toward the plus end of the microtubule (anterograde), whereas dynein transport in the minus end direction (retrograde) (Maday et al., 2014). Kinesin can impact on the stability of microtubules, and expression of KIF5, a kinesin motor protein isoform, has been found to be decreased in the spinal cord and sciatic nerves of a mutant SOD1 mouse model (Maximino et al., 2014). This indicates that altered microtubule dependent transport may be depleting a-MNs via the generation of an energy and signalling deficit. This is also substantiated in a study by Tateno et al (2009), who showed that kinesin-associated protein 3 (KAP3), a kinesin subunit responsible for binding cargo such as choline acetyltransferase (ChAT), was selectively vulnerable to co-aggregation with misfolded SOD1 (Tateno et al., 2009). This phenomenon was also reported to occur in human *SOD1* fALS patients, possibly illuminating a further source of a-MN vulnerability to dysfunctional transport of specific cargos in ALS.

Dynein, in conjunction with its molecular binding partner and activator, dynactin (DCTN1), is also vulnerable, both as a primary driver of ALS, but also as a site of convergence of ALS insults

(Ligon et al., 2005). Dynein interacts with mutant SOD1 and is located in proteinacious aggregates in SOD1 mice (Ligon et al., 2005) (Figure 1.7 B). Mutant SOD1 also interacts directly with the assembled dynein-dynactin complex, occurring prior to disease onset, at a similar age when retrograde dynein mediated axonal transport dysfunction occur in $SOD1^{G93A}$ mice (Zhang et al., 2007b; Bilsland et al., 2010). The functional consequence of this is yet to be determined, however detrimental impacts of transport dysfunction on the ubiquitin-proteasome system and protein autophagy may create a positive feedback loop, whereby proteins are caught in the incorrect cellular compartment, which compounds aggregation (Goldberg, 2003; Strom et al., 2008; Takalo et al., 2013). Similarly, bidirectional transport of mitochondria is affected presymptomatically, highlighting the cargo and directional specificity of axonal transport dysfunction in this model; however, the exact mechanism is not well understood (Bilsland et al., 2010). Mutations to the $p150^{Glued}$ subunit of DCTN1 are associated with MN degeneration and ALS (Munch et al., 2004; Munch et al., 2005; Levy et al., 2006; Laird et al., 2008). The mutation distorts the folding of the microtubule-binding domain. An autosomal dominant variant has also been reported to concurrently cause FTD (Munch et al., 2005), highlighting the role of motor proteins in other neurodegenerative diseases.

Expression of motor protein genes is altered in sALS patients and in mutant SOD1 mouse models. A reduction in dynactin-1 expression is observed, in the absence of alterations to kinesin and dynein expression; down regulation occurs prior to the deposition of neurofilament protein aggregates (Jiang et al., 2007; Rustici et al., 2013). Furthermore, a polymorphism and reduced expression in kinesin-associated protein 3 (KIFAP3) correlates with an extended life span in sALS patients (Landers et al., 2009); however, how this affects transport is unknown. Interestingly, in mutant SOD1 mice, KIFAP3 expression in increased early in the diseases clinical course (Dupuis et al., 2000). Similarly, a number of cytoskeletal genes are altered in the $SOD1^{G93A}$ mouse spinal cord and sciatic nerve, dependant on both age and a-MN sub compartment evaluated (Maximino et al., 2014). Similar gene expression changes were found in sALS patients, having a decrease in MAP2, MAP1b and tau protein expression, which is also seen in the mutant $SOD1^{G37R}$ mouse model (Farah et al., 2003; Jiang et al., 2007). Motor proteins are also susceptible to alterations in tau levels, as observed in tauopathies, which retard anterograde motor transport (Ebneth et al., 1998). Tau alters the flux at which kinesin and dynein motor complexes bind to the microtubules, but not the speed at which they travel the microtubule tracks (Trinczek et al., 1999), suggesting alterations to tau levels on microtubules may impact

transport where tau pathology and dysfunction is present. Indeed, multiple upstream effectors such as altered dynamics, MAP dysfunction, and protein-protein interactions can produce aberrant axonal transport.

1.4.7 Targeting neuronal microtubules for therapy: an approach for ALS

The only available treatment for ALS is the anti-excitotoxic drug, Riluzole, which acts on the presynaptic neuron to limit the release of glutamate into the synapse, reducing the excitotoxic effect of glutamate on the postsynaptic cell (Bensimon et al., 1994). Notwithstanding the reduction in excitotoxicity, treatment strategies involving Riluzole have limited effectiveness, and are only able to extend patient life by approximately 3-6 months (Gurney et al., 1998). ALS is a multi-factorial disease, with many cellular components affected; therefore there are a range of available targets for therapy, however many of them have had limited success (Turner and Talbot, 2008). Microtubule involvement in ALS and in particular how dynamics and function are impaired in disease states is an attractive target for pharmacological manipulation to improve disease phenotype. Indeed, this therapeutic approach has previously been undertaken in multiple neurodegenerative disease models, including ALS.

Fanara et al (2007), established that hyperdynamic neuronal microtubules were present in a SOD1 mouse model of ALS and administered the microtubule modulating agent noscapine to attenuate this phenotype (Fanara et al., 2007). Noscapine, which can cross the blood brain barrier (BBB) effectively dampens hyperdynamics, leading to less depolymerisation and polymerisation events from occurring at the growing plus tip of the microtubule (Landen et al., 2002; Landen et al., 2004). Noscapine treatment extended lifespan, attenuated microtubule dynamics and normalised aspects of axonal transport. This in itself gives evidence for hyperdynamics driving transport deficits in these mice. However, more cargo-specific and rate-specific transport assays are required to identify if this is the case. This therapy did not investigate whether stabilising the microtubule cytoskeletal network prevented axonal degeneration from progressing in these mice; a pathological phenomenon that requires attention. However, this study provides supporting evidence for the use of microtubule stabilising agents in the treatment of ALS.

Histone deacetylase 6 (HDAC6) inhibitors and HDAC knockout mice have also been trialled to improve outcomes in ALS models, with the intention of increasing the acetylation of stable microtubules to improve stability and axonal transport. The inhibition or removal of HDAC6 was

found to improve the phenotype of mutant SOD1 mice (Taes et al., 2013). However, axonal transport was not directly measured. A similar study utilising HDAC6 inhibition in Charcot-Marie-Tooth (CMT) disease showed an improvement in axonal mitochondrial transport, supporting HDAC6 inhibition as a candidate therapeutic for multiple neurodegenerative diseases (d'Ydewalle et al., 2011).

Direct microtubule stabilising agents have been previously used in the medical setting in the treatment of cancers, as the addition of these agents perturb the formation of the mitotic spindle and therefore inhibit cell division (Schiff et al., 1979). The most studied microtubule targeting compound, taxol, has in the last decade developed a newfound use in modulating microtubules in neurodegenerative diseases (Michaelis et al., 2006; Brunden et al., 2011; Das and Miller, 2012; King et al., 2013). At high doses, taxol treated systems develop hyper-stabilised microtubules, preventing cell division in cancer cells; however, this can generate a painful peripheral neuropathy (Reyes-Gibby et al., 2009). At lower doses taxol has been found to limit microtubule depolymerisation and stabilise the microtubule network in a number of neurodegenerative models (Michaelis et al., 2006; Brunden et al., 2011; Das and Miller, 2012; King et al., 2013). Indeed, treatment of an *in vivo* tauopathy model with taxol improves MN fast axonal transport, highlighting the therapeutic potential of taxol for disorders effecting MNs (Zhang et al., 2005). The range of taxol concentrations which yield beneficial effects on neurodegeneration are very narrow (Shemesh and Spira, 2011). Coupled with the off target effects identified due to taxol therapy, limited crossover at the BBB and the dramatic alterations to microtubule stability that it delivers, the benefits of taxol administration in neurodegenerative disease have been brought into question (Baas and Ahmad, 2013; Baas, 2014). Indeed, some opponents of using taxol or taxol based/like compounds have highlighted that normal neuronal functioning is aberrantly effected including microtubule polarity reversal, microtubule dynamic changes and axonal transport dysfunction (Shemesh and Spira, 2010; Baas and Ahmad, 2013; Benbow et al., 2016).

In relation to ALS, taxol has been shown to reduce microtubule disintegration in an *in vitro* kainic acid excitotoxic model of ALS (King et al., 2013). Excitotoxicity exposure was reported to induce microtubule instability upstream of caspase-3 activation, which is mitigated with taxol treatment. However, as characterisation of microtubule dynamics has not been completed in regards to excitotoxicity due to kainic acid exposure, it is difficult to assess whether taxol is indeed limiting the hypothesised dynamic instability of microtubules, or preventing the

breakdown of the microtubule network. Indeed, inhibition of caspase-3 activation in other excitotoxicity models reports neuroprotection and increased cell survival (Chen et al., 2001). However, it is important to note that taxol derivatives, which exhibit higher blood brain barrier permeability, need to be investigated to determine if this form of microtubule stabilisation is a is a viable treatment for ALS. Moreover, the impact that these derivatives have on normal neuronal functioning is a necessary step to ensure that these therapeutics have limited to no aberrant off-target effects in the nervous system.

1.5 Thesis hypothesis and aims

Despite decades of research regarding distal pathology in ALS, the time course of degenerative events of the distal neuromuscular circuitry is yet to be fully characterised. As discussed in this chapter, research has highlighted that distal neuromuscular pathology is an early event in ALS, and occurs presymptomatically, due in most part to plasticity in the neuromuscular system. However, investigations of presymptomatic changes to the NMJ pre and post synapse are yet to be fully completed, particularly in regard to identifying early therapeutically targetable pathology. Establishing a clear time course of distal axon and NMJ alterations, particularly focusing on distal morphology, denervation, plasticity, and NMJ architectural proteins, will determine the earliest pathology to target in ALS. Indeed, microtubule involvement in ALS, as described in section 1.4, suggests that microtubule-targeting drugs may be of benefit in ALS, as they have shown promise in other neurodegenerative diseases with similar disease mechanisms. Stabilising the axonal microtubule cytoskeleton may offer protection against ALS pathogenesis, particularly axonal degeneration and the alterations identified to microtubule dynamics in ALS.

Identification of distal targets for therapeutics is attractive, as distal pathology produces the ALS phenotype due to a loss of muscle innervation. Further, development of treatments for ALS has been limited in both efficacy and clinical translation. This thesis aims to investigate the time course of pathological alterations of the distal neuromuscular circuitry in an animal model of ALS. Further, it focuses on the potential for axonal protection in ALS using a microtubule stabilising agent, specifically targeting distal events in the neuromuscular circuitry. The impact of pharmacologically stabilising microtubules on neuronal development and function are also determined, as alterations to microtubule stability are associated with pharmacologically induced microtubule dysfunctions and neuropathy.

Thesis hypothesis: *Axonal degeneration is an early pathological phenomenon in ALS, and protecting axonal integrity through pharmacological stabilisation of microtubules in the distal neuromuscular circuitry will improve outcomes in ALS.*

Aim 1: Characterise axonal and neuromuscular junction degeneration in the YFPxSOD1^{G93A} mouse model of ALS.

Hypothesis 1: Pathology of the distal neuromuscular circuitry is an early event in ALS, evidenced by presymptomatic pathology of the axon and NMJ.

Investigations focusing on degeneration of the distal axonal segments of a-MNs, and specific alterations to NMJ architectural proteins in ALS are still incomplete. The first aim of this thesis will investigate specific alterations in axonal and NMJ morphology utilising YFP expressing mice to visualise the distal neuronal anatomy. In addition, alterations to NMJ architectural proteins will be investigated. This will be completed utilising the SOD1^{G93A} mouse model of ALS, coupled with immunohistochemical and confocal microscopy techniques.

Aim 2: Pharmacologically stabilise microtubules to improve outcomes in the SOD1^{G93A} mouse model of ALS using Epothilone D.

Hypothesis 2: Pharmacologically stabilising microtubules will protect the distal neuromuscular circuitry and improve outcomes in ALS.

Cytoskeletal disintegration during axonopathy is a well-characterised event. Further, hyperdynamics of the microtubule cytoskeleton occurs early in ALS, and promotes axonal transport dysfunction. Stabilising axonal microtubules has been shown to halt axonal degeneration and improve microtubule function in various models of neurodegenerative disease. This has previously been shown to be beneficial in ALS, utilising the microtubule-modulating agent noscapine. Thus, aim 2 will determine the efficacy of pharmacologically stabilising microtubules against disintegration and aberrant dynamics in the SOD1^{G93A} mouse model of ALS using the microtubule stabilising compound Epothilone D. The therapeutic efficacy of Epothilone D will be measured through survival, behavioural, clinical progression and histological analysis.

Aim 3: Identify the impact Epothilone D has on neuronal development. *Hypothesis 3: Epothilone D will affect the normal development and function of cortical neurons in a dose-dependant manner.*

Microtubule stabilisation, whilst being an attractive therapeutic target for many neurodegenerative diseases, is not without its caveats. Aberrant and off-target effects of various microtubule targeting compounds, such as taxol, lead to painful peripheral neuropathies, altered cytoskeletal organisation and microtubule dysfunction. Using an *in* vitro model system, aim 3 will investigate the impact of Epothilone D on normal neuronal development and function, by examining the initiation of polarity, neuronal growth, neuronal health, microtubule dependant transport and microtubule chemical and protein expression in cells treated with Epothilone D.

Chapter 2

2 General Methods

2.1 Animal Models

The hSOD1^{G93A} mouse model of ALS was utilised in these studies. Transgenic mice expressing a high copy number of mutant human SOD1 with a glycine (G) to Alanine (A) substitution at position 93 (SOD1^{G93A}), strain number B6.Cg-Tg (SOD1*G93A)1Gur/J (Gurney *et al*.,1994) were obtained from the Jackson Laboratories (stock number 004435). A second transgenic strain (male) that express yellow fluorescent protein (YFP) under the control of the neuron specific *Thy1* promoter, strain number B6.Cg-Tg (*Thy1*-YFP)16Jra/J was also obtained from the Jackson Laboratories (stock number 003709). This line exhibits high YFP expression in cortical projection neurons and a-MNs, making it possible to visualise cellular processed with high resolution and fidelity. Both transgenic strains were bred on a C57BL/6 background. Pups were weaned at 28 days post-natal. Mice were housed in micro isolator cages on a 12 hour light/dark cycle with free access to food and water, and maintained at a temperature of 20°C. Water, food and bedding were replenished twice weekly. Animals were monitored daily and weighed weekly (unless stated otherwise). In accordance with ethical guidelines associated with the SOD1^{G93A} mutant line, animals reaching 80% of their maximum weight or had increasingly affected righting reflexes were considered at the end stage of the disease and sacrificed. This was done by euthanizing in CO_2 for 5 minutes, after which signs of life were checked, or transcardially perfused for histological or molecular analysis as described in subsections below. All animal experiments were approved by the Ethics Committee (Animal Experimentation) of the University of Tasmania (approval numbers A11952, A14233, A13183 for the principal investigator Associate Professor Tracey Dickson).

2.2 Genotyping

Mice were genotyped at the time of weaning (28 days post-natal) using a clipping from the end portion of the tail or ear, which was removed and stored at -20°C until DNA extraction was undertaken. DNA was extracted using an Extract-N-Amp Tissue PCR tissue kit (Sigma-Aldrich) according to the manufacturer's instructions and stored at -4°C.

All offspring of the SOD1^{G93A} cross were genotyped to identify gene status. A qPCR approach was utilised to identify both SOD1 transgene presence and to monitor genetic drift through copy

number analysis (Leitner et al., 2009). This was to ensure high copy number animals (~ 23 copies) were being utilised for both experiments and breeding. The primer and labelled oligonucleotide sequences for $SOD1^{G93A}$ and the internal control ApoB are shown in Table 2.1, (GeneWorks). qPCR DNA amplification and quantitation was completed on a Qiagen Rota-gene Q (Qiagen), according to the reaction conditions outlined in Table 2.2.

YFP status was determined utilising traditional PCR methods. Amplification of the *YFP* transgene resulted in a PCR product of 300bp, and *Tcrd*, used as an internal control, resulting in a PCR product of 200bp. The primer sequences are shown in Table 2.1. DNA was amplified by PCR in a Veriti thermalcycler (Life Technologies) according to the reaction conditions outlined in Table 2.3. A typical YFP PCR gel is shown in Figure 2.1.

Primer	**Sequence (5' – to 3')**
SOD1 Forward primer (qPCR, oIMR-9665)	**gggaagctgttgtcccaag**
SOD1 Reverse primer (qPCR oIMR-9666)	**caaggggaggtaaaagagagc**
Human SOD1 oligos (qPCR, TmolMR-0147)	**ctgcatctggttcttgcaaaacacca**
ApoB Forward primer (qPCR, oIMR-1544)	**cacgtgggctccagcatt**
ApoB Reverse primer (qPCR, oIMR-3580)	**tcaccagtcatttctgcctttg**
Mouse ApoB oligos (qPCR, TmolMR-0105)	**ccaatggtcgggcactgctcaa**
YFP Forward primer (oIMR-1258)	**TCTgAgTggCAAAggACCTTAgg**
YFP Reverse primer (oIMR-1260)	**CgCTgAACTTgTggCCgTTTACg**
TCRD Forward primer (oIMR-015)	**CAAATgTTgCTTgTCTggTg**
TCRD Reverse primer (oIMR-016)	**gTCAgTCgA gTgCAC AgT TT**

Table 2.1 qPCR and PCR primer and oligonucleotide names and sequences

Step	**Temp (°C) & Time**
Initiation	95°C 5 mins
Denaturation	95°C 15 sec
Annealing and elongation	60°C 15 sec (35 cycles)

Table 2.2 SOD1 qPCR reaction conditions

Step	Temp (°C) & Time
Initialisation	94°C 3 mins
Denaturation	94°C 30 secs
Annealing	60°C 30 secs
Elongation	72°C 45 secs
Final Elongation	72°C 2 mins
Hold	4°C <24 hours

Table 2.3 YFP PCR reaction conditions

2.3 Mouse tissue preparation and sectioning

2.3.1 Perfusion and tissue dissection

Mice were terminally anaesthetised (pentabarbitone sodium, 140mg/kg, intraperitoneal) and transcardially perfused with either 4% PFA/0.01M PBS for immunohistochemical and microscopy analysis, or ice-cold 0.01M PBS for protein quantitation. PFA fixed tissue was dissected and stored in 0.02% sodium azide tissue storage solution or bathed in increasing concentrations (4%, 16%, 30%) of sucrose cryoprotectant solution for 24 hours. PBS perfused tissue was snap frozen in liquid nitrogen, followed by storage at -80°C until tissue lysis was performed.

2.3.2 Tissue sectioning

PFA fixed tissue specimens were frozen in Tissue-Tek O.C.T sectioning compound (Sakura) and cut to the desired thickness using a Leica CM1850 cryostat (Leica) followed by mounting onto frosted glass slides (Dako). Sections were then dried overnight in the dark, followed by immunohistochemical labelling.

2.4 Cell culture

2.4.1 Preparation of coverslips and cell culture trays

Glass coverslips were etched in nitric acid (70% v/v) overnight, followed by 5 milliQ® washes. Coverslips were then dried at 60°C overnight and autoclaved. Utilising a laminar flow hood,

FIGURE 2.1. YFP transgene genotyping using gel electrophoresis. YFP (300bp) and TCRD (200bp) PCR products were separated on an agarose gel containing a UV excitable DNA label, followed by image capture under UV light. The presence of the YFP transgene was shown by a positive band at the corresponding PCR product size for YFP, plus the presence of the TCRD housekeeping PCR product.

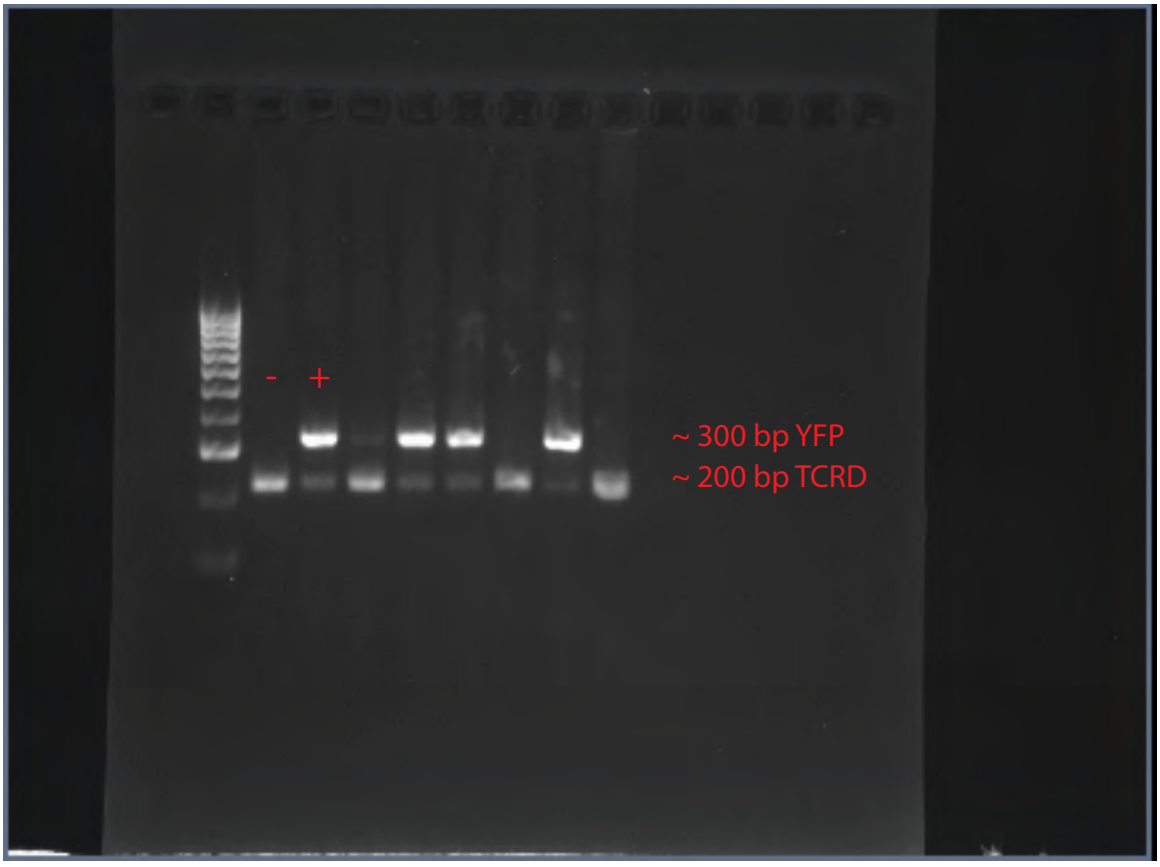
-
+
~ 300 bp YFP
~ 200 bp TCRD

coverslips were then placed singularly into either 6- or 24-well micro plates (Iwaki), followed by ultraviolet sterilisation for 30 mins. Live cell imaging 3 well micro culture vessels were placed on coverslips in 6 well micro plates (refer to Chapter 5). Coverslips were then coated with 1mg/ml poly-L-lysine (Poly-L) (Sigma) in 0.1M PBS (pH 7.4) for a minimum of 4 hours prior to addition of cells. Coverslips were then rinsed (1x) in sterile PBS followed by the addition of initial plating media: Neurobasal™ media supplemented with 2% B27, 10% foetal calf serum, (all from Invitrogen), 0.5mM L-glutamine, 25μM glutamate and 1% penicillin/streptomycin antibiotics (all from Gibco BRL, Thermo Scientific). Micro plates were then incubated at 37°C in 5% CO_2 until the addition of cells.

2.4.2 Cortical neuron cultures

Primary cortical cultures were prepared from embryonic day 15.5 (E15.5) YFP or C57Bl/6 embryos. In brief, cortices were removed from the skull, followed by the careful removal of attached meninges. Cortical tissue was then mechanically disassociated with forceps, collected into sterile HBSS containing 0.0125% trypsin and incubated at 37°C for 5 mins. The HBSS and trypsin was carefully removed, followed by trypsin inactivation and cellular disassociation by triturating with initial plating media. Cell viability and counts were determined utilising trypan blue vital dye exclusion (Sigma). Cells were then plated to the desired density into pre-prepared micro plates and returned to the incubator.

2.4.3 Maintenance of cortical neuronal cultures

24 hours after plating, initial plating media was removed and replaced with Neurobasal™ media supplemented with 2% B27, 0.5mM L-glutamine and 1% penicillin/streptomycin antibiotics. This promoted the selective growth of neurites (Brewer, 1995). Half of the media was replaced every three to four days with fresh media. Cells were maintained at 37°C and 5% CO_2 for up to 10 days *in vitro* (DIV). Following experiments cultures were either fixed in 4% PFA for immunocytochemical analysis, or treated with lysis buffer for protein quantification.

2.4.4 Live cell imaging

Live cell imaging was completed utilising fluorescence, differential interference contrast (DIC) and phase-contrast microscopy on a Nikon Eclipse Ti inverted microscope (Nikon) within an enclosed incubator maintained at 37°C and 5% CO_2. For live cell imaging experiments, cell cultures were grown and maintained in indicator free Neurobasal™ media. Selected cover slips were transferred to the microscope and appropriate areas for imaging were selected, as discussed

in relevant chapters. Live cell images were captured using a Zyla CMDS camera (Andor), and controlled by NIS elements (Nikon). Images were subsequently analysed using FIJI software (NIH).

2.5 Immunohistochemistry and immunocytochemistry

Animal tissue and cultures that had been previously fixed were incubated in primary antibody combinations in diluent (0.3% or 1% Triton-x-100 in 0.01M PBS) for the durations indicated hereafter at 4°C (see table 2.4 for antibody information). Following primary antibody incubation, specimens were washed in 0.01M PBS three times for ten minutes. Specimens were then incubated in secondary antibodies in PBS for 90 minutes at 4°C. Generally DAPI (1:10000 dilution, 5mg/ml stock) was added for the final ten minutes, followed by washing with PBS and mounting with mounting media (Permaflur, DAKO; or ProLong® Gold, Life Technologies).

2.6 Protein quantitation

2.6.1 Tissue and cell lysis

Tissue from animal's transcardially perfused with PBS, or cortical cell cultures were prepared in application specific tissue lysis buffer. Generally, RIPA buffer (50mM Tris-HCL, 150mM NaCl, 1% NP-40, 1% Sodium deoxycholate, 0.1%SDS) with EDTA free protease inhibitor tablets (Roche) was used for the majority of experiments, unless stated otherwise. In brief, tissue or cells were rinsed 1-2 times with ice cold sterile PBS, followed by the addition of RIPA lysis buffer. Tissue was briefly homogenised utilising a T10 basic Ultra-Turrax homogeniser (IKA). Cell cultures were incubated in RIPA buffer for 10 mins at 4°C, followed by cell scrapping. Both tissue and cells lysates were subsequently centrifuged at 15,800 RCF for 10 mins, followed by snap freezing in liquid nitrogen and storage at -80°C.

2.6.2 SDS-PAGE and Western blot

Protein concentration was determined by utilising a micro-plate DC-protein assay kit (BioRad). Protein lysates were separated using an SDS-PAGE mini gel tank system, generally on precast 4-12%, 1.5mm gradient gels, using power and duration settings specified in the manufacturers instructions (Thermo Scientific). Separated proteins were transferred to PVDF membrane, normally for 60 mins at 20 volts, followed by blocking in 5% skim milk powder in TBS-T for 60 mins. Some experiments utilised overnight transfer for high molecular weight proteins, using an XCell Surelock™ system at 8 volts for 12 hours at 4°C, followed by blocking (Thermo Scientific). Membranes were then incubated in relevant primary antibodies overnight at 4°C,

Primary Antibodies

Species	Antibody	Company	IHC/ICC dilution (1:x)	WB Dilution (1:x)
Conjugated stain	aBT AlexaFluor 594	Molecular probes	200	N/A
Mouse monoclonal	Acetylated-tubulin	Sigma Aldrich	N/A	5000
Mouse polyclonal	Alpha-tubulin	Abcam	N/A	5000
Goat polyclonal	Choline Acetyltransferase	Millipore	N/A	200
Rabbit polyclonal	Dystrophin	Abcam	100	500
Rat monoclonal	EB3	Abcam	N/A	500
Rabbit polyclonal	GAPDH	Millipore	N/A	5000
Mouse monoclonal	GFAP	Abcam	1000	N/A
Rat monoclonal	GFP	Nacalai tesque	3000	N/A
Rabbit polyclonal	Iba1	Wako	1000	N/A
Rabbit polyclonal	LRP-4	Millipore	100	200
Mouse monoclonal	MAP2	Millipore	1000	N/A
Mouse monoclonal	Nestin	BD Transduction	500	N/A
Rabbit polyclonal	Nestin	Covance	N/A	200
Rabbit monoclonal	NFM	Millipore	1000	1000
Mouse monoclonal	Rapsyn	Sigma Aldrich	200	N/A
Rabbit monoclonal	Rapsyn	Abcam	N/A	200
Mouse monoclonal	SMI-312	Covance	1000	N/A
Mouse monoclonal	SMI32	Covance	1000	N/A
Mouse monoclonal	STOP/MAP6	Millipore	N/A	500
Rabbit polyclonal	Synaptophysin	Abcam	500	N/A
Rabbit polyclonal	Tau	Dako	2000	N/A

Secondary Antibodies

Species	Conjugate	Company	IHC/ICC dilution (1:x)	WB Dilution (1:x)
Anti-Mouse	AlexaFluor 488	Molecular Probes	750	N/A
Anti-Mouse	AlexaFluor 568	Molecular Probes	750	N/A
Anti-Rat	AlexaFluor 488	Molecular Probes	750	N/A
Anti Rabbit	AlexaFluor 488	Molecular Probes	750	N/A
Anti Rabbit	AlexaFluor 568	Molecular Probes	750	N/A
Anti Rabbit	AlexaFluor 647	Molecular Probes	750	N/A
Anti-Goat	HRP	Dako	N/A	5000
Anti-Rat	HRP	Invitrogen	N/A	2000
Anti-Mouse	HRP	Dako	N/A	5000
Anti-Rabbit	HRP	Dako	N/A	5000

Table 2.4

followed by 4, 5 min washed with chilled TBS-T. Secondary HRP conjugated antibodies (DAKO anti mouse and rabbit, 1:5000; Invitrogen anti rat, 1:2000) were incubated for 1.5 hours, followed by rinsing with TBS-T. Membranes were then probed by incubating with Immobilon chemiluminescence HRP substrate (Millipore) for 5 mins, followed by detection with Chemi-Smart 5000 image station (Vilber Lourmat). Band quantitation was completed using ImageJ, and is represented as the area of pixels per band (pix^2). This was then followed by analysis in Graphpad Prism.

Chapter 3

3 Pathology of the distal neuromuscular circuitry is an early, presymptomatic event in the disease course of the SOD1^{G93A} mouse model of ALS

3.1 Introduction

There is increasing evidence that the a-MN distal axon and synapse is an early target for pathology in ALS patients (Raff et al., 2002; Wishart et al., 2006). As described previously in Chapter 1 of this thesis, similar degenerative changes have been widely reported in the SOD1^{G93A} transgenic mouse model of ALS (Gurney et al., 1994; Fischer et al., 2004). High-copy number SOD1^{G93A} mice are reported to develop progressive muscle weakness and hindlimb paralysis at 110 days of age, compared to an onset in forelimbs at 136 days, despite similar a-MN loss and pathology in corresponding spinal regions (Karlsson et al., 2004; Dodge et al., 2008; Schafer and Hermans, 2011). These symptoms progress to a strain-dependent end-point, typically reached at 157 days in mice on a C57Bl/6 background (Wooley et al., 2005). Symptom onset in the SOD1^{G93A} mouse is largely attributed to dysfunction and degeneration of the a-MN distal axons, however some evidence suggests that NMJ abnormalities may precede both distal axon degeneration and loss of the a-MN soma in transgenic mouse models (Gurney et al., 1994; Fischer et al., 2004; Carrasco et al., 2016). Although, degeneration of the distal components appears to be a key process in ALS, the sequence of pathological changes is not fully known. Investigations into the evolution of this pathology may shed light on possible targets for therapeutic intervention; a much needed advancement in ALS research.

Axonal pathology is a complex and evolving degenerative process in ALS, and has been reported to occur in a fibre-type specific manner (Frey et al., 2000; Banks et al., 2003). Fast-firing phasic a-MNs are preferentially vulnerable in both SOD1^{G93A} models and human disease (Frey et al., 2000; Atkin et al., 2005; Pun et al., 2006), conversely, small-calibre type I axons persist later in disease (Kawamura et al., 1981; Bruijn et al., 1997). It has been identified that axon degeneration in the distal neuromuscular circuitry occurs early in the disease time course of both human cases and animal models (Frey et al., 2000; Fischer et al., 2004). This degeneration includes intra-axonal accumulations of protein aggregates, cytoskeletal breakdown and eventual fragmentation of the axonal membrane via Wallerian-like mechanisms (Frey et al., 2000; Vickers et al., 2009; Wang et al., 2012). However presymptomatic observations of axonal degeneration are yet to be fully comprehended. Symptom onset in the SOD1^{G93A} mouse model occurs firstly in the

hindlimbs, with forelimb function remaining spared until the later stages of the disease (Schafer and Hermans, 2011). However, it is currently unknown whether this preserved function is due to decreased axonal and NMJ degeneration in the forelimb, in comparison to hindlimb muscles. Identification and comparisons of pathology between forelimb and hindlimb neuromuscular circuitry will increase our understanding of anatomical vulnerability in these mice.

It is widely accepted that some axonal responses to ALS disease mechanisms identified in the $SOD1^{G93A}$ mouse may be beneficial. For example, and as discussed in Chapter 1, the surviving distal neuromuscular circuitry shows a remarkable ability to reinnervate recently denervated muscle, with collateral branches forming from axons in close proximity to AChR patterned muscle that lack the pre-synaptic apparatus (Hegedus et al., 2008; Moloney et al., 2014). This phenomenon is hypothesised to occur relatively early in the pathogenesis of ALS, prior to the onset of motor symptoms. Ultimately the decrease in a-MN survival and increase in pathology overwhelms any regenerative capacity, resulting in loss of the neuromotor unit and symptoms (Williams et al., 2009; Taetzsch et al., 2017). Identification of collateral capacity early and late in the disease is incomplete, and offers an interesting and necessary avenue of research to focus on. Furthermore, although having been investigated in other ALS mouse models, distal axonal and NMJ alterations in the high copy number $SOD1^{G93A}$ mice are yet to be fully characterised using YFP as the primary label of the distal axon and pre-synaptic compartment (Feng et al., 2000b; Wong et al., 2009).

The NMJ has also been implicated in the disease process, with 'dying back' degeneration of the synapse and distal axon also occurring early in the disease time course (Frey et al., 2000; Fischer et al., 2004). Recently it has also been identified that NMJs in $SOD1^{G93A}$ mice have impaired presymptomatic neuromuscular transmission (Rocha et al., 2013). Similarly, $SOD1^{G93A}$ dependant alterations to skeletal muscle gene expression occur presymptomatically (de Oliveira et al., 2014). Terminal schwann cells, which are specialised schwann cells that facilitate neurotransmission at the NMJ are also abnormally affected presymptomatically in SOD1 mouse models of ALS (Carrasco et al., 2016). However, identification of early NMJ morphological alterations and the implications of specific protein changes are still poorly understood in the $SOD1^{G93A}$ mouse model of ALS.

Appropriate expression and localisation of post-synaptic architectural proteins in the NMJ are necessary for NMJ maturation, function and maintenance. Indeed, a loss or mutation of such proteins has been shown to lead to a number neuromotor disorders due to either aberrant NMJ development, or denervation in childhood or early adulthood (Frail et al., 1989; Ohno et al., 2002; Li et al., 2010; Pilgram et al., 2010; Pevzner et al., 2012; Ohkawara et al., 2014). Remarkably, there is limited research investigating NMJ post-synaptic architectural proteins in ALS (Perez-Garcia and Burden, 2012). This is significant, as the NMJ is a neuroanatomical site where in both patients and animal models show the greatest amount of degeneration and neurocircuitry loss; a direct correlation to motor/clinical phenotype (see review (Moloney et al., 2014)). Interestingly, myocytes in the SOD1^{G93A} mouse model show alterations in gene expression, endoplasmic reticulum stress and dysfunctional protein folding, suggesting the myocyte proteome (and thus post-synaptic proteins) may be vulnerable in ALS (de Oliveira et al., 2014; Chen et al., 2015). However, limited evidence exists surrounding age dependant alterations in NMJ protein localisation and alterations in protein expression in the SOD1^{G93A} mouse model.

The current investigations utilised the SOD1^{G93A} mouse model of ALS. It also utilised the novel SOD1^{G93A} x *Thy1*YFP (SOD1^{G93A}xYFP henceforth) mice to facilitate morphological analysis of distal axons and NMJs. The *Thy1*YFP mouse demonstrates yellow fluorescent protein (YFP) expression in spinal a-MNs (Feng et al., 2000b). The aim of this investigation was to characterise axonal and pre and post-synaptic NMJ degeneration, utilising YFP as a morphological visualisation aid. Investigations into specific alterations to the hindlimb (gastrocnemius) and forelimb (extensor muscles) YFP expressing distal axons and NMJs in the SOD1^{G93A}xYFP mouse were completed. Identification of axonopathy and the extent of collateral branching at presymptomatic and symptomatic time points were also undertaken. This was followed by assessment of gross NMJ degeneration and morphological alterations at similar time points. Post-synaptic architectural markers of the NMJ were also probed over the disease time course as well as protein levels at end stage of disease.

3.2 Methods

3.2.1 Animals

Male transgenic SOD1^{G93A} mice and the double transgenic SOD1^{G93A}xYFP cross mice (see Chapter 2) were used for histological analysis. SOD1^{G93A} and SOD1^{G93A}xYFP mice were assessed daily for overt clinical symptoms and weighed weekly from 58-140 days of age to

evaluate disease progression. The mice used for these studies were humanely killed before reaching an ethical end-point, which is generally 157 days of age in this $SOD1^{G93A}$ model (Wooley et al., 2005). Motor testing demonstrated that there was no difference in Rotarod performance or weight between YFP transgenic mice and wild-type littermates (Figure 3.1). Age matched control mice (non $hSOD1^{G93A}$ expressing C57BL/6 and YFP mice) were used for all immunohistochemical and imaging analysis.

3.2.2 Immunohistochemistry and quantitation

Mice were terminally anaesthetised and transcardially perfused with 4% PFA (28, 56, 84, 112 and 140 days of age for $SOD1^{G93A}$; 56 and 140 days of age for $SOD1^{G93A}$xYFP). The hindlimb gastrocnemius and forelimb extensor muscles (extensor carpi radialis longus, extensor digitorum communis, extensor digitorum lateralis and extensor carpi ulnaris) were dissected and cryoprotected. $SOD1^{G93A}$ muscle was cryosectioned longitudinally at 40µm to improve antibody penetration, whereas $SOD1^{G93A}$xYFP muscle was cryosectioned at 80µm (Figure 3.2). All sections were stained for post-synaptic acetylcholine receptors (AChRs) using AlexaFluor conjugated 594nm α-bungarotoxin (α-BTx, 1:200, Molecular Probes/Invitrogen) for 30 minutes. Sections for immunohistochemical analysis were washed once in ice-cold methanol (Sigma-Aldrich) for 30seconds and permeablised with 0.1% Triton-X-100 (Sigma-Aldrich) for 4 hours at room temperature. Pre-synaptic motor terminals were labelled using a cocktail of mouse-anti phosphorylated neurofilaments (SMI-312; 1:1000; Sternberger Monoclonals/Covance), dephosphorylated neurofilaments (SMI-32; 1:1000; Sternberger Monoclonals/Covance) and rabbit-anti synaptophysin (1:500, Millipore) (Mozaffar et al., 2009). Post-synaptic structural proteins were labelled using antibodies to dystrophin (1:100; rabbit polyclonal; Abcam/Sapphire Bioscience), nestin (1:500; BD Transduction), rapsyn (1:200; Sigma-Aldrich) and LRP-4 (1:100; intracellular domain, Millipore). Primary antibodies or isotype controls were incubated for 1 hour at room temperature followed by $4^{o}C$ overnight. Species-specific Alexa488 secondary antibodies (1:750; Molecular Probes) were incubated for 2 hours at room temperature. Sections were thoroughly washed and mounted with ProLong® Gold antifade mounting medium (Life Technologies) and fully dried prior to analysis.

3.2.3 Quantitation of colocalisation and distal axonopathy

$SOD1^{G93A}$xYFP en-face NMJs and terminal axons were imaged using a Zeiss scanning confocal microscope (Zeiss 510 laser scanning microscope). Z-stacks (40µm stack, 2µm interval, 512x512 pixels, voxel = $1.68mm^3$) were generated using Zen software (Zeiss) and axonal and NMJ

morphologies were analysed using Image J (NIH) (Valdez et al., 2010). Only en-face NMJs were included for morphological analysis. Analysis of immunohistochemical labels relative to α-BTx staining was performed using fluorescence microscopy (Leica DM-LB2). NMJs were considered occupied if there was evidence of complete or partial association between pre-synaptic markers and α-BTx (Cappello et al., 2012). Similarly, post-synaptic proteins were considered to be present if there was complete or partial colocalisation with α-BTx. NMJs from the gastrocnemius muscles were counted from three fields of view (200x), across two sections from each muscle, ensuring comparable regions of each muscle. All NMJs in the forelimb muscle were counted as part of the analysis. All counts were performed blinded to the genotype and age of the animal.

3.2.4 Western blot quantification of neuromuscular junction protein

End stage $SOD1^{G93A}$ and age matched control gastrocnemius muscle were homogenised in RIPA buffer (50mM Tris-HCL pH 7.4, 150mM NaCl, 1% NP-40, 1% sodium deoxycholate, 0.1% SDS), containing EDTA free protease inhibitor (Roche). The homogenate was centrifuged at 15,800 RCF at 4°C for 10 minutes, after which supernatant was collected and analysed by SDS-PAGE and Western blot (20ug of protein). Detection of postsynaptic NMJ proteins was performed using antibodies for dystrophin (1:500) and LRP4 (1:200) as mentioned previously, as well as nestin (1:200; Covance) and rapsyn (1:200; Abcam). GAPDDH (1:5000; Millipore) immunoblots were prepared from cut blots for LRP-4, Nestin and Dystrophin. Rapsyn blots were subsequently stripped and re-probed for GAPDH. Antibody binding was detected utilising anti-rabbit and anti-mouse HRP-conjugated secondary antibodies (1:5000; Dako) and Immobilon chemiluminescent substrate (Millipore). Densitometry analysis was performed using Image J.

3.2.5 Statistical analysis

The proportion of NMJs with colocalisation of α-BTx and immunohistochemical markers was statistically analysed using GraphPad Prism (Version 5.00) using two-way analysis of variance (ANOVA) with Tukey's post-hoc correction for multiple comparisons. $p < 0.05$ was considered significant. Data is expressed ± standard error of the mean (SEM). Unless otherwise stated, a minimum of four separate animals was used for each genotype and age ($n = 4$).

FIGURE 3.1. YFP transgene does not affect weight or motor behaviour measures. **(A)** YFP transgene does not affect weight gain. **(B)** YFP transgene does not affect Rotarod performance when measured by latency to fall (seconds) and corrected for mouse weight (grams), (seconds per gram, sec/g). Wild-type (black) and YFP expressing mice (grey) were tested from 63 to 140 days of age.

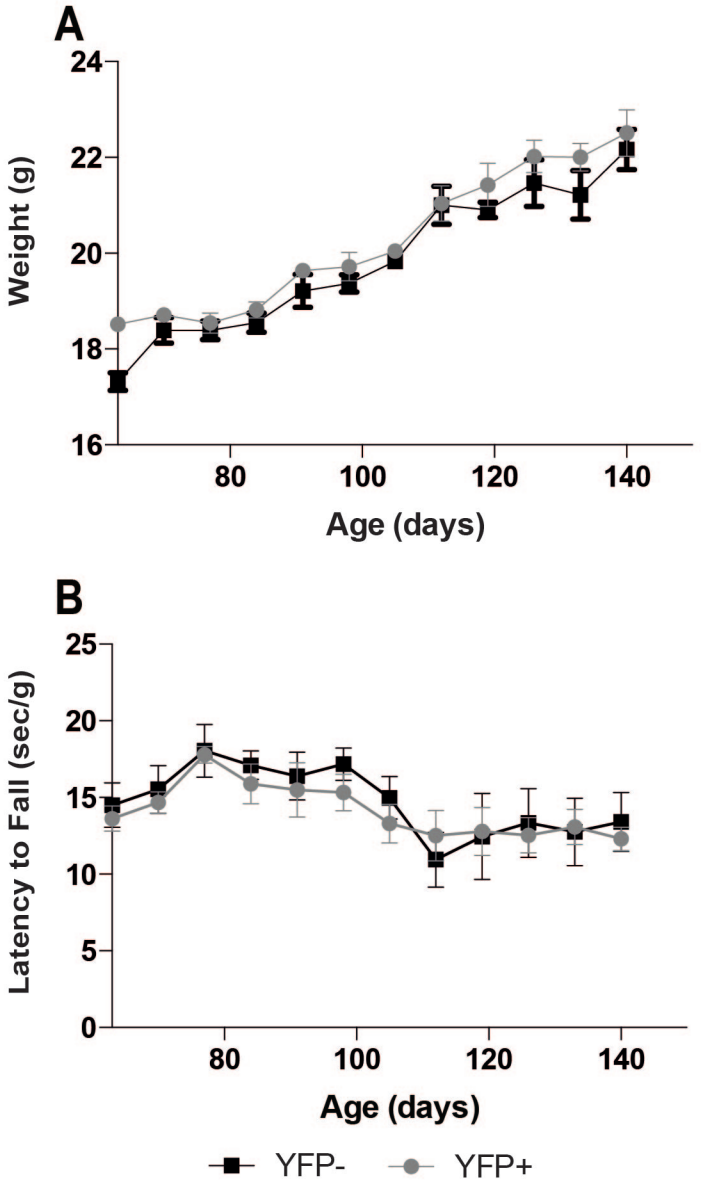
A
24
22
20
18
16
Weight (g)
80
100
120
140
Age (days)
B
25
20
15
10
5
0
Latency to Fall (sec/g)
80
100
120
140
Age (days)
YFP-
YFP+

FIGURE 3.2. The name and anatomical position for the muscles used in this study (grey). Muscles of the **(A)** hindlimb and **(B)** forelimb are shown in lateral view. Not to scale.

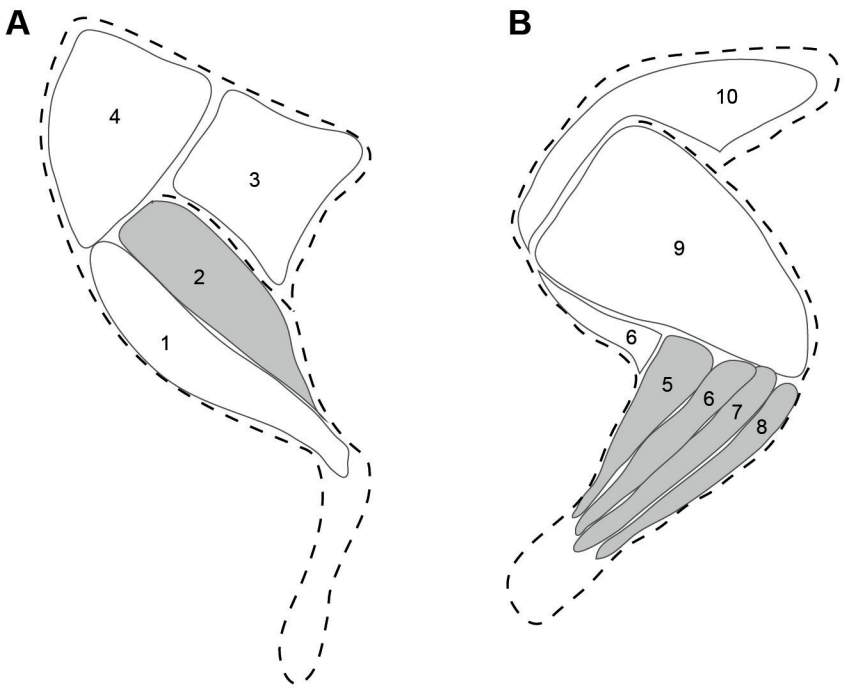

1 Extensor digitorum longus and tibialis cranialis
2 Gastrocnemius
3 Vastus lateralis, biceps feboris, adductor, semimebranosus, semitendinosus
4 Rectus femoris

5 Extensor carpi radialis longus
6 Extensor digitorum communis
7 Extensor digitorum lateralis
8 Extensor carpi ulnaris
9 Triceps brachii
10 Biceps brachii

3.3 Results

3.3.1 SOD1^{G93A} mice exhibit hindlimb distal axonopathy and increased axonal branching prior to symptom onset

To characterise changes to distal axon morphology in the hindlimb, SOD1^{G93A}xYFP transgenic gastrocnemius muscle sections were examined at 56 days (presymptomatic) and 140 days (late disease). Examination of distal axons terminating at the NMJ in YFP control mice demonstrated that the majority of axons exhibited intact morphology, with uninterrupted YFP expression along the axon length (Figure 3.3 A). However, in SOD1^{G93A}xYFP mice it was evident that a small subset of axons demonstrated evidence of abnormal and pathological morphology, including beading and fragmentation. Beaded axons had segments that were thin and were separated by large concentrated membranous beads of YFP (Figure 3.3.B). Fragmented axons however, showed interrupted YFP expression, with large zones of axonal membrane loss (Figure 3.3 C). For the purpose of this study, both beaded and fragmented axons were pooled as a degenerative pathological phenotype. Quantitation revealed a significant ($p < 0.05$) decrease in the proportion of intact distal axons at 56 days of age in SOD1^{G93A}xYFP mice compared with YFP controls (Figure 3.3 G) (SOD1^{G93A}xYFP: 81.2% ± 4.62%; YFP: 97.5% ± 2.1%, $n = 6$). There was a further significant ($p < 0.05$) decrease in the proportion of intact axons at 140 days of age in SOD1^{G93A}xYFP mice, with over half of the axons showing degenerative morphologies, compared to YFP controls, where nearly 100% remained intact (Figure 3.3 G) (SOD1^{G93A}xYFP: 49.77% ± 6.66%; YFP: 98.06% ± 1.70%, $n = 6$).

Following the establishment of presymptomatic axonal degeneration, collateral branch analysis of SOD1^{G93A}xYFP distal axons was undertaken (Figure 3.3.D). Intact primary axons with at least one fully colocalised NMJ structure projecting from nerve bundles were selected, and collateral branch numbers were determined. The majority of YFP control mice presented with limited axonal collaterals (Figure 3.3 E). However, at presymptomatic day 56, SOD1^{G93A}xYFP mice displayed a significant ($p < 0.05$) increase in the number of collateral branches compared to YFP controls (SOD1^{G93A}xYFP: 1.409 ± 0.025; YFP: 1.248 ± 0.044, $n = 5$) (Figure 3.3 H). This was visualised as generally 1-2 primary axonal segment terminating at a NMJ (Fig. 1F). At 140 days the number of collateral branches increased further, with axonal segments in SOD1^{G93A}xYFP mice having significantly ($p < 0.0001$) more branch points (SOD1^{G93A}xYFP: 2.023 ± 0.055;

FIGURE 3.3. Confocal images from SOD1^{G93A}xYFP mice displaying distal axonopathy and an increase in axon collateral branches over the disease time course. (A) Control mice had mostly intact axons. (B) Degenerating axons were increased in 56 day old SOD1^{G93A}xYFP mice, mostly presenting a beaded morphology, (C) or a fragmented morphology. (D) Schematic of axonal branch quantification, as shown by branch order of distal axons. (E) Wild-type YFP axons had fewer branches. (F) SOD1^{G93A}xYFP mice had a significant increase in axonal branches. (G) Statistical analysis showed that intact axons were significantly ($p < 0.05$) decreased at 56 days, and decreased further by 140 days in SOD1^{G93A}xYFP mice. (H) Axonal branches were significantly ($p < 0.0001$) increased at 56 days in SOD1^{G93A}xYFP mice, and increased further at 140 days (mean ± SEM, $n = 6$). Scale = 15μm.

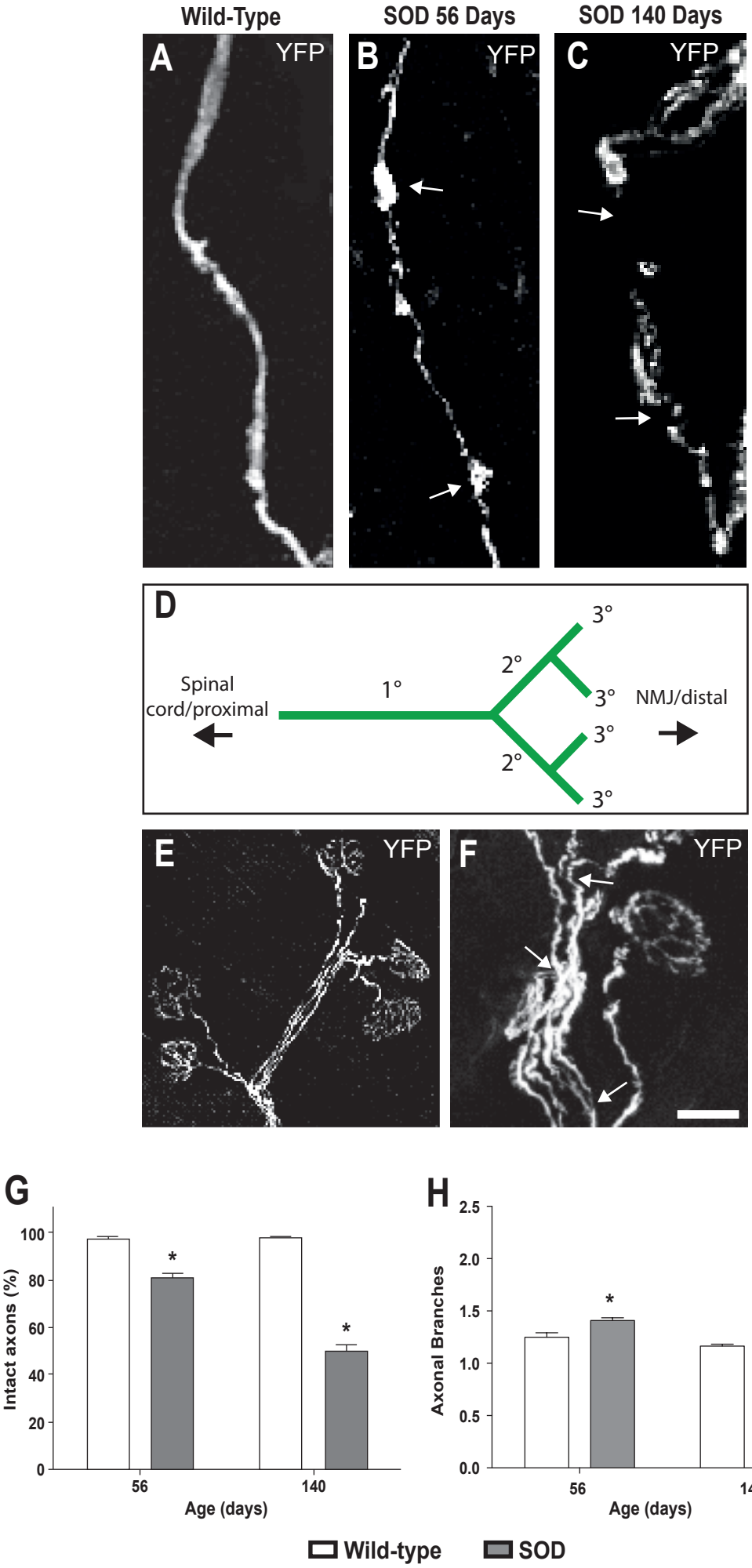
Wild-Type
SOD 56 Days
SOD 140 Days
A
YFP
B
YFP
C
YFP
D
3°
2°
Spinal
cord/proximal
1°
3°
NMJ/distal
3°
2°
3°
E
YFP
F
YFP
G
Intact axons (%)
100
80
60
40
20
0
*
*
56
140
Age (days)
H
Axonal Branches
2.5
2.0
1.5
1.0
0.5
0.0
*
****
56
140
Age (days)
Wild-type
SOD

YFP: 1.164 ± 0.0188, n = 5), as well as an increase in the typical degenerative axonal morphology reported previously (Figure 3.3 H).

3.3.2 Hindlimb distal axonopathy is accompanied by increased NMJ morphological alterations

This chapter sought to investigate whether the expression of $SOD1^{G93A}$ altered NMJ morphology in the gastrocnemius muscle of $SOD1^{G93A}$xYFP mice. Firstly, $SOD1^{G93A}$xYFP gastrocnemius tissue sections were stained with α-BTx, followed by the generation of confocal images of the pre- and post-synapse. Three morphologically distinct categories of NMJs were revealed. Firstly, intact and complex junctions were present, identifiable by the typical 'pretzel' morphology of the post-synaptic apparatus (Figure 3.4 A), and were noted to be present in presymptomatic $SOD1^{G93A}$xYFP mice. However, abnormal NMJ morphologies were also identified, presenting as either less complex or degenerative. These NMJs were identified as NMJs with only one or two synaptic branches instead of the normal 'pretzel' morphology (Figure 3.4 B). Statistical analysis identified that there were significantly ($p < 0.001$) fewer complex NMJs at 56 days of age in $SOD1^{G93A}$xYFP mice, compared to YFP controls ($SOD1^{G93A}$xYFP: 76.45% ± 4.13%; YFP: 92.38% ± 4.30%) (Figure 3.4 D). At the later disease stage NMJs showed highly degenerative morphology, such as blebbing and fragmentation of the membrane folds and sparse post-synaptic labelling (Figure 3.4 C). Further analysis found that at 140 days of age there was a significant ($p < 0.0001$) 32.17% additional decrease in intact NMJs in $SOD1^{G93A}$xYFP mice ($SOD1^{G93A}$xYFP: 44.29% ± 8.39%) (Figure 3.4 D). These two abnormal NMJ morphological subtypes were also pooled during analysis as a 'degenerative morphology'.

3.3.3 $SOD1^{G93A}$ mice have reduced hindlimb NMJ innervation throughout disease course

Evaluation of the colocalisation between pre- and post-synaptic labels in the gastrocnemius muscle of $SOD1^{G93A}$xYFP hindlimb was also completed at presymptomatic and late stage disease, as well as immunohistochemical methods at 28, 56, 84, 112, and 140 days in non-crossed $SOD1^{G93A}$ mice. Innervation was defined as NMJs demonstrating either complete or partial colocalisation of pre-synaptic elements with α-BTx; degeneration was defined as total loss of colocalisation, resulting in only post-synaptic density labelling. At 56 days of age there was no significant ($p > 0.05$) difference in the proportion of NMJs with full colocalisation of YFP positive terminals and α-BTx staining in $SOD1^{G93A}$xYFP mice compared with YFP controls (Figure 3.5 A). However, by 140 days of age, there was a significant ($p < 0.0001$) decrease in the proportion of NMJs with colocalisation between YFP and α-BTx staining in $SOD1^{G93A}$xYFP

FIGURE 3.4. NMJ analysis highlighted the presence of morphological abnormalities at pre-symptomatic and late disease stages. (A) Wild-type YFP control mice exhibited NMJs with the typical complex 'pretzel' morphology. (B) SOD1^{G93A}xYFP mice demonstrated NMJ morphological abnormalities, with many having less complex synaptic structures at 56 days, (C) as well as the increasing proportion of NMJs with fragmented and beaded presynaptic membrane folds (arrow). (D) Intact NMJ morphology was significantly ($p < 0.05$) decreased by 56 days of age in SOD1^{G93A}xYFP mice, decreasing further by 140 days (mean ± SEM, $n = 6$). NMJs counted from three fields of view (200x), across two sections from each muscle. Scale = 15μm.

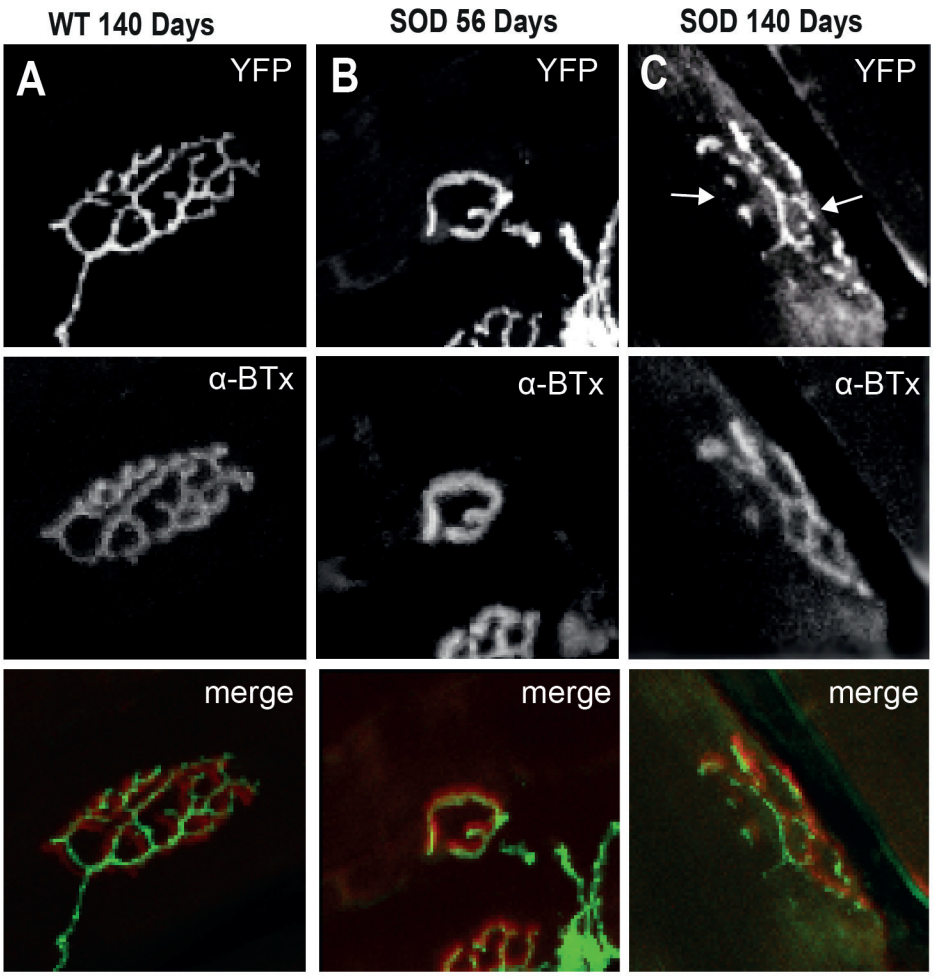
WT 140 Days
SOD 56 Days
SOD 140 Days
A
YFP
B
YFP
C
YFP
α-BTx
α-BTx
α-BTx
merge
merge
merge

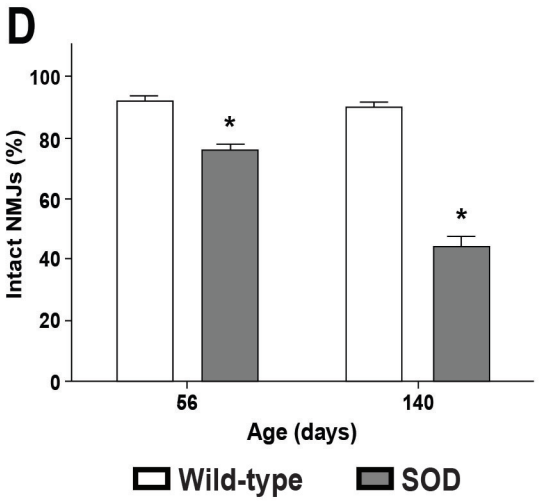
D
Intact NMJs (%)
100
80
60
40
20
0
*
*
56
140
Age (days)
Wild-type
SOD

FIGURE 3.5. The proportion of NMJs demonstrating colocalisation between pre- and post-synaptic components was reduced in older $SOD1^{G93A}$ mice. (A) NMJs imaged by confocal microscopy were either fully colocalised between YFP (green) and α-BTx (red), (B) or demonstrated non-colocalisation between YFP and α-BTx, due to presynaptic loss of YFP, leaving a denervated endplate. (C) Immunohistochemical presynaptic markers imaged by fluorescence microscopy were either fully colocalised with α-BTx, (D) or the presynapse was lost, with only the α-BTx endplate visible. (E) $SOD1^{G93A}$xYFP mice showed no decrease in the proportion of NMJs with colocalised YFP and α-BTx at 56 days of age ($p > 0.05$), however at 140 days there was a significant decrease ($p < 0.05$) in the proportion of NMJs colocalised with YFP and α-BTx in the gastrocnemius, compared to YFP controls ($n = 6$). (F) Immunohistochemical analysis demonstrated a significantly ($p < 0.05$) reduced proportion of NMJs with pre-synaptic terminals colocalised with α-BTx at 84, 112 and 140 days of age compared with controls (mean ± SEM, $n = 4$). NMJs counted from three fields of view (200x), across two sections from each muscle. Scale = 15μm.

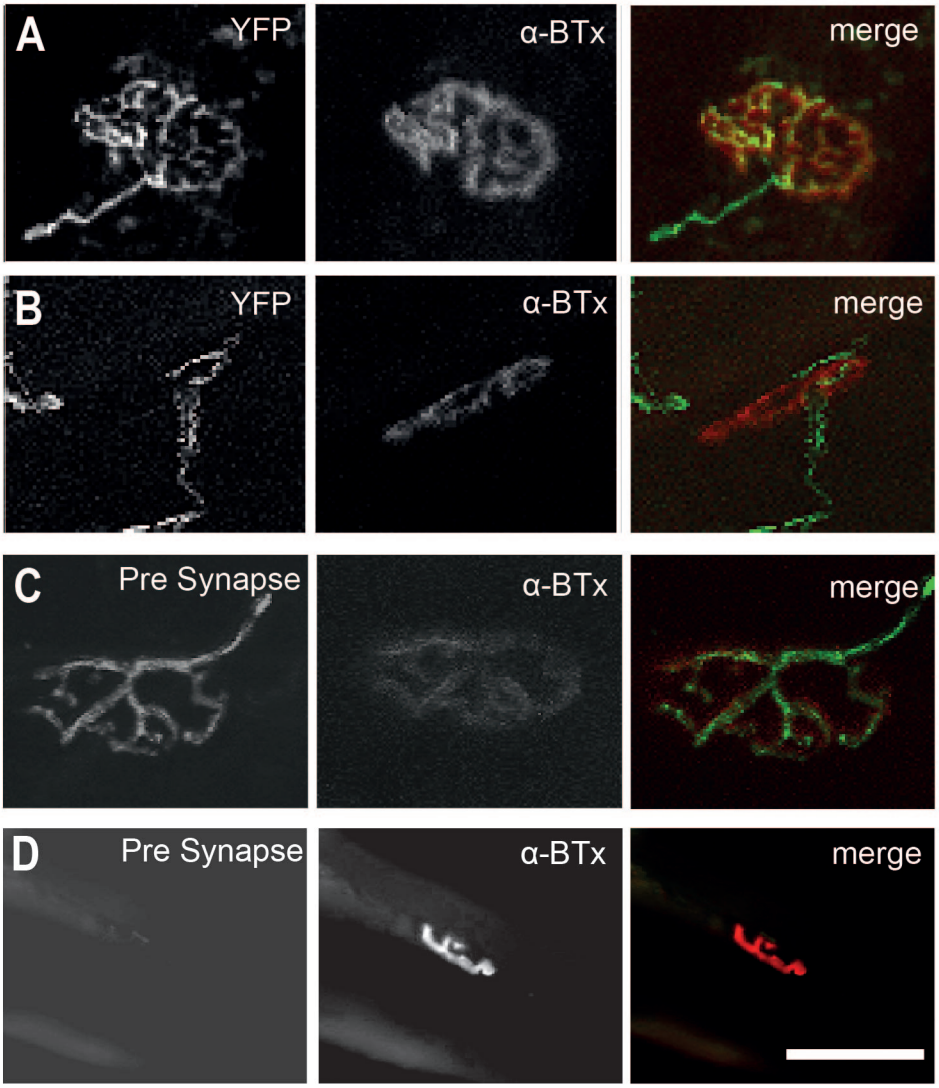
A
YFP
α-BTx
merge
B
YFP
α-BTx
merge
C
Pre Synapse
α-BTx
merge
D
Pre Synapse
α-BTx
merge

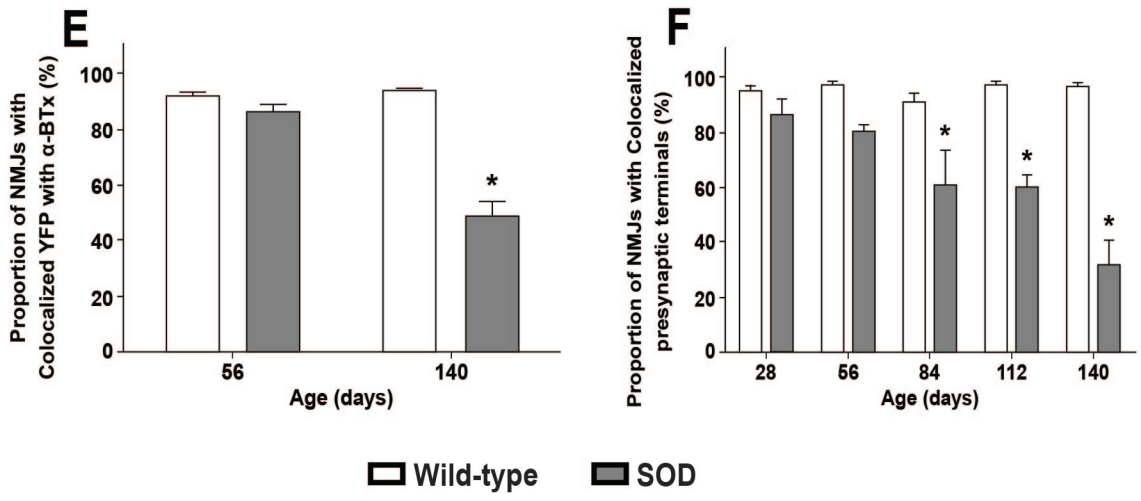
E
Proportion of NMJs with Colocalized YFP with α-BTx (%)
100
80
60
40
20
0
56
140
Age (days)
*
F
Proportion of NMJs with Colocalized presynaptic terminals (%)
100
80
60
40
20
0
28
56
84
112
140
Age (days)
*
*
*
Wild-type
SOD

mice compared with YFP controls ($SOD1^{G93A}$xYFP: 51.60% ± 13.3%; YFP: 99.36% ± 0.82%) (Figure 3.5 B, E).

To investigate protein expression changes associated with the pre-synaptic changes in the hindlimb, non-YFP crossed $SOD1^{G93A}$ and wild-type control gastrocnemius muscle sections were immunolabelled with a cocktail of antibodies to neurofilaments and synaptophysin to visualise the pre-synaptic terminal (Figure 3.5 C). Denervated NMJs had no pre-synaptic labelling colocalised with α-BTx (Figure 3.5 D). There was no significant ($p > 0.05$) difference in the proportion of NMJs with pre-synaptic terminal colocalisation with α-BTx staining in wild-type and $SOD1^{G93A}$ at 28 days of age. In agreement with the $SOD1^{G93A}$xYFP data, there was no significant ($p > 0.05$) change in the proportion of NMJs with colocalised pre-synaptic immunolabelling and α-BTx staining at 56 days of age ($SOD1^{G93A}$: 83.1% ± 1.10%; wild-type: 97.3% ± 1.45%). However, at 84 and 112 days of age, there were significant ($p < 0.05$) 44% and 50% decreases in the proportion of NMJs with colocalised pre-synaptic immunolabelling and α-BTx staining (84 days, $SOD1^{G93A}$: 49.5% ± 5.26%; wild-type: 88.7% ± 2.74%. 112 days, $SOD1^{G93A}$: 58.0% ± 5.77%; wild-type: 96.5% ± 1.51%) (Figure 3.5 F). Corroborating results reported above in $SOD1^{G93A}$xYFP mice, at 140 days of age there was a significant ($p < 0.05$) decrease in NMJ marker colocalisation, compared to wild-type controls ($SOD1^{G93A}$: 23.4% ± 6.79%; wild-type: 96.4% ± 2.0%).

3.3.4 Hindlimb NMJ degeneration in $SOD1^{G93A}$ mice is accompanied by loss of post-synaptic structural proteins

To determine whether there is a sequential loss of specific post-synaptic proteins due to $SOD1^{G93A}$ expression, gastrocnemius muscle sections from the same mice were examined using immunohistochemical labelling. At 28 and 56 days of age there was no significant ($p > 0.05$) difference in the degree of colocalisation of either nestin, LRP-4, rapsyn or dystrophin with α-BTx in the gastrocnemius muscle of wild-type and $SOD1^{G93A}$ mice. At 84 days of age, there was a significant ($p < 0.05$) decrease in the proportion of NMJs showing colocalisation of nestin with α-BTx in $SOD1^{G93A}$ gastrocnemius muscles compared to controls ($SOD1^{G93A}$: 43.6% ± 4.24%; wild-type: 89.1% ± 3.56%) (Figure 3.6 A & B). Decreased numbers of NMJs with colocalisation of nestin with α-BTx was associated with a change in immunoreactivity to a more dispersed expression throughout the muscle fibre as previously reported following denervation (Vaittinen et al., 1999). Colocalisation of nestin immunoreactivity with α-BTx was further decreased at 112

FIGURE 3.6. NMJ post-synaptic structural proteins are progressively lost over the disease time course in SOD1^{G93A} mice, compared to age matched controls. (A) Nestin (green) immunoreactivity is present surrounding the healthy wild-type control NMJ stained with α-BTx (red) but was not colocalised with α-BTx in SOD1^{G93A} NMJs. (B) The proportion of NMJs with colocalised nestin and α-BTx was significantly ($p < 0.05$) reduced at 84, 112 and 140 days of age in SOD1^{G93A} mice compared with controls. (C) LRP-4 (green) immunoreactivity is present surrounding the healthy wild-type control NMJ stained with α-BTx (red), with LRP-4 colocalisation with α-BTx progressively decreasing in SOD1^{G93A} NMJs from 84 days of age. (D) The proportion of NMJs with colocalised LRP-4 and α-BTx was significantly ($p < 0.05$) reduced at 84, 112 and 140 days of age in SOD1^{G93A} mice compared with controls. (E) Dystrophin (green) immunoreactivity colocalised with α-BTx staining (red) and extends beyond the synapse in the wild-type NMJ, however dystrophin staining was absent from some SOD1^{G93A} NMJs. (F) The proportion of NMJs with colocalised dystrophin and α-BTx was significantly ($p < 0.05$) reduced at 112 and 140 days of age in SOD1^{G93A} mice compared with controls. (G) Rapsyn (green) immunoreactivity was localised to α-BTx staining (red) in the wild-type NMJ, however rapsyn staining was absent from SOD1^{G93A} NMJs. (H) The proportion of NMJs with colocalised rapsyn and α-BTx was significantly ($p < 0.05$) reduced at 140 days of age in SOD1^{G93A} mice compared with controls (mean ± SEM, $n = 4$). Scale = 15μm.

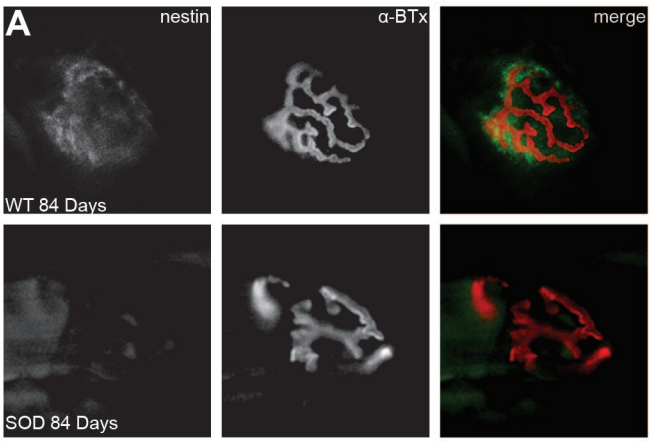
A
nestin
α-BTx
merge
WT 84 Days
SOD 84 Days

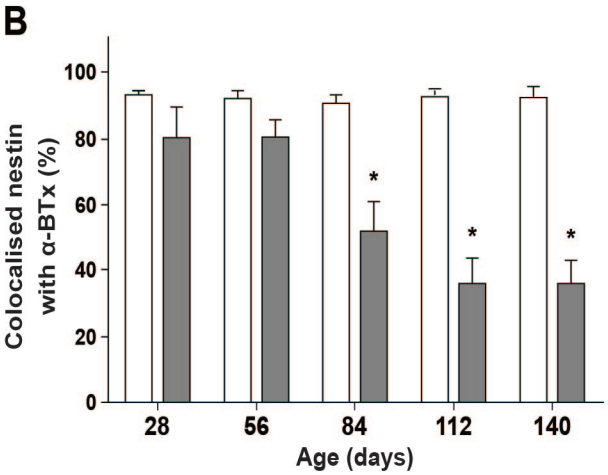
B
Colocalised nestin with α-BTx (%)
100
80
60
40
20
0
28
56
84
112
140
Age (days)
*
*
*

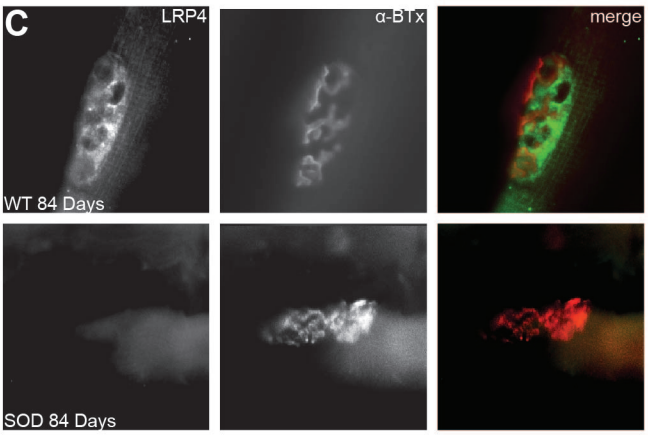
C
LRP4
α-BTx
merge
WT 84 Days
SOD 84 Days

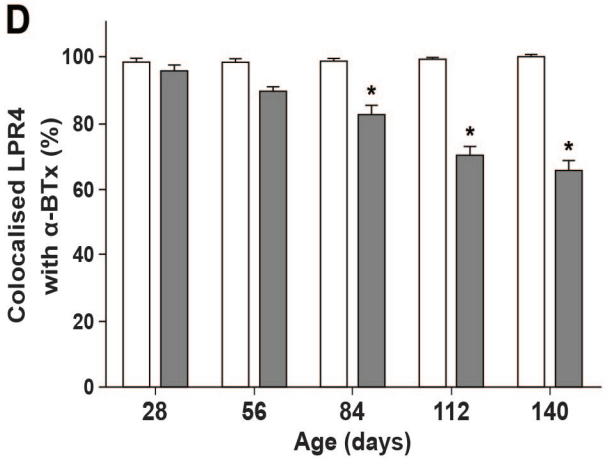
D
Colocalised LPR4 with α-BTx (%)
100
80
60
40
20
0
28
56
84
112
140
Age (days)
*
*
*

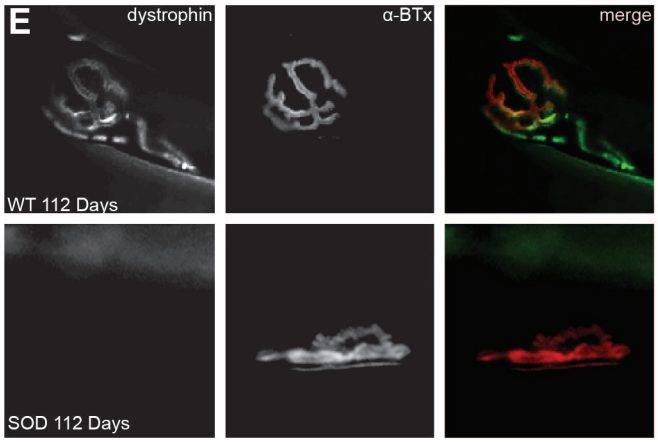
E
dystrophin
α-BTx
merge
WT 112 Days
SOD 112 Days

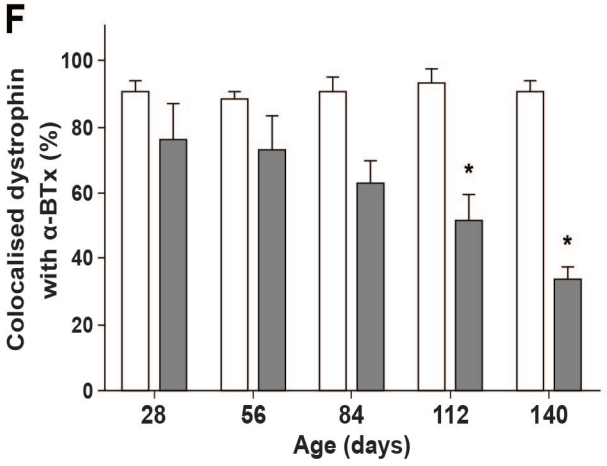
F
Colocalised dystrophin with α-BTx (%)
100
80
60
40
20
0
28
56
84
112
140
Age (days)
*
*

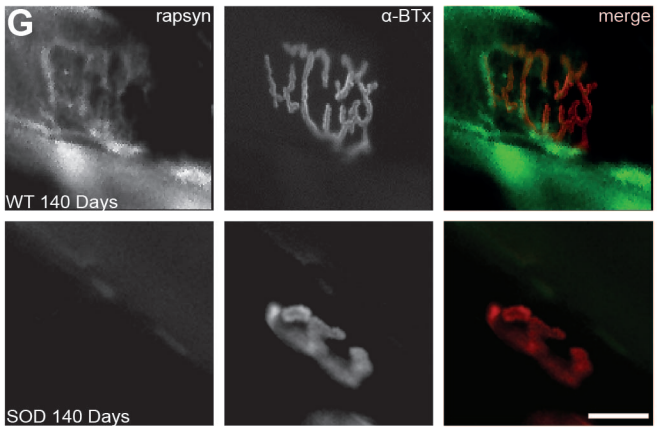
G
rapsyn
α-BTx
merge
WT 140 Days
SOD 140 Days

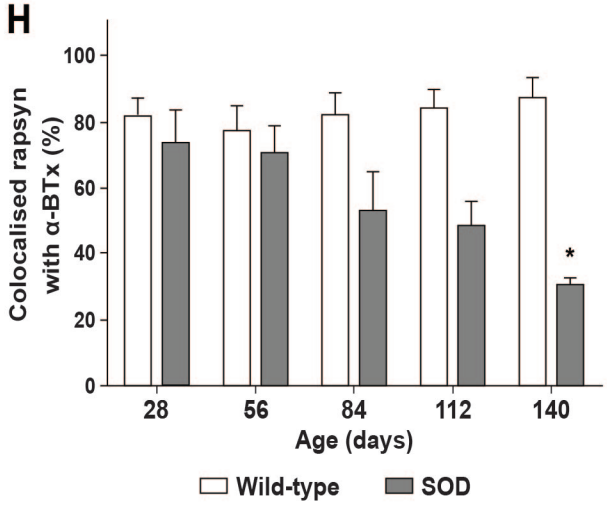
H
Colocalised rapsyn with α-BTx (%)
100
80
60
40
20
0
28
56
84
112
140
Age (days)
*
Wild-type
SOD

and 140 days of age, representing a final loss of 70% of α-BTx NMJs colocalised with nestin at 140 days of age. Similarly, LRP-4 colocalisation with α-BTx in the gastrocnemius muscles was significantly ($p < 0.01$) decreased in SOD1^{G93A} mice at 84 days of age (SOD1^{G93A}: 82.1± 2.90%; wild-type: 98.68% ± 0.71%) (Figure 3.6 C & D). This also decreased further at 112 and 140 days, with a final loss of 35% of α-BTx labelled NMJs colocalised with LRP-4. At 112 days of age, the proportion of NMJs with dystrophin colocalised with α-BTx in SOD1^{G93A} gastrocnemius was significantly ($p < 0.05$) decreased compared to wild-type tissue (SOD1^{G93A}: 44.09% ± 5.19%; wild-type: 90.58% ± 5.62%) (Figure 3.6 E & F). Colocalisation of dystrophin immunoreactivity with α-BTx was further decreased at 140 days of age. By 140 days of age, there was a significant ($p < 0.05$) reduction in the proportion of NMJs with colocalised rapsyn and α-BTx (SOD1^{G93A}: 30.75% ± 2.04%; wild-type: 87.33% ± 5.91%) (Figure 3.6 G & H).

3.3.5 Forelimb distal axonopathy, morphological alterations and synapse loss are evident at late stage disease, but are not accompanied by the loss of post-synaptic apparatus

Disease onset in the SOD1^{G93A} mouse characteristically begins in the hindlimbs, with the forelimb function remaining comparatively spared throughout disease progression (Schafer and Hermans, 2011). To determine whether this preservation of function is reflected by preservation of NMJs and whether NMJ degeneration is preceded by early structural changes, the forelimb muscles of SOD1^{G93A}xYFP and SOD1^{G93A} mice were examined using the same analysis criteria as used for the gastrocnemius muscle. In the forelimb, there was a significant ($p < 0.0001$) 23% decrease in the proportion of intact distal axons at 140 days of age in SOD1^{G93A}xYFP mice compared with YFP controls (SOD1^{G93A}xYFP: 73.37% ± 3.55%; YFP: 96.28% ± 1.87%) (Figure 3.7 A). Similar to axonal degeneration, there was a significant ($p < 0.05$) 14% decrease in the proportion of α-BTx labelled NMJs demonstrating normal morphology in SOD1^{G93A} mice (SOD1^{G93A}xYFP: 72.92% ± 6.84%; YFP: 86.77% ± 3.25%) (Figure 3.7 A), suggesting that this morphological phenomenon is not limited to the pathophysiology of only the SOD1^{G93A} gastrocnemius.

NMJ synaptic colocalisation demonstrated a significant ($p < 0.0001$) 22% decrease in the proportion of YFP axon terminals colocalised with α-BTx in SOD1^{G93A}xYFP mice at 140 days of age compared to YFP controls (SOD1^{G93A}xYFP: 77.29% ± 8.58%; YFP: 98.97% ± 0.39%) (Figure 3.7 B and D). Similarly, there was also a significant ($p < 0.05$) decrease in the proportion

FIGURE 3.7. Distal axon and NMJ degeneration is delayed in the forelimbs of $SOD1^{G93A}$ mice. (A) There was a significant ($p < 0.05$) decrease in the proportion of distal axons displaying a normal, intact morphology at 140 days of age in $SOD1^{G93A}$xYFP mice compared with YFP controls; and significant ($p < 0.05$) decrease in the proportion of NMJs demonstrating a normal complex morphology at 140 days in $SOD1^{G93A}$xYFP mice compared with YFP controls. (B) There was a significant ($p < 0.05$) decrease in the proportion of NMJs demonstrating colocalised YFP and pre-synaptic terminal immunolabelled for neurofilaments and synaptophysin with α-BTx at 140 days of age in $SOD1^{G93A}$xYFP and $SOD1^{G93A}$ mice forelimbs compared with respective controls. However, there was no significant ($p > 0.05$) change in the proportion of NMJs showing colocalised nestin, dystrophin or rapsyn with α-BTx at 140 days of age (mean ± SEM, $n = 4$ mice). (C) There was a significant ($p < 0.05$) decrease in the proportion of NMJs demonstrating colocalised LRP-4 with α-BTx at 84, 112 and 140 days of age in $SOD1^{G93A}$ mice compared to controls. However, the loss of LRP-4 is not progressive. (D) Forelimb NMJs were either fully colocalised between YFP (green) and α-BTx (red), (B) or demonstrated non-colocalisation between YFP and α-BTx, due to presynaptic loss of YFP, leaving a denervated endplate. (E) Immunohistochemical presynaptic markers were either fully colocalised with α-BTx, (D) or the presynapse was lost, with only the α-BTx endplate visible. (F) In the forelimb LRP-4 (green) immunoreactivity is present surrounding the healthy wild-type control NMJ stained with α-BTx (red), with LRP-4 colocalisation with α-BTx progressively decreasing in the forelimb of $SOD1^{G93A}$ NMJs from 84 days of age in the forelimb. Scale = 15μm.

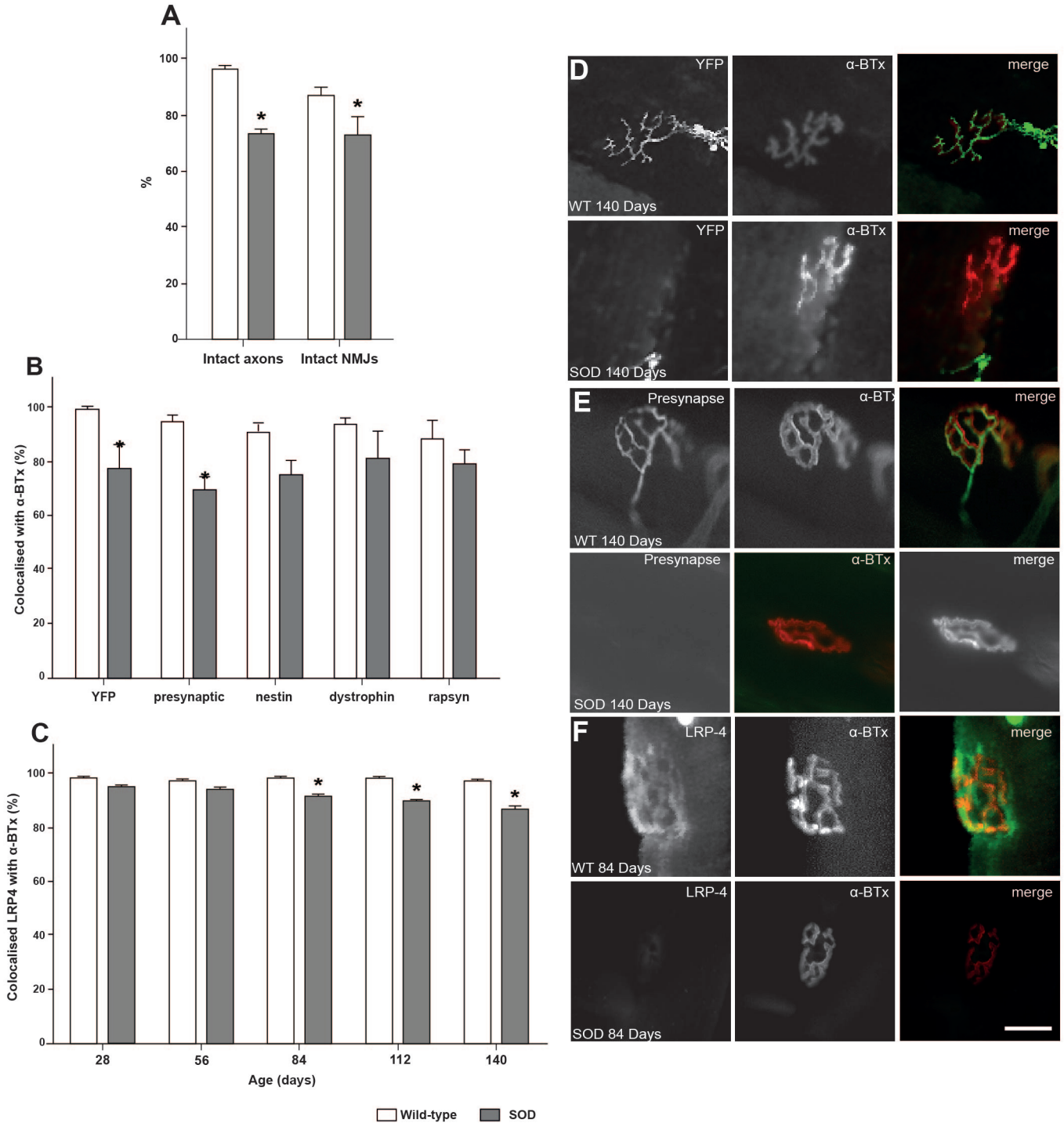
A
100
80
60
40
20
0
%
*
*
Intact axons
Intact NMJs
B
Colocalised with α-BTx (%)
100
80
60
40
20
0
*
*
YFP
presynaptic
nestin
dystrophin
rapsyn
C
Colocalised LRP4 with α-BTx (%)
100
80
60
40
20
0
*
*
*
28
56
84
112
140
Age (days)
Wild-type
SOD
D
YFP
α-BTx
merge
WT 140 Days
YFP
α-BTx
merge
SOD 140 Days
E
Presynapse
α-BTx
merge
WT 140 Days
Presynapse
α-BTx
merge
SOD 140 Days
F
LRP-4
α-BTx
merge
WT 84 Days
LRP-4
α-BTx
merge
SOD 84 Days

of NMJs with pre-synaptic immunolabelling for neurofilaments and synaptophysin colocalised with α-BTx at 140 days of age, reflecting a 27% decrease in colocalisation ($SOD1^{G93A}$: 69.8% ± 4.75%; wild-type: 95.1% ± 2.17%) (Figure 3.7 B and E). Furthermore, there was no significant ($p > 0.05$) difference in colocalisation between pre- and post-synaptic structures prior to 140 days of age. Axonal degeneration and NMJ morphology was only measured at 140 days of age.

To identify the differential vulnerability of forelimb NMJs to architectural protein loss, we evaluated the colocalisation of post-synaptic proteins identified previously in the hindlimb. There was no significant ($p > 0.05$) change in the proportion of NMJs with nestin, rapsyn and dystrophin colocalised with α-BTx compared to wild-type animals at any age (Figure 3.7 C). Conversely, analysis of LRP-4 in forelimb tissue of $SOD1^{G93A}$ mice demonstrated a significant ($p < 0.01$) loss of LRP-4 colocalisation at with α-BTx at 84 days of age, compared to age matched wild-type control mice ($SOD1^{G93A}$: 91.4% ± 1.19%; wild-type: 98.2% ± 0.71%) (Figure 3.7 C and F). The loss of LRP-4 at 112 and 140 days was significant, but not as pronounced as found at matching ages in the gastrocnemius muscles, nor was it progressive between 84, 112 and 140 day old $SOD1^{G93A}$ mutant animals. These data suggest that NMJ degeneration is delayed in the forelimb despite axonal degeneration occurring in both hindlimb and forelimb of $SOD1^{G93A}$ muscles, however loss of LRP-4 localisation to the post-synapse occurs in both hindlimb and forelimbs muscle, but appears to occur at different rates.

3.3.6 Post-synaptic structural protein levels are altered in $SOD1^{G93A}$ mice

To identify if the loss of colocalisation of post-synaptic proteins with α-BTx is due to a loss of protein levels or a loss of protein trafficking/localisation, Western blot analysis was performed. End stage gastrocnemius muscle revealed alterations in protein levels, as well as unconfirmed protein-processing deficits. Western blot showed a significant ($p < 0.05$) decrease in total nestin in the gastrocnemius muscle in end-stage $SOD1^{G93A}$ mice, compared with wild-type controls ($SOD1^{G93A}$: 0.19pix^2 ± 0.01pix^2; wild-type: 0.30pix^2 ± 0.01 pix^2) (Figure 3.8 A). However, as shown in Fig. 6A, a shift from 260kDa nestin to a larger nestin isoform of 350kDa occurs in $SOD1^{G93A}$ mice; 260kDa ($SOD1^{G93A}$: 0.02pix^2 ± 0.005pix^2; wild-type: 0.28pix^2 ± 0.03pix^2), 350kDa ($SOD1^{G93A}$: 0.17pix^2 ± 0.01pix^2; wild-type: 0.02pix^2 ± 0.007pix^2). Conversely, there was a significant ($p < 0.05$) increase in protein levels of LRP-4, dystrophin and rapsyn in end-stage in the gastrocnemius muscle of end stage $SOD1^{G93A}$ mice; LRP-4 ($SOD1^{G93A}$: 0.12pix^2 ± 0.022pix^2; wild-type: 0.016pix^2 ± 0.001pix^2) (Figure 3.8 B), dystrophin ($SOD1^{G93A}$: 0.25pix^2 ± 0.06pix^2;

FIGURE 3.8. Post-synaptic protein levels are altered in SOD1^{G93A} mice at end stage. (A) LRP-4 levels were significantly ($p < 0.05$) increased in SOD1^{G93A} mice at, compared with age-matched controls. (B) Total nestin levels were significantly ($p < 0.05$) decreased in SOD1^{G93A} mice compared with age-matched controls. However, there was a significant ($p < 0.001$) shift in protein size from 260kDa to 350kDa in SOD1^{G93A} mice. (C) Dystrophin levels were significantly ($p < 0.05$) increased in SOD1^{G93A} mice compared with age-matched controls. (D) Rapsyn levels were significantly ($p < 0.05$) increased in SOD1^{G93A} mice compared with age-matched controls.

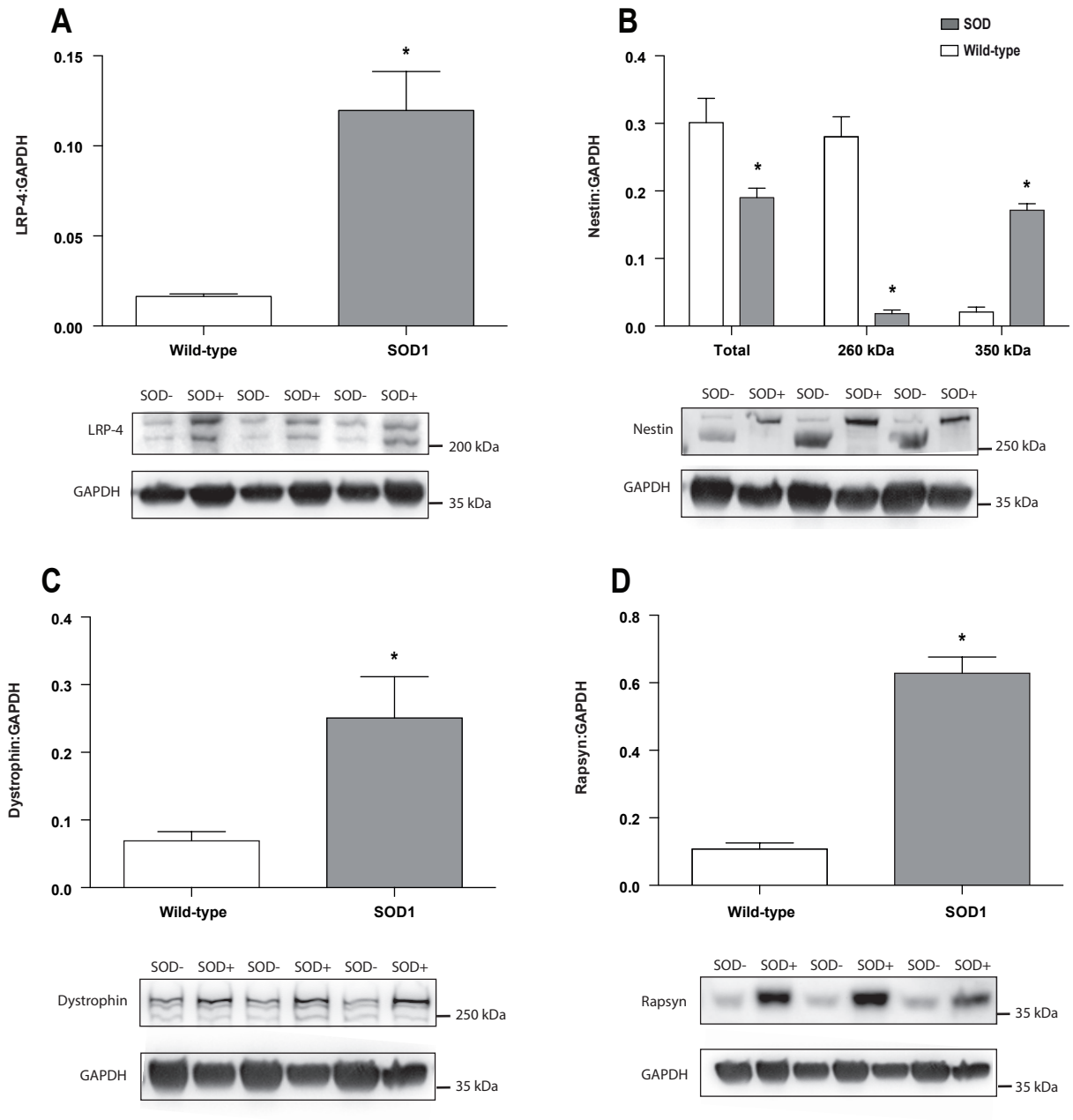
A
LRP-4:GAPDH
0.15
0.10
0.05
0.00
*
Wild-type
SOD1
SOD- SOD+ SOD- SOD+ SOD- SOD+
LRP-4
200 kDa
GAPDH
35 kDa
B
SOD
Wild-type
Nestin:GAPDH
0.4
0.3
0.2
0.1
0.0
*
*
*
Total
260 kDa
350 kDa
SOD- SOD+ SOD- SOD+ SOD- SOD+
Nestin
250 kDa
GAPDH
35 kDa
C
Dystrophin:GAPDH
0.4
0.3
0.2
0.1
0.0
*
Wild-type
SOD1
SOD- SOD+ SOD- SOD+ SOD- SOD+
Dystrophin
250 kDa
GAPDH
35 kDa
D
Rapsyn:GAPDH
0.8
0.6
0.4
0.2
0.0
*
Wild-type
SOD1
SOD- SOD+ SOD- SOD+ SOD- SOD+
Rapsyn
35 kDa
GAPDH
35 kDa

wild-type: 0.07pix^2 ± 0.014pix^2) (Figure 3.8 C) and rapsyn (SOD1^{G93A}: 0.6284pix^2 ± 0.048pix^2; wild-type: 0.11pix^2 ± 0.018pix^2) (Figure 3.8 D).

3.4 Discussion

This chapter investigated the sequence of axonal and NMJ degenerative events in the SOD1^{G93A} mouse model of ALS. It focused observations on pathological changes to the distal axon, alterations to synaptic morphology and key post-synaptic structural proteins of the NMJ in the hindlimb (gastrocnemius) and the less studied forelimb (extensor) muscles. The chapter highlighted that YFP is a highly detailed marker of distal axon and pre-synaptic alterations, with its expression confirming hallmark axonal pathology, as well as key early alterations to NMJ morphology. Novel alterations to YFP expressing axonal branch complexity and key post-synaptic protein localisation and total protein levels in the hindlimb of the SOD1^{G93A} mouse model were also identified in this chapter.

3.4.1 Degeneration of the motor neuron distal axon and NMJ pathology occurs prior to symptom onset in SOD1^{G93A} mice

Distal axon degeneration, including axonal beading and fragmentation, and alterations to the hindlimb NMJ, are considered key and early features of pathology in the SOD1^{G93A} mouse (Gurney et al., 1994; Frey et al., 2000). The process of degeneration in ALS is thought to occur in a 'dying back' fashion, with degenerative changes beginning in the a-MN axon and progressing proximally (Fischer et al., 2004). With the aid of the YFP reporter, hallmarks of the disease are shown at an early, presymptomatic time point in the gastrocnemius muscle, and these pathological and morphological changes can be detected in the axon and NMJ by assessing changes to YFP distribution (Frey et al., 2000; Fischer et al., 2004; Pun et al., 2006). These results are comparable to previously reported studies utilising YFP to aid in axonal and NMJ characterisation using confocal microscopy (Schaefer et al., 2005; Wong et al., 2009).

It has been previously reported that both low and high copy number SOD1^{G93A} mice exhibit axonal fragmentation, NMJ denervation, as well an increase in collateral branches over an imaging time course (Frey et al., 2000; Schaefer et al., 2005; Pun et al., 2006; Wong et al., 2009). Ngo and Colleagues (2012) have previously shown that NMJ denervation occurs at symptom onset, at approximately 63 – 75 days, in the gastrocnemius of the SOD1^{G93A} mouse (Ngo et al., 2012). Indeed, results from this chapter identified a significant decline in of NMJ innervation of

the gastrocnemius at 84 days, a similar age to the previously mentioned study. However, unlike the study in Chapter 3, Ngo and Colleagues (2012) did not study axonal or NMJ morphological alterations, which were identified to occur at a presymptomatic age in the $SOD1^{G93A}$ mouse. Indeed, this Chapter demonstrated that the previously reported onset of hindlimb weakness/loss of motor performance is preceded by degenerative axonal pathology within the gastrocnemius muscles in the $SOD1^{G93A}$ model. The lack of correlation between the appearance of pathology and symptom onset is often attributed to compensatory reinnervation and NMJ structural plasticity from remaining a-MNs following loss of vulnerable a-MN subtypes. The current data supports this finding, with evidence of compensatory resprouting from YFP positive axons in the $SOD1^{G93A}$xYFP crossed transgenic mouse at a presymptomatic time point (Frey et al., 2000; Fischer et al., 2004; Pun et al., 2006). Collateral sprouting and attempted reinnervation in the $SOD1^{G93A}$ mouse gastrocnemius was measured by increased terminal axon branching in addition to an increase in the number of NMJs with reduced synaptic complexity (Feng et al., 2000b; Li et al., 2011).

The NMJ is a highly dynamic structure, which has been shown to undergo reactive changes in other pathologies, such as following experimental pre-synaptic distal nerve ablation (Li et al., 2011). Indeed, during development NMJs undergo transformation from being multi-axon innervated with a plaque-like morphology, to a single axon innervated pretzel morphology (Balice-Gordon and Lichtman, 1993). In the current study, a small subset of NMJs demonstrating reduced complexity whilst retaining full colocalisation between pre- and post-synaptic markers. Such NMJs may be newly formed synapses or attempted re-innervation in the $SOD1^{G93A}$ tissue. However, analysis used in the current study, whilst being highly stringent on NMJ selection, did not select specifically for NMJs with the aforementioned immature 'plaque-like' appearance (Balice-Gordon and Lichtman, 1993), which is indicative of newly formed synapses. Further, using the current model it was unfeasible to determine whether there are any fundamental abnormalities in NMJ formation as a result of SOD1 transgene expression, however the lack of an overt NMJ phenotype in younger animals and normal distribution of post-synaptic proteins in young animals was suggestive of degenerative changes occurring after NMJ formation. Although not quantified in the current study, others have shown that the pre-synaptic motor endplate undergoes axonal sprouting, similar to axonal collateral branching discussed previously (Ngo et al., 2012). Future research would benefit from perusing this observation further using YFP

expressing animal models, particularly as YFP axon volumetric analysis can help to identify fibre type specific regenerative capacity (Pun et al., 2006).

The use of YFP expressing distal axons and NMJs highlights a novel way to identify alterations to cellular structures in other disease models, where axonopathy and synaptic alterations are an early or primary event in their pathogenesis (Vickers et al., 2009). Although these morphological alterations were evident in early disease in the $SOD1^{G93A}$ mouse, loss of pre-synaptic structures were only detected at 84 days, through the significant loss of colocalisation between pre- and post-synaptic structures of the NMJ prior to symptom onset (Frey et al., 2000; Fischer et al., 2004; Hegedus et al., 2008). This highlights that compensatory plasticity likely plays a major role in ALS, with reinnervation of skeletal muscle fibres delaying the loss of muscle function.

3.4.2 Loss of structural proteins precedes loss of post-synaptic receptors in the hindlimb

The current chapter aimed to investigate how NMJ changes affected a number of structural components of the synapse, beyond the pre-synaptic axon terminal and post-synaptic AChRs. Surprisingly, structural proteins such as nestin, rapsyn, dystrophin and LRP-4 are all lost from the NMJs prior to complete disassembly of AChRs.

The intermediate filament nestin provides structural support to the NMJ (Herrmann and Aebi, 2000; Kang et al., 2007; Mohseni et al., 2011; Yang et al., 2011), however is also a substrate for phosphorylation by a large number of kinases, including CDk5 (Sahlgren et al., 2003). Phosphorylation of nestin at Thr316 allows for AChR dissociation. During skeletal muscle development, nestin is distributed throughout the muscle fibre, localising to the neuromuscular and myotendious junctions following NMJ formation (Lendahl et al., 1990; Vaittinen et al., 1999). Following nerve transection injury, nestin expression increases in skeletal muscle (Vaittinen et al., 1999) and has been shown to be increased in the cortex of the $SOD1^{G93A}$ mouse (Lee et al., 2011). Nestin colocalisation to the NMJ is progressively lost in $SOD1^{G93A}$ mice, however there were also changes to overall nestin levels. As with many other intermediate filaments, nestin is a target for post-translational modifications, in particular, phosphorylation and ubiquitination (Snider and Omary, 2014). It currently remains unclear whether the size-shift of nestin from our experiments could be due to aberrant processing from $SOD1^{G93A}$ overexpression, or whether there is abnormal post-translational modification occurring, such as

hyperphosphorylation and ubiquitination as occurs with related intermediate filaments (Ku and Omary, 2000; Snider and Omary, 2014).

LRP-4 is a correceptor for agrin and forms an intracellular signalling complex with muscle specific kinase (MuSK) (Kim and Burden, 2008; Zhang et al., 2008a). The agrin-LRP-4-MuSK complex is required for both NMJ formation, but also NMJ maintenance and stability (Barik et al., 2014). Furthermore, a loss of LRP-4 can lead to a-MN pre-synaptic retraction from the NMJ (Barik et al., 2014). Mutations to LRP-4 result in the development of congenital myasthenic syndromes (CMS), and Cenani–Lenz syndrome, with autoantibodies for LRP-4 also causing myasthenia gravis (Li et al., 2010; Pevzner et al., 2012; Ohkawara et al., 2014). Our identification of LRP-4 loss may indicate a loss of the agrin-LRP-4-MuSK signalling complexes ability to effect both NMJ formation in the reinnervation attempt, but also a loss of NMJ maintenance that may lend pathogenicity to both a-MN and NMJ degeneration. This phenomenon of LRP-4 pathology in the current chapter was identified at the approximate age of reported symptom onset in these mice (84 days), possibly illuminating a mechanism behind the apparent inability for effective reinnervation to occur to stave off motor symptoms. Indeed, the identified increase in LRP-4 levels could indicate a regenerative attempt by the muscle, or that mislocalisation of LRP-4 is occurring and mutant SOD1 is driving both mislocalisation of LRP-4, up-regulation or both.

Rapsyn is primarily a structural protein for post-synaptic AChR aggregation. In addition to AChR binding (Frail et al., 1987; Gautam et al., 1995; Zuber and Unwin, 2013), rapsyn interacts with the cytoskeleton (Antolik et al., 2007) and molecules such as calpain (Chen et al., 2007), β-catenin (Zhang et al., 2007a) and α-actinin (Dobbins et al., 2008). Rapsyn deficiency results in CMS, and rapsyn mRNA levels has also been shown to increase in muscle following nerve transection (Frail et al., 1989; Ohno et al., 2002). Indeed, increased expression of rapsyn in CMS *in vivo* models improved the pathological outcome of NMJs (Losen et al., 2005). A significant increase in skeletal muscle rapsyn levels in the $SOD1^{G93A}$ mouse was identified. However, this was coupled with a decrease in the proportion of NMJs showing rapsyn colocalisation with α-BTx, possibly suggesting a dysfunction in the aggregation of AChRs at the skeletal muscle membrane.

Dystrophin is a component of the dystrophin glycoprotein complex (DGC) which is required for organisation and stabilisation of synaptic folds (Lyons and Slater, 1991; Knuesel et al., 1999;

Sanes and Lichtman, 1999; Banks et al., 2003; Shiao et al., 2004). Dystrophin also provides a point of linkage between the muscle plasma membrane and the F-actin component of the cytoskeleton (Ervasti and Campbell, 1993; Banks et al., 2009). Importantly, the DGC putatively acts as a scaffold for signalling proteins including nNOS, calmodulin, phosphoinositol triphosphate 3 and may also be involved with mitogen activated protein kinase (MAPK) signalling (Rando, 2001) and maintaining Ca^{2+} homeostasis (Gillis, 1996; Carlson, 1998). In Duchenne muscular dystrophy, loss of dystrophin results in progressive destabilisation of the NMJ (Pilgram et al., 2010). These studies suggest that the loss of dystrophin from the NMJ occurring late in the $SOD1^{G93A}$ model may reflect the increased disassembly of the AChR complex from the skeletal muscle membrane. The identified increase in dystrophin levels suggests, again, a lack of localisation and trafficking to the NMJ. It currently remains unknown how changes to DGC assembly in the $SOD1^{G93A}$ model affect the associated signalling pathways and the structural integrity of the post-synapse. The early and progressive loss of the NMJ structural proteins may have a dramatic effect on the multitude of signalling cascades that are required for NMJ stability, maintenance and plasticity.

A possible mechanism driving the identified increase in post-synaptic protein expression in the $SOD1^{G93A}$ gastrocnemius may be explained by the muscles capacity for activity dependant changes in the architecture of the NMJ, as discussed in Chapter 1, Section 1.2.2 (Misgeld et al., 2005; Morsch et al., 2013). Whilst previous research has shown that increased ACh at the NMJ can alter synaptic performance and maintenance, the innervation of the gastrocnemius muscle at end stage in the $SOD1^{G93A}$ mice is drastically decrease, suggesting that increased synaptic activity is not causing the identified protein expression. As stated throughout Section 3.4.2 of this thesis, it is more likely that surviving, denervated myocytes undergo an increase in NMJ protein synthesis due to a loss of activity, similar to what is identified in nerve transection studies (Frail et al., 1989; Vaittinen et al., 1999; Ohno et al., 2002). However, the increase in protein expression, particularly that of rapsyn, may instead act as the driving force for NMJ degeneration, as rapsyn overexpression has been found to inhibit AchR clustering (Han et al., 1999).

3.4.3 Distal forelimb pathology is only evident in the later stages of disease in the $SOD1^{G93A}$ mouse

The onset of disease in the $SOD1^{G93A}$ mouse classically begins with hindlimb weakness which progresses to a severe motor disability whilst the forelimb muscles remain relatively spared

(Gurney et al., 1994; Bendotti and Carri, 2004). Despite differences in muscle fibre type compositions and vulnerability between the forelimb and hindlimb muscles investigated, Mathewson et al., (2012) have suggested that forelimb musculature is relatively comparable between humans and mice, irrespective of limb function and skeletal muscle biomarkers between humans and mice (Hegedus et al., 2008; Elashry et al., 2009; Mathewson et al., 2012).

In the present study, axonal pathology evident at the later disease stages in the forelimbs, with an increased proportion of beaded and fragmented axons at 140 days. Similarly, increases in morphological abnormalities were also evident at 140 days in SOD1^{G93A}xYFP mice. This highlights that distinctive axonal and NMJ morphology alterations are delayed relative to the hindlimb in SOD1^{G93A} mice. Furthermore, analysis of pre-and post-synaptic components indicated that the delay in functional loss of the forelimbs in SOD1^{G93A} mice is supported by an absence of histological pathology until the disease is well progressed (Gurney et al., 1994). There was a significant decrease in the proportion of NMJs with colocalisation between pre-synaptic terminals and α-BTx at 140 days of age, however only the post-synaptic signalling protein LRP-4 was lost, with no loss of rapsyn, nesting and dystrophin, despite no earlier loss of pre-synaptic markers at similar time points (Schafer and Hermans, 2011; Barik et al., 2014).

Studies have demonstrated that spinal pathology in the SOD1^{G93A} mouse is widespread throughout both the lumbar and thoracic regions (Karlsson et al., 2004; Dodge et al., 2008; Graffmo et al., 2013), however the delayed pathology in the forelimb muscles is suggestive of potential differences in the disease process which may be localised to specific regions. This is highlighted by the differential loss of nestin from the NMJs of the gastrocnemius and forelimb muscles. In the hindlimb, nestin is lost parallel to loss of the pre-synaptic component, and occurs prior to symptom onset, however this loss of nestin was not present in the forelimb. This discrepancy may arise from key differences between the motor units of the forelimb and hindlimb and need to be investigated further (Elashry et al., 2009; Mathewson et al., 2012).

Conversely, the loss of LRP-4 from both hindlimbs and forelimbs suggests that SOD1^{G93A} may play a direct involvement in its loss from the NMJ, independent of muscle fibre type, compared to other post-synaptic proteins studied. It is known that SOD1^{G93A} expression in muscle can both cause a motor phenotype *in vivo* when conditionally expressed and can also lead to the aberrant

expression of a number of genes; however, the proteins identified in this study are yet to be investigated in this manner (Wong and Martin, 2010).

Although the underlying mechanisms for the disparity in axon and NMJ degeneration remain to be fully elucidated, evidence suggests that degeneration of type II fibres occurs in a length-dependent manner in SOD1 mice, with preferential loss of longer axons over shorter (Tallon et al., 2016). This recent finding provides excellent evidence for length-dependent degeneration in the lateral thoracic nerve and cutaneous maximus muscle and further studies may reveal whether a similar pattern of degeneration occurs in the gastrocnemius and forelimb extensor muscles. Interestingly, Nguyen and Colleagues (2012) reported that NMJ degeneration occurs in the forelimb at symptom onset, in the $SOD1^{G85R}$ mouse model, a phenomenon not found in the $SOD1^{G93A}$ model (Nguyen et al., 2012). The denervation was found to predominantly occur in the fast-fatigue fibres. The $SOD1^{G85R}$ mutant has a slower progressing disease course, which may suggest that the fast progressing G93A strain used in the current may be more toxic to the lumbar motor neuron pool, suggesting that the hindlimbs are more vulnerable to this SOD1 mutation than the forelimbs (Bruijn et al., 1997). Further investigations should determine whether subtle differences in degeneration occur from one side of the body to another. ALS in many human cases is characterised by asymmetrical spread of clinical symptoms (Swinnen and Robberecht, 2014).

3.5 Conclusion

ALS is classically referred to as a distal axonopathy; the resulting pathology following a-MN dysfunction. Although this phenomenon has been known for some years, identification of the earliest pre and post-synaptic changes are yet to be completed. The current chapter attempted to identify the earliest changes to the distal axon and NMJ, with the intention of identifying the most prudent site for therapeutic intervention.

YFP expression was instrumental in identifying axonal and NMJ morphological alterations, with hallmark pathology and plasticity being evident, particularly at the early, presymptomatic time point. This highlights the use of YFP in the detection of axonal and synaptic abnormalities in neurodegenerative diseases. The reported progressive loss of postsynaptic scaffolding in the $SOD1^{G93A}$ gastrocnemius muscle suggests that using α-BTx as a sole marker for the NMJ loss does not provide a full picture of disease progression. This loss of key structural components in

the hindlimb but not in the forelimb indicates that these proteins, which are involved in maintaining post-synaptic integrity, may play an important role in the progressive dysfunction of this specialised synapse. This chapter also highlighted that the post-synaptic integrity of the NMJ may be playing a key pathogenic role in preserving forelimb function in this model. The cause for this phenotypic phenomenon is not well understood, however it may reflect differences in pre- and post-synaptic structures, different skeletal muscle composition, or metabolism, including mutant SOD1 activity. Furthermore, a live imaging approach in the forelimbs and gastrocnemius of the $SOD1^{G93A}$ mouse, utilising the YFP reporter, may offer further insights into axonal degeneration, plasticity and NMJ morphology characterisation to establish a more holistic sequence of pathological events.

Currently, alterations to the pre-synaptic axon and NMJ compartment in the hindlimb are the earliest identified pathology in the $SOD1^{G93A}$ mouse model, followed by alterations to synaptic integrity and gross innervation (Figure 3.9 A). Targeting pathology in ALS at the earliest possible instance will hopefully improve outcomes of the disease. To this end the distal axon in the $SOD1^{G93A}$ mouse should be considered as an attractive therapeutic target, to prevent both its breakdown, but to also preserve its function to limit the classic 'distal axonopathy' of ALS (Figure 3.9 B).

FIGURE 3.9. Timeline of distal pathology and possible therapeutic intervention. **(A)** Axonal degeneration and morphological alterations to hindlimb NMJs are the earliest identified pathology in the distal neuromuscular circuit. **(B)** MT disintegration and altered dynamics are associated with the pathogenesis of ALS. Targeting MTs with stabilising compounds (red circles) may improve outcomes in ALS.

A

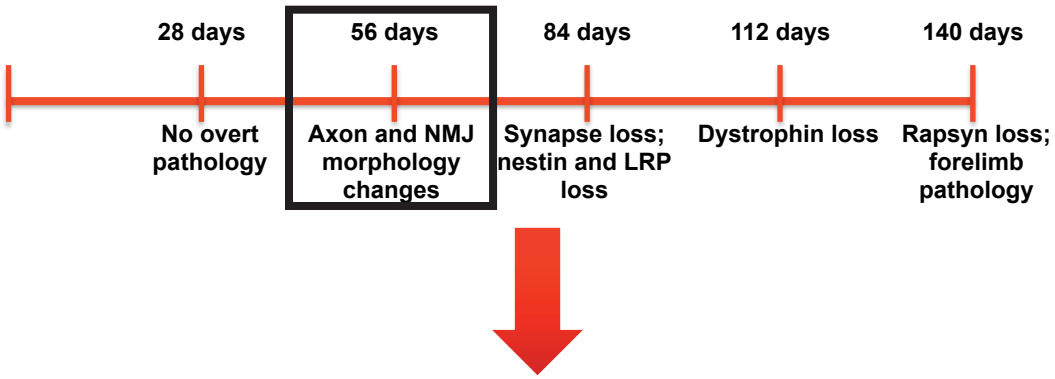
28 days
56 days
84 days
112 days
140 days
No overt pathology
Axon and NMJ morphology changes
Synapse loss; nestin and LRP loss
Dystrophin loss
Rapsyn loss; forelimb pathology

B

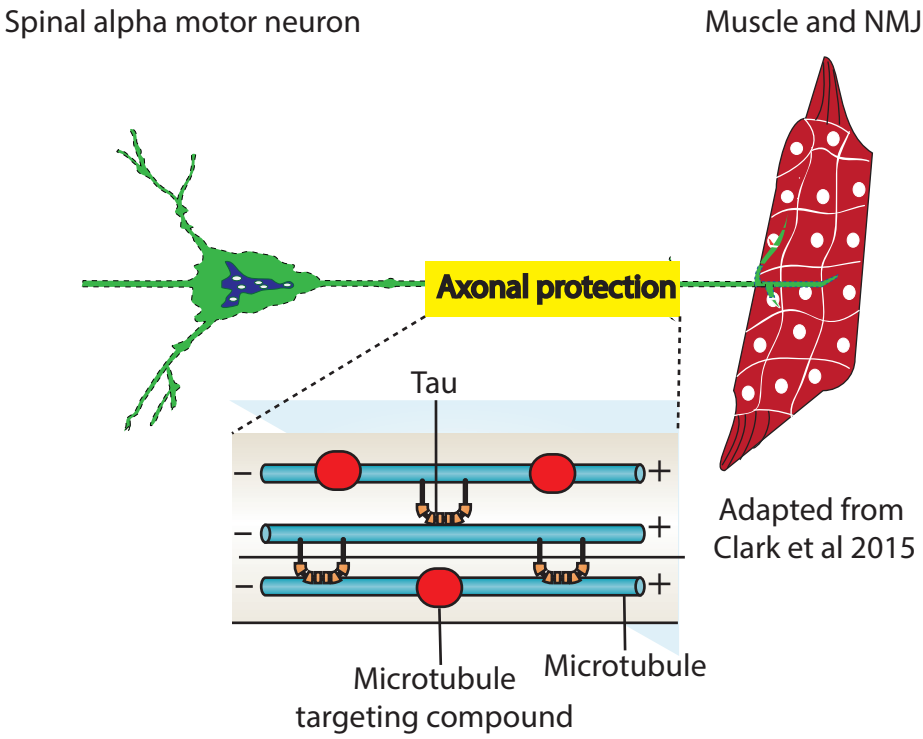
Spinal alpha motor neuron
Muscle and NMJs
Axonal protection
Tau
Microtubule targeting compound
Microtubule
Adapted from Clark et al 2015

Chapter 4

4 The microtubule stabilising agent Epothilone D modifies disease progression in a mouse model of Amyotrophic Lateral Sclerosis.

4.1 Introduction

Although being described and researched extensively for over a century, limited translation of effective therapeutics to combat ALS has occurred. The only current therapy for patients with ALS is the compound Riluzole; a drug that modestly modifies various aspects of glutamatergic signalling (Bensimon et al., 1994; Gurney et al., 1998; Vucic et al., 2013). However, Riluzole does not present a cure, delaying death by only 6-7 months in subset of patients that respond well to the drug (Hardiman et al., 2011). There remains a great need for new drug development, and the identification of novel mechanisms and therapeutic targets.

A pathological hallmark that has the capacity to be targeted is the degeneration of the spinal a-MN distal axon and terminal. As identified in Chapter 3, axonal pathology, consisting of beading and fragmentation, is an early presymptomatic event in ALS. Further, as discussed in Chapter 1 of this thesis, axonal transport dysfunction and aberrant microtubule hyperdynamics is an early occurrence in the pathogenesis of ALS (Fanara et al., 2007; Bilsland et al., 2010; Kleele et al., 2014). Evidence for microtubule involvement in ALS classically stems from the identification of dysfunctional axonal transport; thought to limit the delivery and recycling of mitochondria, proteins, mRNA, vesicles and survival factors necessary for a-MN health and longevity (Bilsland et al., 2010; Alami et al., 2014; Dubey et al., 2015). However, it is becoming increasingly apparent that the phenomenon of microtubule dynamic instability is altered in ALS, resulting in a shift to a hyperdynamic state (Fanara et al., 2007; Kleele et al., 2014). Indeed, many molecular mechanisms associated with MN vulnerability also impact on microtubule functions, as highlighted in Chapter 1. As discussed, Fanara and Colleagues (2007) emphasised that microtubule dynamics initiates the dysfunction of axonal transport in $SOD1^{G93A}$ mice, suggesting that alterations to microtubule dynamics is a primary mechanism in ALS. This is substantiated by the recent identification of the *TUBA4A* rare variant, whereby the various missense mutations to this tubulin isoform decrease its ability to polymerise into the microtubule polymer, altering the dynamics of the microtubule network (Smith et al., 2014). These include changes to tubulin isotype expression, altered tubulin localisation and tubulin aggregation, all of which results in a weakened microtubule network (Smith et al., 2014). Furthermore, Kubota and Colleagues (2009),

found that mutant SOD1 can alter microtubule networks by modulating tubulin polymerization and dynamics (Kabuta et al., 2009). Moreover, microtubules are involved in the process of axonal degeneration, with microtubules being a substrate for caspase and calpain; enzymes that are activated in disease, breaking down the axon during Wallerian-like axonal degeneration in ALS (Wang et al., 2012).

Targeting the cytoskeleton to improve outcomes in neurodegenerative diseases is not a novel concept (Brunden et al., 2011; Baas and Ahmad, 2013; Eira et al., 2016). Diseases where alterations to microtubule dynamics and stability, such as AD, PD, tauopathies and schizophrenia, have shown that using low doses of antimitotic compounds that target microtubules can improve pathology and outcomes in various disease models (Andrieux et al., 2006; Fanara et al., 2007; Green et al., 2008; Kitaoka et al., 2009; Brunden et al., 2011; Zhang et al., 2012; Cartelli et al., 2013). The most well characterised and utilised microtubule stabilising compound, taxol, has been supplemented by other compounds that have greater tubulin affinity, decreased off-target effects and the ability for blood brain barrier permeability and CNS retention (Bollag et al., 1995; Brunden et al., 2011). One such microtubule-targeting compound is Epothilone D (EpoD). EpoD is a member of the epothilones, a group of compounds found naturally in the myxobacterium Sorangium cellulosum (Bollag et al., 1995). EpoD is currently in clinical trials for taxol-resistant malignancies, however it is being increasingly used at lower doses to manipulate the microtubule cytoskeleton in the nervous system (Cheng et al., 2008; Brunden et al., 2010; Zagouri et al., 2015).

Targeting microtubules to improve outcomes in ALS was initially investigated by Fanara et al (2007), where the compound Noscapine was utilised to ameliorate the hyperdynamic microtubule phenotype identified in the $SOD1^{G93A}$ mouse model (Fanara et al., 2007). Noscapine effectively 'stalls' microtubule dynamics, limiting the amount of polymerisation/depolymerisation events that occur, thus decreasing microtubule hyperdynamics. Indeed the authors reported that noscapine attenuates microtubule dynamics, which directly improved axonal transport. Clinically the animals showed slower pathology progression and extended survival. However, noscapine is still in preclinical trials, highlighting the need to test novel compounds that also selectively target microtubule stability for use in ALS. Targeting the distal axon with calpain inhibitors has also been shown to decrease microtubule disintegration and improve outcomes in models of peripheral neuropathy, suggesting that protecting the distal axonal cytoskeleton is a viable approach to limiting pathology in diseases such as ALS (O'Hanlon et al., 2003; Moloney et al.,

2014). These previous studies highlight that microtubule stabilisation may be an attractive target for ALS, to alleviate not only aberrant dynamics, but to also stabilise the microtubule cytoskeleton against enzymatic disintegration.

The current investigation utilised the SOD1^{G93A} mouse model of ALS to identify the efficacy of the microtubule-targeting compound EpoD to modify disease progression by targeting the distal axon. Investigations into the ability of EpoD to increase the stability of the microtubule network in the spinal cord were initially undertaken, as SOD1^{G93A} mouse models spinal onset ALS. Treatment of SOD1^{G93A} mice with low dose EpoD began at 50 days of age, in accordance with recommended treatment paradigms for this model and was carried out until endpoint (Scott et al., 2008). Behavioural, clinical and pathological characterisation of disease progression was completed, followed by analysis of time of disease onset and survival. These investigations determined how EpoD modifies disease progression in ALS and develop insights into not only the efficacy of microtubule-targeting therapies for the disease, but also the scope for improvements for combination therapies. Moreover, it will further highlight the important role microtubules have on disease progression and maintenance.

4.2 Methods

4.2.1 Animals

C57BL/6 mice were used to probe the efficacy of EpoD to induce microtubule stability in a-MNs. Male transgenic SOD1^{G93A} mice were used for behavioural, clinical and pathological evaluation after EpoD treatment. Double transgenic SOD1^{G93A}xYFP mice (see Chapter 2) were used for histological analysis of the distal axon and NMJs. All mice were assessed daily for clinical symptoms and weighed daily from 50 days of age (trial start) until end stage. End stage in these investigations was considered as 80% of maximal weight or an inability for the mouse to right itself (righting reflex) within 15 seconds. Following the onset of hindlimb paralysis, SOD1 mice were given the nutrient supplement NutraGel (Bioserve), generally from 120-130 days of age, to aid in dietary and water supplementation. Further, normal mouse chow was placed on the cage floor and moistened with drinking water.

4.2.2 Therapeutic regime

For initial microtubule stabilisation assay C57BL/6 mice (n=8) were injected intraperitonealy with either EpoD (Abcam) (2mg/kg, 50ul injection volume) or DMSO (100%, 50ul injection volume) every five days for two weeks. For EpoD treatment trial SOD1^{G93A} transgenic mice

(n=28), their wild-type (WT) littermates (n=16), and SOD1^{G93A}xYFP mice (*n* = 18), were randomly allocated to either EpoD (2mg/kg) or vehicle (DMSO) groups. Injections were administered every 5 days, starting from 50 days of age (Kennel et al., 1996; Scott et al., 2008). Mice were weighed at the same time daily to account for diurnal cycles. No adverse effects due to the vehicle were seen. Mice were injected according to this regime until the required time point or endpoint was reached. Mice were then terminally anesthetised with sodium pentabarbitone and perfused with 4% paraformaldehyde or ice cold 0.01M PBS. All researchers were blinded to genotype and drug administration for the duration of the experiments.

4.2.3 Clinical assessment

Clinical evaluation was completed from 50 days of age until disease end stage. Mice were examined daily and assessed using an amended four point scoring system, with the mode score for the week being recorded and evaluated (Weydt et al., 2003). Evaluation categories included 'normal clinical presentation' (score of 4); 'hindlimb tremors or 'waddle' when motile' (score of 3); 'dragging of hindlimbs, or decreased ability to extend hindlimbs when suspended by the tail' (score of 2), 'paralysis of hindlimbs and substantial decrease in ability to ambulate around the cage' (score of 1); 'inability to right within 15 seconds, or 20% loss of body weight from maximum, and inability to ambulate around cage' (score of 0). Weight was also utilised as a clinical assessment of disease progression.

4.2.4 Rotarod performance test

Motor behaviour was evaluated using rotarod performance testing (TSE Systems). The rotarod performance test measures strength, endurance and coordination, and is considered a gold standard in motor phenotype testing (Weydt et al., 2003; Bohlen et al., 2009). Mice were trained one week prior to the commencement of experiments by experiencing various rotational speeds (10rpm, 20rpm and 40rpm), with an acceleration of 8rpm/minute, ensuring the mouse had to increase its pace to remain on the rotating rod (Galante et al., 2009). On the day of testing, mice were habituated in the testing room for 15 minutes. Mice were then placed on the rotating rod at 4rpm, which served as a minimum cut-off speed for mice with later stage clinical progression, which can no longer grip the rod. The test program consisted of an acceleration phase from 4rpm to 40rpm over 300 seconds, followed by a further 60 seconds at 40rpm (Galante et al., 2009; Perry et al., 2010). For all experiments latency to first rotation and latency to fall were recorded. Rotarod performance testing was repeated three times per session with a 15 minute inter-trial-interval between tests. Testing was completed three times per week.

4.2.5 Grip strength test

Grip strength was evaluated using a digital force gauge (Ametek). Grip strength measures the strength of the limbs, and is a measure of both the muscle mass and innervation of the muscle groups concerned (Schafer and Hermans, 2011). Grip strength of the hindlimbs and forelimbs were evaluated, consisting of three successive measurements. This was repeated three times with a five-minute inter-trial-interval between tests. Grip strength (kilograms of force (kgf)) was measured three times a week.

4.2.6 Behavioural statistical methods

The primary aim of behavioural analysis was to model rotarod performance, grip strength and weight, investigating the relationships between treatment and genotype. This was completed in collaboration with the Menzies Institute for Medical Research statistics department. The goal was to obtain a model trajectory, which represents our mice in the current behavioural conditions over time, without over fitting, so that the trajectory might reasonably be generalised to the greater population. Due to the general non-linear nature of the behavioural and biological outcomes measured in the current study, we used smooth non-linear polynomials to fit the data where appropriate (Grajeda et al., 2016). However, much of the data presented in the current study employed piece wise non-linear polynomial models, where individual break points and cubic splines are applied concurrently in the same model to best represent, and thus fit, the data (Durban et al., 2005; Chen and Stanley, 2012; Grajeda et al., 2016). 'Cut-Points' can be added to non-linear models to improve fit by increasing the number of possible maxima and minima ('bends') in the curve. In some cases, they can also be used to estimate when the data significantly deviates from previous time points.

The smooth or piecewise functions were applied within the fixed effects component of a linear mixed model. This approach was applied in the case of all behaviour outcomes. Linear mixed effect models are becoming more popular for modelling longitudinal data, as they are able to deal with the correlation between repeated measurements, as well as investigate variation between individual trajectories. This combination of piecewise polynomials within a mixed effects model has high utility for longitudinal biological data (Naumova et al., 2001). The final models selected are outlined below. Values are represented as mean plus lower and upper level confidence intervals. An unstructured covariance structure for random effects was applied throughout. The software package used was STATA 12 (StataCorp LP).

Latency to rotation model fit: Separate straight-line functions were fitted to the wild-type and SOD1^{G93A} data, coupled with optimal 'break points' for SOD1^{G93A} mice for each treatment, identified through a grid search. Random slopes were allowed for mouse. *Latency to fall model fit:* A straight-line fit was applied to wild-type curve and a quadratic term for SOD1^{G93A} mice. Separate terms for treatments were added with 5 cut-points to improve model fit. Random slopes were allowed for mouse. *Forelimb grip strength model fit:* Utilised the incorporation of both linear and cubic terms, with the addition of an optimal break point, as data suggested two stages of disease progression. Random slopes were allowed for mouse. *Hindlimb grip strength model fit:* Two straight-line functions were fitted for both SOD1^{G93A} and wild-type mice coupled with the fit of separate break points. Random slopes were allowed for mouse. *Weight model fit:* A separate straight line for wild-type and SOD1^{G93A} was fit, as well as a cubic spline function with three cut-points, due to the subtle curvature of the data. Random slopes were allowed for mouse.

4.2.7 Histopathology

Mice were transcardially perfused and relevant tissue was cryosectioned as described in Chapter 2, followed by histological analysis outlined below.

4.2.7.1 Spinal motor neuron visualisation and quantitation

Spinal a-MNs were quantified by firstly isolating the lumbar region of the spinal cord as described previously (Gunther et al., 2012; Harrison et al., 2013), followed by sectioning at 30μm onto slides. Every fourth lumbar section was selected for quantitation. Lumbar a-MN numbers were evaluated by staining with 0.125% toluidine blue in 0.75% acetic acid for 10 minutes. Lumbar sections (L1 – L5) were imaged using a Zeiss LAB A1, fitted with a bright field light source and a Zeiss AxioCam iCc5 camera (Zeiss) Images were analysed in image J, with counted cells being selected based on pre-reported a-MN cell area (cell area ≥450 μm^2, ≤745 μm^2), dark staining cytoplasm, a dark nucleolus and ventral horn location (Friese et al., 2009). Lateral and medial motor neuron columns were pooled during counts. Immunohistochemical quantitation of a-MNs was also used by labelling for dephosphorylated neurofilaments (SMI-32; 1:1000; Sternberger Monoclonals/Covance), with a-MNs selected based on diameter (≥20μm) and ventral location (Blizzard et al., 2015). SMI-32 immunohistochemistry was quantitated using dual cube immunofluorescence (Leica DM-LB2, Leica).

4.2.7.2 Quantitation of glial immunoreactivity

Lumbar spinal sections were prepared as described above. Every fourth 30μm slide mounted section was firstly rehydrated and then permeablised for 4 hours in blocking diluent (1% Triton-X 100, 5% BSA in 0.01M PBS). Primary antibodies for microglia (rabbit-anti Iba1; 1:1000; WAKO) and astrocytes (mouse-anti GFAP; 1:1000; Abcam) in blocking diluent were used to identify changes to glial activation. Primary antibodies were incubated at 4°C for a minimum of 16 hours, followed by 4x10 minute washes in PBS. Secondary antibodies (mouse Alexa568, rabbit Alexa647) were diluted in PBS (1:750; Molecular Probes) and sections were incubated for 2 hours at room temperature. Secondary antibodies were washed thoroughly and coverslipped as described in Chapter 2. Analysis of immunolabelled glia was performed using spinning disk confocal microscopy and the area of fluorescence was calculated using Image J (NIH), as described in Chapter 2.

4.2.7.3 Quantitation of distal axonopathy, NMJ colocalisation and NMJ morphology

EpoD treated SOD1^{G93A} and SOD1^{G93A}xYFP were perfused and the gastrocnemius muscles dissected and cryosectioned at 80μm onto glass slides. At 50, 70, 140 days (end stage not completed as hindlimb is fully paralysed). Forelimbs extensor muscles (extensor carpi radialis longus, extensor digitorum communis, extensor digitorum lateralis and extensor carpi ulnaris) were dissected and sectioned at 40μm and probed with a presynaptic antibody cocktail (as in Chapter 3, section 3.2.2) to visualise the NMJ. All sections were stained for post-synaptic acetylcholine receptors (AChRs) using AlexaFluor conjugated 594nm α-bungarotoxin (α-BTx, 1:200, Molecular Probes/Invitrogen) for 30 minutes. Sections were washed thoroughly in PBS followed by mounting in Permafluor mounting media. Gastrocnemius sections were imaged using confocal microscopy (80μm stacks, 2μm interval, NIKON). Distal axons and NMJs were analysed using Image J. Forelimb muscle immunohistochemistry was quantitated using dual cube immunofluorescence (Leica DM-LB2, Leica).

4.2.8 Western blot

PBS perfused lumbar spinal cords (15μg) were homogenised in RIPA-Inhibit (RIPA-INH) buffer (RIPA buffer + trichostatin-a, (Sigma)), followed by centrifugation at 70,000g for 30 minutes at 4°C and re-suspension in RIPA-INH buffer. Protein expression was then evaluated by Western blot (Brunden et al., 2010; Cartelli et al., 2013). Blots were cut to remove the need for antibody stripping. Tubulin acetylation levels were used as a marker of microtubule stability (mouse monoclonal, 1:5000, Sigma Aldrich) and neurofilament M (NFM) for a cytoskeletal loading

control (rabbit polyclonal, 1:1000, Millipore). Choline acetyltransferase (ChAT) levels were measured as an indicator of a-MN loss (goat polyclonal, 1:200, Millipore) with GAPDH (rabbit polyclonal, 1:5000, Millipore) used as a loading control. Blots were imaged using a Chemi-Smart 5000 chemiluminescent imager and subsequent analysis completed using Image-J (NIH).

4.2.9 Pathology and Western blot statistical analysis

Analysis was performed using MS-Excel (Microsoft). Histological and Western blot analysis was completed using GraphPad Prism using one-way ANOVA with Tukey's post-hoc correction for multiple comparisons, or t-tests, respectively. Clinical evaluation was analysed using two-way analysis of variance (ANOVA) with Bonferroni post-hoc correction. Survival curve analysis (log-rank) was completed. $p < 0.05$ was considered significant. All results are expressed as mean ± standard deviation, or median for survival analysis.

4.3 Results

4.3.1 Epothilone D administration increases tubulin acetylation in the lumbar spinal cord

It has been previously reported that EpoD increases biomarkers of microtubule stability in the cortex of mice (Brunden et al., 2010). To evaluate whether EpoD had similar effects on the microtubule network in the spinal cord, mice were injected twice (day 1 and day 6) with 2mg/kg of EpoD, followed by Western blot analysis of the lumbar spinal cord. A monoclonal antibody specific for acetylated tubulin chemical modifications was utilised, as acetylation is enriched on stable microtubules (Janke, 2014). After two injections of 2mg/kg EpoD, Western blot of the lumbar region showed a significant ($p < 0.001$) increase in the levels of tubulin acetylation (EpoD: 2.296 $pix^2 \pm 0.3205$ pix^2; vehicle: 0.9402 $pix^2 \pm 0.1984$ pix^2) (Figure 4.1). This suggests that recurrent injections of 2mg/kg of EpoD are sufficient to increase microtubule stability in the CNS, specifically in the lumbar spinal cord.

4.3.2 Epothilone D treatment does not induce gliosis

Microtubule-targeting compounds such as EpoD are associated with the development of painful peripheral neuropathies when used at high doses (Argyriou et al., 2011). Although the dose used in the current investigation is approximately 1/20 the average dose used in cancer therapies, the large number of repeated injections used in the current study have not been previously reported. To investigate whether the treatment regime of 2mg/kg of EpoD (20 injections over 16 weeks) induced pathology associated with peripheral neuropathy, glia were specifically evaluated in the dorsal and ventral horns of the lumbar spinal cord (Figure 4.2 A) of wild-type mice. Astrocytes

FIGURE 4.1. Western blot of acetylated tubulin in the lumbar spinal cord of EpoD treated mice. Increased acetylated tubulin levels suggest an increase in the stability of the microtubule network in EpoD treated mice, compared to vehicle treated controls. ($P < 0.001$) (mean ± SD, n = 4 & 4 respectively).

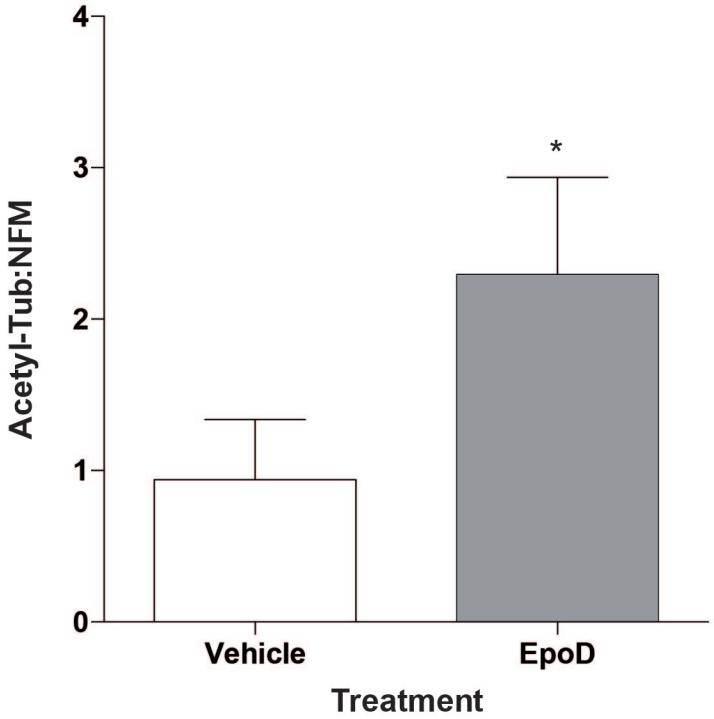
4
3
2
1
0
Acetyl-Tub:NFM
*
Vehicle
EpoD
Treatment

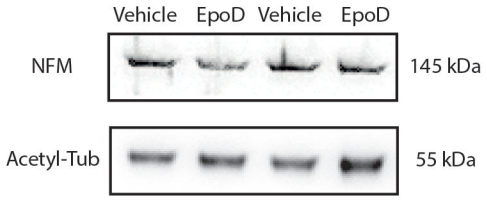
Vehicle
EpoD
Vehicle
EpoD
NFM
145 kDa
Acetyl-Tub
55 kDa

Figure 4.2. Confocal images of glia in the lumbar spinal cord of EpoD and vehicle treated wild-type mice. (A) Diagram of the mouse lumbar (L3) spinal cord, highlighting the dorsal and ventral horn, and the ventrally located spinal MNs. Medial motor neuron columns (A1) and lateral motor neuron columns (A2) are also highlighted. (B) Neither GFAP labelled astrocytes, (C) or Iba1 labelled microglia were activated by EpoD or vehicle treatment. Panels 1 – 8 represent higher magnification of dorsal and ventral horn. ($P > 0.05$) (mean ± SD, n = 6 & 4 respectively). Scale = 60 & 500μm.

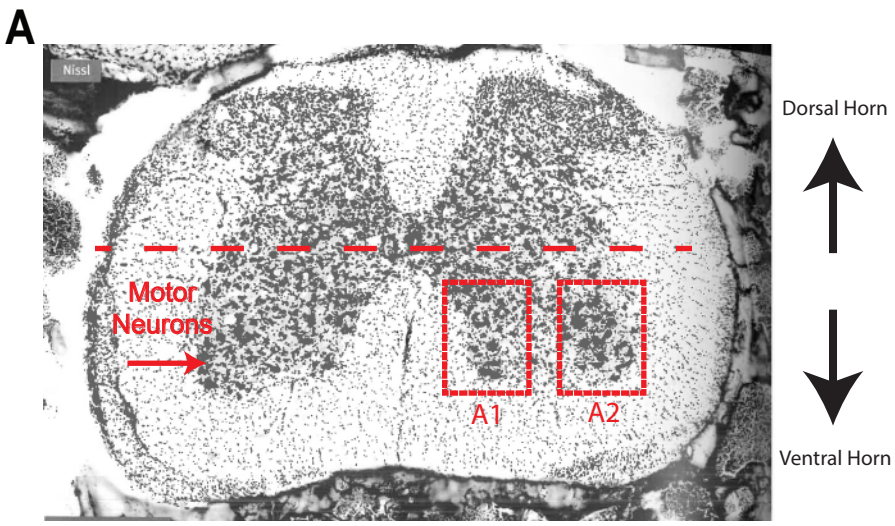

Mouse L3

Adapted from Watson, Paxinos and Kayalioglua (2009) 'The Spinal Cord'

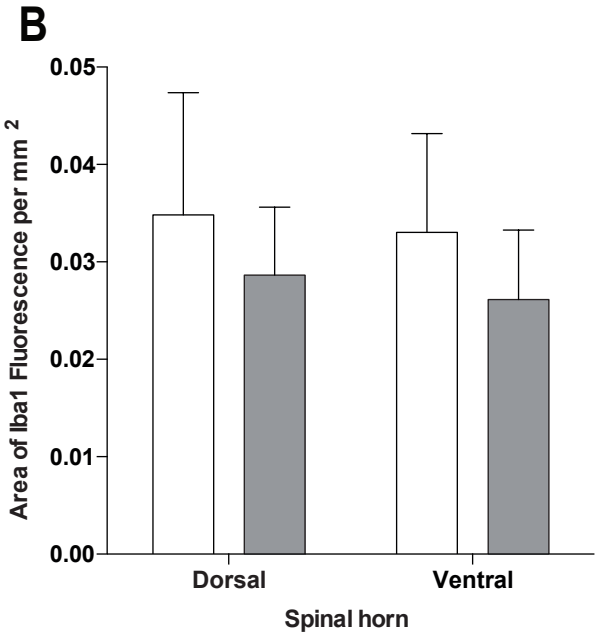

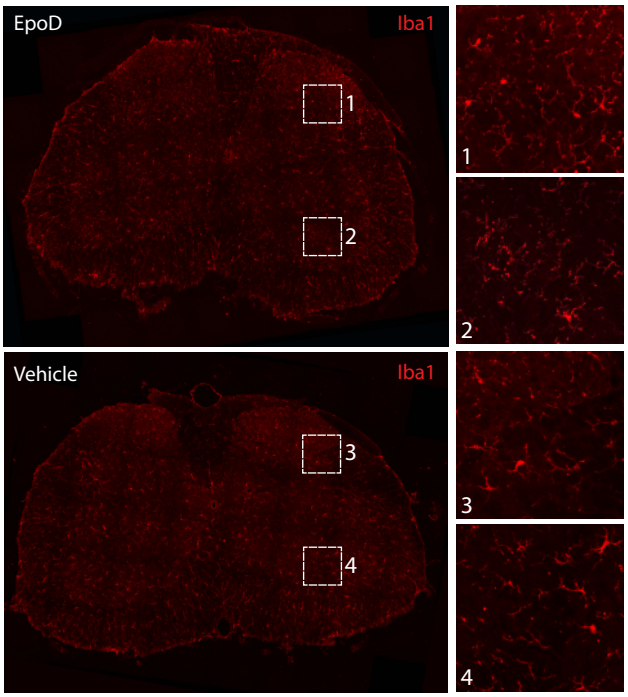

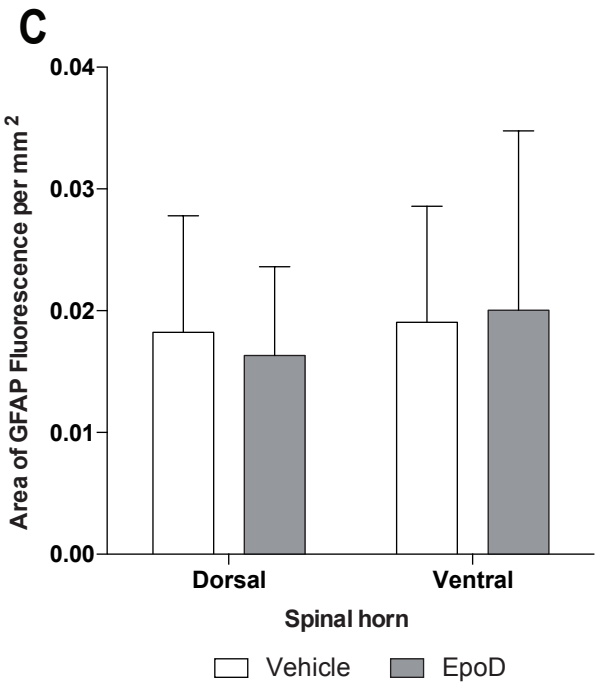

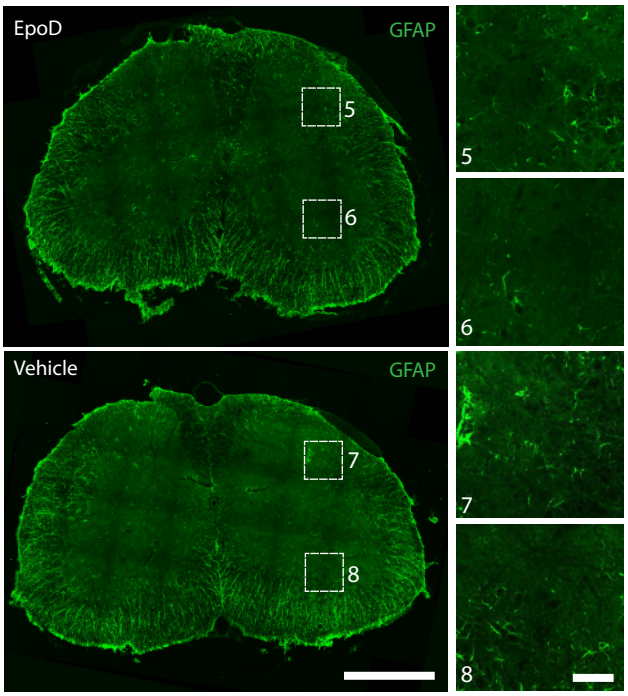

were labelled with GFAP, and the area of labelling compared between EpoD and vehicle treated wild-type mice. There was no significant difference ($p > 0.05$) between EpoD and vehicle treated mice in either the ventral horn (EpoD: 0.020 mm^2 ± 0.015; vehicle: 0.019 mm^2 ± 0.0095) or dorsal horn (EpoD: 0.016 mm^2 ± 0.007; vehicle: 0.018 mm^2 ± 0.0096) regions of the lumbar spinal cord (Figure 4.2 B). Similarly, microglia were labelled with Iba1, and the area of labelling compared between EpoD and vehicle treated wild-type mice. Again, there was no significant difference ($p > 0.05$) between EpoD and vehicle treated mice in either the ventral horn (EpoD: 0.026 mm^2 ± 0.007; vehicle: 0.033 mm^2 ± 0.010) or the dorsal horn (EpoD: 0.029 mm^2 ± 0.007; vehicle: 0.035 mm^2 ± 0.013) regions of the lumbar spinal cord (Figure 4.2 C). These results suggest that the current treatment regime does not induce glial activation in the lumbar spinal cord of mice.

4.3.3 Epothilone D treatment does not alter motor neuron survivability in wild-type mice

To ensure that chronic, low dose injections of EpoD were not neurotoxic, evaluation of a-MN number was undertaken in wild-type treated mice. Toluidine blue stained sections were used to identify large a-MNs located in the ventral horn of the lumbar spinal cord (Friese et al., 2009). The number of a-MNs per lumbar section was not significantly different ($p > 0.05$) between treatment groups (EpoD: 10.82 ± 2.51; vehicle: 11.13 ± 2.03) (Figure 4.3). This suggests that chronic low dose EpoD treatment is not neurotoxic to a-MNs of the lumbar spinal cord.

After initial experiments confirmed that the proposed treatment dosage altered acetylation in the spinal cord but did not trigger gliosis of a-MN toxicity, the proposed trial utilising both wild-type and $SOD1^{G93A}$ mice commenced. The trial consisted of 2mg/kg injections of EpoD every 5 days from 50 days of age. Disease progression was evaluated with motor behaviour (beginning at a baseline age of 49 days of age) consisting of rotarod performance and grip strength, neurological scoring and weight analysis, and survival. Subsequent pathology and molecular alterations were also evaluated.

4.3.4 Epothilone D treatment alters rotarod performance in $SOD1^{G93A}$ mice

Rotarod performance testing is an indirect measure of muscle strength, endurance and coordination of mice. Mice are placed on an accelerating rotating wheel, with latency until first rotation and latency until fall being recorded. In the current study it was measured three times a week between 49 and 145 days of age.

Figure 4.3. Histological analysis of toluidine blue stained MNs in EpoD treated wild-type mice. Quantitation of motor neuron numbers in toluidine blue stained sections (cell area ≥450 μm^2, ≤745 μm^2), dark staining cytoplasm, a dark nucleolus and ventral horn location (both lateral and medial motor columns). There was no significant difference in MN numbers between EpoD and vehicle treated wild-type mice ($P > 0.05$) (mean ± SD, n = 6 & 4 respectively). Scale = 30μm.

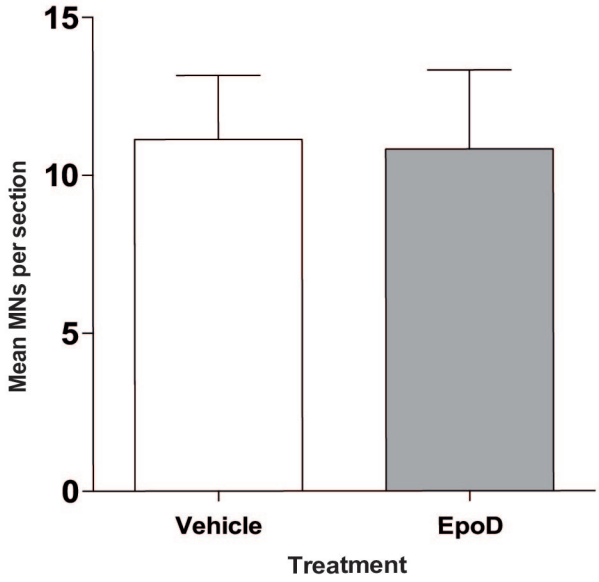
15
10
5
0
Mean MNs per section
Vehicle
EpoD
Treatment

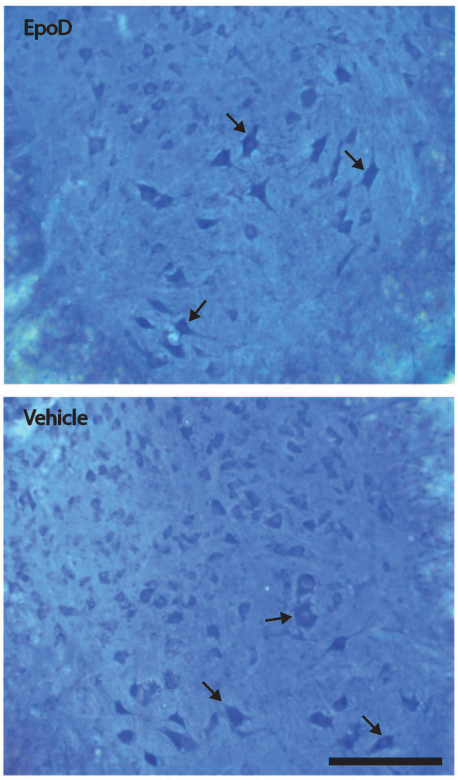
EpoD
Vehicle

4.3.4.1 Latency to first rotation

Rotarod performance, as measured by Latency to first rotation, is a measure of the time at which the mice can no longer walk continuously on the top of the rotating rod, and experience a full rotation without falling off (Figure 4.4 A). Statistical modelling using mixed-effect, piece wise polynomial models show no statistically significant difference between treatment groups at the start of measurement (Figure 4.4 B). However, it was revealed that $SOD1^{G93A}$ mice showed a deficit in rotarod performance when measured by latency to first rotation at the beginning of the study. Interestingly, wild-type mice showed a gradual decline in performance. At the conclusion of rotarod performance testing EpoD treated $SOD1^{G93A}$ mice could no longer balance on the rotarod bar at the 4rpm cut-off speed. During the trial wild-type mice were always able to complete the rotarod test regime.

Estimation of the age at which transgenic $SOD1^{G93A}$ mice show a significant decrease in rotarod performance identified that there was an earlier decrease in rotarod performance as measured by rotation at 114.0 days in EpoD treated mice. This occurred when their performance had reached 201.0 (187.1, 214.9) sec, compared to vehicle treated mice at 125.5 days, with a performance of 202.5 (187.5, 217.5) sec (Figure 4.4 B). This suggests that $SOD1^{G93A}$ mice have an early deficit in rotarod performance as measured by latency to first rotation, and that EpoD treatment is detrimental to muscle strength, endurance and/or coordination in the later stages of the disease.

4.3.4.2 Latency to fall

Rotarod performance, as measured by latency to fall, measures the time at which the mice can no longer grip/run on the rotating bar, thus falling into the enclosure (Figure 4.5 A). Statistical modelling of latency to fall using non-linear regression for wild-type mice and quadratic terms with spline functions for $SOD1^{G93A}$ mice determined that $SOD1^{G93A}$ mice showed a deficit in rotarod performance from the beginning of the study, with the two curves always significantly different ($p < 0.05$) (Figure 4.5 B). Modelling estimated that when comparing genotype, independent of treatment, $SOD1^{G93A}$ mice have a peak rotarod performance at 60.9 days of age, with a latency to fall of 304.7 (292.5, 315.9) sec, followed by deterioration in performance. In the later stages of the disease EpoD treated $SOD1^{G93A}$ mice deteriorate slightly more rapidly than vehicle treated controls, similar to rotarod performance when measured by latency to first rotation. These results suggest that $SOD1^{G93A}$ mice show symptoms at the commencement of the study, as revealed by latency to fall rotarod performance, compared to wild-type controls.

Figure 4.4. EpoD treatment alters rotarod performance, as measured by latency to rotate, in the later stages of the disease. (A) Behavioural data, with lines representing the mean of each genotype and treatment group. Grey dots signify individual mice. (B) Fitment of mixed effect polynomial models improves data representation. No effect due to EpoD treatment was identified early in the disease. However, at later stages, EpoD is significantly detrimental to rotarod performance, with performance declining in EpoD treated mice earlier than respective vehicle controls. Interestingly, $SOD1^{G93A}$ mice performance, regardless of treatment, was significantly worse than wild-type mice for the duration of the study. ($P < 0.05$), time in seconds (s), ($n = 12$ $SOD1^{G93A}$ + EpoD, $n = 12$ $SOD1^{G93A}$ + vehicle, $n = 8$ WT + EpoD, $n = 8$ WT + vehicle).

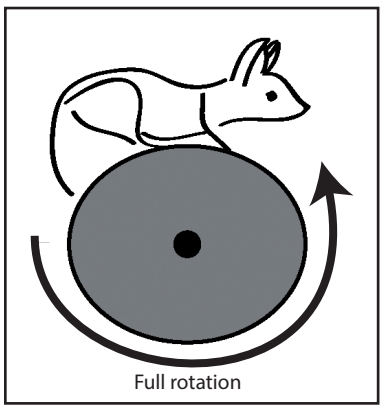

Adapted from McGee Lab, 2016

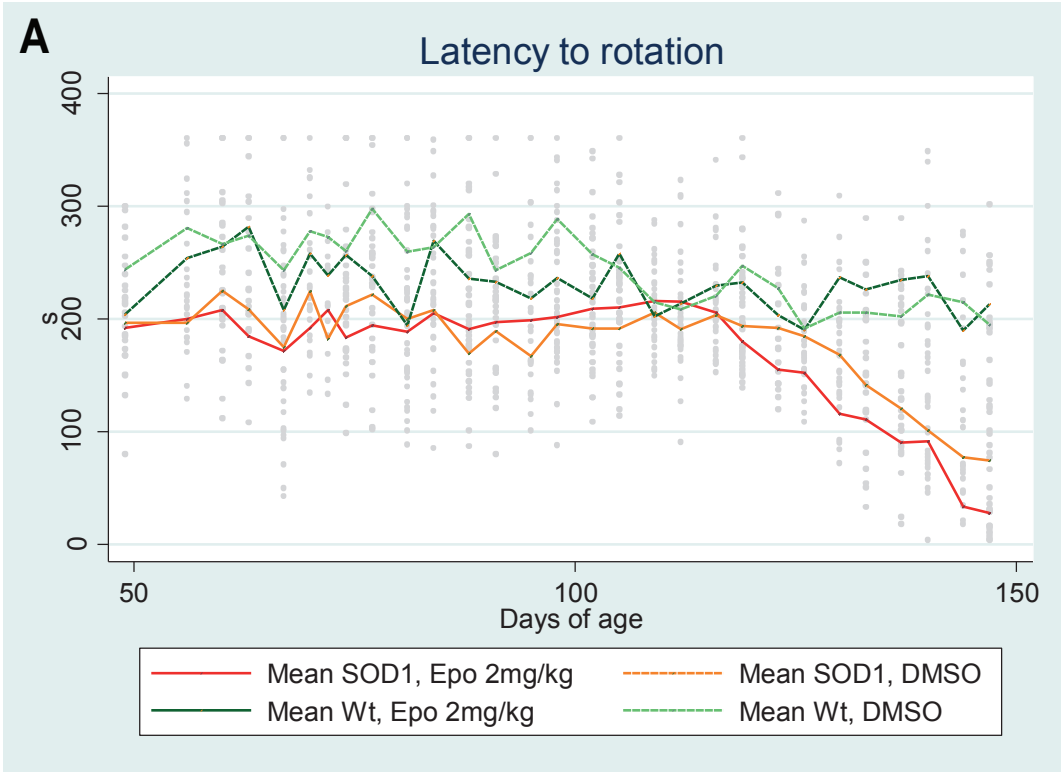

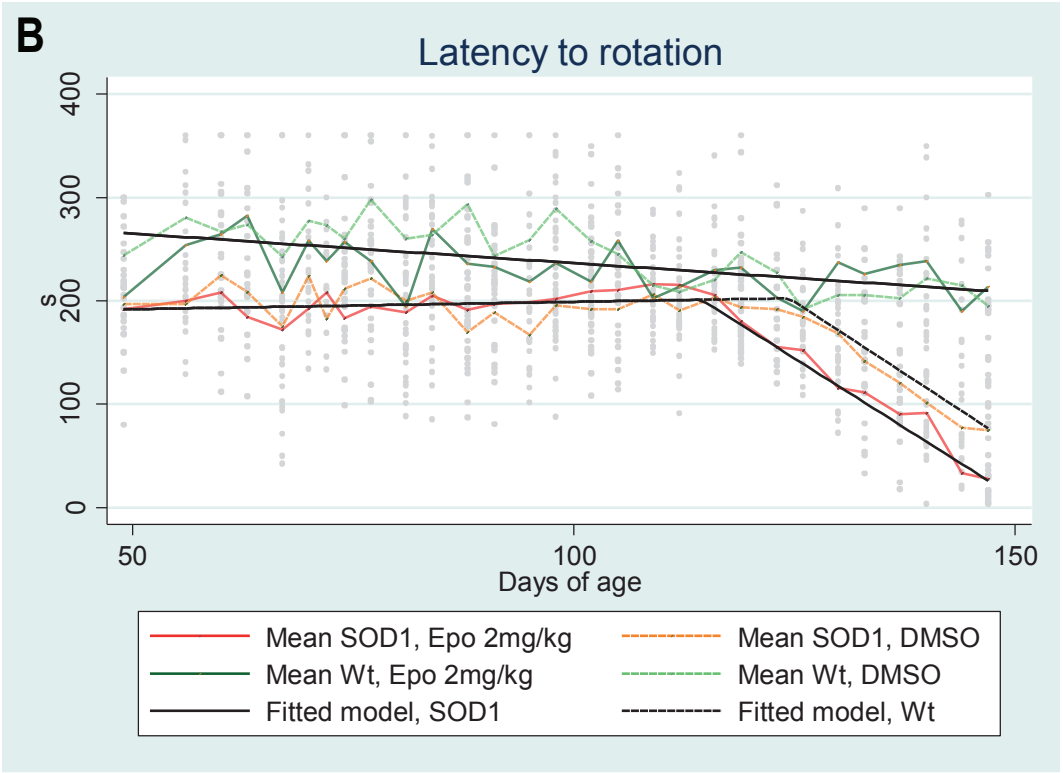

Figure 4.5. EpoD treatment alters rotarod performance, as measured by latency to fall, in the later stages of the disease. (A) Behavioural data, with lines representing the mean of each genotype and treatment group. Grey dots signify individual mice. (B) Fitment of non-linear regression for wild-type and quadratic terms for $SOD1^{G93A}$ mice. No effect due to EpoD treatment was identified early in the disease. The solid vertical red line represents peak performance for both EpoD and vehicle treated $SOD1^{G93A}$ mice. At later stages, EpoD is significantly detrimental to rotarod performance, with performance declining in EpoD treated mice earlier than respective vehicle controls. Similar to latency to first rotation, the performance of $SOD1^{G93A}$ mice, regardless of treatment, was significantly worse than wild-type mice for the duration of the study. ($P < 0.05$), time in seconds (s), (n = 12 $SOD1^{G93A}$ + EpoD, n = 12 $SOD1^{G93A}$ + vehicle, n = 8 WT + EpoD, n = 8 WT + vehicle).

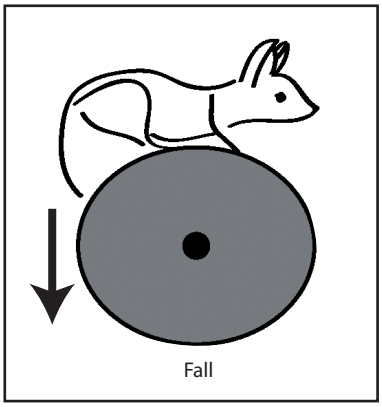

Adapted from McGee Lab, 2016

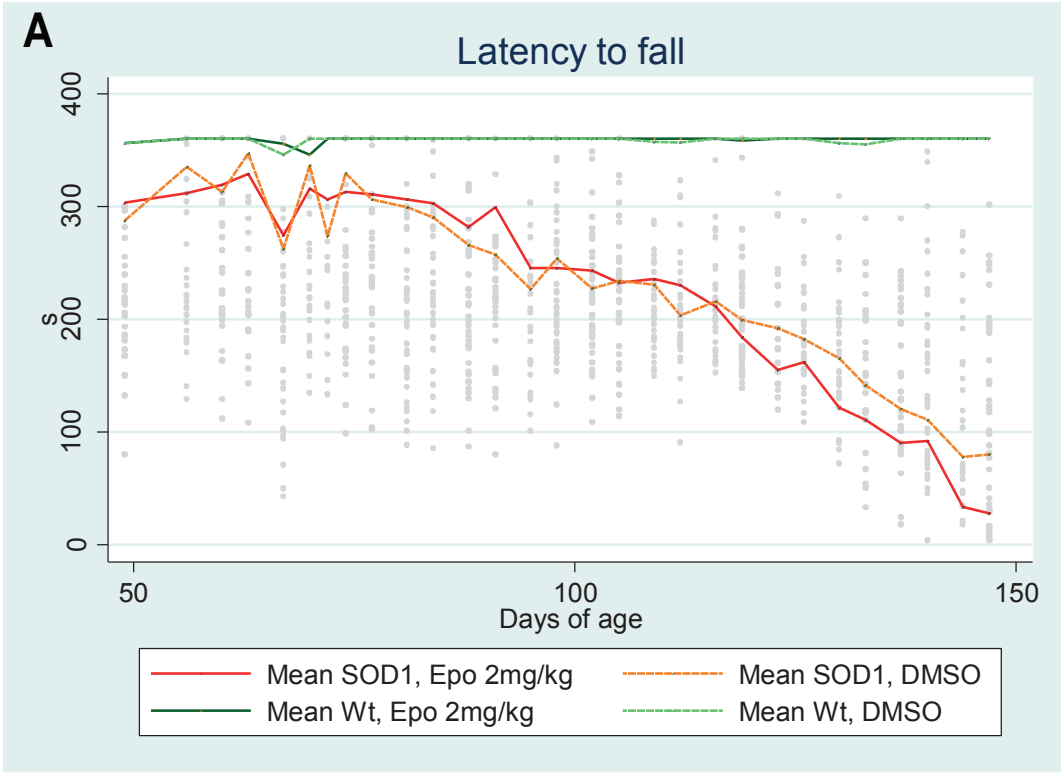

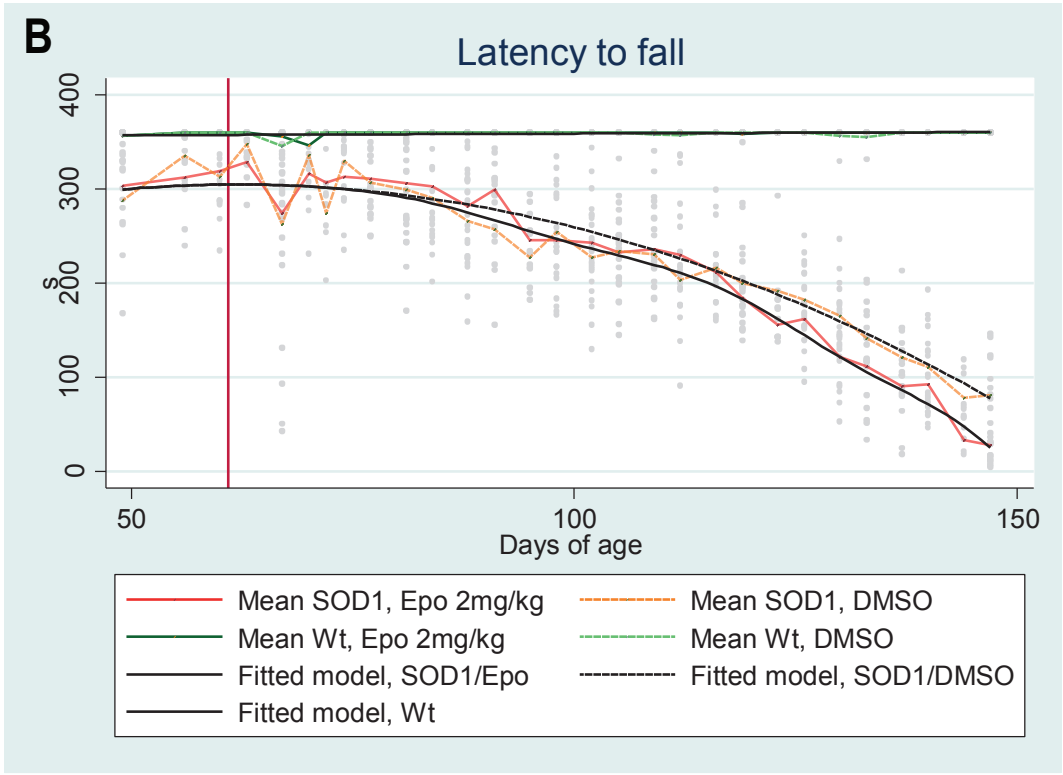

Further, it suggests that EpoD is detrimental to rotarod performance in the later stages of the disease.

4.3.5 Epothilone D treatment alters grip strength in SOD1^{G93A} mice

Grip strength measurements determine the highest force each animal can apply to the grip bars. As the SOD1^{G93A} mouse model is a model of hindlimb onset, with differential forelimb and hindlimb pathology (as identified in Chapter 3), forelimb alone and hindlimb alone measurements were taken.

4.3.5.1 Forelimbs

To determine whether EpoD effects disease progression, statistical modelling of forelimb grip strength using multi-level mixed effect non-linear regression was performed, coupled with fitting of break points. These measurements were taken between 49 and 145 days of age. There was no significant ($p > 0.05$) difference in disease progression as measured by forelimb grip strength between treatment groups in SOD1^{G93A} mice (Figure 4.6 A). Further, SOD1^{G93A} and wild-type mice had comparable forelimb grip strength at the beginning of the trial. However, SOD1^{G93A} mice showed a significant decline in grip strength until 75.5 days, when their forelimb grip was 0.095 (0.091, 0.099) kilograms of force (kgf), followed by a period of improvement, then a second decline at 98.8 days, with a local maximum of 0.099 (0.097, 0.102) kgf (Figure 4.6 B). These results suggest that EpoD treatment does not alter disease progression in the forelimb of SOD1^{G93A} mice.

4.3.5.2 Hindlimb analysis

To model hindlimb grip strength (Figure 4.7 A), multi-level non-linear regression models with break points were fitted to the data (Figure 4.7 B). Similar to forelimb data, no significant ($p > 0.05$) changes to hindlimb grip strength were identified when comparing treatment groups in in SOD1^{G93A} mice. Interestingly, when modelling data by genotype, irrespective of treatment, it was identified that SOD1^{G93A} and wild-type mice first become significantly different ($p < 0.05$) from each other at 49.60 days, with SOD1^{G93A} mice having an estimated grip strength of 0.084 (0.081, 0.088) kgf, and wild-type of 0.092 (0.086, 0.094) kgf. Hindlimb grip strength of SOD1^{G93A} mice is decreased from the beginning of measurements, compared to wild-type mice, with the optimal breakpoint of data suggesting a sharp decline at 93.0 days of age, where hindlimb grip strength is 0.078 (0.076, 0.081) kgf. This suggests that EpoD does not effect disease progression as

Figure 4.6. EpoD treatment does not alter forelimb grip strength during the disease time course. (A) Fitment of a multi-level mixed effect non-linear regression model accurately estimates forelimb grip strength. Grey dots signify individual mice. Forelimb grip strength was not significantly different between $SOD1^{G93A}$ mice treated with either EpoD or vehicle over the course of the study. Forelimb grip strength of $SOD1^{G93A}$ mice was not significantly different from wild-type controls at the beginning of the study, regardless of treatment. However, there was a significant decline in $SOD1^{G93A}$ mice as the disease progressed, compared to wild-type mice. (B) Mixed effect model representing two 'phases' of forelimb grip strength. Initially, $SOD1^{G93A}$ mice show an early, linear decline. This is then followed by a subtle improvement in grip strength, culminating in a slow, second decline in forelimb grip strength. ($P < 0.05$), (n = 12 $SOD1^{G93A}$ + EpoD, n = 12 $SOD1^{G93A}$ + vehicle, n = 8 WT + EpoD, n = 8 WT + vehicle).

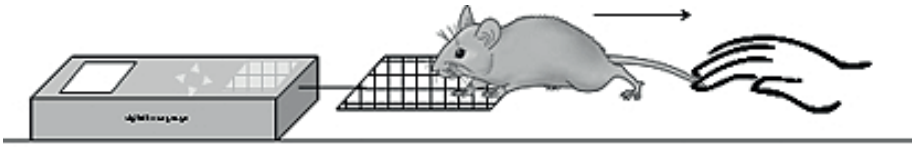

Adapted from Pirog et al 2010

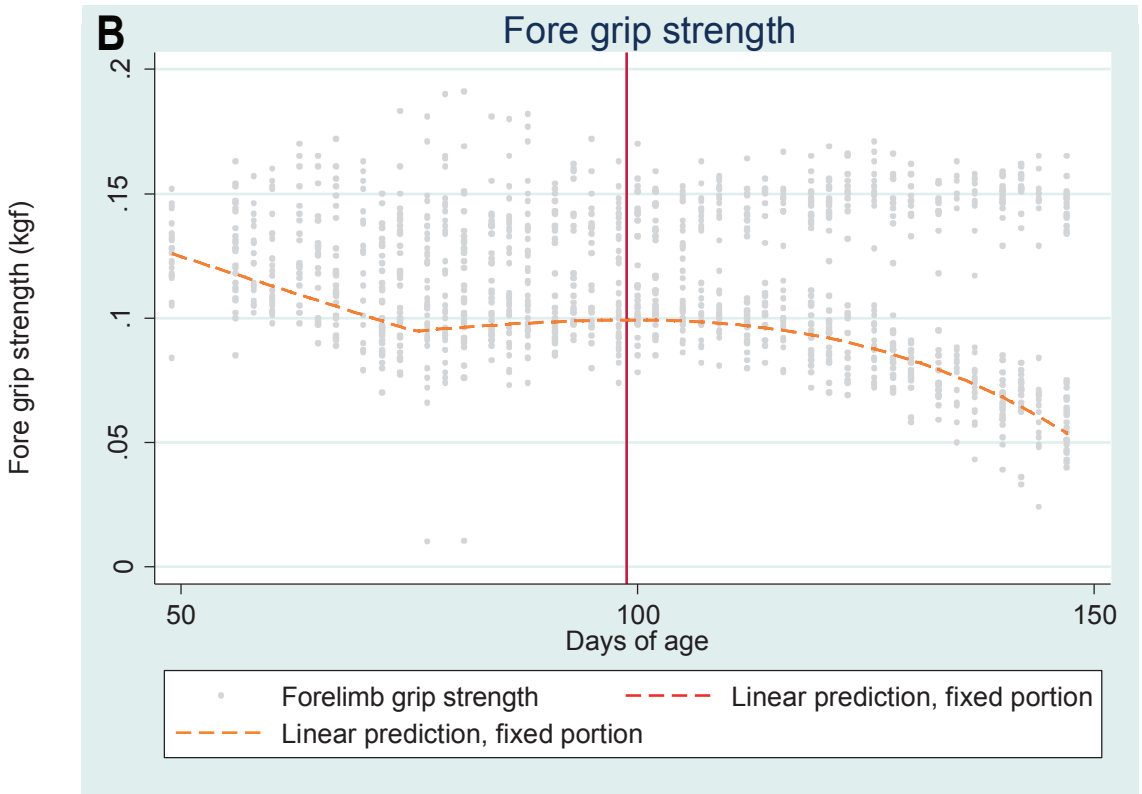

Figure 4.7. EpoD treatment does not alter hindlimb grip strength during the disease time course. (A) Behavioural data, with lines representing the mean of each genotype and treatment group. Grey dots signify individual mice. (B) Fitment of a multi-level mixed effect non-linear regression model accurately estimates hindlimb grip strength. Hindlimb grip strength was not significantly different between $SOD1^{G93A}$ mice treated with either EpoD or vehicle over the course of the study. Hindlimb grip strength was significantly different between $SOD1^{G93A}$ mice and wild-type early in the study, regardless of treatment. Hindlimb grip strength of $SOD1^{G93A}$ mice decreased from the beginning of measurements, with a notable decline in grip strength occurring mid way through the study. ($P < 0.05$), ($n = 12$ $SOD1^{G93A}$ + EpoD, $n = 12$ $SOD1^{G93A}$ + vehicle, $n = 8$ WT + EpoD, $n = 8$ WT + vehicle).

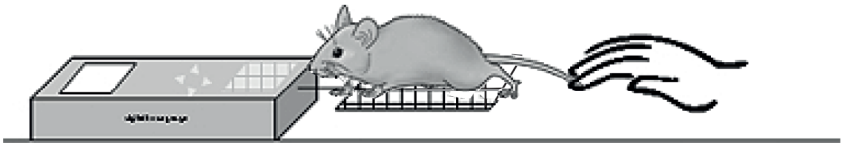

Adapted from Pirog et al 2010

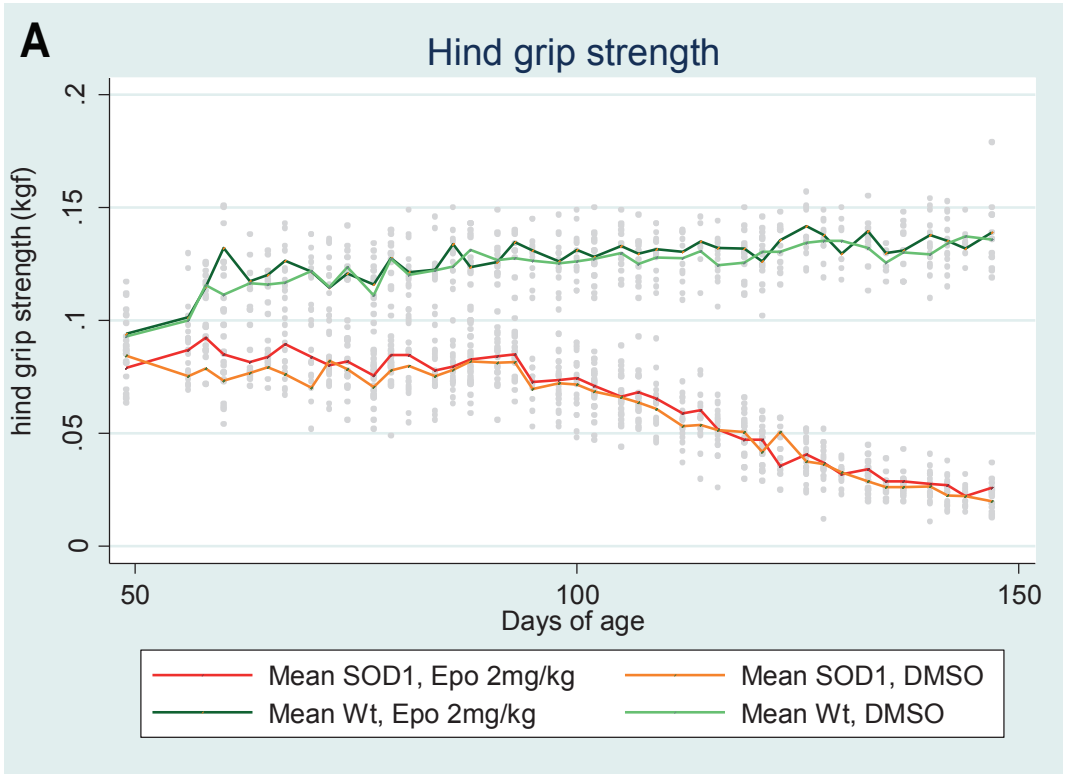

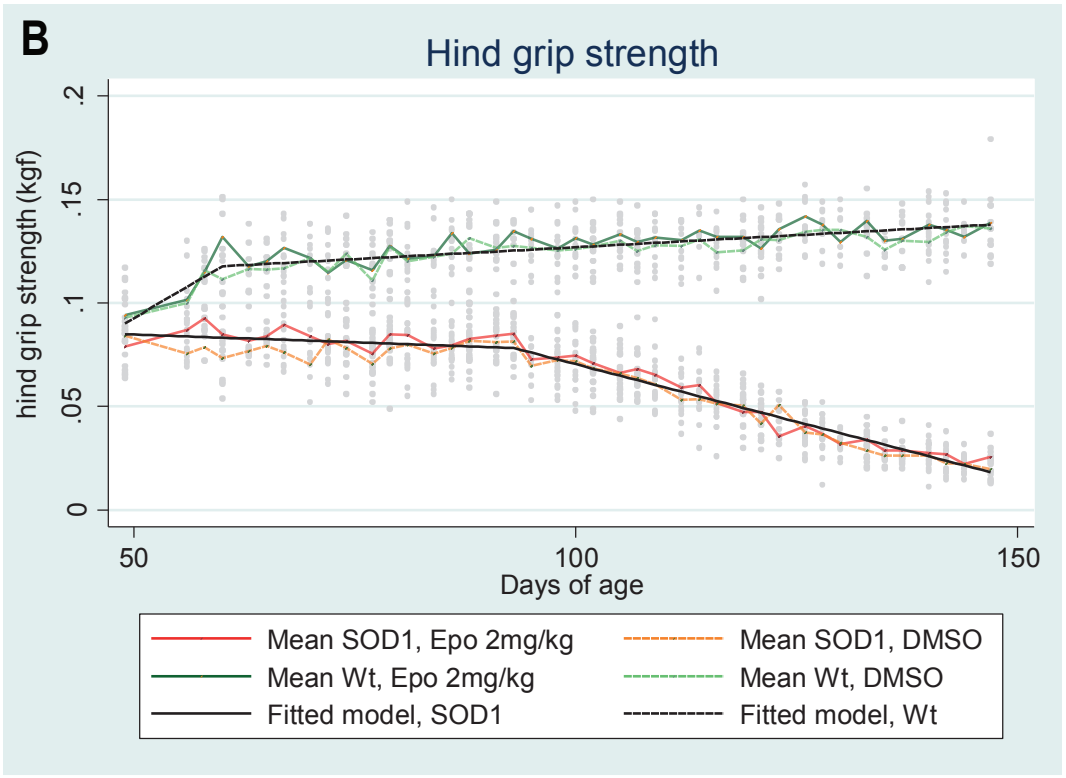

measured by hindlimb grip strength, and that SOD1^{G93A} mice show early onset disease, compared to wild-type mice, as measured by hindlimb grip strength.

4.3.6 Epothilone D treatment does not alter weight loss trajectory in SOD1^{G93A} mice

Utilising weight to track disease progression is a standard method of analysis for the SOD1^{G93A} mouse model (Schafer and Hermans, 2011). The effects of time, genotype and treatment on body weight were evaluated from 49 to 150 days of age (Figure 4.8 A). Statistical modelling of weight used cubic spline functions for both SOD1^{G93A} and wild-type mice (Figure 4.8 B). It was determined that there was no significant ($p > 0.05$) difference between treatment groups in SOD1^{G93A} mice, suggesting EpoD treatment does not effect weight. However, modelling estimated that SOD1^{G93A} mice weighed significantly ($p < 0.05$) less than their wild-type littermates, regardless of treatment, at 49.10 days of age (SOD1^{G93A}: 23.1g (22.7, 23.6); wild-type: 23.8g (23.4, 24.4). This is followed by a gradual decline in weight of SOD1^{G93A} mice from their predicted maximum at 116.4 days of age, where the estimated weight is 24.2g (23.8, 24.7). This surprising result suggests that SOD1^{G93A} mice already show symptoms (independent of treatment) at the commencement of the trial. This suggests that either our SOD1^{G93A} high copy number colony shows onset prior to 50 days of age when determined by weight and that the methods of measurement and analysis (statistical modelling) have increased fidelity.

4.3.7 Epothilone D treatment effects neurological symptoms in the later stages of disease in SOD1^{G93A} mice

A neurological evaluation based on the appearance of the SOD1^{G93A} mice is used to track the progression of the clinical phenotype (Weydt et al., 2003). The first clinical sign of onset identified in the SOD1^{G93A} mice was hindlimb tremors and difficulty extending hindlimbs whilst suspended by the tail, followed by progressive or simultaneous gait abnormalities, ultimately leading to paralysis and death (Weydt et al., 2003). Using an amended 4-point scoring system described by Weydt and Colleagues (2003), representing clinical progression as a percentage of the maximum clinical score, neurological assessment of mice revealed EpoD treatment significantly ($p < 0.01$) accelerated the time of disease onset, compared to vehicle controls, with onset in the EpoD treated mice occurring at 77 days of age (EpoD: 88.46% ± 12.97%), compared to EpoD treated wild-type controls, which showed no overt neurological symptoms throughout the trial. This presented as an increase in hindlimb tremors and decreased leg extension (Figure 4.9 A). Vehicle treated SOD1^{G93A} mice significantly ($P < 0.001$) differed from vehicle treated wild-type controls one week later, at 84 days of age (vehicle: 80.77% ± 10.96%).

Figure 4.8. EpoD treatment does not alter weight during the disease time course. (A) Behavioural data, with lines representing the mean of each genotype and treatment group. Grey dots signify individual mice. (B) Fitment of a cubic spline function accurately estimates weight trajectory. Hindlimb grip strength was not significantly different between EpoD or vehicle treated $SOD1^{G93A}$ mice over the course of the study. Weight, and its trajectory, was significantly different between $SOD1^{G93A}$ mice and wild-type, regardless of treatment, from the beginning for the study. ($P < 0.05$), (*n* = 12 $SOD1^{G93A}$ + EpoD, *n* = 12 $SOD1^{G93A}$ + vehicle, *n* = 8 WT + EpoD, *n* = 8 WT + vehicle).

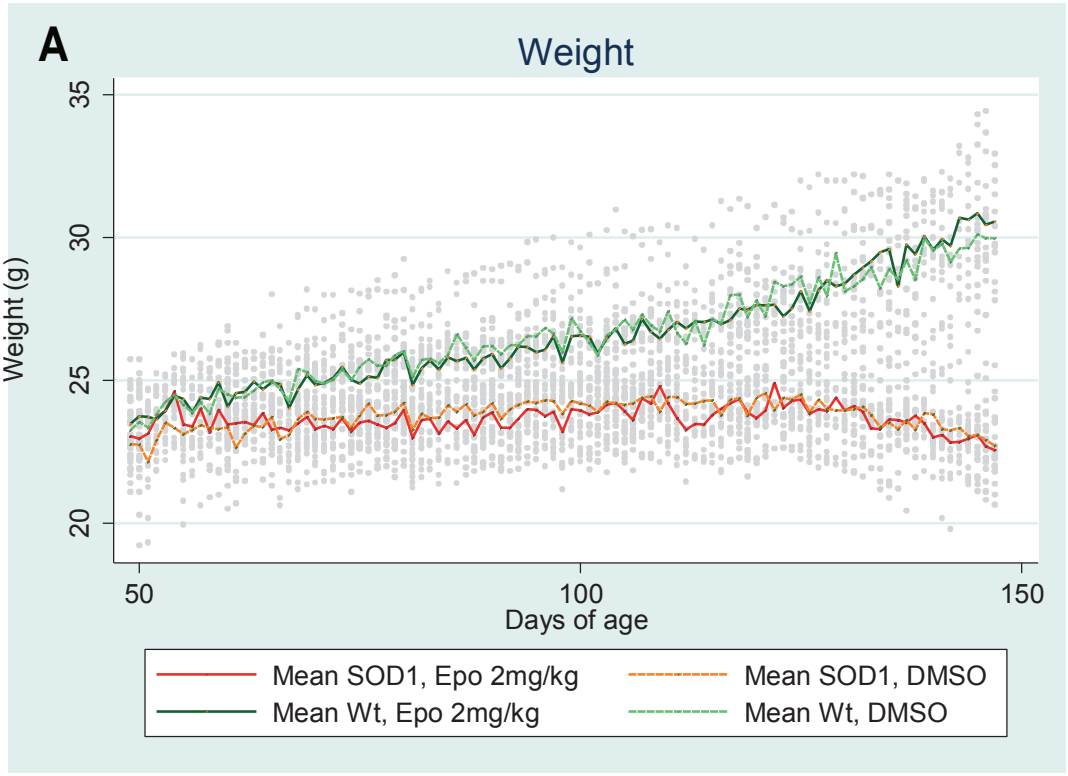
A
Weight
Weight (g)
35
30
25
20
50
100
150
Days of age
Mean SOD1, Epo 2mg/kg
Mean Wt, Epo 2mg/kg
Mean SOD1, DMSO
Mean Wt, DMSO


B
Weight
Weight (g)
35
30
25
20
50
100
150
Days of age
Mean SOD1, Epo 2mg/kg
Mean Wt, Epo 2mg/kg
Fitted model, SOD1
Mean SOD1, DMSO
Mean Wt, DMSO
Fitted model, Wt

Figure 4.9. EpoD treatment is detrimental to neurological score and survival. (A) EpoD treated $SOD1^{G93A}$ mice exhibit a significantly ($p < 0.01$) worse neurological phenotype one week earlier than vehicle treated $SOD1^{G93A}$ mice, when compared to respective wild-type controls. In the later stages of the disease, EpoD treated $SOD1^{G93A}$ mice show a greater decline in neurological score, compared to vehicle treated $SOD1^{G93A}$ mice. (B) EpoD treated $SOD1^{G93A}$ mice have a significantly ($p < 0.01$) reduced life span, compared to vehicle treated $SOD1^{G93A}$ controls. (mean ± SD, $n = 12$ $SOD1^{G93A}$ + EpoD, $n = 12$ $SOD1^{G93A}$ + vehicle, $n = 8$ WT + EpoD, $n = 8$ WT + vehicle.

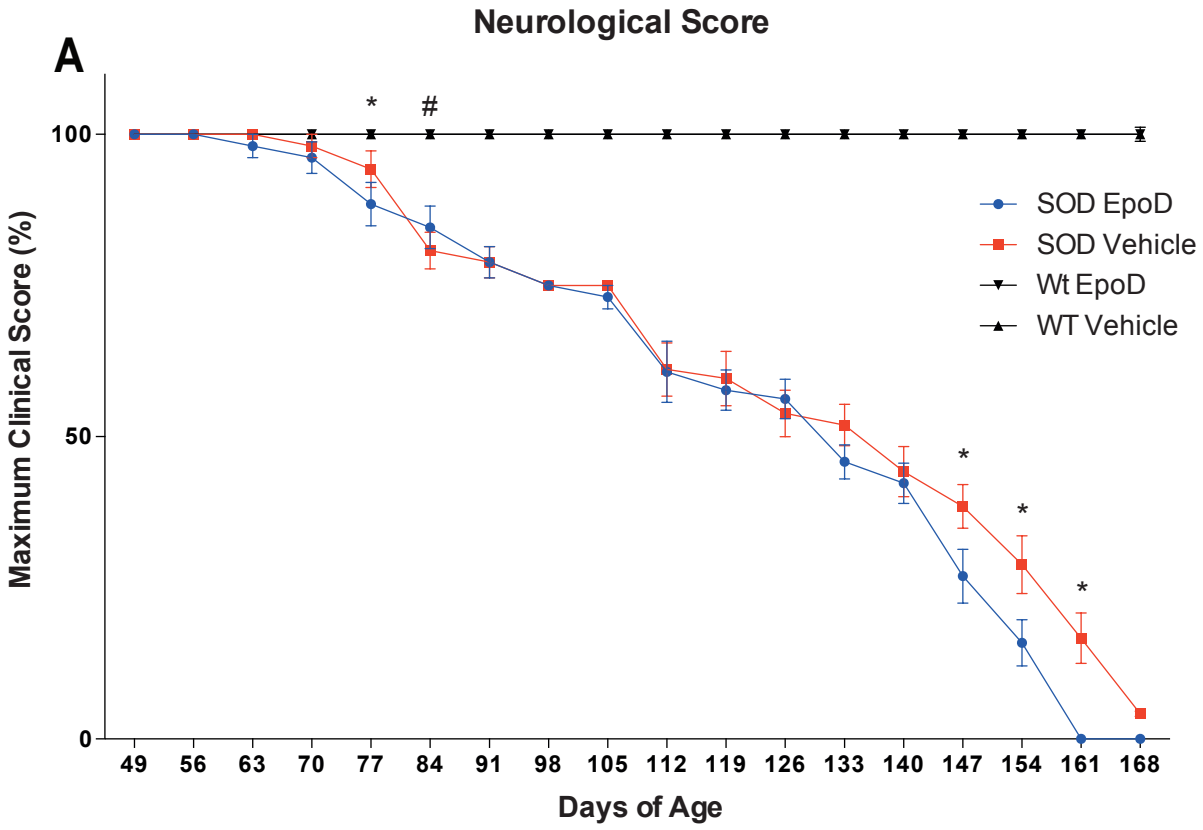
A
Neurological Score
Maximum Clinical Score (%)
100
50
0
*
#
*
*
*
SOD EpoD
SOD Vehicle
Wt EpoD
WT Vehicle
49 56 63 70 77 84 91 98 105 112 119 126 133 140 147 154 161 168
Days of Age

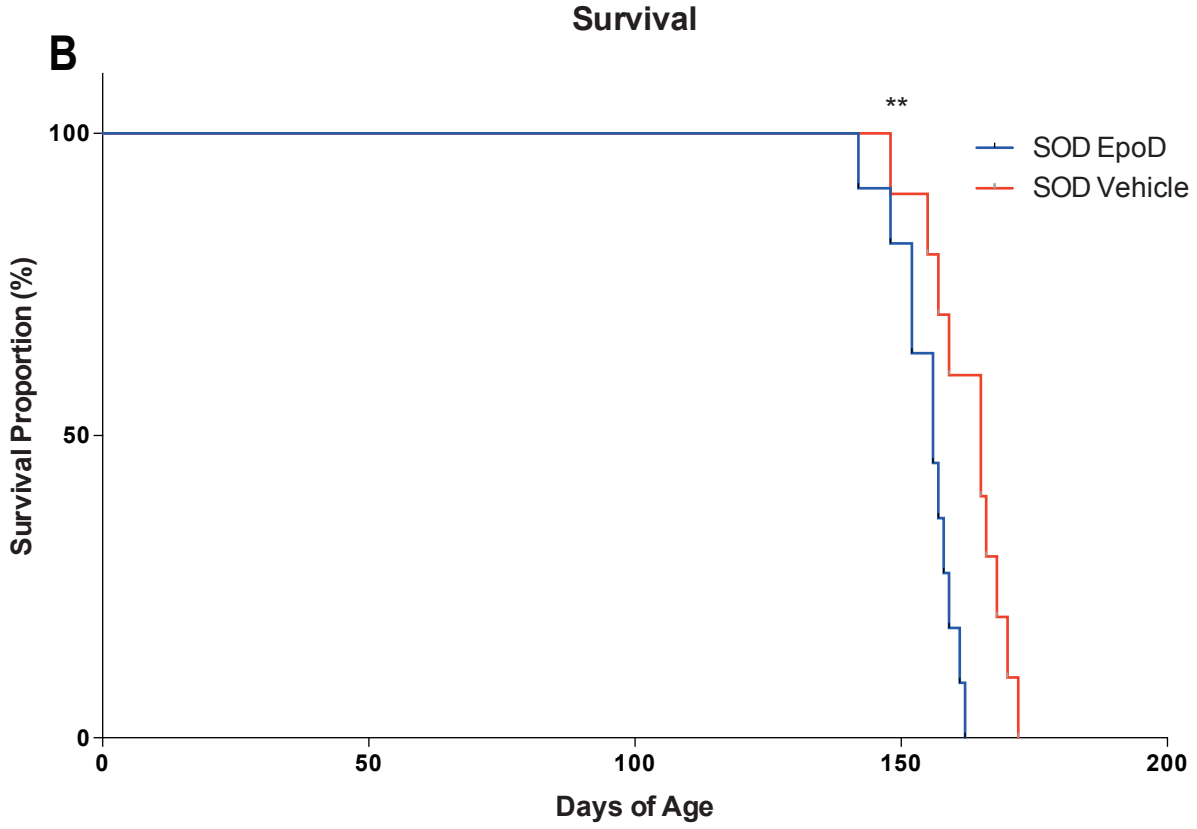
B
Survival
Survival Proportion (%)
100
50
0
**
SOD EpoD
SOD Vehicle
0 50 100 150 200
Days of Age

Neurological symptoms continued to deteriorate in EpoD treated mice at a higher rate, compared to vehicle controls, with EpoD injected $SOD1^{G93A}$ mice showing significantly ($P < 0.01$) reduced clinical scores compared to vehicle treated $SOD1^{G93A}$ mice at 147 days of age, and continuing until end stage (EpoD: 26.92% ± 16.01%; vehicle: 38.46% ± 12.97%) (Figure 4.9 A). This suggests that EpoD treatment hastens neurological symptoms in both early and late stages of the disease, and is detrimental to neurological functions in $SOD1^{G93A}$ mice. Wild-type mice treated with either EpoD or vehicle showed no overt neurological symptoms due to treatment.

4.3.8 Epothilone D treatment decreases the life span of $SOD1^{G93A}$ mice

To determine whether there was an effect of EpoD treatment on survival, the age of mice (days) was recorded until the mice reached the studies ethical end stage cut off, defined as mice that reach 80% of their maximal weight or had increasingly affected righting reflexes. Once this stage was research the mice were perfused. Survival analysis estimated that EpoD treatment significantly ($p < 0.01$) decreased the life span of $SOD1^{G93A}$ mice, compared to vehicle treated controls (mode days of age, EpoD: 156 days; vehicle: 165 days) (Figure 4.9 B). This suggests that the treatment regime of 2mg/kg EpoD is toxic to $SOD1^{G93A}$ mice, and taken with rotarod and neurological data, is detrimental in the later stages of the disease.

4.3.9 Epothilone D treatment alters gliosis in $SOD1^{G93A}$ mice

Cellular pathology was evaluated to determine specific cell type and structural changes after EpoD treatment. Immunohistochemical analysis of astrocytes using GFAP as a marker showed a significant ($p < 0.01$) increase in GFAP fluorescence area in the ventral, and surprisingly also the dorsal, lumbar spinal cord of EpoD treated mice, compared with vehicle treated controls (dorsal, EpoD: $0.185mm^2 \pm 0.039mm^2$; vehicle: $0.088mm^2 \pm 0.021mm^2$) (Figure 4.10 A), (ventral, EpoD: $0.159mm^2 \pm 0.035mm^2$; vehicle: $0.088\ mm^2 \pm 0.138mm^2$) (Figure 4.10 B). There was no significant difference between treatment groups at earlier time points, however a steady increase in GFAP expression area was noted as the disease phenotype progresses. Cellular morphology appeared similar between both treatment groups.

Similarly, immunohistochemical analysis of microglia found a significant ($p < 0.05$) increase in Iba1 fluorescence area in both the ventral and dorsal horn at end stage (dorsal, EpoD: $0.170mm^2 \pm 0.048mm^2$; vehicle: $0.099mm^2 \pm 0.023mm^2$) (Figure 4.10 C), (ventral, EpoD: $0.216mm^2 \pm 0.058$; vehicle: $0.122\ mm^2 \pm 0.025$) (Figure 4.10 D). There was no significant difference between

Figure 4.10. EpoD treatment induces gliosis in $SOD1^{G93A}$ mice. (A) Astrocyte (GFAP) activation is significantly ($p < 0.01$) increased at end stage in the dorsal, (B) and ventral horns, of the lumbar spinal cord in EpoD treated $SOD1^{G93A}$ mice, compared to vehicle controls. (C) Similarly, microglial (Iba1) activation is significantly ($p < 0.05$) increased at end stage in the dorsal, (D) and ventral horns, of the lumbar spinal cord in EpoD treated $SOD1^{G93A}$ mice, compared to vehicle controls. Both astrocytes and microglia morphology appear similar between EpoD and vehicle treated controls. ($P < 0.05$) (mean ± SD, n = 4 (50 & 70 days of age), 3 (140 days of age) and 5 (end stage), Scale = 500μm.

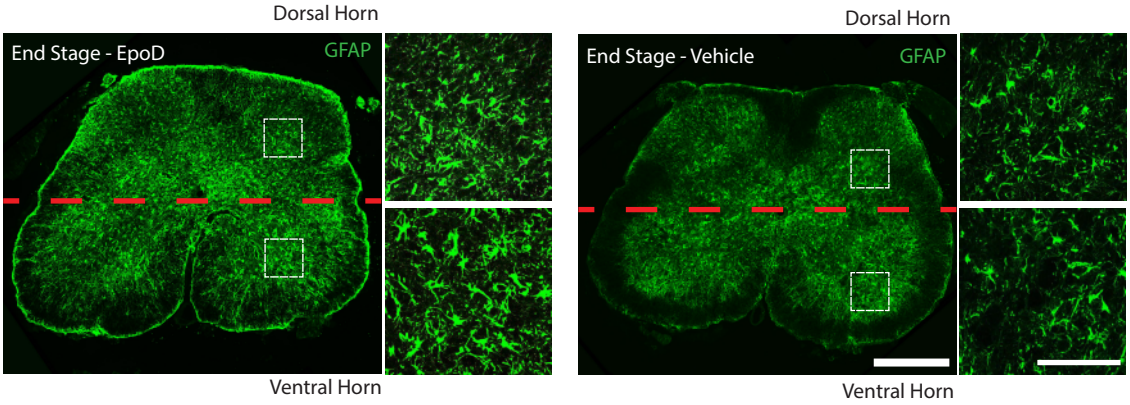
Dorsal Horn
End Stage - EpoD
GFAP
Ventral Horn
Dorsal Horn
End Stage - Vehicle
GFAP
Ventral Horn

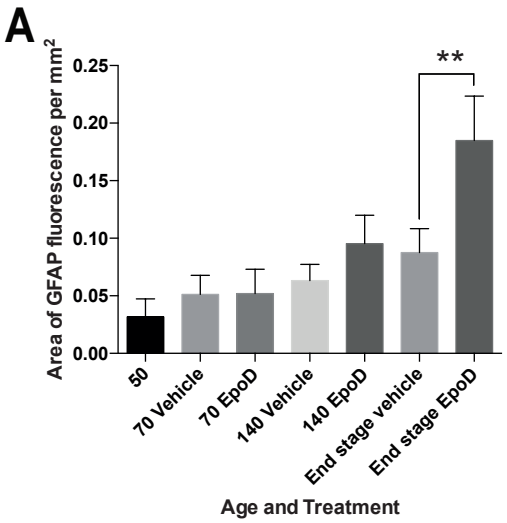
A
Area of GFAP fluorescence per mm2
0.25
0.20
0.15
0.10
0.05
0.00
**
50
70 Vehicle
70 EpoD
140 Vehicle
140 EpoD
End stage vehicle
End stage EpoD
Age and Treatment

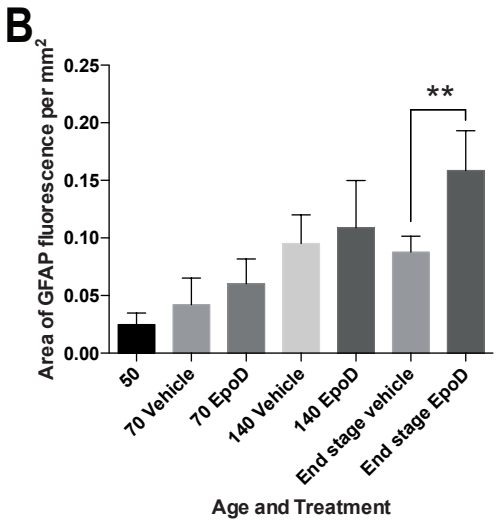
B
Area of GFAP fluorescence per mm2
0.25
0.20
0.15
0.10
0.05
0.00
**
50
70 Vehicle
70 EpoD
140 Vehicle
140 EpoD
End stage vehicle
End stage EpoD
Age and Treatment

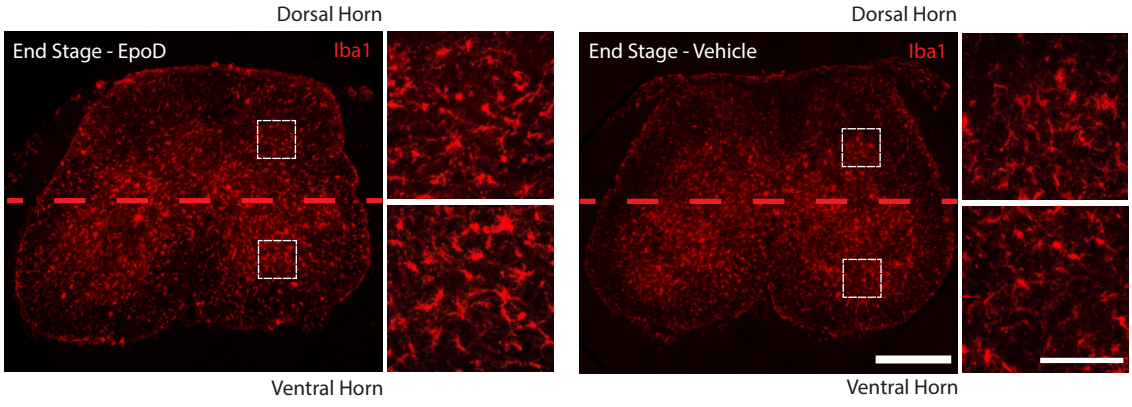
Dorsal Horn
End Stage - EpoD
Iba1
Ventral Horn
Dorsal Horn
End Stage - Vehicle
Iba1
Ventral Horn

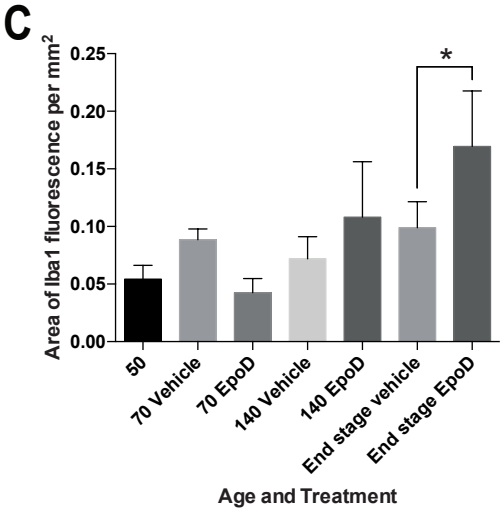
C
Area of Iba1 fluorescence per mm2
0.25
0.20
0.15
0.10
0.05
0.00
*
50
70 Vehicle
70 EpoD
140 Vehicle
140 EpoD
End stage vehicle
End stage EpoD
Age and Treatment

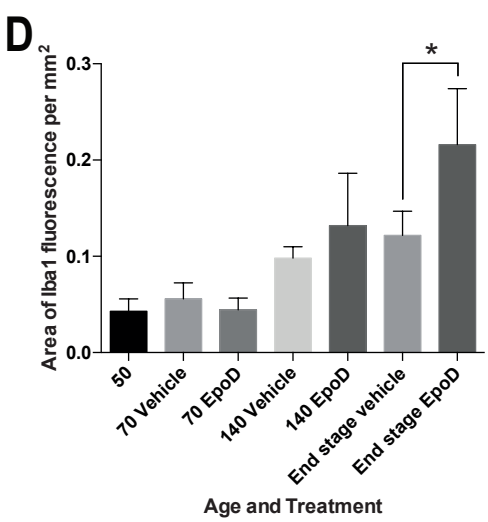
D
Area of Iba1 fluorescence per mm2
0.3
0.2
0.1
0.0
*
50
70 Vehicle
70 EpoD
140 Vehicle
140 EpoD
End stage vehicle
End stage EpoD
Age and Treatment

treatment groups at earlier time points. However, Iba1 fluorescence area increases as the disease progresses, irrespective of treatment. Cellular morphology appeared similar between both treatment groups.

4.3.10 Epothilone D may protect motor neurons from degeneration early in the disease time course of SOD1^{G93A} mice

The number of a-MNs in the lumbar spinal cord were compared between EpoD and vehicle treated SOD1^{G93A} mice. Investigations of toluidine blue stained lumbar spinal cord sections determined that treatment with EpoD protected a-MNs from degeneration at 70 days of age, with a-MN numbers per section comparable ($p > 0.05$) to that of 50 day old SOD1^{G93A} mice (50 day: 9.551 ± 2.111; 70 EpoD: 8.971 ± 2.583; 70 vehicle: 5.099 ± 1.143) (Figure 4.11 A). Indeed, 70 day old EpoD treated SOD1^{G93A} mice had significantly ($p < 0.05$) more a-MNs than 70 day old vehicle treated SOD1^{G93A} controls. However, a-MN numbers were similar (non-significantly different ($p > 0.05$)) between treatment groups in 140 days old and end stage SOD1^{G93A} mice.

To further investigate the number of a-MNs at end stage, specific quantitation using immunolabelling for SMI32, a marker for a-MNs (Tsang et al., 2000), and Western blot analysis was used. Using these approaches determined there was a significant ($p < 0.01$) decrease in SMI32 positive a-MN numbers in EpoD treated mice, compared to vehicle treated controls (EpoD: 2.797 ± 0.0687; vehicle: 3.373 ± 0.08862) (Figure 4.11 B). Further, Western blot analysis using anti-choline acetyltransferase (ChAT), an enzyme specific to a-MNs in the spinal cord, identified a significant ($p < 0.05$) decrease in ChAT protein levels in EpoD treated end stage spinal cords (EpoD: 0.412 pix^2 ± 0.024 pix^2; vehicle: 1.000 pix^2 ± 0.181 pix^2) (Figure 4.11 C). This suggests that although EpoD confers a-MN protection early in the disease, it appears to be neurotoxic in the later stages of disease.

4.3.11 Epothilone D treatment protects axons early in the disease time course of SOD1^{G93A} mice

As discussed in Chapter 1 and further determined in Chapter 3, axonal degeneration is a hallmark pathological event in the ALS distal neuromuscular circuitry, particularly in the hindlimb of the SOD1^{G93A} mouse model. For these studies SOD1^{G93A}xYFP mice were used to visualise distal morphology in 50, 70 and 140 day old mice, as in Chapter 3. Stabilisation of the microtubule cytoskeleton with EpoD resulted in a decrease in axonal pathology early in the disease. 70 day old EpoD treated SOD1^{G93A}xYFP mice showed a similar proportion of intact axons to the earlier

Figure 4.11. Possible early protection of MNs (arrows) in the lumbar spinal cord of EpoD treated SOD1^{G93A} mice. (A) MNs were protected at 70 days of age in EpoD treated SOD1^{G93A} mice, with significantly ($p < 0.05$) more MNs per section, compared to 70 day old vehicle treated mice. Indeed, 70 day old EpoD treated mice had comparable levels of MNs per section to the earlier, 50 day time point. However, at 140 days of age and end stage, MN numbers were not significantly ($p > 0.05$) different between EpoD and vehicle treated mice. (B) Further evaluation of end stage mice using immunohistochemical and fluorescence microscopy identified that there was a significant ($p < 0.01$) decrease in MN numbers (closed arrow) in the lumbar spinal cord in EpoD treated SOD1^{G93A} mice, with an increasing presence of dark 'voids' in the tissue (open arrow). (C) MN loss at end stage was confirmed with a significant ($p < 0.05$) decrease in choline acetyltransferase levels in the lumbar spinal cord of EpoD treated SOD1^{G93A} mice. ChAT (5 minute exposure) and GAPDH (20 second exposure) were measured on same membrane. ($P < 0.05$) (mean ± SD, n = 4 (50 & 70 days of age), 3 (140 days of age) and 5 (end stage). Scale (A) = 200μm, (B) = 50μm.

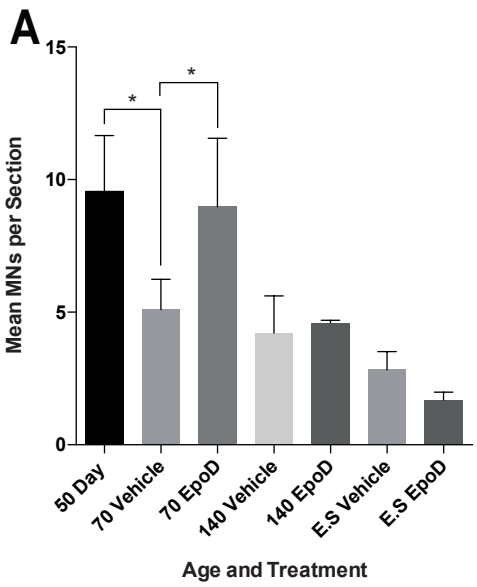
A
Mean MNs per Section
15
10
5
0
*
*
50 Day
70 Vehicle
70 EpoD
140 Vehicle
140 EpoD
E.S Vehicle
E.S EpoD
Age and Treatment

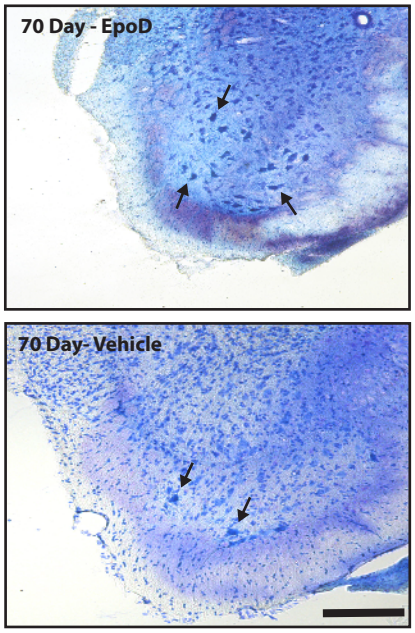
70 Day - EpoD
70 Day- Vehicle

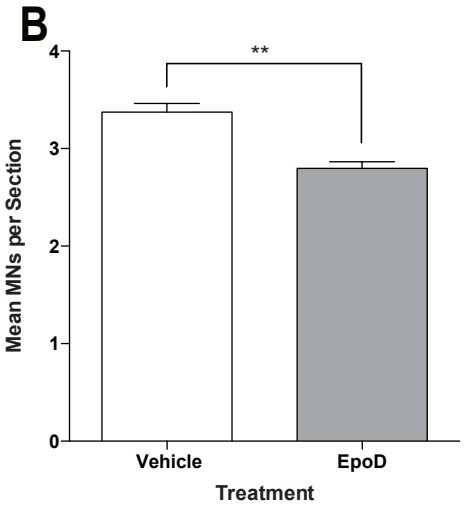
B
Mean MNs per Section
4
3
2
1
0
**
Vehicle
EpoD
Treatment

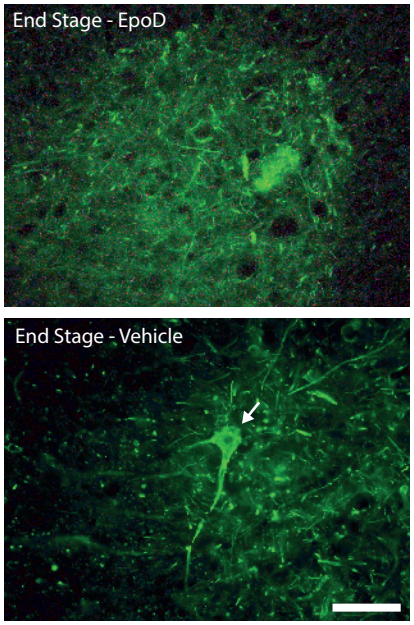
End Stage - EpoD
End Stage - Vehicle

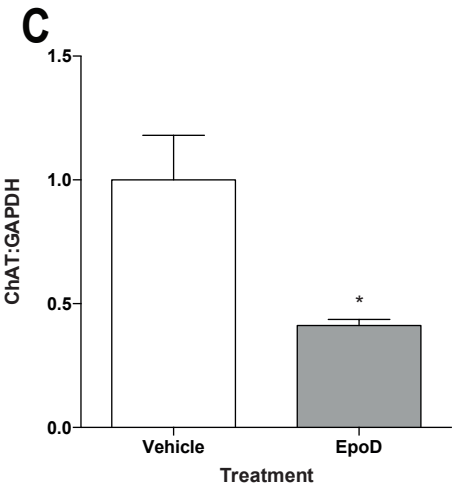
C
ChAT:GAPDH
1.5
1.0
0.5
0.0
*
Vehicle
EpoD
Treatment

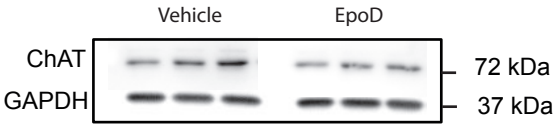
Vehicle
EpoD
ChAT
GAPDH
72 kDa
37 kDa

50 day time point, with vehicle treated mice SOD1^{G93A}xYFP mice having a significantly ($p < 0.05$) decreased proportion of intact axons compared to 50 day old mice (50 day: 82.253% ± 2.849; 70 EpoD: 77.773% ± 2.855; 70 vehicle: 68.988% ± 3.863) (Figure 4.12 A & C). However, the proportion of intact axons was not significantly ($p > 0.05$) different between treatments at 140 days of age in SOD1^{G93A}xYFP. This suggests that EpoD offers early axonal protection in the SOD1^{G93A}xYFP mouse model, limiting axonal degeneration.

Axonal branching was evaluated in EpoD treated SOD1^{G93A}xYFP mice. It was identified that there was no significant ($p > 0.05$) differences in axonal branch order between treatment groups in SOD1^{G93A}xYFP mice at any stage of the disease (Figure 4.11 B & D). However, as identified in the previous chapter, axonal branch order increased over the disease time course, suggesting increased collateral sprouting as the disease progresses.

4.3.12 Epothilone D treatment effects NMJ morphology but not synaptic colocalisation

To determine whether EpoD altered NMJ pathology, SOD1^{G93A}xYFP mice were used to probe for degeneration of the presynaptic compartment over the disease time course (Figure 4.13 A, Fully colocalised; B, partially colocalised; C, non-colocalised). Investigations found that there was no significant ($p > 0.05$) difference in the proportion of NMJs with fully colocalised YFP and α-BTx between treatment groups in SOD1^{G93A}xYFP mice (Figure 4.13 E). However, there was an age dependant loss of NMJ pre- and post-synaptic colocalisation as the disease progressed, independent of treatment. This suggests that EpoD treatment does not protect the synaptic compartment of the distal neuromuscular circuitry in the gastrocnemius muscle.

To investigate NMJ pathology at end stage, forelimb muscles were evaluated using presynaptic antibody cocktail as utilised in Chapter 3. This consisted of antibodies targeting the neurofilaments SMI-32 and SMI-312, as well as the pre-synaptic marker synaptophysin. Forelimb muscles were used at end stage, as the hindlimbs of SOD1^{G93A} mice are fully paralysed at end stage. As forelimbs are spared until later in the disease, these were chosen for end stage analysis. It was identified that there was no significant ($p > 0.05$) difference in pre-synaptic labelling between treatment groups in the forelimbs of SOD1^{G93A} mice (EpoD: 46.59% ± 3.30; vehicle: 42.73% ± 4.51) (Figure 4.13 F). This further suggests that EpoD does not have an effect on modifying NMJ pre- and post-synaptic colocalisation in SOD1^{G93A} mice.

Figure 4.12. Early protection of distal axons in the gastrocnemius muscle in EpoD treated $SOD1^{G93A}$ mice. (A) Axonal degeneration was decreased in EpoD treated $SOD1^{G93A}$ mice at 70 days, with EpoD treated mice showing comparable levels to the previous, 50 day old time point. Indeed, vehicle treated mice showed a significant decrease in the proportion of intact axons at 70 days, compared to the previous, 50 day old time point. However, at 140 days of age there was no significant difference in the proportion of intact axons between EpoD and vehicle treated mice. (B) Axonal branching was not significantly altered due to EpoD treatment, however, branching complexity increased as the disease progressed. (C) Confocal image of YFP labelled axons in $SOD1^{G93A}$ mice show beaded axons (open arrow) and fragmented axons (closed arrow). (D) Branch points (indicated by numbers 1 – 3) increased over the disease time course (arrow), with axonal branches numbered. ($P < 0.05$) (mean ± SD, n = 4 (50 & 70 days of age), 3 (140 days of age). Scale = 40μm.

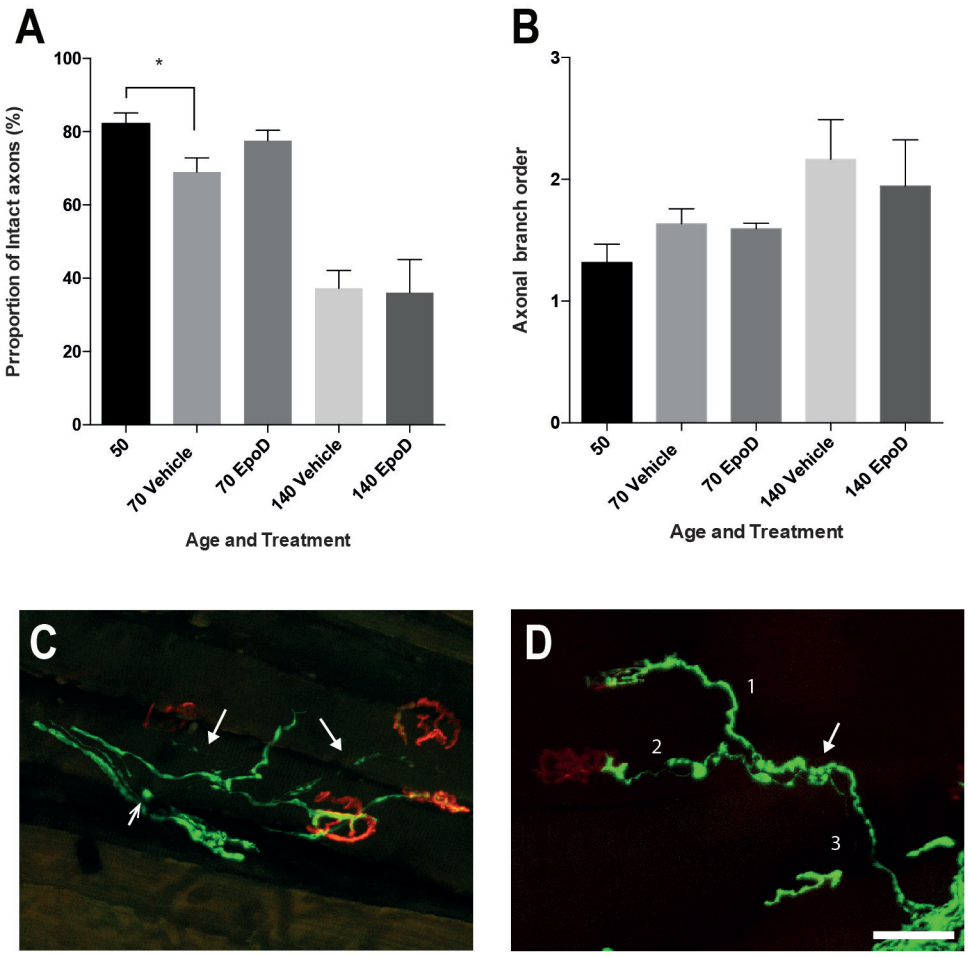
A
100
80
60
40
20
0
*
Prroportion of Intact axons (%)
50
70 Vehicle
70 EpoD
140 Vehicle
140 EpoD
Age and Treatment
B
3
2
1
0
Axonal branch order
50
70 Vehicle
70 EpoD
140 Vehicle
140 EpoD
Age and Treatment
C
D
1
2
3

Figure 4.13. No alterations to synaptic colocalisation, but improvements to NMJ morphology in EpoD treated $SOD1^{G93A}$ mice. (A) The normal 'pretzel' morphology of the NMJ with fully colocalised pre- and post-synaptic labelling. (B) As the disease progressed, partially colocalised NMJs, (C) and fully denervated NMJs became more pronounced. The overall size of NMJs also appeared smaller. (D) Remaining, fully colocalised NMJs showed altered morphology. (E) Statistical analysis revealed no significant difference in the proportion of full pre- and post-synapse colocalisation of NMJs between EpoD and vehicle treated $SOD1^{G93A}$ mice at any time point in the hindlimb gastrocnemius, (F) nor at end stage in the forelimb. (G) EpoD treated $SOD1^{G93A}$ mice showed improved NMJ morphology at 140 days, compared to vehicle treated controls. ($P < 0.05$) (mean ± SD, n = 4 (50 & 70 days of age), 3 (140 days of age); 80-100 NMJs, 4 sections. Scale = 20μm.

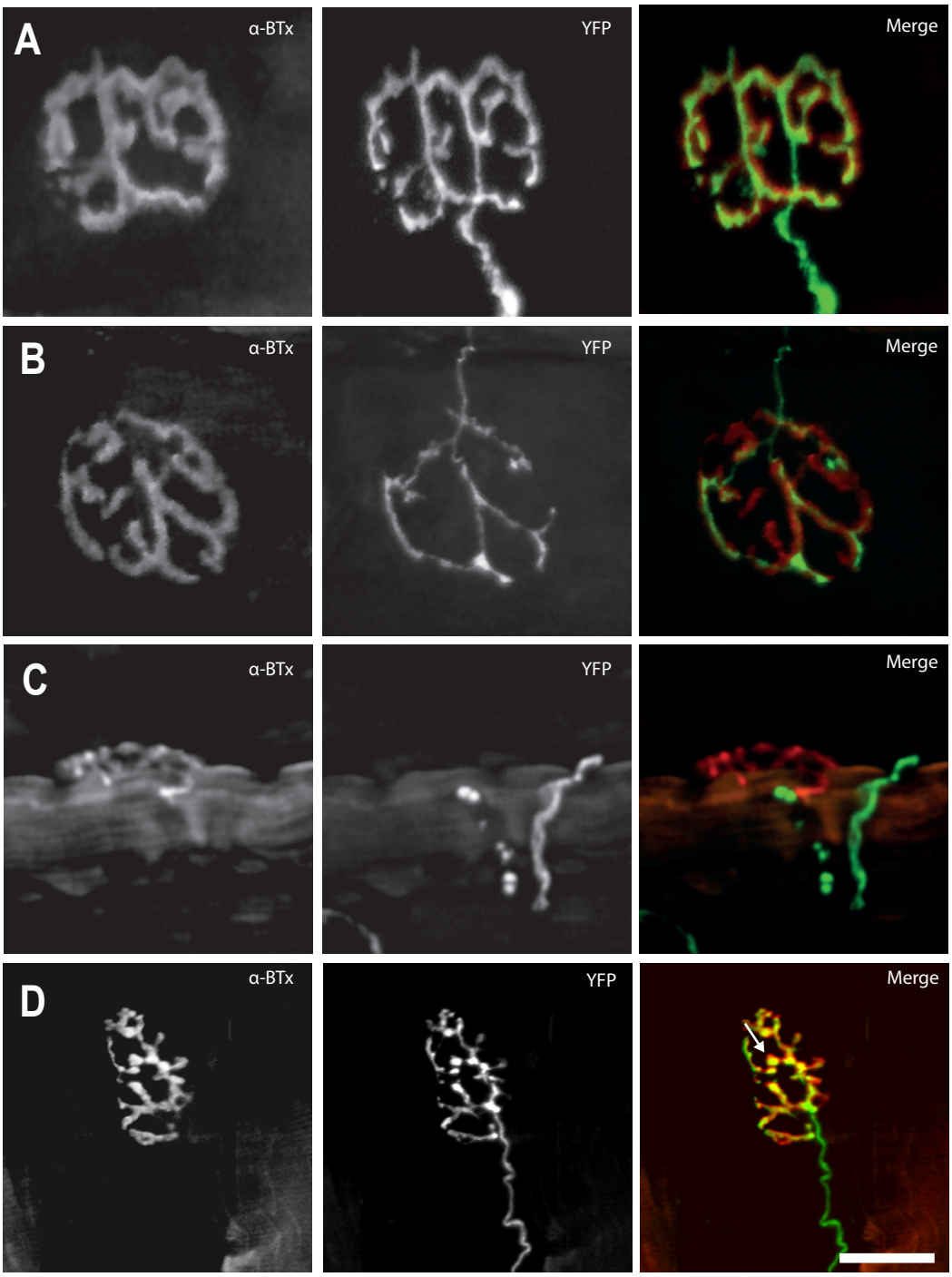
A
α-BTx
YFP
Merge
B
α-BTx
YFP
Merge
C
α-BTx
YFP
Merge
D
α-BTx
YFP
Merge

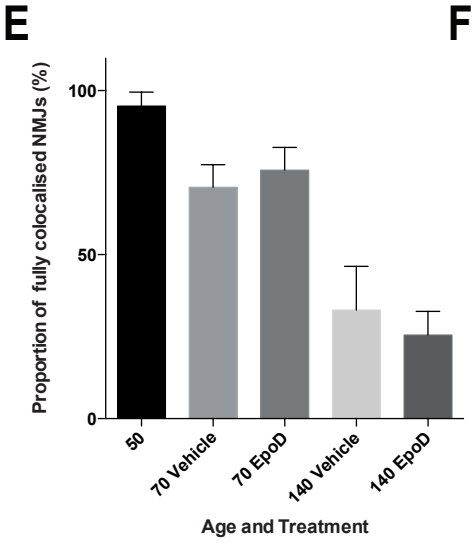
E
Proportion of fully colocalised NMJs (%)
100
50
0
50
70 Vehicle
70 EpoD
140 Vehicle
140 EpoD
Age and Treatment

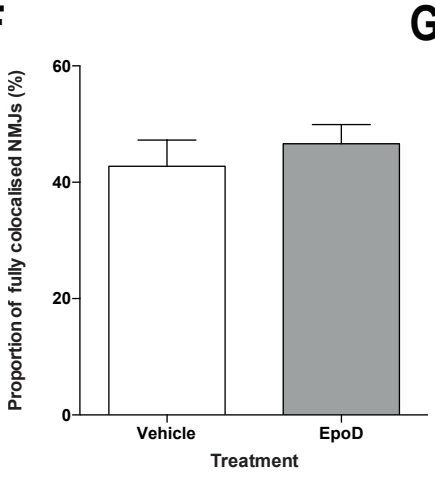
F
Proportion of fully colocalised NMJs (%)
60
40
20
0
Vehicle
EpoD
Treatment

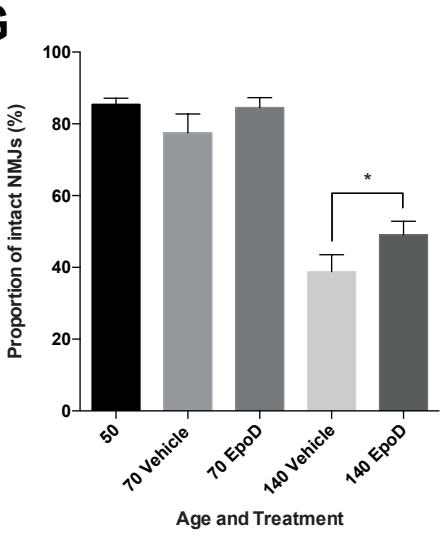
G
Proportion of intact NMJs (%)
100
80
60
40
20
0
*
50
70 Vehicle
70 EpoD
140 Vehicle
140 EpoD
Age and Treatment

As NMJ morphology alterations occur over the disease time course in SOD1^{G93A} mice (as in Chapter 3), the morphology of fully colocalised (pre- and post-synapse) NMJs were evaluated in EpoD treated SOD1^{G93A}xYFP mice (Figure 4.13 D) (Ngo et al., 2012). It was found that at 140 days of age there was a significant ($p < 0.05$) reduction in the proportion of NMJs with degenerative morphology in EpoD treated mice, compared to vehicle treated controls (EpoD: 49.023% ± 3.853; vehicle: 38.840% ± 4.715) (Figure 4.13 G). Furthermore, the NMJs in EpoD treated animals have reduced presynaptic YFP beading compared to vehicle treated controls (such as comparisons between Figure 4.13 panels A & D). This suggests that EpoD treatment reduces the degeneration of the NMJ pre-synapse by improving the morphological stability of the NMJ.

4.4 Discussion

Degeneration of the distal neuromuscular axon is a hallmark pathology of ALS, in both patients and in mouse models of the disease (Fischer et al., 2004). The 'die back' degeneration associated with ALS highlights the innate vulnerability of the distal axon and NMJ, both of which degenerate prior to the a-MN, which resides in the ventral horn of the spinal cord (Moloney et al., 2014). The current chapter investigated the efficacy of using a microtubule stabilising agent to target the distal neuromuscular circuitry and prevent degeneration in the SOD1^{G93A} mouse model of ALS. EpoD was hypothesised to protect microtubules of a-MNs from degeneration against Wallerian-like mechanisms, and by ameliorating microtubule hyperdynamics associated with ALS pathogenesis (Fanara et al., 2007; Kleele et al., 2014; Smith et al., 2014). The current chapter focused on a variety of behavioural, histological and molecular outcomes to determine the efficacy of EpoD treatment. The chapter highlighted that EpoD protects a-MNs and their axons from degeneration early in the disease course, and NMJs later in disease; however, this is not translated to improved synaptic health. Furthermore, results suggest early but modest improvements to aspects of motor behaviour, but with an ultimately detrimental effect on clinical and motor behaviour outcomes in the later stages of disease. Indeed, EpoD was found to decrease the life span of SOD1^{G93A} mice and result in end stage a-MN neurotoxicity and increased gliosis.

4.4.1 Epothilone D is a novel therapeutic for targeting microtubules in the lower neuromuscular circuitry

There has been limited success in identifying compounds and treatments to modify or cure ALS. Although the initial disease causing mechanism is yet to be elucidated, many contributing mechanisms have been identified, as have therapeutics to target them, however, the translation

from preclinical to clinical trials has, thus far, been disappointing (Mitsumoto et al., 2014; Ittner et al., 2015; Garbuzova-Davis et al., 2016). Identification of mechanisms common to other neurodegenerative disorders has allowed for further development of targeted therapies for ALS. As described in Chapter 1, many neurodegenerative diseases feature the common cellular pathology of a dysfunctional microtubule environment (Dubey et al., 2015; Clark et al., 2016a). This dysfunction can manifest as altered dynamics of the microtubule network, aberrant axonal transport, or a combination of both, as is reportedly the case in ALS (Fanara et al., 2007; Bilsland et al., 2010; Kleele et al., 2014). However, pharmacologically targeting microtubules in a selective manner presents a conundrum, as intracellular signalling cascades, small molecules and MAPs that alter the microtubule environment can interact with a plethora of other targets and functions (Alami et al., 2014; Wojnacki et al., 2014; Mohan and John, 2015; Sayas et al., 2015). Appealingly, anti-mitotic compounds used for cancer therapies typically have higher selectivity for microtubules by binding to and inducing conformational changes to tubulin, thus their attractiveness as a repurposed therapeutic method for neurodegenerative disease (Brunden et al., 2011; Eira et al., 2016). Indeed, the current investigation has highlighted that a low dose of EpoD can target and modify the microtubule environment of spinal cord a-MNs.

To date the majority of microtubule-targeting compounds have aimed to alter microtubule dynamics in the cortex of the CNS, focusing primarily on disorders such as AD, PD, schizophrenia and tauopathies (Andrieux et al., 2006; Brunden et al., 2010; Zhang et al., 2012; Baas and Ahmad, 2013; Cartelli et al., 2013). These studies focused on stabilising the microtubule cytoskeleton by modifying aberrant microtubule dynamics, reducing it to normal physiological levels. Indeed, this method of treatment has been found to improve outcomes in *in* vitro and *in vivo* models of the aforementioned diseases.

Of interest to the current thesis is a study by Hellal and Colleagues (2011), where the compound taxol was used to stabilise microtubules in a model of spinal cord injury (Hellal et al., 2011). Although used to promote axonal regrowth, and not protection of axons per se, this study highlights that stabilisation of microtubules in the spinal cord can lead to positive outcomes in neurological pathology. Further, targeting spinal cord microtubules with other epothilone analogues, such as epothilone B (EpoB), has been shown to increase the stability of microtubule network in the spinal cord, with positive outcomes in spinal cord injury models (Ruschel et al.,

2015). These results suggest that epothilone analogues, such as EpoD, can target and modify the stability of microtubule networks in the spinal cord.

More recently, Brill et al 2016 showed that epothilones stabilise microtubules in the distal axons of the neuromuscular circuitry, affecting axonal pruning and maintenance (Brill et al., 2016). Indeed, results from the current chapter support that EpoD, a compound with increased BBB permeability and CNS retention, compared to taxol or other epothilone analogues, can stabilise microtubule networks in a-MNs and their peripheral processes, identifying it as a compound that can potentially be used to target a-MNs in ALS (Cheng et al., 2008; Brunden et al., 2010). Attractively, the low dose of EpoD used in the current investigation, coupled with the increase in a microtubule stability marker, showed no identifiable neuropathology due to aberrant microtubule stabilisation, as is attributed to higher doses used in anti-mitotic caner therapy (Argyriou et al., 2011; Benbow et al., 2016). Further, chronic injection of EpoD (~20 weeks), did not lead to the development of aberrant behavioural clinical manifestations in wild-type mice, as shown with weight, motor function and neurological analysis. This suggested that EpoD at bioactive doses (to modify but not abolish microtubule dynamics) may be of use as a therapeutic in ALS to targets the distal neuromuscular circuitry (Brunden et al., 2014). Findings in the current chapter suggested that EpoD may protect the distal neuromuscular circuitry, particularly the a-MN soma and distal axon, at early stages of the disease. A similar study using noscapine to stabilise microtubules has previously been shown to improve outcomes in the $SOD1^{G93A}$ mouse model (Fanara et al., 2007). However, unlike this study, and regardless of the early benefits to pathology, chronic treatment with EpoD culminates in a neurotoxic effect, accelerating cellular pathology, motor behaviour deficits, and decreasing the lifespan of the $SOD1^{G93A}$ mouse. This suggests that whilst EpoD is a novel and attractive target for stabilising microtubules in the distal neuromuscular circuitry, it may have limited eficay.as a therapeutic strategy in ALS (Baas, 2014).

4.4.2 Axonal protection as a therapy for neuromuscular disorders

In the current investigation, low dose EpoD treatment was found to delay axonal degeneration early in the disease course of the $SOD1^{G93A}$ mouse model of ALS; however, this protection was not afforded later in the disease. Furthermore, early axon protection was also associated with improved a-MN survival. However, EpoD treatment only modestly protected NMJs by decreasing the proportion of NMJs with degenerative 'beaded' pre-synaptic morphology, and did not affect the proportion of NMJs with full pre-synaptic occupation of the postsynaptic endplate.

Similar axonal protection has been identified in an *in vitro* model of excitotoxicity, with microtubule stabilisation using taxol improving axonal pathology and cell survival, albeit in a caspase dependant manner (King et al., 2013). However, direct alterations to microtubule stability were not tested, with inhibition of enzymatic caspase action thought to offer axonal protection. Axonal protection using calpain inhibitors has also been shown to limit axonal degeneration in models of neuropathy (O'Hanlon et al., 2003). Interestingly, this method of axonal protection prevents microtubule disintegration via enzymatic digestion by calpain, the main enzyme utilised in dismantling axonal proteins, including the microtubule cytoskeleton (Wang et al., 2012). The effects of EpoD on caspase or calpain dependant cytoskeletal degenerative pathways were not directly tested in the current chapter. However, microtubule stabilisation has been shown to protect against Wallerian degeneration during phasic pruning of the a-MN distal axon, further suggesting that microtubule targeting compounds can prevent axonal degeneration in the distal neuromuscular circuitry (Brill et al., 2016).

The use of noscapine, a microtubule-targeting compound, and alterations to microtubule acetylation via genetic ablation of HDAC6, has shown promise in improving outcomes in ALS, supporting the use of microtubule-targeting methods to modify dynamics (Fanara et al., 2007; Taes et al., 2013). Utilising EpoD to target microtubules was shown to improve a-MN and axonal pathology early in the disease course, supporting the hypothesis that EpoD can improve axonal pathology. However, there were no additional benefits later in disease. EpoD was found to cause detrimental outcomes in motor function, survival and clinical readouts later in the disease course, with increased a-MN cell death and glial activation; a phenomenon that was not identified in previous microtubule targeting treatments (Fanara et al., 2007; Taes et al., 2013). Others have shown that gliosis is associated with increased a-MN death in ALS (Boillee et al., 2006a; Gowing et al., 2008), and taken with previously described results of limited glial activation in neuropathy analysis of EpoD in wild-type mice, suggests that EpoD may not be impacting directly on either astrocytes or microglia in the current study (Friedlander, 2003). To evaluate this further, drugs such as minocycline, which inhibits microglial activation, may be utilised to determine if EpoD is causing a-MN toxicity through microglial dependant mechanisms (Kriz et al., 2002; Zhu et al., 2002).

The current chapter determined that EpoD does not affect collateral branching in the distal neuromuscular circuitry, a reactive phenomenon that occurs in ALS, mediated in party by changes to microtubule dynamics in distal axons (Pun et al., 2006; Brill et al., 2016). This suggests that the levels of altered microtubule dynamics in the current study are not significant enough to impact collateral sprouting over the disease time course (Ketschek et al., 2015a), and that the capacity for branching is still available to the distal neuromuscular circuitry. Interestingly, microtubule stabilisation using taxol only affects branching during neurite elongation, and not during collateral formation, suggesting that microtubule stabilisation using EpoD may not affect the ability for distal axons to sprout and reinnervate vacant NMJ endplates (Letourneau et al., 1986; Gallo and Letourneau, 1999).

EpoD dose not improve presynaptic colocalisation and NMJ innervation over the disease time course, suggesting EpoD stabilises microtubules and offers protection only in distal axons, allowing presynaptic degeneration to continue. However, later in the disease, alterations to NMJ morphology are apparent in EpoD treated mice, with NMJs showing less YFP 'blebbing' of the pre-synaptic membrane, a phenomenon associated with degeneration of the NMJ pre-synapse (Li and Thompson, 2011). The microtubule environment between axons and NMJs is different, suggesting EpoD may have different effects in these two distinct cellular compartments (Godena et al., 2011; Bodaleo and Gonzalez-Billault, 2016). For example, NMJ microtubules have the capacity to become increasingly dynamic during bouts of plasticity and phasic pruning (Bodaleo and Gonzalez-Billault, 2016; Brill et al., 2016). NMJ microtubules also rely heavily on axonal transport to recycle synaptically localised mitochondria and vesicles. Additionally, it may be surmised that NMJs are more vulnerable to pathogenic mechanisms in ALS than axons, with both pre- and post-synaptic involvement of the NMJ leading to degeneration independent of microtubule stabilisation (Santos and Caroni, 2003; Moloney et al., 2014).

4.4.3 Behavioural outcomes and statistical modelling of SOD1^{G93A} mice

Identification of the earliest behavioural deficits in disease models is imperative to understanding the disease phenotype, and also to identify appropriate ages in which to draw comparisons to the human disease. The use of advanced statistical modelling, not typically utilised in animal behavioural studies, has made it easier to visualise and interpret the data from the current therapeutic trial (Naumova et al., 2001). Fitment of either smooth non-linear polynomials, or multi-level piece wise non-linear polynomial models to the data to obtain the most valid data

representation is used extensively for population based studies, particularly in with biological data, such as age and height (Durban et al., 2005; Grajeda et al., 2016). Moreover, fitment of break points to the data (where the fitment of two lines and their intersection represents the age at which the readout changes), allows for an increasingly accurate estimation of either onset, or how the disease is progressing due to variables such as treatment or genotype (Muggeo, 2003; Schafer and Hermans, 2011). Indeed, mixed effect modelled grip strength data suggests differential progression of the disease, with definable 'phases' of grip strength loss. Initially, $SOD1^{G93A}$ mice show an early sharp 1st phase linear decline of the forelimb. Contrastingly, there is a gentle decline in gripstrength identified in the 1st phase decline of the hindlimb. Both forelimb and hindlimb gripstrength then have a 2nd phase decline. Further, forelimb gripstrength deficits occur at an age prior to NMJ degeneration as discussed in Chapter 3, suggesting that NMJ pathology in the forelimbs may not be the most appropriate readout of disease progression, and a greater emphasis on function may be required, such as electromyography (Kennel et al., 1996). Taken together, this suggests that differential progression of both pathology and gripstrength occurs between the forelimb and hindlimb muscles in the $SOD1^{G93A}$ mouse.

Current results suggest that $SOD1^{G93A}$ mice perform significantly worse than wild-type mice from the beginning of the trial, approximately 50 days of age, using weight analysis, rotarod performance and grip strength testing. This is comparable to other reported alterations to motor behaviour in $SOD1^{G93A}$ mice, with abnormal gait (56 days of age) in $SOD1^{G93A}$ mice on a C57Bl/6 background, which was used in this study (Wooley et al., 2005; Kanning et al., 2010). Genetic background has a large influence on symptom progression and survival in SOD1 mice, and must be taken into account when comparing between studies (Leitner et al., 2009). Interestingly, a meta-analysis of C57Bl/6 $SOD1^{G93A}$ mice, the most common combination of background/transgenic mutant, estimated onset at 103 days when measuring hindlimb tremors (neurological onset) (Pfohl-Leszkowicz et al., 2015). Indeed, hindlimb tremors are thought to occur prior to generalised motor deficits in SOD1 models (Kasai et al., 2011), whereas the current study identified neurological onset at 70 days of age in EpoD treated mice, and 77 days for vehicle mice, compared to wild-type controls. Indeed, Lee and Colleagues (2013) found that hindlimb gripstrength and motor neuron loss occur concurrently from 70 days in C57Bl/6 $SOD1^{G93A}$ mice, suggesting a strong behavioural-pathology correlation (Lee et al., 2013a). However, the early onset of behavioural deficits in the current chapter (gripstrength decline occurred 20 days earlier than Lee and Colleagues, 2013) highlights a significantly earlier presence of clinical symptoms in the $SOD1^{G93A}$ mice used in this study, compared to many others

(Gurney et al., 1994; Pfohl-Leszkowicz et al., 2015). Arguably, there is still not a sound consensus on the best measure for onset in mouse models of ALS, although deficits to maximal running speed seems to be the earliest measure reported, and may be the most effective measure of motor behaviour alterations (Veldink et al., 2003).

Furthermore, as highlighted in Figure 4.14, comparisons of pathology data from Chapter 3, and grip strength behavioural data from Chapter 4, suggest that hindlimb motor behavioural deficits occur prior to the identified axonal and NMJ pathology by approximately one week. However, no pathological investigations occurred between 28 and 56 days of age in the $SOD1^{G93A}$ mice in Chapter 3. Therefore, results from Chapter 4 suggest that future research should focus on this age range of the $SOD1^{G93A}$ when focusing on distal neuromuscular pathology, such as in the axon and NMJ. Correlation studies using sophisticated modelling techniques, such as those employed in this chapter may elucidate a more holistic representation and comparison of pathology and behavioural phenotype.

4.4.4 Microtubule stabilisation alters behavioural outcomes

As described previously, EpoD treatment improved a-MN and axonal pathology early in the disease course. Interestingly, this was not associated with improvements in motor behaviour and neurological scoring. This suggests that pathology and behaviour do not always match, and in this case, may be explained by the lack of protection at the NMJ, as destruction of synaptic colocalisation continued unabated. Later disease stages showed a hastened deterioration in motor performance and neurological scoring in EpoD treated mice, mirroring the loss of a-MNs and increased gliosis in the lumbar spinal cord of end stage $SOD1^{G93A}$ mice. This suggests that even at the low dose used in the current study EpoD is potentially neurotoxic, causing greater a-MN degeneration and aberrant glial activation, and thus negatively effecting behavioural and neurological outcomes (Fischer et al., 2004; Hegedus et al., 2008). Further, EpoD decreased the survival of $SOD1^{G93A}$ mice, significantly reducing the disease time course.

4.4.5 The evolving complications of the microtubule environment in ALS

Whilst microtubule involvement in ALS is increasingly being appreciated (Dubey et al., 2015; Clark et al., 2016a), the cause of microtubule dysfunction is still largely unknown. Current results suggest that age dependant alterations to microtubules may occur, as EpoD treated $SOD1^{G93A}$ mice show differential disease progression in pathology, and modest alterations in behaviour. Indeed, many age dependant pathological and molecular alterations in the $SOD1^{G93A}$ mouse

FIGURE 4.14. Timeline of distal pathology and motor behaviour deficits as measured by grip strength. Deficits to hindlimb grip strength occur prior to the presence of axonal and NMJ pathology. Both hindlimb and forelimb gripstrength occur in two stages. Forelimb grip strength loss occurs well before the loss of the corresponding forelimb distal neuromuscular circuitry (64.5 days), compared to the hindlimb (6.4 days).

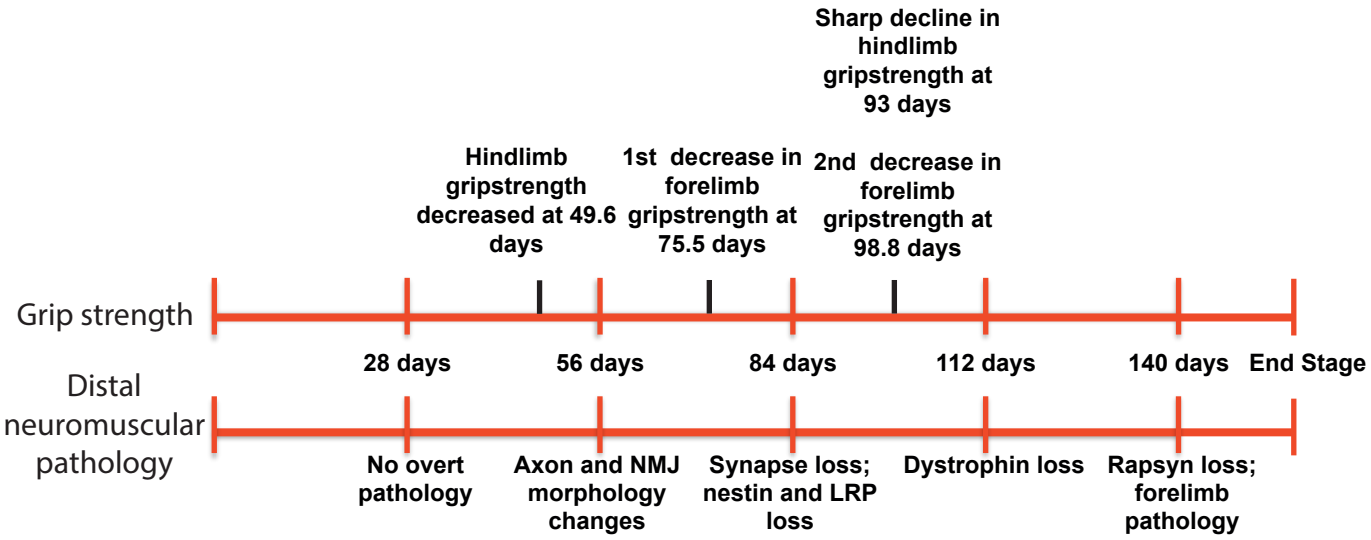
Sharp decline in hindlimb gripstrength at 93 days
Hindlimb gripstrength decreased at 49.6 days
1st decrease in forelimb gripstrength at 75.5 days
2nd decrease in forelimb gripstrength at 98.8 days
Grip strength
28 days
56 days
84 days
112 days
140 days
End Stage
Distal neuromuscular pathology
No overt pathology
Axon and NMJ morphology changes
Synapse loss; nestin and LRP loss
Dystrophin loss
Rapsyn loss; forelimb pathology

model have been documented (Kanning et al., 2010; Redler and Dokholyan, 2012). Further, signalling pathways that directly impact normal microtubule dynamics and function are also affected over the disease course; however, the direct impact these mechanisms have on microtubules are yet to be investigated (Palazzo et al., 2001; Tudor et al., 2005; D'Ambrosi et al., 2014; Wojnacki et al., 2014). Investigation of microtubule alterations over the disease time course, particularly between age, genotype and associated pathogenic mechanism are needed to elucidate the full involvement of microtubules disease pathogenesis.

The current results suggest that reassessment of age, timing and duration of EpoD delivery will need to be completed, as well as the capacity for combination therapy, to improve the efficacy of microtubule stabilisation in ALS (Pandya et al., 2012). Further, comparing the mode of action between noscapine, a compound that improves the ALS phenotype, and EpoD, is necessary. EpoD binds the taxol binding site on β-tubulin, promoting a GTP independent conformational change that promotes dose dependant microtubule polymerisation and alterations to dynamics (Cheng et al., 2008). Conversely, the binding site on tubulin for noscapine is unknown (Ye et al., 1998). Further, noscapine does not significantly alter microtubule mass or promote polymerisation. Instead, noscapine supresses microtubule dynamics by 'stalling' the growth and shrinkage phases of microtubules, thus decreasing the overall dynamics of the microtubule network (Zhou et al., 2002; Zhou and Giannakakou, 2005). This suggests that gross microtubule stabilisation may not be the best way to improve pathology in ALS. Rather, subtly altering microtubule dynamics in a-MNs may be a more attractive therapeutic approach to target pathology.

Another consideration is the copy number variant of the SOD1^{G93A} mouse model. High copy number mice (23-25 copies) have a significantly shorter life span and faster progressing pathology than low copy SOD1^{G93A} models. Due to the high rate of disease progression, potential therapeutics may have benefits or positive outcomes masked, further complicating the design and interpretation of therapeutic trials (Zwiegers et al., 2014). Repeating therapeutic interventions in a slower progressing SOD1 model (for example, the low copy SOD1^{G93A} mouse), TDP-43 and newer C9ORF72 animal models, may uncover a greater number of pathological and behavioural changes during EpoD treatment (Stallings et al., 2010; Acevedo-Arozena et al., 2011; Liu et al., 2016).

The highly multifactorial nature of pathogenic mechanisms in ALS suggests that any therapy to modify or cure the disease will most likely be a combination-based therapy, with adjusted treatment type, dosage and time as the disease progresses (Bucchia et al., 2015; Goutman and Feldman, 2015). Indeed, EpoD treatment regimes used in cortical degenerative models may not be appropriate for long term management of ALS, a conclusion which is supported by the current study (Brunden et al., 2014). EpoD's positive effect early in the disease, followed by deterioration of behavioural outcomes and pathology, suggest the disease pathology is heterogeneous and evolving, and that to manage this change a multi drug approach, with alterations to dosage and timing is necessary. Indeed, the lack of impact on NMJ pathology, whilst axonal pathology was reduced early in the disease, suggests that the two distinctly different cellular sites may require multiple targeted treatment regimes to obtain benefits. Further, EpoD may differentially affect microtubules over the disease time course in an age and cellular compartment manner, however this is still poorly understood.

4.4.6 Conclusion

Stabilising microtubules to attenuate axonal degeneration is an attractive therapeutic approach for many neurodegenerative diseases. The current chapter utilised the microtubule targeting compound EpoD, with the aim of protecting axons of the neuromuscular circuitry in ALS and improving the disease phenotype. EpoD was identified to increase microtubule stability markers in the lumbar spinal cord, suggesting EpoD has the capacity to modify the microtubule network in the distal neuromuscular circuitry. Furthermore, early protection offered by EpoD suggests that targeting the distal axon with low dose EpoD may only be of benefit in the earlier stages of the disease, with the need for adjusted treatment strategies or other combined therapies as the disease progresses. The current results highlight the highly heterogeneous nature of disease pathogenesis in ALS.

Age dependant effects of EpoD on pathological, neurological and behavioural outcomes in the current study suggest that microtubules play an evolving role over the entire disease course. The role they play is still largely unknown, however, as our understanding of the normal neuronal function of microtubules increases, so will the complexity and targeted nature of research question surrounding microtubules in ALS. Similarly, the impact EpoD has on neuronal microtubules is still underappreciated. Future investigations into dose dependant effects of EpoD on normal neuronal functioning should be considered a priority due to the attractive of such

compounds as neurodegenerative treatments. Due to the complexity of *in vivo* systems, and the difficulty of measuring outcomes with microtubule targeting compound, whether morphological or functional, *in vitro* approaches should be considered as an appropriate method for evaluating the microtubule dependant effects of EpoD on neurons.

Chapter 5

5 The impact of microtubule stabilisation by Epothilone D on neuronal growth, viability and function

5.1 Introduction

Defects to the neuronal cytoskeleton occur in various neurodegenerative disorders. Compounds targeting cytoskeletal elements, such as microtubules, are becoming an increasingly popular therapeutic intervention strategy to improve cytoskeletal dysfunction and outcomes in disease (Eira et al., 2016). This philosophy was applied in Chapter 4, where the microtubule-targeting compound EpoD was used to stabilise the microtubule cytoskeleton in the SOD1^{G93A} mouse model of ALS. Results showed early beneficial actions on improving a-MN survival and distal axonal pathology. However, this protection was not extended to the synapse or translated into improved motor behaviour, although modest improvements to hindlimb grip strength were identified. Indeed, age dependent acceleration of symptoms in EpoD treated SOD1^{G93A} mice suggest that both genotype and treatment are having a detrimental effect on late stage disease progression. However, how this particular epothilone analogue (EpoD) alters normal neuronal function is poorly understood.

A common misconception with the neuronal cytoskeleton is that as mature neurons are non-mitotic, their cytoskeletal elements, such as actin, neurofilaments and microtubules are stable entities (Baas et al., 2016). However, as our understanding and documentation of the plastic nature of the nervous system increases, so does our appreciation of the similar dynamic nature the in neuronal cytoskeleton. Our understanding of non-dynamic stable domains, and highly dynamic labile domains in the normal neuronal microtubule network has highlighted that the microtubule system may be vulnerable to changes in this dynamic state. Indeed, changes to microtubule dynamics and proteins associated with the control of microtubule dynamics are associated with the pathogenesis of multiple neurological disorders, including ALS (Fanara et al., 2007; Kleele et al., 2014).

Microtubule-targeting compounds are among the most successful means by which to target and treat various types of malignancies (Dumontet and Jordan, 2010). This is mainly due to the importance of microtubules in the development and mechanical action of the mitotic spindle during cell division, which, in cancer, develops into an uncontrolled and hyper activated process

(Zhou and Giannakakou, 2005). When used at concentrations high enough to inhibit cell division, compounds such as the taxanes and epothilones have been shown to be highly effective treatments for patients suffering from cancer (Dumontet and Jordan, 2010). However these drugs, regardless of their intended use, are not without their caveats. High doses of microtubule-targeting drugs can hyper-stabilise the microtubule network, causing a painful and debilitating peripheral neuropathy (reviewed previously in (Lee and Swain, 2006; Carlson and Ocean, 2011)). Indeed, brain penetrant microtubule-targeting compounds such as EpoD cause similar symptoms, however the effect of these drugs on neuronal health in the CNS is still not well documented (Konner et al., 2012). Highlighting the importance of increased understanding, Masocha and colleagues described increased astrocyte activation and altered expression of glutamate receptor subunits in the cortex of mice treated with paclitaxel, suggesting that microtubule stabilisation which typically causes peripheral neuropathic pain, also affect cells of the CNS (Masocha, 2015).

It is becoming increasingly apparent that microtubule-targeting compound concentration, target and measurement (outcome) are all important and intertwined in both study design and interpretation. Indeed, the concentration range of such compounds to obtain optimal stabilisation in neural systems is extremely narrow (Bollag et al., 1995). For example, studies using low dose of microtubule-targeting compounds (approximately $1/20^{th}$ to $1/30^{th}$ of the doses used in cancer therapy (rodent equivalent), were found to improve outcomes in models of neurodegeneration or cortical injury (Brunden et al., 2010; Brunden et al., 2011; Zhang et al., 2012; Cartelli et al., 2013; Brizuela et al., 2015). These studies generally used tubulin chemical modifications as a biomarker for microtubule network stabilisation; a valid and reproducible test, which highlights the dose dependant increase in microtubule stability with increasing compound concentration (Brunden et al., 2011; Magiera and Janke, 2014). However, microtubule-targeting compounds can, like in cancer therapy, abolish microtubule dynamics via hyper-stabilisation, causing a loss of +TIP protein localisation and expression (Kleele et al., 2014; Benbow et al., 2016; Brill et al., 2016). Indeed, paclitaxel has been identified to induce polar reconfiguration of axonal microtubules and impair axonal transport of organelles and vesicles *in vitro*, with no recovery of the resultant phenotype upon compound removal (Shemesh and Spira, 2010).

Of the epothilones, EpoB has been investigated with regards to dose-dependant neuronal impact, with results suggesting that low to moderate concentrations cause decreased neuronal development, axonal health and decreased electrophysiological properties by lowering nerve

transduction velocities, both *in vitro* and *in vivo* (Chiorazzi et al., 2009; Jang et al., 2016). Indeed, considerations of dose and target must be evaluated when developing therapeutic strategies utilising microtubule-targeting compounds for neurodegenerative diseases and CNS injury, as evidence suggests that these compounds can cause drastic microtubule changes in dose-dependant manner.

The current investigation utilised a primary *in vitro* cortical model to identify alterations to normal neuronal growth, development and function caused by the dose-dependant application of EpoD, a process that is still poorly understood. Utilising cultured cortical neurons, a subtype of projection neurons expressing endogenous YFP will be selected to aid in decreasing cell variability. Tau immuno-staining will be utilised to separate tau positive and negative processes for analysis, as tau localises mainly to axonal microtubules (Conde and Caceres, 2009). The current investigation aims to determine the impact of EpoD on a subset of cortical neurons to better understand and interpret outcomes of stabilising neuronal microtubules with EpoD.

5.2 Methods

5.2.1 Cell culture

As described in Chapter 2, section 2.5, neurons were isolated from the dissected and disassociated neocortex of 15.5-day-old embryonic *thy1*-YFP mice, and plated onto poly-l-lysine coated surface (glass or plastic) in 24 well plates (1.9 cm^2), 6 well plates (3.48 cm^2) or live imaging micro chambers (1.5 cm^2), at the following densities: 24 well plate, 3 x 10^4 cells; 6 well plate, 6 x 10^6 cells; imaging chambers, 5 x 10^3 cells.

Transgenic YFP expressing embryos and wild-type littermates were used for experiments. Cultures were grown according to the procedures described in Chapter 2, section 1.5.

5.2.2 Treatment paradigms

In order to study the effects of EpoD on normal neuronal development, neurite growth and function, cells were exposed to a variety of drug concentrations (0.1nM, 1nM, 10nM, 100nM EpoD), for 2 hours and 24 hours in mature neurons (10DIV), or 24 hours with media replacement (conditioned +treatment) for growth and development experiments. Naïve, untreated neurons and vehicle (DMSO) treated neurons were utilised as controls.

5.2.3 Quantification of cell viability

Cell health was determined by either using the alamarBlue® cell viability assay (Thermo Fisher Scientific) or by quantifying nuclear morphological alterations with DAPI staining (Kihlmark et al., 2001). AlamarBlue® reagent was diluted (1:10) in conditioned cell culture medium, followed by incubation with neurons for 2 hours. Redox reactions, as a measure of cell viability, was measured by fluorescence on a FLUOstar OPTIMA plate reader (excitation 570 nm, emission 580; BMG Labtech).

5.2.4 Immunocytochemistry of microtubule cytoskeleton

Neuronal cultures were fixed in 4% PFA and were probed using immunocytochemistry methods described in Chapter 2, section 1.6 for: cell processes (anti-rat GFP, 1:3000, Nacalai tesque), axons (anti- rabbit tau, 1:2000, DAKO) and dendrites (anti-mouse MAP2, 1:1000, Millipore). Secondary antibodies (rat Alexa488, mouse Alexa568, rabbit Alexa647) were diluted in PBS (1:750; Molecular Probes) and incubated for 1.5 hours at room temperature, followed by DAPI nuclear staining.

5.2.5 Confocal microscopy of neuronal cultures

Cells were visualised using a spinning disk laser confocal (UltraVIEW® VOX, Perkin Elmer) on an inverted microscope (Nikon TiE, Nikon) fitted with 20x (Plan-Apo N.A. 0.75) and 40x (Plan-Apo N.A. 0.95) objective lenses. Images were acquired using an Orca R^2 camera (C10600, Orca, Hamamatsu) and analysed using imaging capture software (Velocity v6.3.0, 2013, Perkin Elmer).

5.2.6 Image analysis and cell tracing

Neurite extension was evaluated in YFP expressing cells with healthy nuclear morphology and robust YFP cytoplasmic fluorescence in Image J (Schneider et al., 2012). Tracings of neuronal cell bodies, developing axons (described as tau positive YFP processes henceforth) and dendrites (described as tau – negative YFP processes henceforth) were completed utilising Neurolucida software (MBF Bioscience).

5.2.7 Mitochondrial transport analysis

Culture media containing EpoD/vehicle treatment was removed from the cells and kept at 37°C for reapplication following staining. Cells were incubated in conditioned culture media containing Mitotracker® Red FM (200nM final concentration, Thermo Fischer Scientific) for 15 minutes, followed by a 5 minute wash in conditioned culture media. EpoD/vehicle media was

reapplied to the cells and live cell imaging was performed as described in Chapter 2, section 1.5.4.

5.2.8 Western blot protein quantification

Neuronal cultures were rinsed twice in ice-cold PBS, followed by lysis in RIPA-Inhibit buffer (RIPA buffer + 1μM trichostatin-a), and centrifugation at 15,800 RCF for 10 minutes at 4°C to remove cell debris, as described in full in Chapter 2, section 1.7.1. Protein levels were then evaluated by Western blot. Tubulin chemical modifications were probed to identify changes to microtubule stability using an antibody to acetylated tubulin (mouse monoclonal, 1:5000, Sigma Aldrich). Antibodies for STOP (mouse monoclonal, 1:500, Millipore) and EB3 (rat monoclonal, 1:500, Abcam) and GAPDH (rabbit polyclonal, 1:5000, Millipore) were used. Secondary HRP conjugated antibodies were then used, followed by imaging, as described in Chapter 2, section 1.7.2.

5.2.9 Statistical analysis

To determine the effect of EpoD on normal neuronal growth, development, function and protein levels data was statistically analysed using GraphPad Prism (Version 5.00, La Jolla, CA) using one-way analysis of variance (ANOVA) with Dunnets post-hoc correction for multiple comparisons. $p < 0.05$ was considered significant. Data is expressed ± standard deviation of the mean (SD). Unless otherwise stated, a minimum of three separate cultures was used for each experiment, with 3 technical replicates per culture ($n = 3$).

5.3 Results

5.3.1 Epothilone D causes dose a dependant decrease in neuronal viability

Stabilisation of microtubules with compounds such as EpoD were originally utilised to induce cytotoxicity in tumorigenic and malignant cells. Such approaches cause painful neuropathies due to aberrant stabilisation of the neuronal microtubule cytoskeleton. To date, the dose dependant cytotoxicity of EpoD on primary neurons are yet to be investigated. Utilising a commercial cell viability assay, the current investigation identified that growing and developing neurons treated with varying doses of EpoD showed no significant changes in neuronal viability compared to vehicle treated control neurons between 1DIV and 2DIV (Figure 5.1 A & B). By 3DIV (3 days of recurrent treatment), 100nM EpoD treated neurons showed significantly ($p < 0.05$) decreased viability compared to age matched, vehicle treated control neurons (100nM EpoD: 434.39 ± 53.58; vehicle: 694.56 ± 87.27) (Figure 5.1 C). This trend continued at 4DIV, with 100nM EpoD

FIGURE 5.1. Cell viability of EpoD treated cortical neurons during initial growth. (A) EpoD treatment does not alter neuronal cell viability when measured by the alamarBlue® cell viability assay at any dose at 1 DIV, (B) or at 2 DIV. (C) However at 3 DIV, (D) and 4 DIV, 100nM concentrations of EpoD were detrimental to cell viability, with a significant drop in assay fluorescence ($P < 0.1$). (E) Evaluation of nuclear health determined a decreased proportion of healthy nuclei, with non-condensed chromatin staining and a rounded morphology (DAPI), compared to unhealthy (F), which present as an increased proportion of shrunken nuclei (F, open arrow head), or fully condensed nuclei (F, closed arrowhead), (G) at 1 DIV in 100nM EpoD treated YFP neurons. Data shown are: mean ± SD, (n = 3). * $P < 0.05$, ** $P < 0.01$, One-Way ANOVA with Dunnett's post hoc test. Scale = 15μm. Abbreviations: NC, Naïve control.

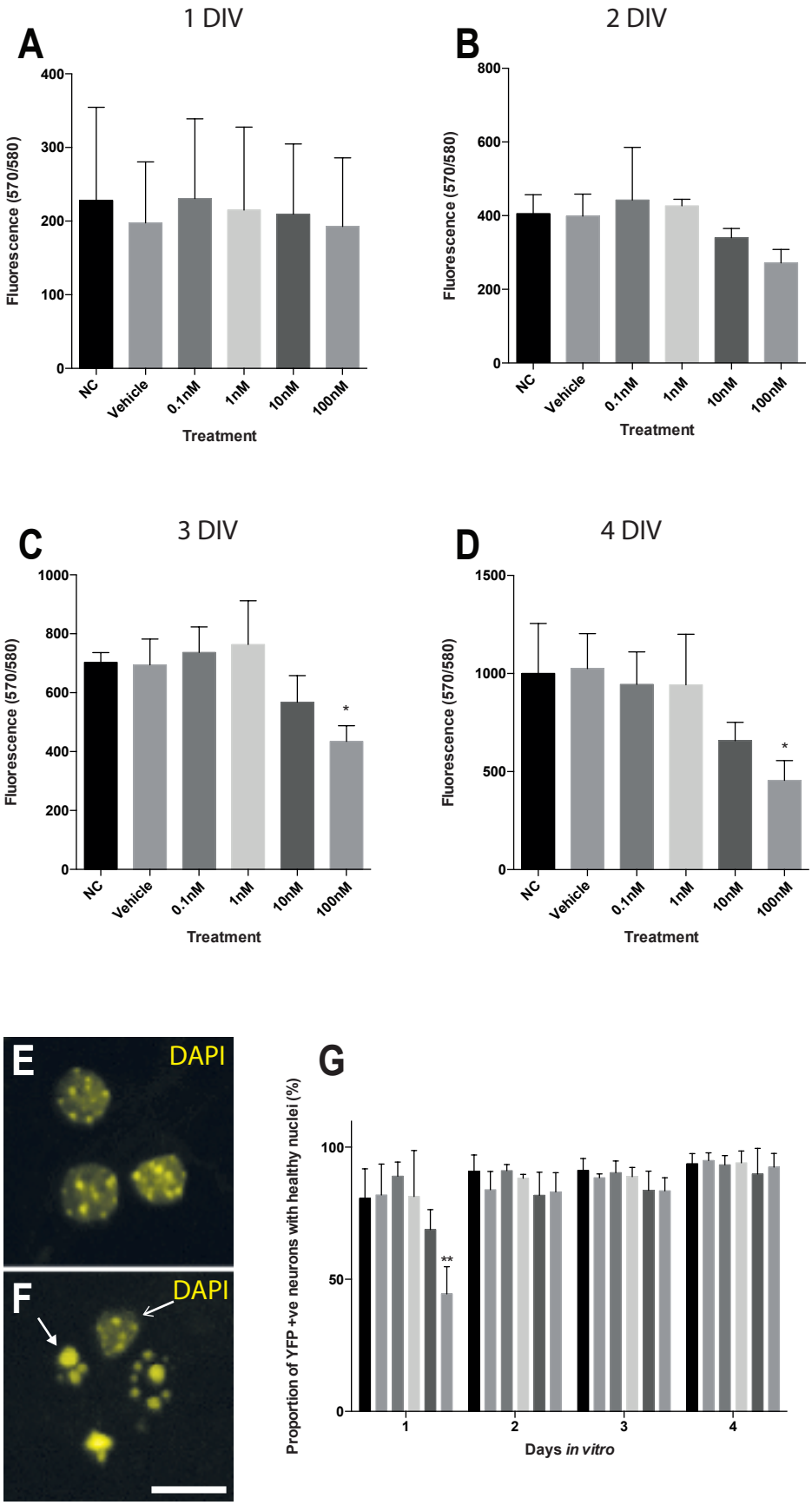
A
1 DIV
Fluorescence (570/580)
400
300
200
100
0
NC
Vehicle
0.1nM
1nM
10nM
100nM
Treatment
B
2 DIV
Fluorescence (570/580)
800
600
400
200
0
NC
Vehicle
0.1nM
1nM
10nM
100nM
Treatment
C
3 DIV
Fluorescence (570/580)
1000
800
600
400
200
0
*
NC
Vehicle
0.1nM
1nM
10nM
100nM
Treatment
D
4 DIV
Fluorescence (570/580)
1500
1000
500
0
*
NC
Vehicle
0.1nM
1nM
10nM
100nM
Treatment
E
DAPI
F
DAPI
G
Proportion of YFP +ve neurons with healthy nuclei (%)
100
50
0
**
1
2
3
4
Days in vitro
NC
Vehicle
0.1nM
1nM
10nM
100nM

treated cells showing significantly ($p < 0.05$) less neuronal viability, compared to vehicle treated controls (100nM EpoD: 454.67 ± 101.58; vehicle: 1025.22 ± 178.11) (Figure 5.1 D). This suggests that high doses of EpoD are toxic to neuronal cell growth and survival.

The morphology of the nucleus was also evaluated to determine the health of YFP positive cortical neurons, as during apoptotic cellular demise a series of morphological alterations to the nucleus occurs that can be quantified into stages of degeneration (Kihlmark et al., 2001). It was determined that there was a significant ($p < 0.05$) decrease in the proportion of healthy nuclei (Figure 5.1 E) at 1DIV, with an increase in condensed and degenerating nuclei (Figure 5.1 F) in 100nM EpoD treated cells, compared to vehicle treated controls (100nM EpoD: 44.45% ± 10.29%; vehicle: 85.48% ± 11.67%) (Figure 5.1 G). At later time points (2, 3 & 4DIV) there was no significant ($p > 0.05$) difference in nuclei morphology in EpoD treated YFP neurons, compared to controls. This suggests that EpoD impairs the health and development of primary cortical neurons in a dose/and age-dependant manner. Further, it suggests that subpopulations of YFP positive cortical neurons may exist, which are resistant to EpoD induced microtubule hyper stabilisation (Jang et al., 2016).

5.3.2 Epothilone D causes dose dependant effects on neuronal viability in relatively mature primary cortical neurons

The majority of situations in which microtubule-targeting compounds will be used in disease models or in patients are where mature neuronal networks are fully developed. Although now appreciated to contain labile domains, microtubules in mature neurons are generally more stable than those in developing neurons, as microtubule dynamics evident during axonal path finding and mass network plasticity are not as essential to mature neuronal function (Kapitein and Hoogenraad, 2015). Neurons at 10DIV were considered relatively mature, as an increase in synaptic proteins, glutamate receptors, axon/dendrite connections and altered electrophysiological properties occur at this age (Lesuisse and Martin, 2002; Wang et al., 2008). Similar to developing neurons, relatively mature primary cortical neurons at 10DIV were treated with varying doses of EpoD and neuronal viability was assessed at 2 hours and 24 hours post treatment. Cortical neurons evaluated two hours post-treatment showed no significant ($p > 0.05$) changes viability in both the Alamar blue cell viability assay (Figure 5.2 A), and no alterations to the morphology of nuclei in YFP positive neurons (Figure 5.2 B). However, 24 hours post treatment, 10nM and 100nM concentrations of EpoD were found to significantly ($p < 0.001$ &

FIGURE 5.2. Cell viability of EpoD treated mature cortical neurons as measured by the alamarBlue® cell viability assay. (A) EpoD treatment does not alter neuronal cell viability at two hours post treatment, (B) or cause a loss of healthy morphology of YFP positive neuronal nuclei. (C) However, 24 hours post treatment 10nM and 100nM concentrations of EpoD were detrimental to cell viability ($p < 0.05$) (D) and nuclear morphology ($p < 0.01$), in cortical neurons. Data shown are: mean ± SD, (n = 3). * $P < 0.05$, ** $P < 0.01$, One-Way ANOVA with Dunnett's post hoc test. Scale = 15μm. Abbreviations: NC, Naïve control.

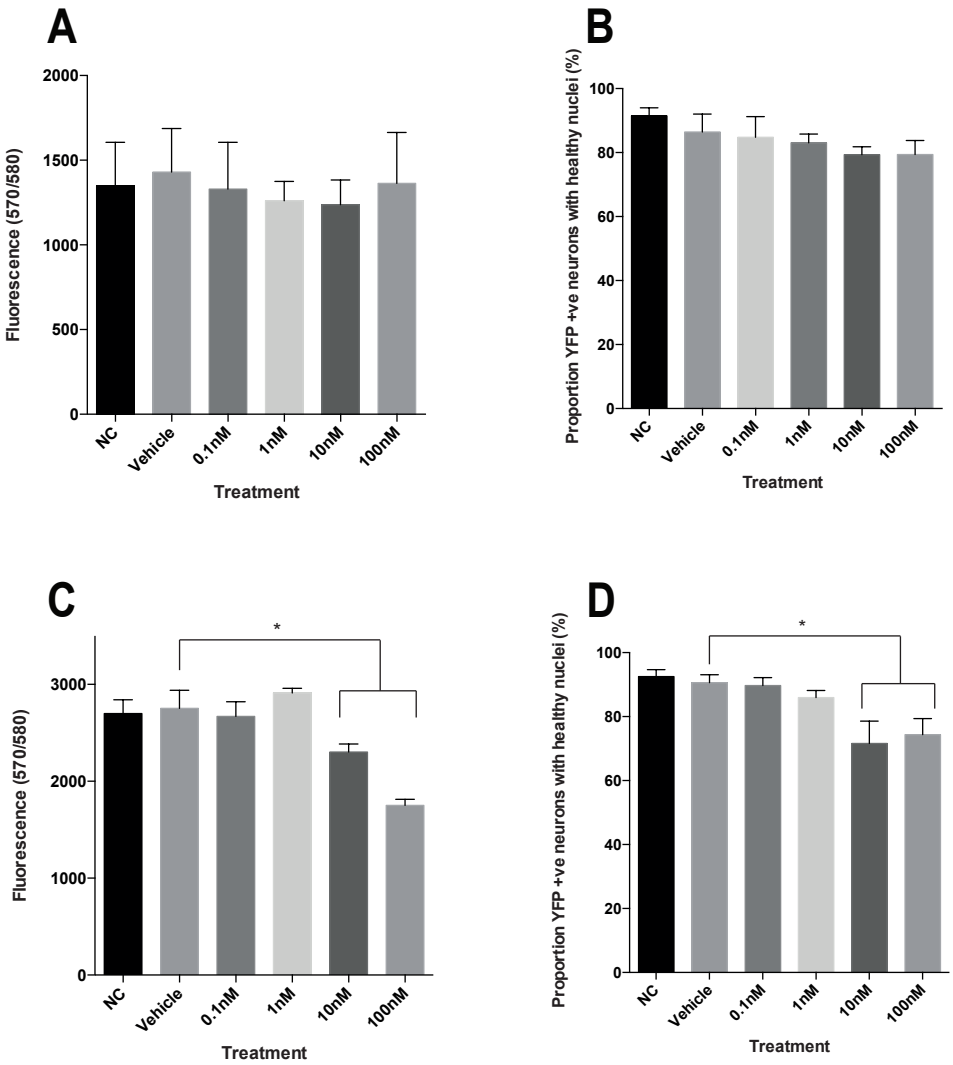
A
Fluorescence (570/580)
2000
1500
1000
500
0
NC
Vehicle
0.1nM
1nM
10nM
100nM
Treatment
B
Proportion YFP +ve neurons with healthy nuclei (%)
100
80
60
40
20
0
NC
Vehicle
0.1nM
1nM
10nM
100nM
Treatment
C
Fluorescence (570/580)
3000
2000
1000
0
*
NC
Vehicle
0.1nM
1nM
10nM
100nM
Treatment
D
Proportion YFP +ve neurons with healthy nuclei (%)
100
80
60
40
20
0
*
NC
Vehicle
0.1nM
1nM
10nM
100nM
Treatment

0.01, respectively) reduce cell viability, compared to vehicle treated controls (10nM EpoD: 2301.67 ± 82.35; 100nM EpoD: 1750.67 ± 63.69; Vehicle: 2699 ± 141.86) (Figure 5.2 C). Similar results were discerned upon evaluation of nuclei morphology in YFP expressing neurons, showing that neurons treated with both 10nM and 100nM EpoD had significantly ($p < 0.05$) decreased proportion of healthy nuclei, compared to vehicle treated control neurons (10nM EpoD: 71.59% ± 6.97%; 100nM EpoD: 74.33% ± 5.06%; vehicle: 90.60% ± 2.48%) (Figure 5.2 D). These results suggest that treatment of relatively mature (10DIV) primary cortical neurons with EpoD has dose-dependant effects on neuronal viability.

5.3.3 EpoD impacts the initial outgrowth of neurites in primary cortical neurons

The initiation of neurite outgrowth, particularly of the axon, is dependant on rearrangement and signalling actin, neurofilaments and microtubules to engage and promote neurite extension (Letourneau and Ressler, 1984; Kapitein and Hoogenraad, 2015). The initiation of neurite extension in EpoD treated cortical neurons was evaluated in YFP positive neurons with healthy nuclear morphology and robust YFP positive cytoplasmic volume (Figure 5.3 A & B). It was found that the proportion of neurons with evidence of neurite extension (such as Figure 5.3 A) was significantly ($p < 0.001$) decreased in neurons treated with 100nM of EpoD at 1DIV, compared to vehicle treated controls (100nM EpoD: 36.45% ± 10.50%; vehicle: 84.26% ± 10.50%) (Figure 5.3 C). Neurons with healthy nuclear morphology and robust YFP labelling showed no significant ($p > 0.05$) difference in the proportion of neurons with neurite extension at 2, 3 and 4DIV (Figure 5.3 C). This suggests that high doses or EpoD inhibit initial neurite extension in primary cortical neurons, however, surviving neurons are able to develop processes at later stages of development.

5.3.4 EpoD impacts on growth and complexity of neurites in primary cortical neurons

As well as being important for neurite initiation, microtubules are also important for axonal and dendrite growth and circuit complexity (Lewis et al., 2013; Kapitein and Hoogenraad, 2015). To determine whether EpoD treatment has microtubule dependant effects on these parameters, developing YFP positive cortical neurons were treated with varying doses of EpoD, followed by evaluation of neurite complexity using tracing software at 1DIV and 4DIV. Immunocytochemistry was utilised to specifically evaluate tau positive and tau negative neurites. High doses of EpoD was found to increase the proportion of less complex cortical neurons at 1DIV (Figure 5.4 A), compared to vehicle treated neurons (Figure 5.4 B). There was no significant ($p > 0.05$) difference in the total length of tau positive processes in EpoD treated

FIGURE 5.3. High doses of EpoD reduce initiation of neurite extension in cortical neurons. (A) Representative image of vehicle treated YFP positive neurons at 1 DIV show robust neurite extension, with tau positive neurites (closed arrowhead) and tau negative neurites (open arrowhead). Scale = 90μm. (B) Representative image of YFP positive neurons at 1 DIV, when treated with 100nM EpoD, show a decrease in identifiable neurites, but still have healthy nuclear morphology and YFP labelling. Scale = 30μm. Neurites were determined as YFP positive processes that were ≥ the diameter of the cell soma. (C) At 1 DIV, cortical neurons treated with 100nM of EpoD have significantly reduced ($P < 0.001$) neurite initiation. Data shown are: mean ± SD, (n = 3). ** $P < 0.01$, One-Way ANOVA with Dunnett's post hoc test. Abbreviations: NC, Naïve control.

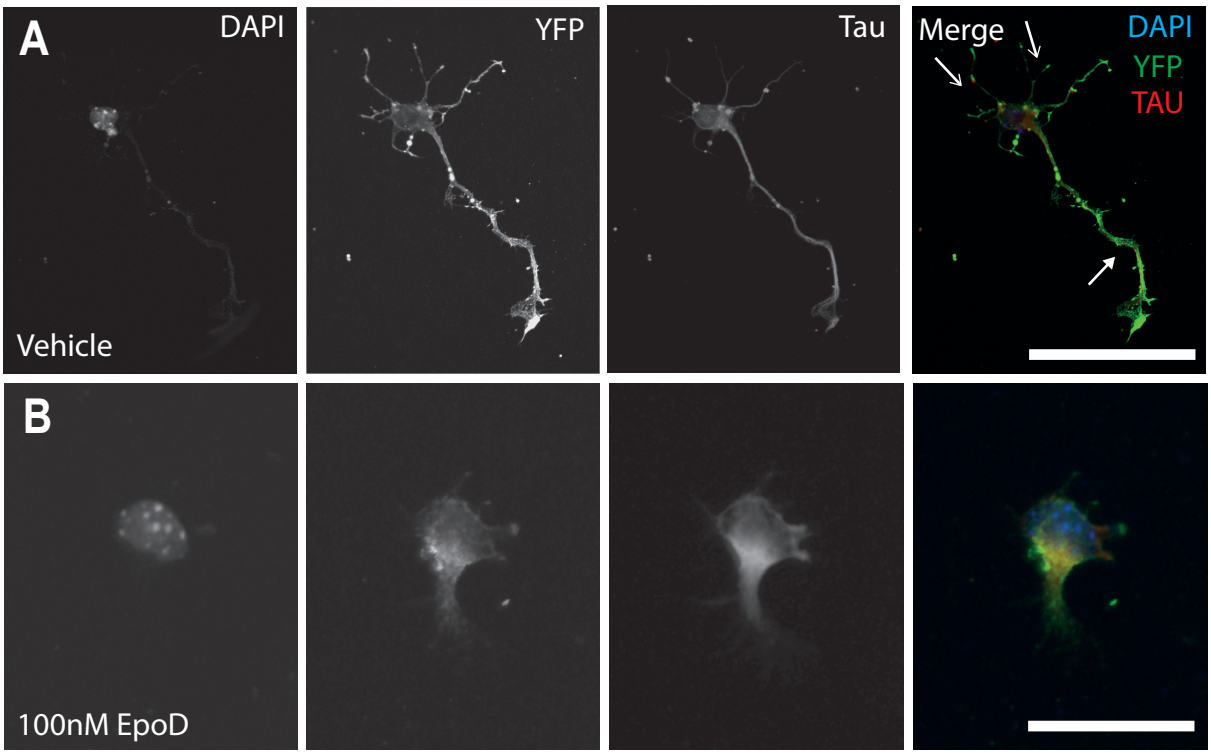
A
DAPI
YFP
Tau
Merge
DAPI
YFP
TAU
Vehicle
B
100nM EpoD

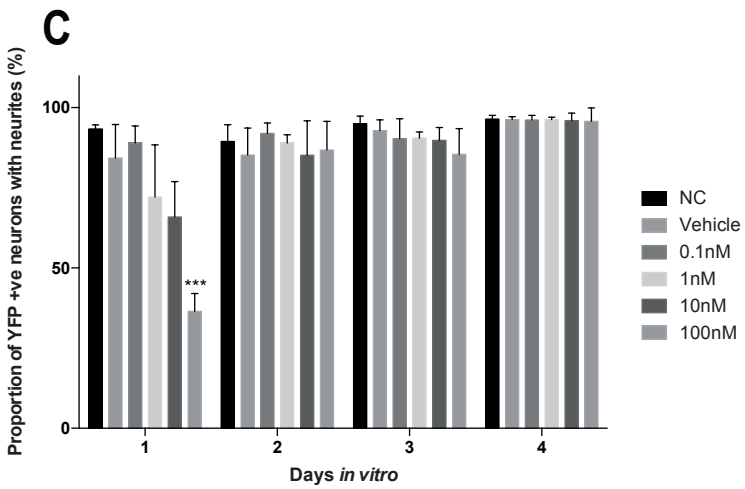
C
Proportion of YFP +ve neurons with neurites (%)
100
50
0
***
1
2
3
4
Days in vitro
NC
Vehicle
0.1nM
1nM
10nM
100nM

FIGURE 5.4. Neuronal process complexity at 1 DIV is affected by treatment with EpoD. (A) Representative tracings of YFP neurons at 4 DIV, which are less complex when treated with EpoD, (B) compared to vehicle treated neurons (tau +ve process, closed arrowhead; tau –ve process, open arrowhead). (C) Total length of tau positive processes are not significantly ($p > 0.05$) altered due to EpoD treatment. (D) Total length of tau negative processes are significantly ($p < 0.05$) decreased at higher doses of EpoD. (E) The proportion of tau +ve secondary order processes is significantly ($p < 0.05$) decreased in 10nM and 100nM EpoD treated YFP neurons. (F) The proportion of tau –ve primary order processes is significantly ($p < 0.01$) reduced in 10nM and 100nM EpoD treated YFP neurons. Scale = 45μm. Data shown are: mean ± SD, (n = 3). * $P < 0.05$, ** $P < 0.01$, One-Way ANOVA with Dunnett's post hoc test. Scale = 15μm. Abbreviations: NC, Naïve control.

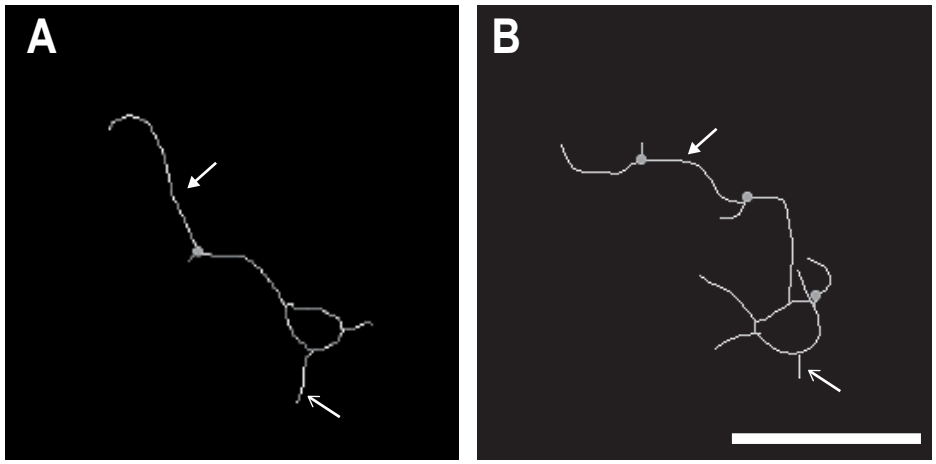
A
B

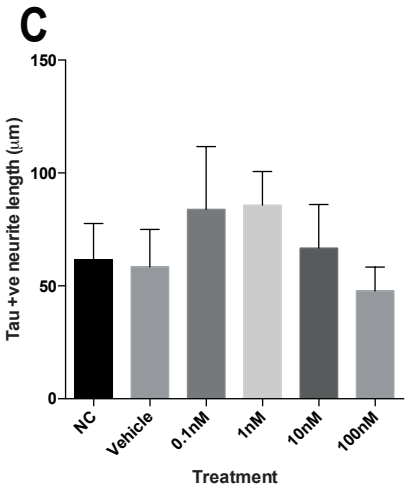
C
Tau +ve neurite length (μm)
150
100
50
0
NC
Vehicle
0.1nM
1nM
10nM
100nM
Treatment

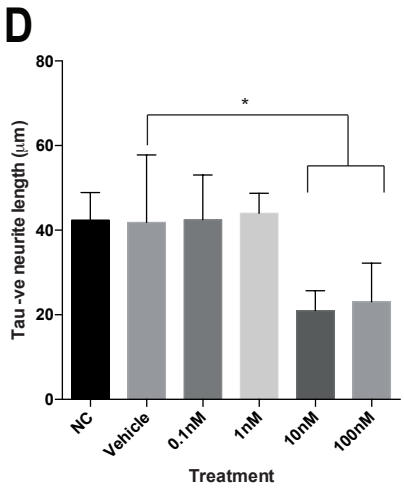
D
Tau -ve neurite length (μm)
80
60
40
20
0
*
NC
Vehicle
0.1nM
1nM
10nM
100nM
Treatment

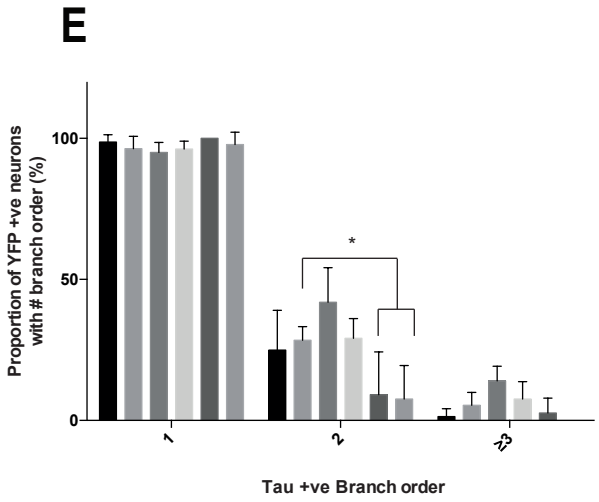
E
Proportion of YFP +ve neurons with # branch order (%)
100
50
0
*
1
2
>3
Tau +ve Branch order

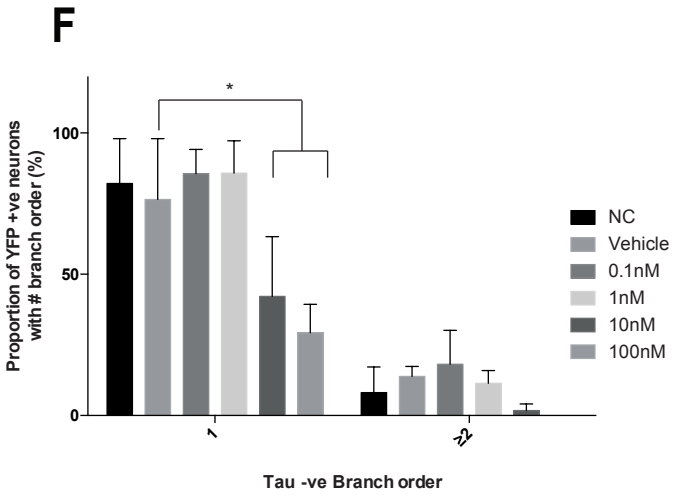
F
Proportion of YFP +ve neurons with # branch order (%)
100
50
0
*
1
≥2
Tau -ve Branch order
NC
Vehicle
0.1nM
1nM
10nM
100nM

neuronal cultures, compared to vehicle treated controls (Figure 5.4 C). However, evaluation of tau negative processes determined a significant ($p < 0.05$) decrease in the total process length in both 10nM and 100nM EpoD treated YFP cortical neurons, compared to vehicle treated controls (10nM EpoD: 20.95µm ± 4.75µm; 100nM EpoD: 23.08µm ± 9.14µm; vehicle: 41.81µm ± 15.97µm) (Figure 5.4 D).

Assessment of the branching complexity of YFP positive neurons was undertaken to determine the impact of EpoD treatment on neuronal development at 1DIV. It was identified that tau positive processes had no significant ($p > 0.05$) difference in the proportion of primary order processes (Figure 5.4 E). However there was a significant ($p < 0.05$) decrease in the proportion of tau positive secondary processes in both 10nM and 100nM EpoD treated YFP neurons, compared to vehicle treated controls (10nM EpoD: 9.14% ± 15.14%; 100nM EpoD: 7.57% ± 11.88%; vehicle: 28.41% ± 4.87%) (Figure 5.4 E). There was no significant ($p > 0.05$) difference in the complexity of YFP positive neurons with tertiary processes due to EpoD treatment (Figure 5.4 E).

Branching complexity of tau negative processes in YFP neurons at 1DIV was also evaluated. It was identified that 10nM and 100nM EpoD treated YFP neurons exhibited a significant ($p < 0.01$) decrease in the proportion of primary order processes, compared to vehicle treated controls (10nM EpoD: 42.17% ± 21.14%; 100nM EpoD: 29.26% ± 10.11%; vehicle: 76.47% ± 21.51%) (Figure 5.4 F). These results suggest that high doses of EpoD impact on the development on neuronal process length and complexity, and impact tau negative processes significantly greater than positive processes.

Similar to the earlier 1DIV time point, high concentrations of EpoD were found to reduce the complexity of cortical neurons at 4DIV (Figure 5.5 A), compared to vehicle treated neurons which had typically more longer and more highly branched neurites (Figure 5.5 B). It was determined that at 4DIV EpoD significantly ($p < 0.05$) reduced the total length of tau positive processes in YFP neurons when treated with 10nM and 100nM EpoD, compared to vehicle controls (10nM EpoD: 214.24µm ± 44.15µm; 100nM EpoD: 141.81µm ± 42.69µm; vehicle: 479.31µm ± 145.60µm) (Figure 5.5 C). Similarly, tau negative processes exhibit significantly ($p < 0.05$) reduced total process length when treated with 10nM and 100nM of EpoD, compared to

FIGURE 5.5. Neuronal process complexity at 4 DIV is affected by treatment with EpoD. (A) Representative tracings of YFP neurons at 4 DIV, which are less complex when treated with EpoD, (B) compared to vehicle treated neurons (tau +ve process, closed arrowhead; tau –ve process, open arrowhead). (C) Total length of tau +ve processes are significantly ($p < 0.001$) decreased in 10nM and 100nM EpoD treated YFP neurons. (D) Total length of tau negative processes are significantly decreased in 10nM ($p < 0.05$) and 100nM ($p < 0.01$) EpoD treated YFP neurons. (E) The proportion of tau +ve secondary order processes is significantly ($p < 0.001$) decreased in 10nM and 100nM EpoD treated YFP neurons. Tertiary order processes are also significantly decreased ($p < 0.0001$) in 1nM and 10nM EpoD treated YFP neurons, with no tertiary tau+ process in 100nM treated cells. (F) The proportion of tau –ve primary order processes is significantly ($p < 0.05$) reduced in 10nM and 100nM EpoD treated YFP neurons. Scale = 75µm. Data shown are: mean ± SD, (n = 3). One-Way ANOVA with Dunnett's post hoc test. Scale = 15µm. Abbreviations: NC, Naïve control.

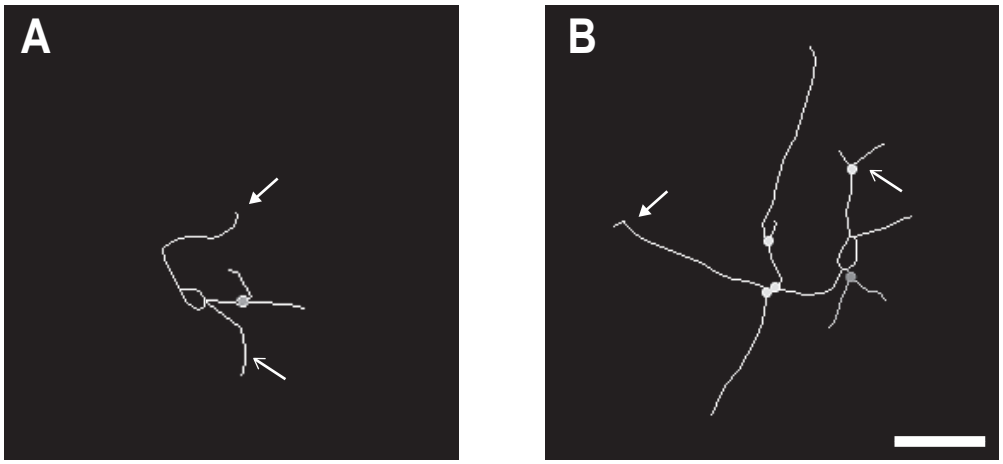
A
B

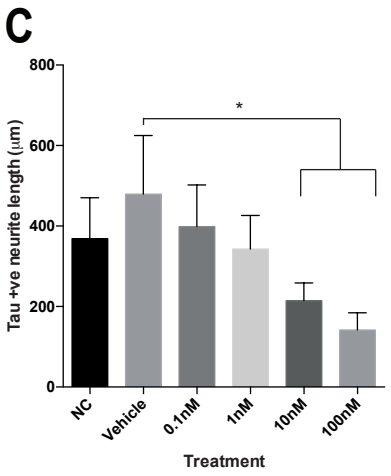
C
Tau +ve neurite length (μm)
800
600
400
200
0
*
NC
Vehicle
0.1nM
1nM
10nM
100nM
Treatment

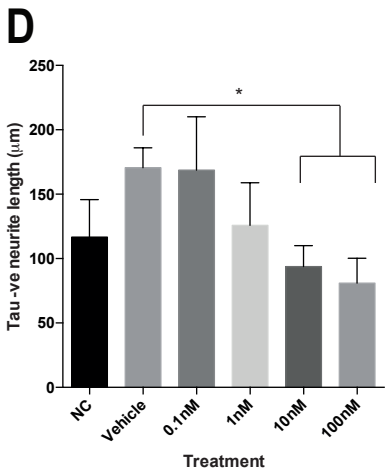
D
Tau -ve neurite length (μm)
250
200
150
100
50
0
*
NC
Vehicle
0.1nM
1nM
10nM
100nM
Treatment

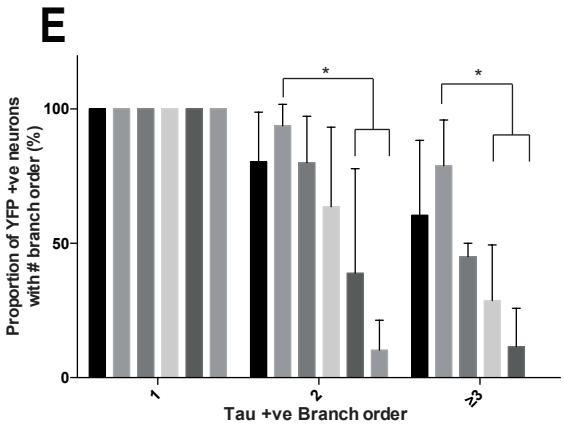
E
Proportion of YFP +ve neurons with # branch order (%)
100
50
0
*
*
1
2
≥3
Tau +ve Branch order

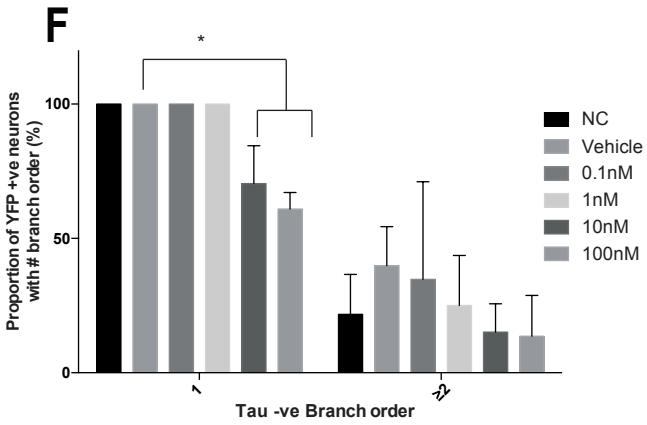
F
Proportion of YFP +ve neurons with # branch order (%)
100
50
0
*
1
≥2
Tau -ve Branch order
NC
Vehicle
0.1nM
1nM
10nM
100nM

vehicle treated controls (10nM EpoD: 93.81µm ± 16.18µm; 100nM EpoD: 80.87µm ± 19.32µm; vehicle: 170.49µm ± 15.59µm) (Figure 5.4 D).

Branching complexity at 4DIV in YFP neurons revealed that primary level tau positive processes were not significantly ($p > 0.05$) altered due to EpoD treatment (Figure 5.5 E). However, the proportion of YFP neurons with secondary order tau positive processes were significantly ($p < 0.001$) decreased in 10nM and 100nM EpoD treated YFP neurons, compared to vehicle treated controls (10nM EpoD: 38.91% ± 38.87%; 100nM EpoD: 10.23% ± 11.16%; vehicle: 93.75% ± 7.98%) (Figure 5.4 E). The proportion of tertiary order tau positive processes were also significantly ($p < 0.0001$) decreased in 1nM and 10nM EpoD treated YFP neurons, with 100nM EpoD treated YFP neurons exhibiting no tertiary order processes (1nM EpoD: 28.66% ± 20.74%; 10nM EpoD: 11.52% ± 14.28%; vehicle: 78.89% ± 17.00%) (Figure 5.5 E).

Evaluation of branching complexity of tau negative processes at 4DIV showed a significant ($p < 0.05$) decrease in the proportion of primary processes in 100nM EpoD treated YFP neurons, compared to vehicle treated controls (100nM EpoD: 60.96% ± 6.14%; vehicle: 100% ± 0%) (Figure 5.5 F). However, there was no significant ($p > 0.05$) decrease in the proportion of secondary processes in EpoD treated YFP neurons. These results suggest that EpoD impacts on the growth and complexity of both tau positive and negative processes, with high doses of EpoD impeding the growth of YFP cortical neurons.

5.3.5 EpoD alters the expression of microtubule proteins and microtubules chemical modifications in cortical neurons

Microtubule-targeting compounds such as EpoD affect the stability of the microtubule network, altering tubulin chemical modifications and the levels of proteins that are associated with both stability and dynamics (Benbow et al., 2011; Brunden et al., 2011). Qualitative evaluation of mature (10DIV) YFP cortical neuronal cultures treated with varying concentrations of EpoD revealed dose-dependant loss of YFP expression and MAP2 expression (Figure 5.6 A - E). It was identified that 0.1nM and 1nM EpoD treatments had no overt effect on YFP or MAP2 immunocytochemical labelling (Figure 5.6 B & C). However, 10nM and 100nM doses showed remarkable decrease in YFP and MAP2 expression (Figure 5.6 D & E). These observations suggest that YFP cells are vulnerable to high concentrations of EpoD, and that EpoD treatment triggers MAP2 loss from dendrites of mature cultured neurons.

FIGURE 5.6. Immunohistochemical analysis of NFM, YFP and MAP2 expression in mature (10 DIV) cortical neurons treated with EpoD. (A) Vehicle treated culture, (B) 0.1nM EpoD treated culture and (C) 1nM EpoD treated culture show no loss of YFP or MAP2 immunofluorescence. (D) 10nM EpoD treated culture and (E) 100nM EpoD treated culture show a reduction in YFP and MAP2 immunofluorescence. NFM appears unaltered due to EpoD treatment. Scale = 120μm.

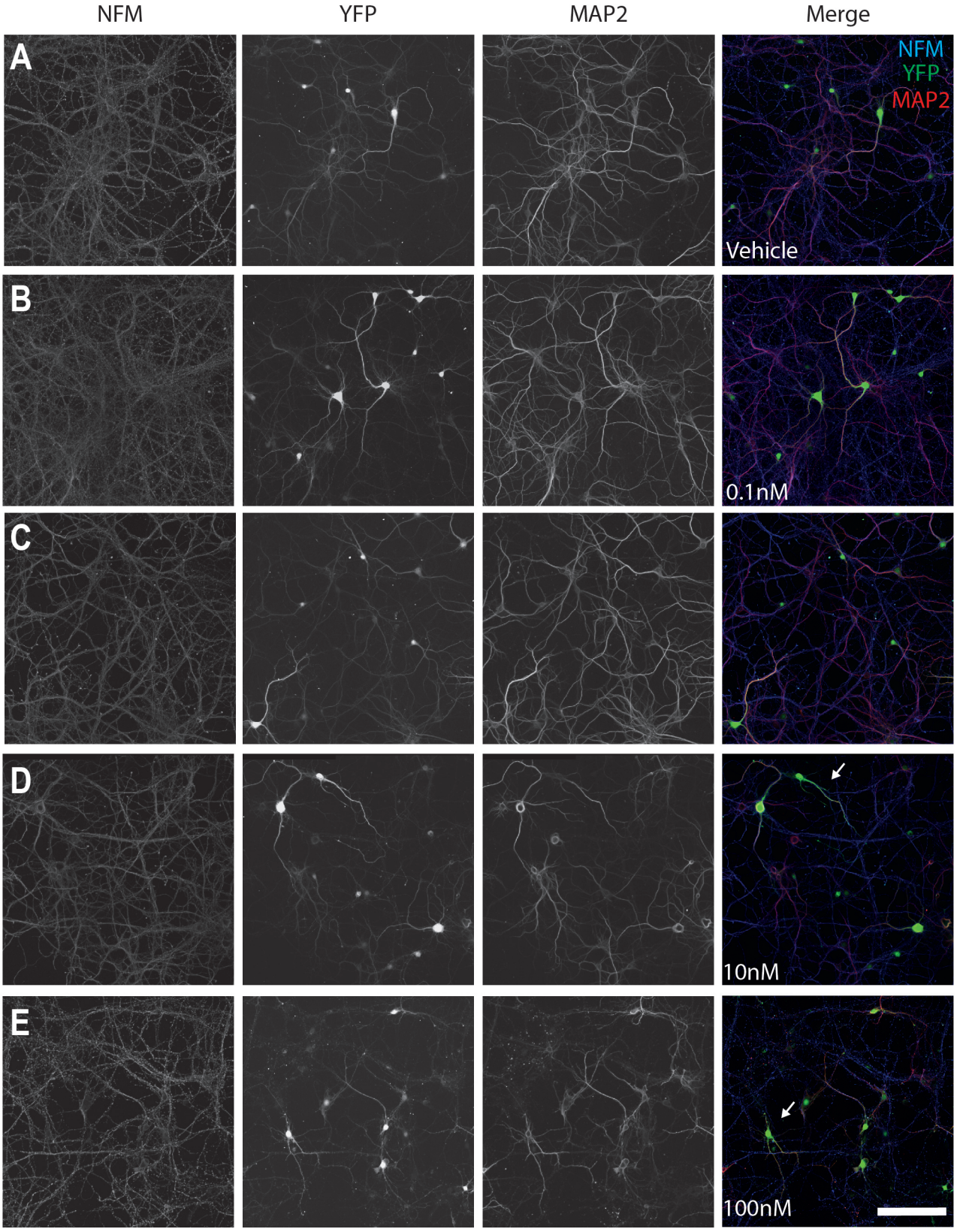
NFM
YFP
MAP2
Merge
A
B
C
D
E
NFM
YFP
MAP2
Vehicle
0.1nM
10nM
100nM

To probe microtubule protein expression further, relatively mature (10DIV) neurons were treated for 24 hours with varying concentrations of EpoD, followed by protein lysis and quantitation by Western blot. It was determined that low concentrations of EpoD does not significantly ($p > 0.05$) alter microtubule mass (α-tubulin levels) (Figure 5.7 A). In order to examine the efficacy of EpoD on microtubule stabilisation *in vitro*, tubulin acetylation, a biomarker for microtubule stability, was evaluated (Brunden et al., 2011). After 24 hours of treatment, tubulin acetylation in 100nM EpoD treated neurons was significantly ($p < 0.01$) increased, compared to vehicle treated controls (100nM EpoD: 2.087 ± 0.437; vehicle: 1.115 ± 0.114) (Figure 5.7 B). Lower doses of EpoD were comparable to vehicle controls.

Levels of EB3, a +TIP protein (as described in Chapter 1) was evaluated, as it is a protein associated with the dynamics of the microtubule network (Benbow et al., 2016). EB3 protein levels following 24 hour EpoD treatment were significantly ($p < 0.01$) decreased in neurons treated with 100nM of EpoD, with no changes in neurons treated with lower concentrations (100nM EpoD: 0.133 ± 0.060; vehicle: 0.384 ± 0.125) (Figure 5.7 C).

STOP is a MAP that is associated with the stable domains of the microtubule network (as in Chapter 1) (Bosc et al., 1996). EpoD stabilises microtubule networks in a dose dependant manner; identification of whether STOP levels also increase in a dose dependant manner during EpoD treatment is important, as altering STOP levels may have effects on microtubule dynamics and function. Indeed, it was determined that STOP levels are significantly ($p < 0.05$) increased in neurons treated with 10nM of EpoD, compared to vehicle treated control neurons (100nM EpoD: 0.471 ± 0.238; vehicle: 0.213 ± 0.190) (Figure 5.7 D). Surprisingly, STOP levels in 100nM EpoD treatments were comparable to vehicle treated controls. These results suggest that alterations to microtubule protein levels are dose dependant in EpoD treatment.

5.3.6 EpoD impairs mitochondrial transport in cortical neurons

Mitochondrial transport is important to meet the energy needs throughout the various compartments of the neuron, relying on the microtubule transport machinery to deliver and recycle mitochondria, as discussed in Chapter 1. Utilising live cell imaging, mitochondrial transport was evaluated in EpoD treated cortical neurons. In vehicle treated control cultures, mitochondrial transport is readily observed at a high speed (Figure 5.8 A). However,

FIGURE 5.7. EpoD alters the expression of MT proteins and a tubulin chemical modification in a dose dependant manner. (A) MT mass, as measured by α-tubulin levels, is not altered by low concentrations of EpoD. (B) Tubulin acetylation, a marker of MT stability, is significantly ($p < 0.01$) increased in 100nM EpoD treated neurons. (C) EB3 levels, a marker of MT dynamics, is significantly ($p < 0.01$) decreased in 100nM EpoD treated neurons. (D) STOP levels, a protein implicated in MT stabilisation, is significantly ($p < 0.05$) increased in 10nM EpoD treated neurons. (mean ± SD, n = 3).

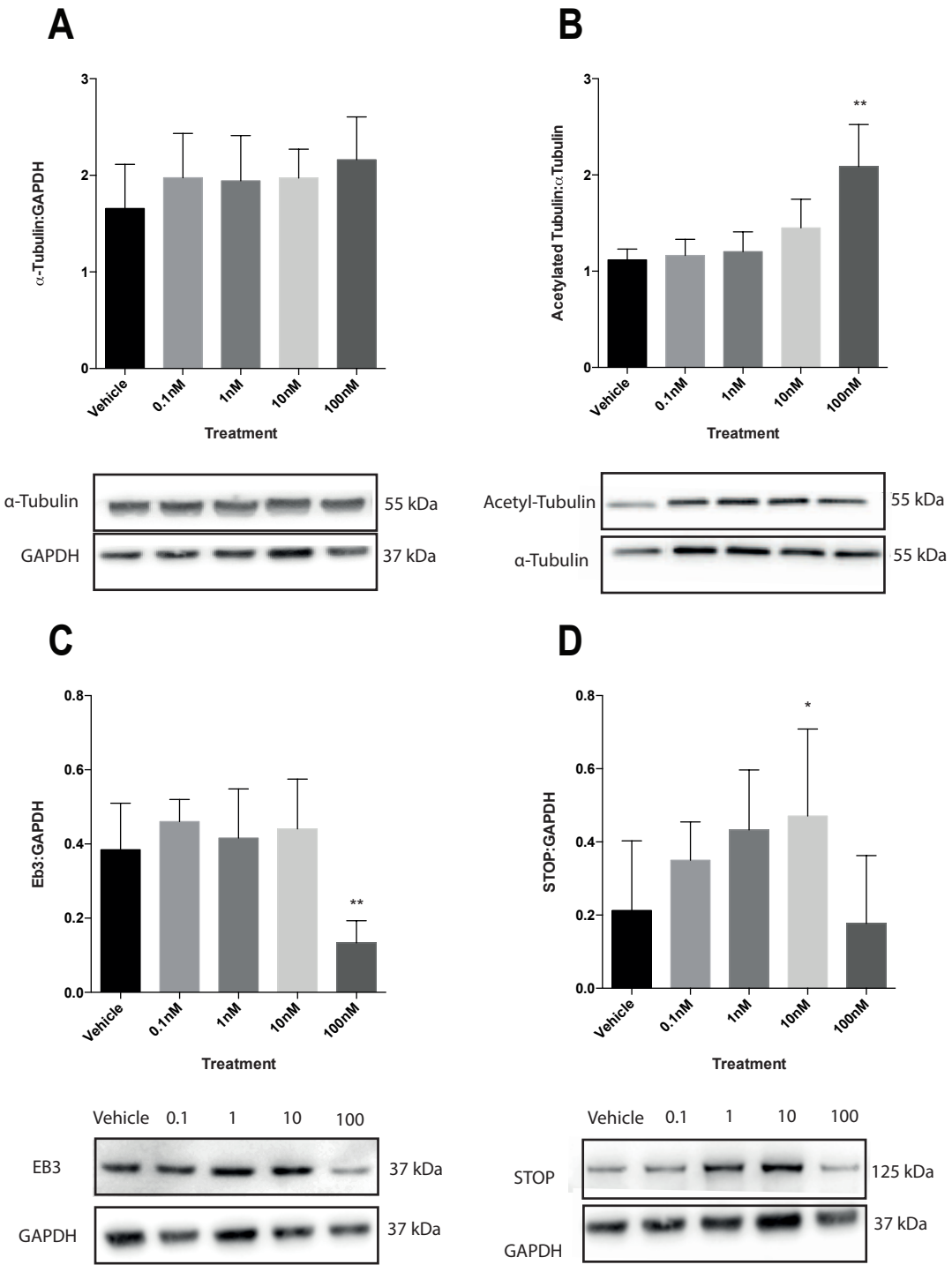
A
α-Tubulin:GAPDH
Vehicle
0.1nM
1nM
10nM
100nM
Treatment
α-Tubulin
GAPDH
55 kDa
37 kDa
B
Acetylated Tubulin:α Tubulin
**
Acetyl-Tubulin
α-Tubulin
55 kDa
55 kDa
C
Eb3:GAPDH
**
Vehicle 0.1 1 10 100
EB3
GAPDH
37 kDa
37 kDa
D
STOP:GAPDH
*
STOP
125 kDa
37 kDa

FIGURE 5.8. Mitochondrial transport in EpoD treated cortical neurons. (A) Mitochondria in vehicle treated controls move at a normal speed (arrows), (B) whereas neurons treated with high concentrations of EpoD show reduced mitochondrial speed. (C) The maximum speed of mitochondria two hours post EpoD treatment is significantly decreased in 10nM ($p < 0.01$) and 100nM EpoD ($p < 0.001$) treated neuronal cultures, compared to vehicle treated cultures. (D) Similarly, the average speed of mitochondria two hours post treatment is significantly ($p < 0.0001$) decreased in 10nM and 100nM EpoD treated neuronal cultures, compared to vehicle treated cultures. (E) The proportion of moving mitochondria is significantly decreased in 10nM ($p < 0.01$) and 100nM ($p < 0.0001$) EpoD treated neuronal cultures, compared to vehicle treated cultures. (F) The maximum speed of mitochondria 24 hours post EpoD treatment is significantly decreased in 0.1nM ($p < 0.05$), 1nM ($p < 0.05$), 10nM ($p < 0.01$) and 100nM ($p < 0.0001$) EpoD treated neuronal cultures, compared to vehicle treated cultures. (G) Similarly, the average speed of mitochondria 24 hours post treatment is significantly decreased in 0.1nM ($p < 0.05$), 1nM ($p < 0.05$), 10nM ($p < 0.0001$) and 100nM ($p < 0.0001$) EpoD treated neuronal cultures, compared to vehicle treated cultures. (H) The proportion of moving mitochondria is significantly ($p < 0.0001$) decreased in 10nM and 100nM EpoD treated neuronal cultures 24 hour post treatment, compared to vehicle treated cultures. Scale = 50μm. Data shown are: mean ± SD, (n = 3). * $P < 0.05$, ** $P < 0.01$, One-Way ANOVA with Dunnett's post hoc test. Scale = 15μm. Abbreviations: NC, Naïve control.

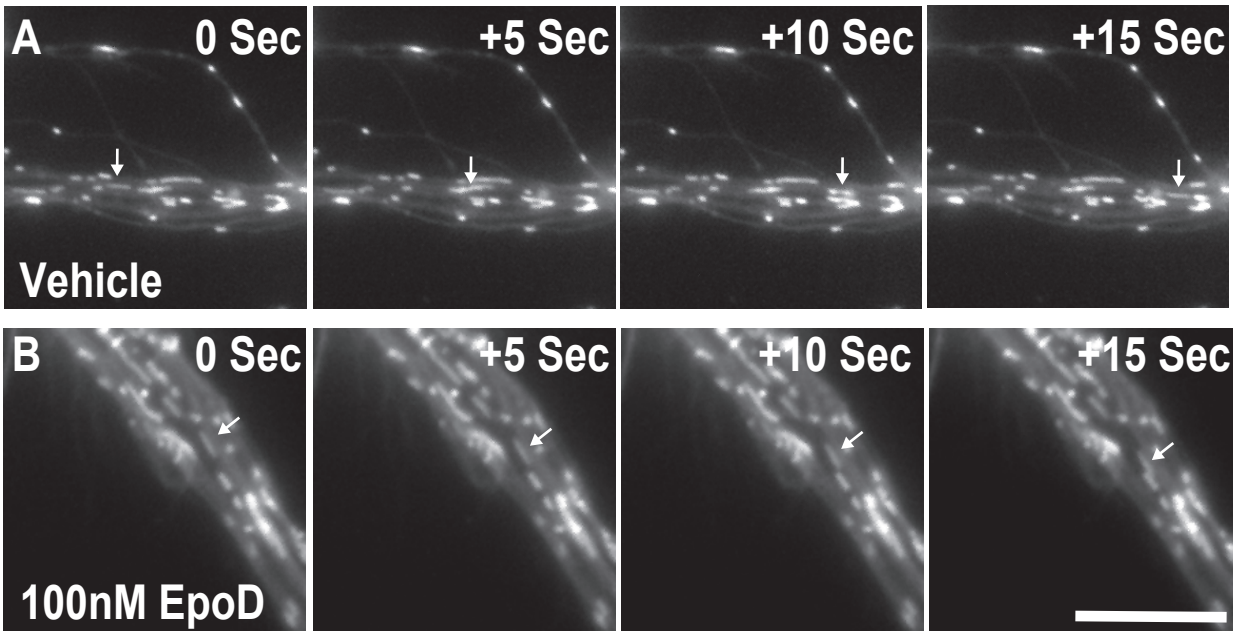
A
0 Sec
+5 Sec
+10 Sec
+15 Sec
Vehicle
B
0 Sec
+5 Sec
+10 Sec
+15 Sec
100nM EpoD

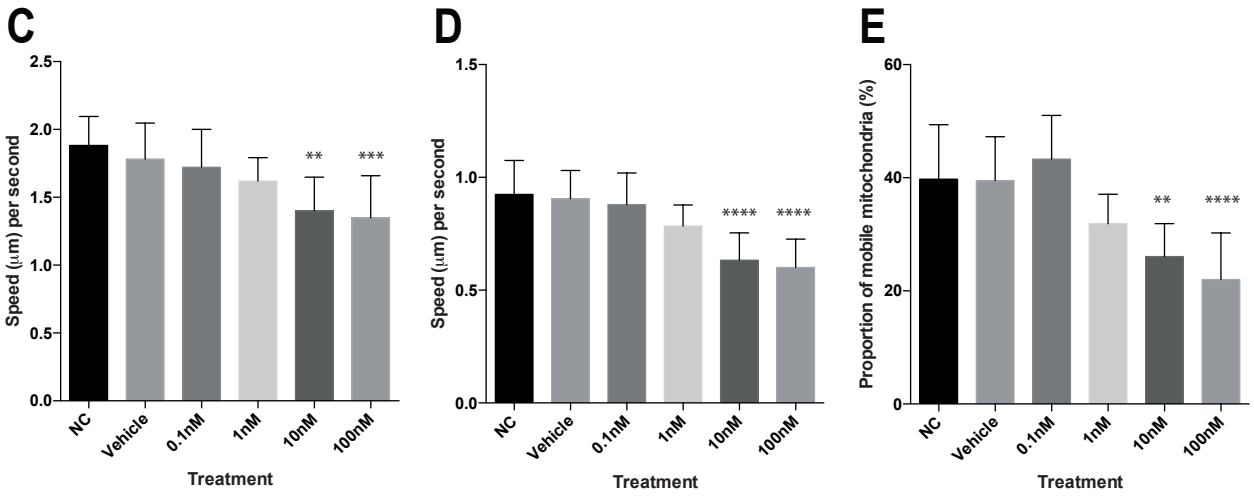
C
Speed (μm) per second
2.5
2.0
1.5
1.0
0.5
0.0
**
***
NC
Vehicle
0.1nM
1nM
10nM
100nM
Treatment
D
Speed (μm) per second
1.5
1.0
0.5
0.0
****
****
NC
Vehicle
0.1nM
1nM
10nM
100nM
Treatment
E
Proportion of mobile mitochondria (%)
60
40
20
0
**
****
NC
Vehicle
0.1nM
1nM
10nM
100nM
Treatment

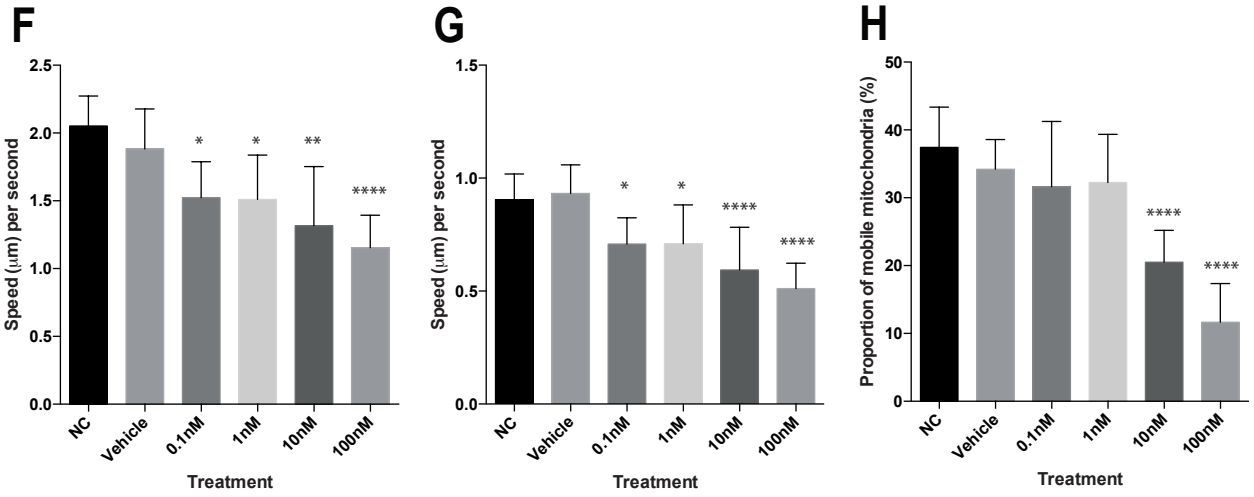
F
Speed (μm) per second
2.5
2.0
1.5
1.0
0.5
0.0
*
*
**
****
NC
Vehicle
0.1nM
1nM
10nM
100nM
Treatment
G
Speed (μm) per second
1.5
1.0
0.5
0.0
*
*
****
****
NC
Vehicle
0.1nM
1nM
10nM
100nM
Treatment
H
Proportion of mobile mitochondria (%)
50
40
30
20
10
0
****
****
NC
Vehicle
0.1nM
1nM
10nM
100nM
Treatment

mitochondrial transport is affected in a dose dependant manner in EpoD treated neurons (Figure 5.8 B). It was determined that the maximum transport speed of mitochondria is significantly ($p < 0.01$) impaired after 2 hours treatment in 10nM and 100nM EpoD treated cortical neurons, compared to vehicle treated controls (10nM EpoD: 1.40μm/s ± 0.25μm/s; 100nM EpoD: 1.35μm/s ± 0.31μm/s; vehicle: 1.78μm/s ± 0.27μm/s) (Figure 5.8 C). Further, the average transport speed of mitochondria 2 hours after treatment is significantly ($p < 0.001$) decreased in 10nM and 100nM EpoD treated neurons, compared to vehicle treated controls (10nM EpoD: 0.63μm/s ± 0.12μm/s; 100nM EpoD: 0.58μm/s ± 0.12μm/s; vehicle: 0.90μm/s ± 0.13μm/s) (Figure 5.8 D). The proportion of moving mitochondria was also evaluated, with 10nM and 100nM EpoD treatments triggering a significant ($p < 0.01$) decrease in the proportion of moving mitochondria in cultured cortical neurons, compared to vehicle treated controls (10nM EpoD: 26.07% ± 5.81%; 100nM EpoD: 21.00% ± 8.25%; vehicle: 39.50% ± 7.76%) (Figure 5.8 E).

Similarly, 24 hours post treatment the maximum transport speed of mitochondrial was significantly ($p < 0.05$) impaired in 0.1nM, 1nM, 10nM and 100nM EpoD treated cortical neurons, compared to vehicle treated controls (0.1nM EpoD: 1.45μm/s ± 0.17μm/s; 1nM EpoD: 1.51μm/s ± 0.33μm/s; 10nM EpoD: 1.32μm/s ± 0.44μm/s; 100nM EpoD: 1.15μm/s ± 0.24μm/s; vehicle: 1.88μm/s ± 0.30μm/s) (Figure 5.8 F). Further, the average transport speed of mitochondria 24 hours after treatment is significantly ($p < 0.05$) decreased in 0.1nM, 1nM, 10nM and 100nM EpoD treated neurons, compared to vehicle treated controls (0.1nM EpoD: 0.71μm/s ± 0.12μm/s; 1nM EpoD: 0.71μm/s ± 0.17μm/s; 10nM EpoD: 0.59μm/s ± 0.19μm/s; 100nM EpoD: 0.51μm/s ± 0.19μm/s; vehicle: 0.93μm/s ± 0.13μm/s) (Figure 5.8 G). The proportion of moving mitochondria was significantly ($p < 0.0001$) reduced in 10nM and 100nM EpoD treatments, compared to vehicle treated controls (10nM EpoD: 20.50% ± 4.70%; 100nM EpoD: 11.66% ± 5.71%; vehicle: 34.19% ± 4.40%) (Figure 5.8 H). These results suggest that EpoD impairs mitochondrial transport in a dose dependant manner, with individual concentrations having an increasingly detrimental effect on transport speed over time.

5.4 Discussion

Targeting microtubules as a pharmacological intervention is becoming an increasingly attractive and investigated therapeutic strategy for various neurodegenerative diseases and injury (Brunden et al., 2010; Brunden et al., 2011; Zhang et al., 2012; Cartelli et al., 2013; Brizuela et al., 2015). However, despite the increased use of these CNS penetrant, microtubule targeting compounds,

the consequence of cortical neurons exposure is still poorly understood (Baas and Ahmad, 2013). The current chapter investigated the effect low concentrations of EpoD has on growth, survival and function of cortical neurons *in vitro*. EpoD was hypothesised to alter microtubule dependant outcomes, such as neurite growth, complexity and length, microtubule stability, microtubule dependant transport and cellular viability in a dose dependant manner. The current chapter highlights that EpoD impairs various aspects of cortical neurons, with a strong emphasis on the dose dependant nature of the compound. Furthermore, results suggest that cultured neurons treated in an environment comparable to EpoD doses previously used in *in vivo* models of neurodegeneration, such as in Chapter 4, may be experiencing microtubule dependant dysfunction, particularly when considering protein levels and organelle transport.

5.4.1 Reported *in vivo* CNS concentrations of Epothilone D effect the health of cortical neurons *in vitro*

Many studies utilising EpoD as a possible neurodegenerative disease therapeutic use doses between 1mg/ml to 3mg/ml (Andrieux et al., 2006; Brunden et al., 2010; Brunden et al., 2011; Zhang et al., 2012). It was reported that low dose EpoD is retained in the CNS at bioactive levels for days, with cells experiencing an environment of low nanomolar concentrations of EpoD (Brunden et al., 2011). In the current investigation concentrations were chosen ranging from picomolar to high nanomolar levels of EpoD to represent these previously reported *in vivo* findings (Brunden et al., 2011). It was identified that EpoD concentrations similar to those reported in the CNS of EpoD treated mice are neurotoxic to cultured cortical neurons. Indeed, low dose EpoD treatment was found to cause decreased cell viability, growth and impair microtubule transport. Similar phenomenon have been reported previously when treating neuronal cultures with microtubule targeting compounds. For example, Letourneau and Ressler (1984) treated cultured chick sensory neurons with various concentrations of taxol, reporting that higher doses cause inhibition of neurite initiation and growth, which is rescued at lower doses (Letourneau and Ressler, 1984).

More relevant to the current study, Jang and Coleagues (2016) treated various types of neurons with EpoB, reporting that EpoB exhibits both beneficial and negative effects depending on both neuronal subtype, dosage and age of the neurons (Jang et al., 2016). For example, EpoB was found to decrease cell viability and prevent axonal growth at nanomolar concentrations. However, the authors report that picomolar concentrations of EpoB promoted axonal growth in

cortical neurons, a phenomenon not identified in the current study utilising EpoD. In the current Chapter, only 0.1nM EpoD treatments were in the picomolar range, suggesting that future experiments may benefit using lower concentrations of EpoD. Indeed, the current chapter did not find any proportion of axonal growth with EpoD treatment. However, one cell population was selected in the current study (YFP positive cortical neurons), whereas Jang et al., did not select for individual cortical subtypes (Jang et al., 2016). Our laboratory has previously shown that picomolar (0.1nM) concentrations of EpoD promotes axonal regeneration in a scratch assay injury model, further promoting the use of sub nanomolar concentrations of EpoD to improve neuronal growth (Brizuela et al., 2015).

Results from the current chapter suggest that doses being used for targeting microtubules in neurodegenerative diseases may be neurotoxic to cortical neurons, however, as such compounds work in a dose-dependant manner, evaluation of target and desired outcome will need to be considered. High doses of microtubule targeting compounds cause painful peripheral neuropathies, whereas the popular conception is that low doses (such as those used to treat neurodegenerative diseases) are safe (Carlson and Ocean, 2011; Baas and Ahmad, 2013). Current results suggest that although high doses of EpoD cause a reduction in cortical neuron viability and healthy, low doses have long lasting effects on organelle transport, as was shown with impaired mitochondrial transport in mature neurons. This highlights that whilst low doses of microtubule targeting compounds, such as EpoD utilised in Chapter 4, may not cause a neuropathic phenotype, there may exist an underlying dysfunction to microtubule dependant processes, such as microtubule dependant transport (Shemesh and Spira, 2010). Similar results were described by Shemesh and Spira (2010), who showed that 10nM and 100nM of paclitaxel causes polar reconfiguration of neuronal microtubules and decreases mitochondrial transport (Shemesh and Spira, 2010). Indeed, others have shown that low doses of taxol decreases the ability for neurons to produce collateral branches, findings which were identified in the current study, with a reduction in complexity of both tau positive and negative (axons and dendrites, respectively) branches (Letourneau et al., 1986). It should be noted that although the current study reports EpoD treatment alters both tau positive and negative processes, our laboratory has also shown that stabilisation of cortical neurons with EpoD can decrease the expression of tau isoforms (Brizuela et al., 2015). Regardless, this Chapters aim was to characterise morphometric analysis of tau positive and negative processes (axons and dendrites respectively). Further, no

gross alterations to tau immunolabelling were evident between EpoD concentrations during image analysis.

5.4.2 Epothilone D effects neurons without increasing microtubule stability

In the current study, alterations to neuronal growth, health and function occurred at concentrations of EpoD that did not increase stability markers of the microtubule network. At 24 hours after treatments, only 100nM EpoD treatments showed increased microtubule stability *in vitro*, and it has been previously reported that even at two hours post treatment 100nM EpoD shows significant increase in microtubule stabilisation (Brizuela et al., 2015). Whilst it was identified that growth, viability and organelle transport was impaired at 100nM, lower doses of EpoD also impair neuronal function (Jang et al., 2016).

Evaluation of mitochondrial transport suggests that higher doses of EpoD have a hastened effect on inducing transport dysfunction, whereas lower concentrations cause transport dysfunction 24 hours post treatment. Further, whilst there is a significant impairment in the transport speed of mitochondria in neurons treated with low concentration of EpoD, the proportion of moving mitochondria remains unchanged until a higher concentration of EpoD is used. The mechanisms behind this were not investigated, however, as dynamics and stability of the microtubule network correlates with microtubule dependent transport efficiency (Fanara et al., 2007; Shemesh and Spira, 2010), it may be due to dose dependent EpoD alterations to microtubule network stability (Brunden et al., 2011).

5.4.3 Epothilone D alters protein levels of MAPs

This chapter determined that alterations to the protein levels of MAPs and tubulin acetylation occur in a dose dependant manner with EpoD treatment. Increases in markers of stability (acetylation and STOP) and a decrease in EB3 levels with increasing EpoD concentrations suggest that the microtubule network becomes increasingly stabilised in treated neurons. Many studies use tubulin acetylation as a biomarker for microtubule stability, however, others evaluate microtubule dynamics and stability by analysing EB3 comets (Shemesh and Spira, 2010; Kleele et al., 2014; Brill et al., 2016). Indeed, using this technique has shown that the microtubule targeting compound paclitaxel reduces the density of EB3 comets, thus signifying a reduction in microtubule dynamics and increased microtubule stability (Shemesh and Spira, 2010). The current chapter showed that 100nM EpoD treated neurons exhibited increased acetylation with a concurrent decrease in EB3 protein levels, suggesting this mechanism may also occur in EpoD

treated neurons. A study by Benbow et al (2016) showed that a similar phenomenon occurs *in vivo*, where mice treated with high doses of paclitaxel, where treated mice showed supressed EB3 immunofluorescence in the sciatic nerve (Benbow et al., 2016). Further, EpoB treatment *in vivo* decreases EB3 comets in the distal axon during phasic pruning (Brill et al., 2016). This suggests that microtubule stabilisation with microtubule targeting compounds such as EpoD causes alterations to EB3 protein levels and microtubule +TIP localisation.

Interestingly, STOP protein levels are increased at 10nM concentrations of EpoD, but were reduced back to levels comparable with vehicle controls in 100nM EpoD treated cultures. The cause of this differential response of STOP protein levels is unknown. However it is quite surprising, as 100nM EpoD doses were shown to increase tubulin acetylation and stability, it would not be unreasonable to assume STOP levels would also be increased at this concentration of EpoD. STOP is a protein that binds to microtubules in response to cold induced depolymerisation (Slaughter and Black, 2003). STOP has a number of calmodulin binding sites (Bosc et al., 2001), and can be regulated by calmodulin (Lefevre et al., 2013), and is susceptible to increasing intracellular calcium levels. Therefore the reduction in STOP levels in 100nM EpoD treatments may be due to increased intracellular calcium due to decreased cellular viability (Job et al., 1981). Interestingly, STOP-null mice are used as a model of schizophrenia, as microtubules have been implicated in the disorder (Andrieux et al., 2006; Fournet et al., 2012; Volle et al., 2013). EpoD treatment of STOP-null mice improves this disorder by stabilising microtubules (Fournet et al., 2012), suggesting the stability properties of both STOP and EpoD affect the stable microtubule domains to a high extent. It will be interesting to identify whether these MAPs (such as STOP and EB3) are affected during dosages of EpoD comparable to those used for cancer therapy (Cheng et al., 2008).

5.4.4 Conclusion

Microtubule targeting compounds are increasingly being considered for their therapeutic potential in various neurodegenerative diseases. However, how these compounds effect normal neuronal functioning is still poorly understood. It was found that EpoD impaired normal neuronal growth, viability and caused dysfunction to microtubule dependant transport at concentrations comparable to those used in Chapter 4 and in previous preclinical neurodegenerative trials (Table 5.1).

EpoD concentration (nM)	1DIV	4DIV	Mature 2hr after treatment	Mature 24 hr after treatment
0.1	No impact	No impact	No impact	↓Mitochondria speed
1	No impact	↓ Tau +ve process complexity	No impact	↓Mitochondria speed
10	↓ Tau +ve & -ve process complexity ↓ Tau –ve process length	↓ Tau +ve process complexity ↓ Tau +ve/-ve process process length	↓ Cell viability ↓ Nuclear health ↓ mitochondria speed and movement	↓ Cell viability ↓ Nuclear Health ↓Mitochondria speed and movement ↓MAP2 expression ↑ STOP levels
100	↓ Nuclear health ↓ neurite extension ↓ Tau +ve/-ve process complexity ↓ Tau –ve process length	↓ Cell viability ↓ Tau +ve process complexity ↓ Tau +ve/-ve process length	↓ Cell viability ↓ Nuclear health ↓ Mitochondria speed and movement	↓ Cell viability ↓ Nuclear health ↓Mitochondria speed and movement, ↓MAP2 expression ↑ Tubulin acetylation levels ↑ STOP levels

Table 5.1

These findings suggest that consideration of dose of EpoD, as well as the intended target or outcome are of vital consideration when utilising EpoD as a potential therapeutic intervention in neurodegenerative diseases. Indeed, this becomes of greater importance where the microtubule network may be differentially altered in disease states, where both timing and dose then become relevant. Future studies utilising pharmacological manipulation of microtubule stability would benefit from a greater understanding of the microtubule environment, and how such microtubule targeting compounds affect the microtubule cytoskeleton.

Chapter 6

6 General discussion

Although having been researched for over a century, there has been limited to no translation of treatment strategies to modify disease outcomes in ALS. ALS is thought to have a long pre clinical stage, hampering early detection of the disease, particularly in the vast majority of sporadic ALS cases who have no underlying familial link (Eisen et al., 2014). Currently ALS research is heavily focused on the development of biomarkers to detect ALS, allowing for an earlier window of treatment that may improve patient outcomes (Cudkowicz et al., 2010; Shepheard et al., 2014; Thompson et al., 2016). However, such strategies are complex in ALS, as ALS is considered a highly heterogeneous disease in its mechanisms. This is highlighted by the plethora of ALS causing mutations, where seemingly unrelated mutations culminate in the degeneration of MNs (Ticozzi et al., 2011; Marangi and Traynor, 2015). Indeed, ALS is also multifaceted in its pathophysiological mechanisms for which both the upper and lower motor circuitry is vulnerable. The clinical phenotype of ALS, such as muscle paralysis and wastage, which is described in Chapter 1 of this thesis, is caused by the destruction of the neuromuscular circuitry necessary for activation of muscle movement and survival (Miller et al., 2006; Moloney et al., 2014). When a critical portion of this circuit is lost from a given anatomical location, symptoms of ALS appear (Kennel et al., 1996; Hegedus et al., 2008). Identification of the earliest pathology in the distal portion of this circuit, such as the axon and NMJ synapse, is crucial for the design and implementation of treatment strategies to improve outcomes in ALS.

The loss of muscle innervation in ALS is thought to progress in a ‘distal die-back’ manner, where the synaptic and axonal processes degenerate prior to the loss of the a-MN soma (Fischer et al., 2004; Fischer and Glass, 2007; Moloney et al., 2014). Microtubules are implicated not only in axonal degeneration, but are also reported to be hyperdynamic (Fanara et al., 2007; Kleele et al., 2014), and are implicated in axonal transport dysfunction in ALS (Bilsland et al., 2010). Targeting microtubules to improve axonal pathology has been shown to improve outcomes in models of neurodegenerative diseases with similar pathological mechanisms to ALS (Brunden et al., 2010; Cartelli et al., 2013; King et al., 2013). Such treatment strategies hold promise in ALS, where stabilising microtubules in the distal neuromuscular circuitry may improve outcomes and prevent degeneration and modify disease progression (Fanara et al., 2007). This thesis has explored the concept of protecting the distal neuromuscular circuitry with microtubule targeting

compounds. This thesis characterised the progression of pathology in the distal neuromuscular circuitry to determine the earliest pathological phenomenon to target in a new treatment strategy. Further, this thesis explored the utility of a microtubule stabilising compound EpoD, and impact EpoD may have in normal neuronal systems, raising considerations for their use.

6.1 Characterisation of the distal neuromuscular circuit

Characterisation of the early changes to the distal neuromuscular circuitry to aid in identification of therapeutic targets is still not fully complete. Chapter 3 of this thesis evaluated the time course of pathology in pre- and post-synaptic compartments of the NMJ, with particular focus on the distal axon, NMJ degeneration and morphology, as well as synaptic architectural proteins. Data obtained from the SOD1^{G93A} mouse model of ALS determined that the earliest pathological phenomenon identified in the distal neuromuscular circuitry is the generation of axonal and NMJ pathology (Pun et al., 2006; Fischer and Glass, 2007; Hegedus et al., 2008). This degeneration occurs firstly in the hindlimb of the SOD1^{G93A} mouse model, with delayed pathology in the forelimb, cementing the hindlimb as the primary site of pathological characterisation in this model (Beers et al., 2011). Indeed, data agreed with previous reports that distal pathology is progressive (Frey et al., 2000; Fischer et al., 2004), with presynaptic alterations occurring first (such as axonal and NMJ pathology), followed by novel alterations to the post-synaptic apparatus of the NMJ, particularly a loss of synaptic localisation of architectural protein involved in stability and maintenance (Darabid et al., 2014). Interestingly, these architectural proteins had elevated levels in the SOD1^{G93A} mouse muscle (LRP-4, rapsyn, dystrophin), or showed evidence of misprocessing (nestin). These proteins are either implicated already in ALS pathophysiology, with nestin expression altered in SOD1^{G93A} hippocampus (Lee et al., 2011), or implicated in other genetic neuromuscular disorders, as described in Chapter 1. Collectively, these results suggest the NMJ may be vulnerable to pathology when key architectural proteins are altered in ALS. Early axonal pathology and degeneration of the distal synapse, as stated previously, is thought to begin years to decades prior to the onset of overt symptoms in ALS (Frey et al., 2000; Miller et al., 2006). As disease screening is improved in ALS patients, targeting this pathology may allow for improved outcomes.

The early presence of axonal pathology in the SOD1^{G93A} mouse model identified in this thesis' studies, as well reported in human patients (Ellis et al., 1999; Fischer et al., 2004; Moloney et al., 2014), endorses the use of a therapeutic intervention that has the capacity to protect the distal

axon from degeneration. Chapter 4 explored the efficacy of the microtubule targeting compound EpoD to improve outcomes in the SOD1^{G93A} mouse model by protecting the distal axon (Brunden et al., 2014; Eira et al., 2016).

6.2 Targeting microtubules to protect the distal axon and improve outcomes in ALS

Microtubule involvement in ALS is becoming increasingly more appreciated, particularly being implicated in axonal degeneration (Zhai et al., 2003; Wang et al., 2012; Ma, 2013; Park et al., 2013), and also as a primary mechanisms of disease, leading to a hyperdynamic phenotype of the microtubule network (Devon et al., 2006; Fanara et al., 2007; Bilsland et al., 2010; Alami et al., 2014; Smith et al., 2014). Microtubules are a highly vulnerably intracellular organelle, as they can also be impacted downstream of other identified ALS mechanisms, as described in Chapter 1. Chapter 4 investigated to capacity for axonal protection in ALS by stabilizing microtubules, as axonal degeneration identified in Chapter 3 was the earliest pathological event in the distal neuromuscular circuitry (Clark et al., 2016b). Microtubule stabilization to improve axonal pathology through treatment with EpoD has been shown to improve other models of neurodegenerative disease (Brunden et al., 2010; Zhang et al., 2012; Cartelli et al., 2013). Indeed, these diseases suffer similar microtubule pathology, as identified during axonal degeneration, but also changes to microtubule dynamics; stabilization offers an attractive therapeutic target across multiple neurological diseases (Brunden et al., 2011; Brunden et al., 2014; Eira et al., 2016). Previously, such therapeutics have been used primarily to target pathology in the cortex, generally for neurodegenerative disorders, but also traumatic brain injury (Zhang et al., 2005; Ruschel et al., 2015). A number of studies have utilised taxanes and epothilones to target and improve outcomes in animal models of tauopathies and spinal cord injury (Zhang et al., 2005; Ruschel et al., 2015); however, the current thesis was the first to utilise EpoD to target spinal cord. Epothilones have been reported to stabilize microtubules in the distal processes in which the current thesis endeavoured to target in ALS, suggesting that such treatment strategies have merit (Brill et al., 2016).

Protection of neuronal soma and axons by treatment with microtubule stabilizing compounds was supported in Chapter 4, with EpoD protecting both the cell soma and distal axon of the neuromuscular circuitry early in the disease. Indeed, this treatment was identified to promote soma and axonal protection at an age where mice show similar clinical phenotype of decreased EMG readings, a phenomenon utilized in the diagnosis of ALS patients, suggesting possible

clinical translation (Kennel et al., 1996; Scott et al., 2008). Interestingly, data from Chapter 4 suggests that EpoD does not protect the NMJ from degeneration. The discrepancy between the axon and NMJ but may be explained by the subtle differences in microtubule dynamics and environment between the two distal compartments (Yan and Broadie, 2007; Bodaleo and Gonzalez-Billault, 2016).

The use of multi-level mixed effects linear regression models, non-linear polynomials (cubics) and break point analysis is a sophisticated method for data representation, interpretation and estimation of disease progression and drug effect (Durban et al., 2005; Chen and Stanley, 2012; Grajeda et al., 2016). Indeed, Chapter 4 highlighted the utility of using such methods, with results suggesting somatic and axonal protection was not associated with improvements in motor behaviour. This implies that EpoD is effective at targeting an aspect of distal pathology, with limited to no behavioural or neurological benefits at comparable ages. Indeed, EpoD was concluded to be detrimental to motor and neurological functioning later in disease stages, and decreased the life span of treated $SOD1^{G93A}$ mice. This was also associated with possible neurotoxic effect of EpoD on lumbar a-MNs in the later stages of the disease, and increased levels of gliosis (Clement et al., 2003; King et al., 2011; Radford et al., 2015). This highlights that both dose and timing of EpoD treatments need to be re-evaluated, particularly as ALS pathophysiology is a progressive and evolving process, as described in Chapter 1 and reported in Chapter 3.

Further, whilst microtubule pathology in ALS is increasingly being understood, future research into this increasingly involved mechanism may uncover new targets and ages at which to test pharmacological agents in the various ALS animal models available (Dubey et al., 2015; Clark et al., 2016a; Eira et al., 2016). For example, many downstream signalling mechanisms reportedly altered in ALS are yet to be investigated in regards to microtubule function and dynamics (Hall and Lalli, 2010; Gonzalez-Billault et al., 2012; Wojnacki et al., 2014) These include the Rho-Rac GTPase pathways (Wen et al., 2004; Wojnacki et al., 2014), which have been implicated in altered actin and immunological function in ALS (D'Ambrosi et al., 2014; Droppelmann et al., 2014), as well as the CDK5-p25 pathways (Nikolic et al., 1996; Ahlijanian et al., 2000), which are implicated in excitotoxic dependant phosphorylation events in ALS (Patzke and Tsai, 2002). Indeed, the familial mutations to Alsin are though to alter such signalling pathways, supporting this hypothesis (Kunita et al., 2007). These signalling pathways have the capacity to effect many

different aspects of the microtubule network, and it should be noted, are involved in microtubule network development and dynamics during neurogenesis and axonal path finding (Palazzo et al., 2001; Wojnacki et al., 2014), suggesting aberrant signalling may cause microtubule dysfunction in adult onset disorders.

Regardless of the mechanism behind microtubule dysfunction, many studies report aberrant impacts of utilising microtubule targeting compounds to improve microtubule pathology. This is due to their association with pathologically altering the microtubule environment, causing gross microtubule dysfunction and cellular demise (Shemesh and Spira, 2010; Baas, 2013; Benbow et al., 2016). Although Chapter 3 highlighted that axonal protection is an attractive target, results from Chapter 4 suggest that such a therapeutic model may only work at particular ages, for a particular time. This raises the option of combination therapies for ALS treatment, a direction that is being increasingly considered in ALS research (Turner and Talbot, 2008; Goutman and Feldman, 2015). Re-evaluation of dose and timing of EpoD treatment, coupled with utilising compounds to target other pathology, such as NMJ stabilization and aberrant gliosis, may cumulatively improve pathology and offer beneficial outcomes to the behavioural, clinical and survival phenotypes in ALS (Zhu et al., 2002; Krakora et al., 2012; Musaro, 2013).

The possibility of EpoD dependent neurotoxicity reported in Chapter 4 suggest that the microtubule targeting compounds and their aberrant effect on neuronal function can occur at low-doses (Baas, 2013). Interestingly, limited research has characterized the impact such compounds have on normal neuronal function (Letourneau and Ressler, 1984; Letourneau et al., 1986; Baas and Ahmad, 2013; Jang et al., 2016). Low doses of such compounds, such as those used in Chapter 4, are thought to be safe, limiting changes to microtubule dynamics to levels where microtubule dependent processes can still function at a physiologically normal level (Brunden et al., 2011; Brunden et al., 2014; Eira et al., 2016). However, increasing evidence suggests that even low doses of microtubule targeting compounds can have overt effects on neuronal growth, health and function (Letourneau and Ressler, 1984; Letourneau et al., 1986; Brill et al., 2016; Jang et al., 2016).

6.3 Pharmacological stabilisation of neuronal microtubules is a complex process

As described in Chapters 1, 4 and 5, microtubule targeting compounds are becoming increasingly considered as a potential therapeutic strategy for neurological disorders and injury (Brunden et al., 2014; Brizuela et al., 2015; Ruschel et al., 2015; Eira et al., 2016). However, limited attention has been given to how these compounds impact on normal neuronal function, even when utilized at doses substantially lower than used in cancer therapy (Albright et al., 2011; Brunden et al., 2011). The high doses used in cancer therapies cause aberrant hyper stabilisation of the microtubule network, a process that causes altered microtubule dependent transport (Shemesh and Spira, 2010), expression of microtubule proteins (Benbow et al., 2016), and causes peripheral neuropathy (Lee and Swain, 2006; Argyriou et al., 2011). Surprisingly, lower doses reported to be beneficial in models of neurodegenerative diseases, such as those used in Chapter 4, were found to be detrimental to neuronal growth, health and function in Chapter 5 (Jang et al., 2016).

Data from Chapter 5 suggests that low nanomolar concentrations of EpoD, comparable to the concentration of EpoD reported to be at the cell body in Chapter 4 (Albright et al., 2011; Brunden et al., 2011), are neurotoxic to cultured mouse primary cortical neurons (Jang et al., 2016). This chapter evaluated a number of outcomes that are dependent on microtubules, such as neurite outgrowth and complexity, as well as organelle transport. Similar to data reported previously using paclitaxel and EpoB, EpoD was found to negatively impact neurite outgrowth, length and complexity (Letourneau et al., 1986; Jang et al., 2016). Further, aberrant microtubule stabilization was found to decrease transport of mitochondria (Shemesh and Spira, 2010), a phenomenon that was supported in Chapter 5 with increasing concentrations of EpoD on cultured primary neurons.

Microtubule targeting compounds such as EpoD were designed to be cytotoxic to malignant cells. Data from Chapter 5 suggests that low concentrations of EpoD may significantly alter microtubule dynamics and cause a decrease in neuronal cell viability, both during phases of growth (1-4 days in vitro, DIV) or in relatively mature neurons (10 DIV) (Jang et al., 2016).

Data from this thesis supports that neurotoxicity identified in Chapter 4 may be caused by as yet unreported aberrant effects of low dose EpoD treatments. These effects may be exacerbated in ALS, as microtubule dynamics are thought to be important in disease progression, as discussed in Chapter 1 (Fanara et al., 2007). It should then be reiterated that dose and timing of such therapeutics should be re-evaluated for use in ALS. Regardless, low doses of EpoD was found to

be neuroprotective early in the disease in the SOD1^{G93A} mouse model, limiting the early a-MN soma and axonal degeneration, suggesting that EpoD may still hold promise as a future therapeutic for ALS, most likely in combination with other therapeutic compounds (Goutman and Feldman, 2015; Ittner et al., 2015; Turner and Swash, 2015).

6.4 Future directions and limitations

This thesis focused on the characterisation of the distal neuromuscular circuitry, microtubule targeted axonal protection and the impact of a microtubule targeting compound on normal neuron function. Firstly, characterisation of the distal neuromuscular circuitry in Chapter 3 focused only on static time points in the SOD1^{G93A} mouse model. Our laboratory has previously utilised *in vivo* live-imaging techniques to repeatedly visualise changes to YFP expressing distal axonal and NMJ morphology over a number of weeks (Feng et al., 2000b; Blizzard et al., 2015). Utilising this method would further benefit the characterisation of distal disease progression in the SOD1^{G93A} mouse. Further, only post-synaptic architectural proteins were investigated in the SOD1^{G93A} mouse model. However, formation, maturation and stability of the NMJ rely on both pre- and post-synaptic NMJ proteins, such as those described in Chapter 1. Presynaptic proteins implicated in other neuromuscular disorders such as various laminin isoforms (Nishimune et al., 2004; Chand et al., 2015; Chand et al., 2017; Lee et al., 2017b) would be an interesting avenue of research in ALS, as other architectural proteins were found to be impacted in Chapter 3 of this thesis. This thesis, particularly in Chapters 3 and 4, focused on morphological pathology in the distal neuromuscular circuitry, rather than function aspects. To gain a better understanding of the disease phenotype in the SOD1^{G93A} mouse (Chapter 3), as well as any functional impacts of EpoD in this model (Chapter 4), direct analysis of NMJ function, such as electromyography techniques to measure nerve-synapse-muscle signal transmission, should be utilised (Kennel et al., 1996; Rizzuto et al., 2015).

Although length dependant and fibre type vulnerability of a-MNs was described in Chapter 1, it was not characterised in either Chapter 3, or evaluated with EpoD treatment in Chapter 4. Indeed, longer axons preferentially degenerate prior to shorter axons in ALS (Tallon et al., 2016), suggesting length dependant vulnerability in the neuromuscular circuitry. Similarly, fast-fatigue a-MNs degenerate earlier in disease, followed by fatigue-resistant and slow (Pun et al., 2006). Evaluation of fibre type vulnerability and pathology in both Chapters 3 and 4 would of benefited from 3D rendering of confocal images, coupled with a-MN axonal fiber type selection utilising

volumetric analysis (Pun et al., 2006). Further, correlating a-MN loss in the SOD1^{G93A} mouse model with results obtained in Chapter 3 would build a more holistic picture of distal degeneration and should be considered for future studies (Frey et al., 2000; Hegedus et al., 2008). A more thorough stereological approach to a-MN identification, with particular emphasis on identification and quantitation of the a-MNs located in the lateral and medial motor columns, would be more appropriate approach when investigating a-MN pathology in ALS (Weber et al., 1997; Mohan et al., 2014). Similarly, glial activation was measured by increased immunofluorescence of both astrocyte and microglial markers. Future studies would benefit from assessing changes to glia cell density, as well as changes to their morphology, such as microglia transforming from an inactive stellate morphology, to a rounded and large cell with few processes (David and Kroner, 2011; Brettschneider et al., 2012).

Treatment of the SOD1^{G93A} mouse model of ALS with EpoD was found to improve a-MN soma and axon pathology early in the disease, with late stage deficits and possible neurotoxicity. To further investigate the efficacy of microtubule stabilisation using EpoD in the SOD1^{G93A} mouse model, revaluation of timing and dosage of EpoD treatment should be completed, as Chapter 5 highlighted that even substantial low nanomolar and high picomolar concentrations of EpoD can alter neuronal outcomes (Jang et al., 2016). Indeed, many studies testing new therapies for ALS combine them with riluzole, the only positive disease-modifying agent available for ALS treatment. It would be interesting to identify how EpoD alters outcomes in the SOD1^{G93A} mouse model in combination with Riluzole, coupled with alterations to EpoD dosage and timing of treatment (Waibel et al., 2004; Del Signore et al., 2009). Further, as discussed in Chapter 4, Section 4.4.2, pharmacological inhibition of microgliosis using minocycline, a compound shown to improve outcomes in the SOD1^{G93A} mouse model, may further aid in any positive benefits of EpoD treatment in ALS (Yrjanheikki et al., 1999; Kriz et al., 2002).

Another consideration is testing therapeutics such as EpoD in the SOD1^{G93A} mouse model of ALS. The lack of a cure for ALS is somewhat compounded by the limited success in translating positive findings from preclinical animal studies to human clinical trials (Turner and Talbot, 2008; Ittner et al., 2015). This is mainly due to the use of single ALS models to represent a disease that is multifactorial in both familial and sporadic insults. However, various compounds and molecular pathways have been identified and are currently under clinical trials (Bucchia et al., 2015; Ittner et al., 2015). There are currently over 70 active phase I through to phase III

clinical trials taking place throughout the world (ALS Theraputic Development Institute, 2016). Although the SOD1 mouse model has been instrumental in advances in ALS, recent opinions highlight poor clinical study design, various methodological issues, and unexpected biological and pharmacological issue arising during mouse to human translation (Mitsumoto et al., 2014; Ittner et al., 2015; Garbuzova-Davis et al., 2016). Moreover, a 'one size does not fit all' approach to treatment of ALS is continuing to gain traction, with tailored patient treatment, or combination therapies, most likely to be utilised to combat the disease in the future (Goutman and Feldman, 2015). Another consideration is the copy number variant of the $SOD1^{G93A}$ mouse model. High copy number mice (23-25 copies) have a significantly shorter life span and faster progressing pathology than low copy $SOD1^{G93A}$ models. Due to the high rate of disease progression, potential therapeutics may have benefits or positive outcomes masked, further complicating the design and interpretation of therapeutic trials (Zwiegers et al., 2014). Therefore, it is recommended trials use multiple transgenic mouse models of ALS to gain insight into how potential therapeutics affect different disease mechanisms (Ittner et al., 2015; Philips and Rothstein, 2015).

Data from Chapter 5 of this thesis suggests that low doses of EpoD can have detrimental effects on growth, viability and function of primary cortical neurons (Jang et al., 2016). Paclitaxel, a compound with similar actions to EpoD, has been shown to induce microtubule polarity reconfiguration in axons, creating a 'mixed' microtubule orientation comparable to those in dendrites (Yau et al., 2016), where in normal axons microtubules reside in a 'plus end out', unidirectional configuration (Shemesh and Spira, 2010; Baas and Ahmad, 2013; Kevenaar and Hoogenraad, 2015). Further, end binding protein +TIP density, such as EB3, is a direct measure of microtubule dynamics (Kleele et al., 2014). Identifying both EB3 density and polar configuration with EpoD treatment is an interesting and necessary avenue of research to identify the full impact of EpoD on neuronal microtubules. Further, evaluation of EpoDs affects *in vivo* is also paramount to understand the full extent of EpoDs impact on normal neuronal function. For example, evaluating cellular pathology and microtubule protein expression following treatment with varying doses of EpoD, up to the maximum tolerated dose, will highlight the full extent of EpoDs effect on the neuronal microtubule cytoskeleton (Benbow et al., 2016). In the current thesis, mitochondrial transport was measured with no selection of directionality. Identification of EpoDs impact on anterograde and retrograde transport will identify whether one or both transport directions are vulnerable to stabilisation with Mt targeting compounds such as EpoD. Further, it is also critical to consider evaluating primary a-MN in future experiments, as other have

identified different neuronal populations have dissimilar outcomes when treated with microtubule targeting compounds (Jang et al., 2016).

Data from this thesis has highlighted that microtubule involvement in ALS may be more complex than alterations to microtubule dynamics and axonal transport, with progressive microtubule pathology most likely occurring over the disease course. Further, characterisation of the impact of microtubule targeting compounds on the nervous system needs to be a priority if they are to be promoted as a potential therapeutic strategy for targeting neurological diseases and injury.

6.5 Conclusions

Pathology of the distal neuromuscular circuitry is a complex and evolving process in ALS. This thesis provided significant insight into the characterisation of distal degeneration in the $SOD1^{G93A}$ mouse model of ALS, the efficacy of EpoD in the protection against distal axon degeneration, and the impact of low-dose EpoD on neurons. In summary, the findings in this thesis indicate that axonal pathology is an early targetable event in the pathogenesis of ALS and that EpoD protects a-MNs and axons from degeneration early in the disease. However, EpoD was found to be detrimental to normal neuronal function, with future evaluation of microtubule targeting compounds recommended as these compounds become more popular in the treatment of neurological disorders.

7 References

Acevedo-Arozena, A., Kalmar, B., Essa, S., Ricketts, T., Joyce, P., Kent, R., Rowe, C., Parker, A., Gray, A., Hafezparast, M., Thorpe, J.R., Greensmith, L., and Fisher, E.M. (2011). A comprehensive assessment of the SOD1G93A low-copy transgenic mouse, which models human amyotrophic lateral sclerosis. *Dis Model Mech* 4**,** 686-700.

Ahlijanian, M.K., Barrezueta, N.X., Williams, R.D., Jakowski, A., Kowsz, K.P., Mccarthy, S., Coskran, T., Carlo, A., Seymour, P.A., Burkhardt, J.E., Nelson, R.B., and Mcneish, J.D. (2000). Hyperphosphorylated tau and neurofilament and cytoskeletal disruptions in mice overexpressing human p25, an activator of cdk5. *Proc Natl Acad Sci U S A* 97**,** 2910-2915.

Al-Chalabi, A., Andersen, P.M., Nilsson, P., Chioza, B., Andersson, J.L., Russ, C., Shaw, C.E., Powell, J.F., and Leigh, P.N. (1999). Deletions of the heavy neurofilament subunit tail in amyotrophic lateral sclerosis. *Hum Mol Genet* 8**,** 157-164.

Al-Chalabi, A., Jones, A., Troakes, C., King, A., Al-Sarraj, S., and Van Den Berg, L.H. (2012). The genetics and neuropathology of amyotrophic lateral sclerosis. *Acta Neuropathol* 124**,** 339-352.

Alami, N.H., Smith, R.B., Carrasco, M.A., Williams, L.A., Winborn, C.S., Han, S.S., Kiskinis, E., Winborn, B., Freibaum, B.D., Kanagaraj, A., Clare, A.J., Badders, N.M., Bilican, B., Chaum, E., Chandran, S., Shaw, C.E., Eggan, K.C., Maniatis, T., and Taylor, J.P. (2014). Axonal transport of TDP-43 mRNA granules is impaired by ALS-causing mutations. *Neuron* 81**,** 536-543.

Albright, C.F., Barten, D.M., and Lee, F.Y. (2011). "Use of Epothilone D in Treating Tau-Associated Diseases Including Alzheimer's Disease". Google Patents).

Alim, M.A., Ma, Q.L., Takeda, K., Aizawa, T., Matsubara, M., Nakamura, M., Asada, A., Saito, T., Kaji, H., Yoshii, M., Hisanaga, S., and Ueda, K. (2004). Demonstration of a role for alpha-synuclein as a functional microtubule-associated protein. *J Alzheimers Dis* 6**,** 435-442; discussion 443-439.

Allen, C., and Borisy, G.G. (1974). Structural polarity and directional growth of microtubules of Chlamydomonas flagella. *J Mol Biol* 90**,** 381-402.

Als Theraputic Development Institute (2016). Available: http://www.alstdi.org/ [Accessed 12 October 2016].

Andersen, J.K. (2004). Oxidative stress in neurodegeneration: cause or consequence? *Nat Med* 10 Suppl**,** S18-25.

Andersen, P.M., and Al-Chalabi, A. (2011). Clinical genetics of amyotrophic lateral sclerosis: what do we really know? *Nat Rev Neurol* 7**,** 603-615.

Andrieux, A., Salin, P., Schweitzer, A., Begou, M., Pachoud, B., Brun, P., Gory-Faure, S., Kujala, P., Suaud-Chagny, M.F., Hofle, G., and Job, D. (2006). Microtubule stabilizer ameliorates synaptic function and behavior in a mouse model for schizophrenia. *Biol Psychiatry* 60**,** 1224-1230.

Antolik, C., Catino, D.H., O'neill, A.M., Resneck, W.G., Ursitti, J.A., and Bloch, R.J. (2007). The actin binding domain of ACF7 binds directly to the tetratricopeptide repeat domains of rapsyn. *Neuroscience* 145**,** 56-65.

Arbour, D., Vande Velde, C., and Robitaille, R. (2017). New perspectives on amyotrophic lateral sclerosis: the role of glial cells at the neuromuscular junction. *J Physiol* 595**,** 647-661.

Argyriou, A.A., Marmiroli, P., Cavaletti, G., and Kalofonos, H.P. (2011). Epothilone-induced peripheral neuropathy: a review of current knowledge. *J Pain Symptom Manage* 42**,** 931-940.

Arikawa-Hirasawa, E., Rossi, S.G., Rotundo, R.L., and Yamada, Y. (2002). Absence of acetylcholinesterase at the neuromuscular junctions of perlecan-null mice. *Nat Neurosci* 5**,** 119-123.

Ash, P.E., Bieniek, K.F., Gendron, T.F., Caulfield, T., Lin, W.L., Dejesus-Hernandez, M., Van Blitterswijk, M.M., Jansen-West, K., Paul, J.W., 3rd, Rademakers, R., Boylan, K.B., Dickson, D.W., and Petrucelli, L. (2013). Unconventional translation of C9ORF72 GGGGCC expansion generates insoluble polypeptides specific to c9FTD/ALS. *Neuron* 77**,** 639-646.

Atkin, J.D., Scott, R.L., West, J.M., Lopes, E., Quah, A.K., and Cheema, S.S. (2005). Properties of slow- and fast-twitch muscle fibres in a mouse model of amyotrophic lateral sclerosis. *Neuromuscul Disord* 15**,** 377-388.

Baas, P.W. (2013). Microtubule stability in the axon: new answers to an old mystery. *Neuron* 78**,** 3-5.

Baas, P.W. (2014). Beyond taxol: microtubule-based strategies for promoting nerve regeneration after injury. *Neural Regen Res* 9**,** 1265-1266.

Baas, P.W., and Ahmad, F.J. (2013). Beyond taxol: microtubule-based treatment of disease and injury of the nervous system. *Brain* 136**,** 2937-2951.

Baas, P.W., and Black, M.M. (1990). Individual microtubules in the axon consist of domains that differ in both composition and stability. *J Cell Biol* 111**,** 495-509.

Baas, P.W., and Lin, S. (2011). Hooks and comets: The story of microtubule polarity orientation in the neuron. *Dev Neurobiol* 71**,** 403-418.

Baas, P.W., Rao, A.N., Matamoros, A.J., and Leo, L. (2016). Stability properties of neuronal microtubules. *Cytoskeleton (Hoboken)*.

Baird, F.J., and Bennett, C.L. (2013). Microtubule defects & Neurodegeneration. *J Genet Syndr Gene Ther* 4**,** 203.

Balice-Gordon, R.J., and Lichtman, J.W. (1993). In vivo observations of pre- and postsynaptic changes during the transition from multiple to single innervation at developing neuromuscular junctions. *J Neurosci* 13**,** 834-855.

Banks, G., Fuhrer, C., and Adams, M. (2003). The postsynaptic submembrane machinery at the neuromuscular junction: requirement for rapsyn and the utrophin/dystrophin-associated complex. *J Neurocytol* 726**,** 709-726.

Banks, G.B., Chamberlain, J.S., and Froehner, S.C. (2009). Truncated dystrophins can influence neuromuscular synapse structure. *Mol Cell Neurosci* 40**,** 433-441.

Barik, A., Lu, Y., Sathyamurthy, A., Bowman, A., Shen, C., Li, L., Xiong, W.C., and Mei, L. (2014). LRP4 is critical for neuromuscular junction maintenance. *J Neurosci* 34**,** 13892-13905.

Baumer, D., Hilton, D., Paine, S.M., Turner, M.R., Lowe, J., Talbot, K., and Ansorge, O. (2010). Juvenile ALS with basophilic inclusions is a FUS proteinopathy with FUS mutations. *Neurology* 75**,** 611-618.

Bear, M.F., and Connors, B.C.P., M. A (2007). *Neuroscience - Exploring the Brain.* Lippincoyy Willians and Wilkins.

Beers, D.R., Zhao, W., Liao, B., Kano, O., Wang, J., Huang, A., Appel, S.H., and Henkel, J.S. (2011). Neuroinflammation modulates distinct regional and temporal clinical responses in ALS mice. *Brain Behav Immun* 25**,** 1025-1035.

Belly, A., Moreau-Gachelin, F., Sadoul, R., and Goldberg, Y. (2005). Delocalization of the multifunctional RNA splicing factor TLS/FUS in hippocampal neurones: exclusion from

the nucleus and accumulation in dendritic granules and spine heads. *Neurosci Lett* 379**,** 152-157.
Belzil, V.V., Valdmanis, P.N., Dion, P.A., Daoud, H., Kabashi, E., Noreau, A., Gauthier, J., Hince, P., Desjarlais, A., Bouchard, J.P., Lacomblez, L., Salachas, F., Pradat, P.F., Camu, W., Meininger, V., Dupre, N., and Rouleau, G.A. (2009). Mutations in FUS cause FALS and SALS in French and French Canadian populations. *Neurology* 73**,** 1176-1179.
Benbow, J.H., Degray, B., and Ehrlich, B.E. (2011). Protection of neuronal calcium sensor 1 protein in cells treated with paclitaxel. *J Biol Chem* 286**,** 34575-34582.
Benbow, S.J., Cook, B.M., Reifert, J., Wozniak, K.M., Slusher, B.S., Littlefield, B.A., Wilson, L., Jordan, M.A., and Feinstein, S.C. (2016). Effects of Paclitaxel and Eribulin in Mouse Sciatic Nerve: A Microtubule-Based Rationale for the Differential Induction of Chemotherapy-Induced Peripheral Neuropathy. *Neurotox Res* 29**,** 299-313.
Bendotti, C., and Carri, M.T. (2004). Lessons from models of SOD1-linked familial ALS. *Trends Mol Med* 10**,** 393-400.
Bensimon, G., Lacomblez, L., and Meininger, V. (1994). A controlled trial of riluzole in amyotrophic lateral sclerosis. ALS/Riluzole Study Group. *N Engl J Med* 330**,** 585-591.
Bilsland, L.G., Sahai, E., Kelly, G., Golding, M., Greensmith, L., and Schiavo, G. (2010). Deficits in axonal transport precede ALS symptoms in vivo. *Proc Natl Acad Sci U S A* 107**,** 20523-20528.
Blizzard, C.A., Southam, K.A., Dawkins, E., Lewis, K.E., King, A.E., Clark, J.A., and Dickson, T.C. (2015). Identifying the primary site of pathogenesis in amyotrophic lateral sclerosis - vulnerability of lower motor neurons to proximal excitotoxicity. *Dis Model Mech* 8**,** 215-224.
Bodaleo, F.J., and Gonzalez-Billault, C. (2016). The Presynaptic Microtubule Cytoskeleton in Physiological and Pathological Conditions: Lessons from Drosophila Fragile X Syndrome and Hereditary Spastic Paraplegias. *Front Mol Neurosci* 9**,** 60.
Bohlen, M., Cameron, A., Metten, P., Crabbe, J.C., and Wahlsten, D. (2009). Calibration of rotational acceleration for the rotarod test of rodent motor coordination. *Journal of neuroscience methods* 178**,** 10-14.
Boillee, S., Vande Velde, C., and Cleveland, D.W. (2006a). ALS: a disease of motor neurons and their nonneuronal neighbors. *Neuron* 52**,** 39-59.
Boillee, S., Yamanaka, K., Lobsiger, C.S., Copeland, N.G., Jenkins, N.A., Kassiotis, G., Kollias, G., and Cleveland, D.W. (2006b). Onset and progression in inherited ALS determined by motor neurons and microglia. *Science* 312**,** 1389-1392.
Bollag, D.M., Mcqueney, P.A., Zhu, J., Hensens, O., Koupal, L., Liesch, J., Goetz, M., Lazarides, E., and Woods, C.M. (1995). Epothilones, a new class of microtubule-stabilizing agents with a taxol-like mechanism of action. *Cancer Res* 55**,** 2325-2333.
Bosc, C., Cronk, J.D., Pirollet, F., Watterson, D.M., Haiech, J., Job, D., and Margolis, R.L. (1996). Cloning, expression, and properties of the microtubule-stabilizing protein STOP. *Proc Natl Acad Sci U S A* 93**,** 2125-2130.
Bosc, C., Frank, R., Denarier, E., Ronjat, M., Schweitzer, A., Wehland, J., and Job, D. (2001). Identification of novel bifunctional calmodulin-binding and microtubule-stabilizing motifs in STOP proteins. *J Biol Chem* 276**,** 30904-30913.
Bosco, D.A., Morfini, G., Karabacak, N.M., Song, Y., Gros-Louis, F., Pasinelli, P., Goolsby, H., Fontaine, B.A., Lemay, N., Mckenna-Yasek, D., Frosch, M.P., Agar, J.N., Julien, J.P., Brady, S.T., and Brown, R.H., Jr. (2010). Wild-type and mutant SOD1 share an aberrant conformation and a common pathogenic pathway in ALS. *Nat Neurosci* 13**,** 1396-1403.
Boutte, A.M., Woltjer, R.L., Zimmerman, L.J., Stamer, S.L., Montine, K.S., Manno, M.V., Cimino, P.J., Liebler, D.C., and Montine, T.J. (2006). Selectively increased oxidative

modifications mapped to detergent-insoluble forms of Abeta and beta-III tubulin in Alzheimer's disease. *FASEB J* 20**,** 1473-1483.

Bowen, D.C., Sugiyama, J., Ferns, M., and Hall, Z.W. (1996). Neural agrin activates a high-affinity receptor in C2 muscle cells that is unresponsive to muscle agrin. *J Neurosci* 16**,** 3791-3797.

Brettschneider, J., Libon, D.J., Toledo, J.B., Xie, S.X., Mccluskey, L., Elman, L., Geser, F., Lee, V.M., Grossman, M., and Trojanowski, J.Q. (2012). Microglial activation and TDP-43 pathology correlate with executive dysfunction in amyotrophic lateral sclerosis. *Acta Neuropathol* 123**,** 395-407.

Brewer, G.J. (1995). Serum-free B27/neurobasal medium supports differentiated growth of neurons from the striatum, substantia nigra, septum, cerebral cortex, cerebellum, and dentate gyrus. *J Neurosci Res* 42**,** 674-683.

Brill, M.S., Kleele, T., Ruschkies, L., Wang, M., Marahori, N.A., Reuter, M.S., Hausrat, T.J., Weigand, E., Fisher, M., Ahles, A., Engelhardt, S., Bishop, D.L., Kneussel, M., and Misgeld, T. (2016). Branch-Specific Microtubule Destabilization Mediates Axon Branch Loss during Neuromuscular Synapse Elimination. *Neuron*.

Brites, D., and Vaz, A.R. (2014). Microglia centered pathogenesis in ALS: insights in cell interconnectivity. *Front Cell Neurosci* 8**,** 117.

Brizuela, M., Blizzard, C.A., Chuckowree, J.A., Dawkins, E., Gasperini, R.J., Young, K.M., and Dickson, T.C. (2015). The microtubule-stabilizing drug Epothilone D increases axonal sprouting following transection injury in vitro. *Mol Cell Neurosci* 66**,** 129-140.

Brockington, A., Heath, P.R., Holden, H., Kasher, P., Bender, F.L., Claes, F., Lambrechts, D., Sendtner, M., Carmeliet, P., and Shaw, P.J. (2010). Downregulation of genes with a function in axon outgrowth and synapse formation in motor neurones of the VEGFdelta/delta mouse model of amyotrophic lateral sclerosis. *BMC Genomics* 11**,** 203.

Brockington, A., Wharton, S.B., Fernando, M., Gelsthorpe, C.H., Baxter, L., Ince, P.G., Lewis, C.E., and Shaw, P.J. (2006). Expression of vascular endothelial growth factor and its receptors in the central nervous system in amyotrophic lateral sclerosis. *J Neuropathol Exp Neurol* 65**,** 26-36.

Bruijn, L.I., Becher, M.W., Lee, M.K., Anderson, K.L., Jenkins, N.A., Copeland, N.G., Sisodia, S.S., Rothstein, J.D., Borchelt, D.R., Price, D.L., and Cleveland, D.W. (1997). ALS-linked SOD1 mutant G85R mediates damage to astrocytes and promotes rapidly progressive disease with SOD1-containing inclusions. *Neuron* 18**,** 327-338.

Bruijn, L.I., Miller, T.M., and Cleveland, D.W. (2004). Unraveling the mechanisms involved in motor neuron degeneration in ALS. *Annu Rev Neurosci* 27**,** 723-749.

Brunden, K.R., Trojanowski, J.Q., Smith, A.B., 3rd, Lee, V.M., and Ballatore, C. (2014). Microtubule-stabilizing agents as potential therapeutics for neurodegenerative disease. *Bioorg Med Chem* 22**,** 5040-5049.

Brunden, K.R., Yao, Y., Potuzak, J.S., Ferrer, N.I., Ballatore, C., James, M.J., Hogan, A.M., Trojanowski, J.Q., Smith, A.B., 3rd, and Lee, V.M. (2011). The characterization of microtubule-stabilizing drugs as possible therapeutic agents for Alzheimer's disease and related tauopathies. *Pharmacol Res* 63**,** 341-351.

Brunden, K.R., Zhang, B., Carroll, J., Yao, Y., Potuzak, J.S., Hogan, A.M., Iba, M., James, M.J., Xie, S.X., Ballatore, C., Smith, A.B., 3rd, Lee, V.M., and Trojanowski, J.Q. (2010). Epothilone D improves microtubule density, axonal integrity, and cognition in a transgenic mouse model of tauopathy. *J Neurosci* 30**,** 13861-13866.

Bucchia, M., Ramirez, A., Parente, V., Simone, C., Nizzardo, M., Magri, F., Dametti, S., and Corti, S. (2015). Therapeutic development in amyotrophic lateral sclerosis. *Clin Ther* 37**,** 668-680.

Budini, M., Buratti, E., Stuani, C., Guarnaccia, C., Romano, V., De Conti, L., and Baralle, F.E. (2012). Cellular model of TAR DNA-binding protein 43 (TDP-43) aggregation based on its C-terminal Gln/Asn-rich region. *J Biol Chem* 287**,** 7512-7525.

Bunton-Stasyshyn, R.K., Saccon, R.A., Fratta, P., and Fisher, E.M. (2015). SOD1 Function and Its Implications for Amyotrophic Lateral Sclerosis Pathology: New and Renascent Themes. *Neuroscientist* 21**,** 519-529.

Buratti, E., and Baralle, F.E. (2001). Characterization and functional implications of the RNA binding properties of nuclear factor TDP-43, a novel splicing regulator of CFTR exon 9. *J Biol Chem* 276**,** 36337-36343.

Buratti, E., and Baralle, F.E. (2008). Multiple roles of TDP-43 in gene expression, splicing regulation, and human disease. *Front Biosci* 13**,** 867-878.

Burgess, R.W., Nguyen, Q.T., Son, Y.J., Lichtman, J.W., and Sanes, J.R. (1999). Alternatively spliced isoforms of nerve- and muscle-derived agrin: their roles at the neuromuscular junction. *Neuron* 23**,** 33-44.

Cairns, N.J., Lee, V.M., and Trojanowski, J.Q. (2004). The cytoskeleton in neurodegenerative diseases. *J Pathol* 204**,** 438-449.

Callicott, J.H., Straub, R.E., Pezawas, L., Egan, M.F., Mattay, V.S., Hariri, A.R., Verchinski, B.A., Meyer-Lindenberg, A., Balkissoon, R., Kolachana, B., Goldberg, T.E., and Weinberger, D.R. (2005). Variation in DISC1 affects hippocampal structure and function and increases risk for schizophrenia. *Proc Natl Acad Sci U S A* 102**,** 8627-8632.

Cappelletti, G., Surrey, T., and Maci, R. (2005). The parkinsonism producing neurotoxin MPP+ affects microtubule dynamics by acting as a destabilising factor. *FEBS Lett* 579**,** 4781-4786.

Cappello, V., Vezzoli, E., Righi, M., Fossati, M., Mariotti, R., Crespi, A., Patruno, M., Bentivoglio, M., Pietrini, G., and Francolini, M. (2012). Analysis of neuromuscular junctions and effects of anabolic steroid administration in the SOD1G93A mouse model of ALS. *Mol Cell Neurosci* 15**,** 12-21.

Carletti, B., Passarelli, C., Sparaco, M., Tozzi, G., Pastore, A., Bertini, E., and Piemonte, F. (2011). Effect of protein glutathionylation on neuronal cytoskeleton: a potential link to neurodegeneration. *Neuroscience* 192**,** 285-294.

Carlson, C.G. (1998). The dystrophinopathies: an alternative to the structural hypothesis. *Neurobiol Dis* 5**,** 3-15.

Carlson, K., and Ocean, A.J. (2011). Peripheral neuropathy with microtubule-targeting agents: occurrence and management approach. *Clin Breast Cancer* 11**,** 73-81.

Carrasco, D.I., Bahr, B.A., Seburn, K.L., and Pinter, M.J. (2016). Abnormal response of distal Schwann cells to denervation in a mouse model of motor neuron disease. *Exp Neurol* 278**,** 116-126.

Cartelli, D., Casagrande, F., Busceti, C.L., Bucci, D., Molinaro, G., Traficante, A., Passarella, D., Giavini, E., Pezzoli, G., Battaglia, G., and Cappelletti, G. (2013). Microtubule alterations occur early in experimental parkinsonism and the microtubule stabilizer epothilone D is neuroprotective. *Sci Rep* 3**,** 1837.

Cartelli, D., Ronchi, C., Maggioni, M.G., Rodighiero, S., Giavini, E., and Cappelletti, G. (2010). Microtubule dysfunction precedes transport impairment and mitochondria damage in MPP+ -induced neurodegeneration. *J Neurochem* 115**,** 247-258.

Chand, K.K., Lee, K.M., Lavidis, N.A., and Noakes, P.G. (2017). Loss of laminin-alpha4 results in pre- and postsynaptic modifications at the neuromuscular junction. *FASEB J* 31**,** 1323-1336.

Chand, K.K., Lee, K.M., Schenning, M.P., Lavidis, N.A., and Noakes, P.G. (2015). Loss of beta2-laminin alters calcium sensitivity and voltage-gated calcium channel maturation of neurotransmission at the neuromuscular junction. *J Physiol* 593**,** 245-265.

Chandran, J., Ding, J., and Cai, H. (2007). Alsin and the molecular pathways of amyotrophic lateral sclerosis. *Mol Neurobiol* 36**,** 224-231.

Chang, J., Baloh, R.H., and Milbrandt, J. (2009). The NIMA-family kinase Nek3 regulates microtubule acetylation in neurons. *J Cell Sci* 122**,** 2274-2282.

Charcot, J., and Joffroy, A. (1869). Deux cas d'atrophie musculaire progressive avec lesions de la sunstance grise et des faiseaux antero-lateraux de la moelle epiniere. *Arch Physiol Neurol Pathol* 2**,** 744-754.

Chen, B.F., and Stanley, R.P. (2012). Orientations, Lattice Polytopes, and Group Arrangements II: Modular and Integral Flow Polynomials of Graphs. *Graphs and Combinatorics* 28**,** 751-779.

Chen, B.L., Hall, D.H., and Chklovskii, D.B. (2006). Wiring optimization can relate neuronal structure and function. *Proc Natl Acad Sci U S A* 103**,** 4723-4728.

Chen, D., Wang, Y., and Chin, E.R. (2015). Activation of the endoplasmic reticulum stress response in skeletal muscle of G93A*SOD1 amyotrophic lateral sclerosis mice. *Front Cell Neurosci* 9**,** 170.

Chen, F., Qian, L., Yang, Z.H., Huang, Y., Ngo, S.T., Ruan, N.J., Wang, J., Schneider, C., Noakes, P.G., Ding, Y.Q., Mei, L., and Luo, Z.G. (2007). Rapsyn interaction with calpain stabilizes AChR clusters at the neuromuscular junction. *Neuron* 55**,** 247-260.

Chen, T.A., Yang, F., Cole, G.M., and Chan, S.O. (2001). Inhibition of caspase-3-like activity reduces glutamate induced cell death in adult rat retina. *Brain Res* 904**,** 177-188.

Cheng, K.L., Bradley, T., and Budman, D.R. (2008). Novel microtubule-targeting agents - the epothilones. *Biologics* 2**,** 789-811.

Chiorazzi, A., Nicolini, G., Canta, A., Oggioni, N., Rigolio, R., Cossa, G., Lombardi, R., Roglio, I., Cervellini, I., Lauria, G., Melcangi, R.C., Bianchi, R., Crippa, D., and Cavaletti, G. (2009). Experimental epothilone B neurotoxicity: results of in vitro and in vivo studies. *Neurobiol Dis* 35**,** 270-277.

Clark, J., Yeaman, E., Blizzard, C., Chuckowree, J., and Dickson, T. (2016a). A Case for Microtubule Vulnerability in Amyotrophic Lateral Sclerosis: Altered Dynamics During Disease. *Frontiers in Cellular Neuroscience* 10.

Clark, J.A., Southam, K.A., Blizzard, C.A., King, A.E., and Dickson, T.C. (2016b). Axonal degeneration, distal collateral branching and neuromuscular junction architecture alterations occur prior to symptom onset in the SOD1(G93A) mouse model of amyotrophic lateral sclerosis. *J Chem Neuroanat* 76**,** 35-47.

Clark, R., Blizzard, C., and Dickson, T. (2015). Inhibitory dysfunction in amyotrophic lateral sclerosis: future therapeutic opportunities. *Neurodegener Dis Manag* 5**,** 511-525.

Clement, A.M., Nguyen, M.D., Roberts, E.A., Garcia, M.L., Boillee, S., Rule, M., Mcmahon, A.P., Doucette, W., Siwek, D., Ferrante, R.J., Brown, R.H., Jr., Julien, J.P., Goldstein, L.S., and Cleveland, D.W. (2003). Wild-type nonneuronal cells extend survival of SOD1 mutant motor neurons in ALS mice. *Science* 302**,** 113-117.

Cohen, S., Aizer, A., Shav-Tal, Y., Yanai, A., and Motro, B. (2013). Nek7 kinase accelerates microtubule dynamic instability. *Biochim Biophys Acta* 1833**,** 1104-1113.

Coleman, M.P. (2005). Axon degeneration mechanisms: commonality and diversity. *Nagt Rev Neurosci* 6**,** 889 - 898.

Collard, J.F., Cote, F., and Julien, J.P. (1995). Defective axonal transport in a transgenic mouse model of amyotrophic lateral sclerosis. *Nature* 375**,** 61-64.

Conde, C., and Caceres, A. (2009). Microtubule assembly, organization and dynamics in axons and dendrites. *Nat Rev Neurosci* 10**,** 319-332.

Cookson, M.R. (2016). RNA-binding proteins implicated in neurodegenerative diseases. *Wiley Interdiscip Rev RNA*.

Corrado, L., Ratti, A., Gellera, C., Buratti, E., Castellotti, B., Carlomagno, Y., Ticozzi, N., Mazzini, L., Testa, L., Taroni, F., Baralle, F.E., Silani, V., and D'alfonso, S. (2009). High frequency of TARDBP gene mutations in Italian patients with amyotrophic lateral sclerosis. *Hum Mutat* 30**,** 688-694.

Court, F.A., Gillingwater, T.H., Melrose, S., Sherman, D.L., Greenshields, K.N., Morton, A.J., Harris, J.B., Willison, H.J., and Ribchester, R.R. (2008). Identity, developmental restriction and reactivity of extralaminar cells capping mammalian neuromuscular junctions. *J Cell Sci* 121**,** 3901-3911.

Crozat, A., Aman, P., Mandahl, N., and Ron, D. (1993). Fusion of CHOP to a novel RNA-binding protein in human myxoid liposarcoma. *Nature* 363**,** 640-644.

Cudkowicz, M.E., Katz, J., Moore, D.H., O'neill, G., Glass, J.D., Mitsumoto, H., Appel, S., Ravina, B., Kieburtz, K., Shoulson, I., Kaufmann, P., Khan, J., Simpson, E., Shefner, J., Levin, B., Cwik, V., Schoenfeld, D., Aggarwal, S., Mcdermott, M.P., and Miller, R.G. (2010). Toward more efficient clinical trials for amyotrophic lateral sclerosis. *Amyotroph Lateral Scler* 11**,** 259-265.

D'ambrosi, N., Rossi, S., Gerbino, V., and Cozzolino, M. (2014). Rac1 at the crossroad of actin dynamics and neuroinflammation in Amyotrophic Lateral Sclerosis. *Front Cell Neurosci* 8**,** 279.

D'ydewalle, C., Krishnan, J., Chiheb, D.M., Van Damme, P., Irobi, J., Kozikowski, A.P., Vanden Berghe, P., Timmerman, V., Robberecht, W., and Van Den Bosch, L. (2011). HDAC6 inhibitors reverse axonal loss in a mouse model of mutant HSPB1-induced Charcot-Marie-Tooth disease. *Nat Med* 17**,** 968-974.

Darabid, H., Perez-Gonzalez, A.P., and Robitaille, R. (2014). Neuromuscular synaptogenesis: coordinating partners with multiple functions. *Nat Rev Neurosci* 15**,** 703-718.

Das, V., and Miller, J.H. (2012). Microtubule stabilization by peloruside A and paclitaxel rescues degenerating neurons from okadaic acid-induced tau phosphorylation. *Eur J Neurosci* 35**,** 1705-1717.

David, S., and Kroner, A. (2011). Repertoire of microglial and macrophage responses after spinal cord injury. *Nat Rev Neurosci* 12**,** 388-399.

Davis, C.H., Kim, K.Y., Bushong, E.A., Mills, E.A., Boassa, D., Shih, T., Kinebuchi, M., Phan, S., Zhou, Y., Bihlmeyer, N.A., Nguyen, J.V., Jin, Y., Ellisman, M.H., and Marsh-Armstrong, N. (2014). Transcellular degradation of axonal mitochondria. *Proc Natl Acad Sci U S A* 111**,** 9633-9638.

De Oliveira, G.P., Maximino, J.R., Maschietto, M., Zanoteli, E., Puga, R.D., Lima, L., Carraro, D.M., and Chadi, G. (2014). Early gene expression changes in skeletal muscle from SOD1(G93A) amyotrophic lateral sclerosis animal model. *Cell Mol Neurobiol* 34**,** 451-462.

De Vos, K.J., Chapman, A.L., Tennant, M.E., Manser, C., Tudor, E.L., Lau, K.F., Brownlees, J., Ackerley, S., Shaw, P.J., Mcloughlin, D.M., Shaw, C.E., Leigh, P.N., Miller, C.C., and Grierson, A.J. (2007). Familial amyotrophic lateral sclerosis-linked SOD1 mutants perturb fast axonal transport to reduce axonal mitochondria content. *Hum Mol Genet* 16**,** 2720-2728.

Dechiara, T.M., Bowen, D.C., Valenzuela, D.M., Simmons, M.V., Poueymirou, W.T., Thomas, S., Kinetz, E., Compton, D.L., Rojas, E., Park, J.S., Smith, C., Distefano, P.S., Glass,

D.J., Burden, S.J., and Yancopoulos, G.D. (1996). The receptor tyrosine kinase MuSK is required for neuromuscular junction formation in vivo. *Cell* 85**,** 501-512.

Dejesus-Hernandez, M., Mackenzie, I.R., Boeve, B.F., Boxer, A.L., Baker, M., Rutherford, N.J., Nicholson, A.M., Finch, N.A., Flynn, H., Adamson, J., Kouri, N., Wojtas, A., Sengdy, P., Hsiung, G.Y., Karydas, A., Seeley, W.W., Josephs, K.A., Coppola, G., Geschwind, D.H., Wszolek, Z.K., Feldman, H., Knopman, D.S., Petersen, R.C., Miller, B.L., Dickson, D.W., Boylan, K.B., Graff-Radford, N.R., and Rademakers, R. (2011). Expanded GGGGCC hexanucleotide repeat in noncoding region of C9ORF72 causes chromosome 9p-linked FTD and ALS. *Neuron* 72**,** 245-256.

Del Signore, S.J., Amante, D.J., Kim, J., Stack, E.C., Goodrich, S., Cormier, K., Smith, K., Cudkowicz, M.E., and Ferrante, R.J. (2009). Combined riluzole and sodium phenylbutyrate therapy in transgenic amyotrophic lateral sclerosis mice. *Amyotroph Lateral Scler* 10**,** 85-94.

Deng, H.X., Chen, W., Hong, S.T., Boycott, K.M., Gorrie, G.H., Siddique, N., Yang, Y., Fecto, F., Shi, Y., Zhai, H., Jiang, H., Hirano, M., Rampersaud, E., Jansen, G.H., Donkervoort, S., Bigio, E.H., Brooks, B.R., Ajroud, K., Sufit, R.L., Haines, J.L., Mugnaini, E., Pericak-Vance, M.A., and Siddique, T. (2011). Mutations in UBQLN2 cause dominant X-linked juvenile and adult-onset ALS and ALS/dementia. *Nature* 477**,** 211-215.

Deng, H.X., Hentati, A., Tainer, J.A., Iqbal, Z., Cayabyab, A., Hung, W.Y., Getzoff, E.D., Hu, P., Herzfeldt, B., Roos, R.P., and Et Al. (1993). Amyotrophic lateral sclerosis and structural defects in Cu,Zn superoxide dismutase. *Science* 261**,** 1047-1051.

Deng, H.X., Zhai, H., Bigio, E.H., Yan, J., Fecto, F., Ajroud, K., Mishra, M., Ajroud-Driss, S., Heller, S., Sufit, R., Siddique, N., Mugnaini, E., and Siddique, T. (2010). FUS-immunoreactive inclusions are a common feature in sporadic and non-SOD1 familial amyotrophic lateral sclerosis. *Ann Neurol* 67**,** 739-748.

Desai, A., and Mitchison, T.J. (1997). Microtubule polymerization dynamics. *Annu Rev Cell Dev Biol* 13**,** 83-117.

Devon, R.S., Orban, P.C., Gerrow, K., Barbieri, M.A., Schwab, C., Cao, L.P., Helm, J.R., Bissada, N., Cruz-Aguado, R., Davidson, T.L., Witmer, J., Metzler, M., Lam, C.K., Tetzlaff, W., Simpson, E.M., Mccaffery, J.M., El-Husseini, A.E., Leavitt, B.R., and Hayden, M.R. (2006). Als2-deficient mice exhibit disturbances in endosome trafficking associated with motor behavioral abnormalities. *Proc Natl Acad Sci U S A* 103**,** 9595-9600.

Dobbins, G.C., Luo, S., Yang, Z., Xiong, W.C., and Mei, L. (2008). alpha-Actinin interacts with rapsyn in agrin-stimulated AChR clustering. *Mol Brain* 1**,** 18.

Dobrowolny, G., Aucello, M., Rizzuto, E., Beccafico, S., Mammucari, C., Boncompagni, S., Belia, S., Wannenes, F., Nicoletti, C., Del Prete, Z., Rosenthal, N., Molinaro, M., Protasi, F., Fano, G., Sandri, M., and Musaro, A. (2008). Skeletal muscle is a primary target of SOD1G93A-mediated toxicity. *Cell Metab* 8**,** 425-436.

Dodge, J.C., Haidet, A.M., Yang, W., Passini, M.A., Hester, M., Clarke, J., Roskelley, E.M., Treleaven, C.M., Rizo, L., Martin, H., Kim, S.H., Kaspar, R., Taksir, T.V., Griffiths, D.A., Cheng, S.H., Shihabuddin, L.S., and Kaspar, B.K. (2008). Delivery of AAV-IGF-1 to the CNS extends survival in ALS mice through modification of aberrant glial cell activity. *Mol Ther* 16**,** 1056-1064.

Dormann, D., and Haass, C. (2011). TDP-43 and FUS: a nuclear affair. *Trends Neurosci* 34**,** 339-348.

Dormann, D., Rodde, R., Edbauer, D., Bentmann, E., Fischer, I., Hruscha, A., Than, M.E., Mackenzie, I.R., Capell, A., Schmid, B., Neumann, M., and Haass, C. (2010). ALS-

associated fused in sarcoma (FUS) mutations disrupt Transportin-mediated nuclear import. *EMBO J* 29**,** 2841-2857.
Droppelmann, C.A., Campos-Melo, D., Volkening, K., and Strong, M.J. (2014). The emerging role of guanine nucleotide exchange factors in ALS and other neurodegenerative diseases. *Front Cell Neurosci* 8**,** 282.
Drubin, D.G., and Kirschner, M.W. (1986). Tau protein function in living cells. *J Cell Biol* 103**,** 2739-2746.
Drum, B.M., Yuan, C., Li, L., Liu, Q., Wordeman, L., and Santana, L.F. (2016). Oxidative stress decreases microtubule growth and stability in ventricular myocytes. *J Mol Cell Cardiol* 93**,** 32-43.
Dubey, J., Ratnakaran, N., and Koushika, S.P. (2015). Neurodegeneration and microtubule dynamics: death by a thousand cuts. *Front Cell Neurosci* 9**,** 343.
Dumontet, C., and Jordan, M.A. (2010). Microtubule-binding agents: a dynamic field of cancer therapeutics. *Nat Rev Drug Discov* 9**,** 790-803.
Dupuis, L., De Tapia, M., Rene, F., Lutz-Bucher, B., Gordon, J.W., Mercken, L., Pradier, L., and Loeffler, J.P. (2000). Differential screening of mutated SOD1 transgenic mice reveals early up-regulation of a fast axonal transport component in spinal cord motor neurons. *Neurobiol Dis* 7**,** 274-285.
Durban, M., Harezlak, J., Wand, M.P., and Carroll, R.J. (2005). Simple fitting of subject-specific curves for longitudinal data. *Stat Med* 24**,** 1153-1167.
Ebneth, A., Godemann, R., Stamer, K., Illenberger, S., Trinczek, B., and Mandelkow, E. (1998). Overexpression of tau protein inhibits kinesin-dependent trafficking of vesicles, mitochondria, and endoplasmic reticulum: implications for Alzheimer's disease. *J Cell Biol* 143**,** 777-794.
Eira, J., Silva, C.S., Sousa, M.M., and Liz, M.A. (2016). The cytoskeleton as a novel therapeutic target for old neurodegenerative disorders. *Prog Neurobiol* 141**,** 61-82.
Eisen, A., Kiernan, M., Mitsumoto, H., and Swash, M. (2014). Amyotrophic lateral sclerosis: a long preclinical period? *J Neurol Neurosurg Psychiatry* 85**,** 1232-1238.
Elashry, M.I., Otto, A., Matsakas, A., El-Morsy, S.E., and Patel, K. (2009). Morphology and myofiber composition of skeletal musculature of the forelimb in young and aged wild type and myostatin null mice. *Rejuvenation Res* 12**,** 269-281.
Ellis, C.M., Simmons, A., Jones, D.K., Bland, J., Dawson, J.M., Horsfield, M.A., Williams, S.C., and Leigh, P.N. (1999). Diffusion tensor MRI assesses corticospinal tract damage in ALS. *Neurology* 53**,** 1051-1058.
Ervasti, J.M., and Campbell, K.P. (1993). A role for the dystrophin-glycoprotein complex as a transmembrane linker between laminin and actin. *J Cell Biol* 122**,** 809-823.
Evans, D.B., Rank, K.B., Bhattacharya, K., Thomsen, D.R., Gurney, M.E., and Sharma, S.K. (2000). Tau phosphorylation at serine 396 and serine 404 by human recombinant tau protein kinase II inhibits tau's ability to promote microtubule assembly. *J Biol Chem* 275**,** 24977-24983.
Eymard-Pierre, E., Lesca, G., Dollet, S., Santorelli, F.M., Di Capua, M., Bertini, E., and Boespflug-Tanguy, O. (2002). Infantile-onset ascending hereditary spastic paralysis is associated with mutations in the alsin gene. *Am J Hum Genet* 71**,** 518-527.
Fallini, C., Bassell, G.J., and Rossoll, W. (2012). The ALS disease protein TDP-43 is actively transported in motor neuron axons and regulates axon outgrowth. *Hum Mol Genet* 21**,** 3703-3718.
Fanara, P., Banerjee, J., Hueck, R.V., Harper, M.R., Awada, M., Turner, H., Husted, K.H., Brandt, R., and Hellerstein, M.K. (2007). Stabilization of hyperdynamic microtubules is neuroprotective in amyotrophic lateral sclerosis. *J Biol Chem* 282**,** 23465-23472.

Fang, C., Bourdette, D., and Banker, G. (2012). Oxidative stress inhibits axonal transport: implications for neurodegenerative diseases. *Mol Neurodegener* 7**,** 29.

Farah, C.A., Nguyen, M.D., Julien, J.P., and Leclerc, N. (2003). Altered levels and distribution of microtubule-associated proteins before disease onset in a mouse model of amyotrophic lateral sclerosis. *J Neurochem* 84**,** 77-86.

Feiler, M.S., Strobel, B., Freischmidt, A., Helferich, A.M., Kappel, J., Brewer, B.M., Li, D., Thal, D.R., Walther, P., Ludolph, A.C., Danzer, K.M., and Weishaupt, J.H. (2015). TDP-43 is intercellularly transmitted across axon terminals. *J Cell Biol* 211**,** 897-911.

Feng, G., Laskowski, M.B., Feldheim, D.A., Wang, H., Lewis, R., Frisen, J., Flanagan, J.G., and Sanes, J.R. (2000a). Roles for ephrins in positionally selective synaptogenesis between motor neurons and muscle fibers. *Neuron* 25**,** 295-306.

Feng, G., Mellor, R.H., Bernstein, M., Keller-Peck, C., Nguyen, Q.T., Wallace, M., Nerbonne, J.M., Lichtman, J.W., and Sanes, J.R. (2000b). Imaging neuronal subsets in transgenic mice expressing multiple spectral variants of GFP. *Neuron* 28**,** 41-51.

Ferraiuolo, L., Kirby, J., Grierson, A.J., Sendtner, M., and Shaw, P.J. (2011). Molecular pathways of motor neuron injury in amyotrophic lateral sclerosis. *Nat Rev Neurol* 7**,** 616-630.

Ferreira, A., and Caceres, A. (1989). The expression of acetylated microtubules during axonal and dendritic growth in cerebellar macroneurons which develop in vitro. *Brain Res Dev Brain Res* 49**,** 205-213.

Filezac De L'etang, A., Maharjan, N., Cordeiro Brana, M., Ruegsegger, C., Rehmann, R., Goswami, A., Roos, A., Troost, D., Schneider, B.L., Weis, J., and Saxena, S. (2015). Marinesco-Sjogren syndrome protein SIL1 regulates motor neuron subtype-selective ER stress in ALS. *Nat Neurosci* 18**,** 227-238.

Fischer, L.R., Culver, D.G., Tennant, P., Davis, A.A., Wang, M., Castellano-Sanchez, A., Khan, J., Polak, M.A., and Glass, J.D. (2004). Amyotrophic lateral sclerosis is a distal axonopathy: evidence in mice and man. *Exp Neurol* 185**,** 232-240.

Fischer, L.R., and Glass, J.D. (2007). Axonal degeneration in motor neuron disease. *Neurodegenerative Diseases* 4**,** 431-442.

Forsberg, K., Jonsson, P.A., Andersen, P.M., Bergemalm, D., Graffmo, K.S., Hultdin, M., Jacobsson, J., Rosquist, R., Marklund, S.L., and Brannstrom, T. (2010). Novel antibodies reveal inclusions containing non-native SOD1 in sporadic ALS patients. *PLoS One* 5**,** e11552.

Fournet, V., De Lavilleon, G., Schweitzer, A., Giros, B., Andrieux, A., and Martres, M.P. (2012). Both chronic treatments by epothilone D and fluoxetine increase the short-term memory and differentially alter the mood status of STOP/MAP6 KO mice. *J Neurochem* 123**,** 982-996.

Fox, M.A., Sanes, J.R., Borza, D.B., Eswarakumar, V.P., Fassler, R., Hudson, B.G., John, S.W., Ninomiya, Y., Pedchenko, V., Pfaff, S.L., Rheault, M.N., Sado, Y., Segal, Y., Werle, M.J., and Umemori, H. (2007). Distinct target-derived signals organize formation, maturation, and maintenance of motor nerve terminals. *Cell* 129**,** 179-193.

Frail, D.E., Mudd, J., Shah, V., Carr, C., Cohen, J.B., and Merlie, J.P. (1987). cDNAs for the postsynaptic 43-kDa protein of Torpedo electric organ encode two proteins with different carboxyl termini. *Proc Natl Acad Sci U S A* 84**,** 6302-6306.

Frail, D.E., Musil, L.S., Buonanno, A., and Merlie, J.P. (1989). Expression of RAPsyn (43K protein) and nicotinic acetylcholine receptor genes is not coordinately regulated in mouse muscle. *Neuron* 2**,** 1077-1086.

Francis, F., Meyer, G., Fallet-Bianco, C., Moreno, S., Kappeler, C., Socorro, A.C., Tuy, F.P., Beldjord, C., and Chelly, J. (2006). Human disorders of cortical development: from past to present. *Eur J Neurosci* 23**,** 877-893.

Freibaum, B.D., Chitta, R.K., High, A.A., and Taylor, J.P. (2010). Global analysis of TDP-43 interacting proteins reveals strong association with RNA splicing and translation machinery. *J Proteome Res* 9**,** 1104-1120.

Frey, D., Schneider, C., Xu, L., Borg, J., Spooren, W., and Caroni, P. (2000). Early and selective loss of neuromuscular synapse subtypes with low sprouting competence in motoneuron diseases. *J Neurosci* 20**,** 2534-2542.

Friedlander, R.M. (2003). Apoptosis and caspases in neurodegenerative diseases. *N Engl J Med* 348**,** 1365-1375.

Friese, A., Kaltschmidt, J.A., Ladle, D.R., Sigrist, M., Jessell, T.M., and Arber, S. (2009). Gamma and alpha motor neurons distinguished by expression of transcription factor Err3. *Proc Natl Acad Sci U S A* 106**,** 13588-13593.

Fujiwara, T., and Morimoto, K. (2012). Cooperative effect of p150Glued and microtubule stabilization to suppress excitotoxicity-induced axon degeneration. *Biochem Biophys Res Commun* 424**,** 82-88.

Galante, M., Jani, H., Vanes, L., Daniel, H., Fisher, E.M., Tybulewicz, V.L., Bliss, T.V., and Morice, E. (2009). Impairments in motor coordination without major changes in cerebellar plasticity in the Tc1 mouse model of Down syndrome. *Hum Mol Genet* 18**,** 1449-1463.

Gallo, G., and Letourneau, P.C. (1999). Different contributions of microtubule dynamics and transport to the growth of axons and collateral sprouts. *Journal of Neuroscience* 19**,** 3860-3873.

Garbuzova-Davis, S., Thomson, A., Kurien, C., Shytle, R.D., and Sanberg, P.R. (2016). Potential new complication in drug therapy development for amyotrophic lateral sclerosis. *Expert Rev Neurother***,** 1-9.

Gautam, M., Noakes, P.G., Mudd, J., Nichol, M., Chu, G.C., Sanes, J.R., and Merlie, J.P. (1995). Failure of postsynaptic specialization to develop at neuromuscular junctions of rapsyn-deficient mice. *Nature* 377**,** 232-236.

Gervasio, O.L., and Phillips, W.D. (2005). Increased ratio of rapsyn to ACh receptor stabilizes postsynaptic receptors at the mouse neuromuscular synapse. *J Physiol* 562**,** 673-685.

Getzoff, E.D., Tainer, J.A., Stempien, M.M., Bell, G.I., and Hallewell, R.A. (1989). Evolution of CuZn superoxide dismutase and the Greek key beta-barrel structural motif. *Proteins* 5**,** 322-336.

Ghazanfari, N., Fernandez, K.J., Murata, Y., Morsch, M., Ngo, S.T., Reddel, S.W., Noakes, P.G., and Phillips, W.D. (2011). Muscle specific kinase: organiser of synaptic membrane domains. *Int J Biochem Cell Biol* 43**,** 295-298.

Gijselinck, I., Van Langenhove, T., Van Der Zee, J., Sleegers, K., Philtjens, S., Kleinberger, G., Janssens, J., Bettens, K., Van Cauwenberghe, C., Pereson, S., Engelborghs, S., Sieben, A., De Jonghe, P., Vandenberghe, R., Santens, P., De Bleecker, J., Maes, G., Baumer, V., Dillen, L., Joris, G., Cuijt, I., Corsmit, E., Elinck, E., Van Dongen, J., Vermeulen, S., Van Den Broeck, M., Vaerenberg, C., Mattheijssens, M., Peeters, K., Robberecht, W., Cras, P., Martin, J.J., De Deyn, P.P., Cruts, M., and Van Broeckhoven, C. (2012). A C9orf72 promoter repeat expansion in a Flanders-Belgian cohort with disorders of the frontotemporal lobar degeneration-amyotrophic lateral sclerosis spectrum: a gene identification study. *Lancet Neurol* 11**,** 54-65.

Gillardon, F. (2009). Leucine-rich repeat kinase 2 phosphorylates brain tubulin-beta isoforms and modulates microtubule stability--a point of convergence in parkinsonian neurodegeneration? *J Neurochem* 110**,** 1514-1522.

Gillingwater, T.H., and Ribchester, R.R. (2003). The relationship of neuromuscular synapse elimination to synaptic degeneration and pathology: insights from WldS and other mutant mice. *J Neurocytol* 32**,** 863-881.

Gillis, J.M. (1996). Membrane abnormalities and Ca homeostasis in muscles of the mdx mouse, an animal model of the Duchenne muscular dystrophy: a review. *Acta Physiol Scand* 156**,** 397-406.

Godena, V.K., Romano, G., Romano, M., Appocher, C., Klima, R., Buratti, E., Baralle, F.E., and Feiguin, F. (2011). TDP-43 regulates Drosophila neuromuscular junctions growth by modulating Futsch/MAP1B levels and synaptic microtubules organization. *PLoS One* 6**,** e17808.

Goldberg, A.L. (2003). Protein degradation and protection against misfolded or damaged proteins. *Nature* 426**,** 895-899.

Gomez-Deza, J., Lee, Y.B., Troakes, C., Nolan, M., Al-Sarraj, S., Gallo, J.M., and Shaw, C.E. (2015). Dipeptide repeat protein inclusions are rare in the spinal cord and almost absent from motor neurons in C9ORF72 mutant amyotrophic lateral sclerosis and are unlikely to cause their degeneration. *Acta Neuropathol Commun* 3**,** 38.

Gonzalez De Aguilar, J.L., Niederhauser-Wiederkehr, C., Halter, B., De Tapia, M., Di Scala, F., Demougin, P., Dupuis, L., Primig, M., Meininger, V., and Loeffler, J.P. (2008). Gene profiling of skeletal muscle in an amyotrophic lateral sclerosis mouse model. *Physiol Genomics* 32**,** 207-218.

Gonzalez-Billault, C., Munoz-Llancao, P., Henriquez, D.R., Wojnacki, J., Conde, C., and Caceres, A. (2012). The role of small GTPases in neuronal morphogenesis and polarity. *Cytoskeleton (Hoboken)* 69**,** 464-485.

Goutman, S.A., and Feldman, E.L. (2015). Clinical Trials of Therapies for Amyotrophic Lateral Sclerosis: One Size Does Not Fit All. *JAMA Neurol* 72**,** 743-744.

Gowing, G., Philips, T., Van Wijmeersch, B., Audet, J.N., Dewil, M., Van Den Bosch, L., Billiau, A.D., Robberecht, W., and Julien, J.P. (2008). Ablation of proliferating microglia does not affect motor neuron degeneration in amyotrophic lateral sclerosis caused by mutant superoxide dismutase. *J Neurosci* 28**,** 10234-10244.

Grad, L.I., Yerbury, J.J., Turner, B.J., Guest, W.C., Pokrishevsky, E., O'neill, M.A., Yanai, A., Silverman, J.M., Zeineddine, R., Corcoran, L., Kumita, J.R., Luheshi, L.M., Yousefi, M., Coleman, B.M., Hill, A.F., Plotkin, S.S., Mackenzie, I.R., and Cashman, N.R. (2014). Intercellular propagated misfolding of wild-type Cu/Zn superoxide dismutase occurs via exosome-dependent and -independent mechanisms. *Proc Natl Acad Sci U S A* 111**,** 3620-3625.

Graffmo, K.S., Forsberg, K., Bergh, J., Birve, A., Zetterstrom, P., Andersen, P.M., Marklund, S.L., and Brannstrom, T. (2013). Expression of wild-type human superoxide dismutase-1 in mice causes amyotrophic lateral sclerosis. *Hum Mol Genet* 22**,** 51-60.

Grajeda, L.M., Ivanescu, A., Saito, M., Crainiceanu, C., Jaganath, D., Gilman, R.H., Crabtree, J.E., Kelleher, D., Cabrera, L., Cama, V., and Checkley, W. (2016). Modelling subject-specific childhood growth using linear mixed-effect models with cubic regression splines. *Emerg Themes Epidemiol* 13**,** 1.

Green, K.N., Steffan, J.S., Martinez-Coria, H., Sun, X., Schreiber, S.S., Thompson, L.M., and Laferla, F.M. (2008). Nicotinamide restores cognition in Alzheimer's disease transgenic mice via a mechanism involving sirtuin inhibition and selective reduction of Thr231-phosphotau. *J Neurosci* 28**,** 11500-11510.

Griffin, J.W., George, E.B., Hsieh, S.-T., and Glass, J.D. (1995). 20 Axonal degeneration and disorders of the axonal cytoskeleton. *The Axon: Structure, Function, and Pathophysiology***,** 375.

Gros-Louis, F., Lariviere, R., Gowing, G., Laurent, S., Camu, W., Bouchard, J.P., Meininger, V., Rouleau, G.A., and Julien, J.P. (2004). A frameshift deletion in peripherin gene associated with amyotrophic lateral sclerosis. *J Biol Chem* 279**,** 45951-45956.

Guerrini, R., Dobyns, W.B., and Barkovich, A.J. (2008). Abnormal development of the human cerebral cortex: genetics, functional consequences and treatment options. *Trends Neurosci* 31**,** 154-162.

Gunther, R., Suhr, M., Koch, J.C., Bahr, M., Lingor, P., and Tonges, L. (2012). Clinical testing and spinal cord removal in a mouse model for amyotrophic lateral sclerosis (ALS). *J Vis Exp*.

Gurney, M.E., Fleck, T.J., Himes, C.S., and Hall, E.D. (1998). Riluzole preserves motor function in a transgenic model of familial amyotrophic lateral sclerosis. *Neurology* 50**,** 62-66.

Gurney, M.E., Pu, H., Chiu, A.Y., Dal Canto, M.C., Polchow, C.Y., Alexander, D.D., Caliendo, J., Hentati, A., Kwon, Y.W., Deng, H.X., and Others (1994). Motor neuron degeneration in mice that express a human Cu, Zn superoxide dismutase mutation. *Science* 264**,** 1772.

Hadano, S., Benn, S.C., Kakuta, S., Otomo, A., Sudo, K., Kunita, R., Suzuki-Utsunomiya, K., Mizumura, H., Shefner, J.M., Cox, G.A., Iwakura, Y., Brown, R.H., Jr., and Ikeda, J.E. (2006). Mice deficient in the Rab5 guanine nucleotide exchange factor ALS2/alsin exhibit age-dependent neurological deficits and altered endosome trafficking. *Hum Mol Genet* 15**,** 233-250.

Hadano, S., Hand, C.K., Osuga, H., Yanagisawa, Y., Otomo, A., Devon, R.S., Miyamoto, N., Showguchi-Miyata, J., Okada, Y., Singaraja, R., Figlewicz, D.A., Kwiatkowski, T., Hosler, B.A., Sagie, T., Skaug, J., Nasir, J., Brown, R.H., Jr., Scherer, S.W., Rouleau, G.A., Hayden, M.R., and Ikeda, J.E. (2001). A gene encoding a putative GTPase regulator is mutated in familial amyotrophic lateral sclerosis 2. *Nat Genet* 29**,** 166-173.

Haidet-Phillips, A.M., Hester, M.E., Miranda, C.J., Meyer, K., Braun, L., Frakes, A., Song, S., Likhite, S., Murtha, M.J., Foust, K.D., Rao, M., Eagle, A., Kammesheidt, A., Christensen, A., Mendell, J.R., Burghes, A.H., and Kaspar, B.K. (2011). Astrocytes from familial and sporadic ALS patients are toxic to motor neurons. *Nat Biotechnol* 29**,** 824-828.

Hall, A., and Lalli, G. (2010). Rho and Ras GTPases in axon growth, guidance, and branching. *Cold Spring Harb Perspect Biol* 2**,** a001818.

Han, H., Noakes, P.G., and Phillips, W.D. (1999). Overexpression of rapsyn inhibits agrin-induced acetylcholine receptor clustering in muscle cells. *J Neurocytol* 28**,** 763-775.

Hanger, D.P., Lau, D.H., Phillips, E.C., Bondulich, M.K., Guo, T., Woodward, B.W., Pooler, A.M., and Noble, W. (2014). Intracellular and extracellular roles for tau in neurodegenerative disease. *J Alzheimers Dis* 40 Suppl 1**,** S37-45.

Hardiman, O., Van Den Berg, L.H., and Kiernan, M.C. (2011). Clinical diagnosis and management of amyotrophic lateral sclerosis. *Nat Rev Neurol* 7**,** 639-649.

Harrison, M., O'brien, A., Adams, L., Cowin, G., Ruitenberg, M.J., Sengul, G., and Watson, C. (2013). Vertebral landmarks for the identification of spinal cord segments in the mouse. *Neuroimage* 68**,** 22-29.

Hasegawa, M., Arai, T., Nonaka, T., Kametani, F., Yoshida, M., Hashizume, Y., Beach, T.G., Buratti, E., Baralle, F., Morita, M., Nakano, I., Oda, T., Tsuchiya, K., and Akiyama, H. (2008). Phosphorylated TDP-43 in frontotemporal lobar degeneration and amyotrophic lateral sclerosis. *Ann Neurol* 64**,** 60-70.

Hayashi, S., Sakurai, A., Amari, M., and Okamoto, K. (2001). Pathological study of the diffuse myelin pallor in the anterolateral columns of the spinal cord in amyotrophic lateral sclerosis. *J Neurol Sci* 188**,** 3-7.

He, F., Krans, A., Freibaum, B.D., Taylor, J.P., and Todd, P.K. (2014). TDP-43 suppresses CGG repeat-induced neurotoxicity through interactions with HnRNP A2/B1. *Hum Mol Genet* 23**,** 5036-5051.

Heath, P.R., and Shaw, P.J. (2002). Update on the glutamatergic neurotransmitter system and the role of excitotoxicity in amyotrophic lateral sclerosis. *Muscle Nerve* 26**,** 438-458.

Hegedus, J., Putman, C.T., Tyreman, N., and Gordon, T. (2008). Preferential motor unit loss in the SOD1G93A transgenic mouse model of amyotrophic lateral sclerosis. *J Physiol* 586**,** 3337-3351.

Heidemann, S.R., Landers, J.M., and Hamborg, M.A. (1981). Polarity orientation of axonal microtubules. *J Cell Biol* 91**,** 661-665.

Hellal, F., Hurtado, A., Ruschel, J., Flynn, K.C., Laskowski, C.J., Umlauf, M., Kapitein, L.C., Strikis, D., Lemmon, V., Bixby, J., Hoogenraad, C.C., and Bradke, F. (2011). Microtubule stabilization reduces scarring and causes axon regeneration after spinal cord injury. *Science* 331**,** 928-931.

Henderson, C.E., Phillips, H.S., Pollock, R.A., Davies, A.M., Lemeulle, C., Armanini, M., Simmons, L., Moffet, B., Vandlen, R.A., Simpson, L.C.C.T.S.L., Koliatsos, V.E., Rosenthal, A., and Et Al. (1994). GDNF: a potent survival factor for motoneurons present in peripheral nerve and muscle. *Science* 266**,** 1062-1064.

Henkel, J.S., Engelhardt, J.I., Siklos, L., Simpson, E.P., Kim, S.H., Pan, T., Goodman, J.C., Siddique, T., Beers, D.R., and Appel, S.H. (2004). Presence of dendritic cells, MCP-1, and activated microglia/macrophages in amyotrophic lateral sclerosis spinal cord tissue. *Ann Neurol* 55**,** 221-235.

Herrmann, H., and Aebi, U. (2000). Intermediate filaments and their associates: multi-talented structural elements specifying cytoarchitecture and cytodynamics. *Curr Opin Cell Biol* 12**,** 79-90.

Hersheson, J., Mencacci, N.E., Davis, M., Macdonald, N., Trabzuni, D., Ryten, M., Pittman, A., Paudel, R., Kara, E., Fawcett, K., Plagnol, V., Bhatia, K.P., Medlar, A.J., Stanescu, H.C., Hardy, J., Kleta, R., Wood, N.W., and Houlden, H. (2013). Mutations in the autoregulatory domain of beta-tubulin 4a cause hereditary dystonia. *Ann Neurol* 73**,** 546-553.

Hirano, A., Nakano, I., Kurland, L.T., Mulder, D.W., Holley, P.W., and Saccomanno, G. (1984). Fine structural study of neurofibrillary changes in a family with amyotrophic lateral sclerosis. *J Neuropathol Exp Neurol* 43**,** 471-480.

Hoskison, M.M., Yanagawa, Y., Obata, K., and Shuttleworth, C.W. (2007). Calcium-dependent NMDA-induced dendritic injury and MAP2 loss in acute hippocampal slices. *Neuroscience* 145**,** 66-79.

Howes, S.C., Alushin, G.M., Shida, T., Nachury, M.V., and Nogales, E. (2014). Effects of tubulin acetylation and tubulin acetyltransferase binding on microtubule structure. *Mol Biol Cell* 25**,** 257-266.

Howland, D.S., Liu, J., She, Y., Goad, B., Maragakis, N.J., Kim, B., Erickson, J., Kulik, J., Devito, L., Psaltis, G., Degennaro, L.J., Cleveland, D.W., and Rothstein, J.D. (2002). Focal loss of the glutamate transporter EAAT2 in a transgenic rat model of SOD1 mutant-mediated amyotrophic lateral sclerosis (ALS). *Proc Natl Acad Sci U S A* 99**,** 1604-1609.

Hurd, D.D., and Saxton, W.M. (1996). Kinesin mutations cause motor neuron disease phenotypes by disrupting fast axonal transport in Drosophila. *Genetics* 144**,** 1075-1085.

Ikeda, K., Zhapparova, O., Brodsky, I., Semenova, I., Tirnauer, J.S., Zaliapin, I., and Rodionov, V. (2011). CK1 activates minus-end-directed transport of membrane organelles along microtubules. *Mol Biol Cell* 22**,** 1321-1329.

Ikenaka, K., Katsuno, M., Kawai, K., Ishigaki, S., Tanaka, F., and Sobue, G. (2012). Disruption of axonal transport in motor neuron diseases. *Int J Mol Sci* 13**,** 1225-1238.

Ilieva, H., Polymenidou, M., and Cleveland, D.W. (2009). Non-cell autonomous toxicity in neurodegenerative disorders: ALS and beyond. *J Cell Biol* 187**,** 761-772.

Ingre, C., Roos, P.M., Piehl, F., Kamel, F., and Fang, F. (2015). Risk factors for amyotrophic lateral sclerosis. *Clin Epidemiol* 7**,** 181-193.

Ito, D., and Suzuki, N. (2011). Conjoint pathologic cascades mediated by ALS/FTLD-U linked RNA-binding proteins TDP-43 and FUS. *Neurology* 77**,** 1636-1643.

Ittner, L.M., Halliday, G.M., Kril, J.J., Gotz, J., Hodges, J.R., and Kiernan, M.C. (2015). FTD and ALS--translating mouse studies into clinical trials. *Nat Rev Neurol* 11**,** 360-366.

Jacobson, C., Cote, P.D., Rossi, S.G., Rotundo, R.L., and Carbonetto, S. (2001). The dystroglycan complex is necessary for stabilization of acetylcholine receptor clusters at neuromuscular junctions and formation of the synaptic basement membrane. *J Cell Biol* 152**,** 435-450.

Jaiswal, M.K. (2014). Selective vulnerability of motoneuron and perturbed mitochondrial calcium homeostasis in amyotrophic lateral sclerosis: implications for motoneurons specific calcium dysregulation. *Mol Cell Ther* 2**,** 26.

Jang, E.H., Sim, A., Im, S.K., and Hur, E.M. (2016). Effects of Microtubule Stabilization by Epothilone B Depend on the Type and Age of Neurons. *Neural Plast* 2016**,** 5056418.

Janke, C. (2014). The tubulin code: molecular components, readout mechanisms, and functions. *J Cell Biol* 206**,** 461-472.

Janke, C., and Kneussel, M. (2010). Tubulin post-translational modifications: encoding functions on the neuronal microtubule cytoskeleton. *Trends Neurosci* 33**,** 362-372.

Je, H.S., Yang, F., Ji, Y., Potluri, S., Fu, X.Q., Luo, Z.G., Nagappan, G., Chan, J.P., Hempstead, B., Son, Y.J., and Lu, B. (2013). ProBDNF and mature BDNF as punishment and reward signals for synapse elimination at mouse neuromuscular junctions. *J Neurosci* 33**,** 9957-9962.

Jiang, Y.M., Yamamoto, M., Kobayashi, Y., Yoshihara, T., Liang, Y., Terao, S., Takeuchi, H., Ishigaki, S., Katsuno, M., Adachi, H., Niwa, J., Tanaka, F., Doyu, M., Yoshida, M., Hashizume, Y., and Sobue, G. (2005). Gene expression profile of spinal motor neurons in sporadic amyotrophic lateral sclerosis. *Ann Neurol* 57**,** 236-251.

Jiang, Y.M., Yamamoto, M., Tanaka, F., Ishigaki, S., Katsuno, M., Adachi, H., Niwa, J., Doyu, M., Yoshida, M., Hashizume, Y., and Sobue, G. (2007). Gene expressions specifically detected in motor neurons (dynactin 1, early growth response 3, acetyl-CoA transporter, death receptor 5, and cyclin C) differentially correlate to pathologic markers in sporadic amyotrophic lateral sclerosis. *J Neuropathol Exp Neurol* 66**,** 617-627.

Jo, S.A., Zhu, X., Marchionni, M.A., and Burden, S.J. (1995). Neuregulins are concentrated at nerve-muscle synapses and activate ACh-receptor gene expression. *Nature* 373**,** 158-161.

Job, D., Fischer, E.H., and Margolis, R.L. (1981). Rapid disassembly of cold-stable microtubules by calmodulin. *Proc Natl Acad Sci U S A* 78**,** 4679-4682.

Kabashi, E., Valdmanis, P.N., Dion, P., Spiegelman, D., Mcconkey, B.J., Vande Velde, C., Bouchard, J.P., Lacomblez, L., Pochigaeva, K., Salachas, F., Pradat, P.F., Camu, W., Meininger, V., Dupre, N., and Rouleau, G.A. (2008). TARDBP mutations in individuals with sporadic and familial amyotrophic lateral sclerosis. *Nat Genet* 40**,** 572-574.

Kabuta, T., Kinugawa, A., Tsuchiya, Y., Kabuta, C., Setsuie, R., Tateno, M., Araki, T., and Wada, K. (2009). Familial amyotrophic lateral sclerosis-linked mutant SOD1 aberrantly interacts with tubulin. *Biochem Biophys Res Commun* 387**,** 121-126.

Kanai, Y., Dohmae, N., and Hirokawa, N. (2004). Kinesin transports RNA: isolation and characterization of an RNA-transporting granule. *Neuron* 43**,** 513-525.

Kang, H., Tian, L., Son, Y.J., Zuo, Y., Procaccino, D., Love, F., Hayworth, C., Trachtenberg, J., Mikesh, M., Sutton, L., and Others (2007). Regulation of the intermediate filament protein nestin at rodent neuromuscular junctions by innervation and activity. *The Journal of neuroscience* 27**,** 5948.

Kang, S.H., Li, Y., Fukaya, M., Lorenzini, I., Cleveland, D.W., Ostrow, L.W., Rothstein, J.D., and Bergles, D.E. (2013). Degeneration and impaired regeneration of gray matter oligodendrocytes in amyotrophic lateral sclerosis. *Nat Neurosci* 16**,** 571-579.

Kanning, K.C., Kaplan, A., and Henderson, C.E. (2010). Motor neuron diversity in development and disease. *Annu Rev Neurosci* 33**,** 409-440.

Kapitein, L.C., and Hoogenraad, C.C. (2015). Building the Neuronal Microtubule Cytoskeleton. *Neuron* 87**,** 492-506.

Karlsson, J., Fong, K.S., Hansson, M.J., Elmer, E., Csiszar, K., and Keep, M.F. (2004). Life span extension and reduced neuronal death after weekly intraventricular cyclosporin injections in the G93A transgenic mouse model of amyotrophic lateral sclerosis. *J Neurosurg* 101**,** 128-137.

Kasai, A., Kinjo, T., Ishihara, R., Sakai, I., Ishimaru, Y., Yoshioka, Y., Yamamuro, A., Ishige, K., Ito, Y., and Maeda, S. (2011). Apelin Deficiency Accelerates the Progression of Amyotrophic Lateral Sclerosis. *Plos One* 6.

Kastanenka, K.V., and Landmesser, L.T. (2010). In vivo activation of channelrhodopsin-2 reveals that normal patterns of spontaneous activity are required for motoneuron guidance and maintenance of guidance molecules. *J Neurosci* 30**,** 10575-10585.

Katz, L.C., and Shatz, C.J. (1996). Synaptic activity and the construction of cortical circuits. *Science* 274**,** 1133-1138.

Kawamura, Y., Dyck, P.J., Shimono, M., Okazaki, H., Tateishi, J., and Doi, H. (1981). Morphometric comparison of the vulnerability of peripheral motor and sensory neurons in amyotrophic lateral sclerosis. *J Neuropathol Exp Neurol* 40**,** 667-675.

Keller, A.F., Gravel, M., and Kriz, J. (2009). Live imaging of amyotrophic lateral sclerosis pathogenesis: disease onset is characterized by marked induction of GFAP in Schwann cells. *Glia* 57**,** 1130-1142.

Kenna, K.P., Van Doormaal, P.T., Dekker, A.M., Ticozzi, N., Kenna, B.J., Diekstra, F.P., Van Rheenen, W., Van Eijk, K.R., Jones, A.R., Keagle, P., Shatunov, A., Sproviero, W., Smith, B.N., Van Es, M.A., Topp, S.D., Kenna, A., Miller, J.W., Fallini, C., Tiloca, C., Mclaughlin, R.L., Vance, C., Troakes, C., Colombrita, C., Mora, G., Calvo, A., Verde, F., Al-Sarraj, S., King, A., Calini, D., De Belleroche, J., Baas, F., Van Der Kooi, A.J., De Visser, M., Ten Asbroek, A.L., Sapp, P.C., Mckenna-Yasek, D., Polak, M., Asress, S., Munoz-Blanco, J.L., Strom, T.M., Meitinger, T., Morrison, K.E., Consortium, S., Lauria, G., Williams, K.L., Leigh, P.N., Nicholson, G.A., Blair, I.P., Leblond, C.S., Dion, P.A., Rouleau, G.A., Pall, H., Shaw, P.J., Turner, M.R., Talbot, K., Taroni, F., Boylan, K.B., Van Blitterswijk, M., Rademakers, R., Esteban-Perez, J., Garcia-Redondo, A., Van Damme, P., Robberecht, W., Chio, A., Gellera, C., Drepper, C., Sendtner, M., Ratti, A., Glass, J.D., Mora, J.S., Basak, N.A., Hardiman, O., Ludolph, A.C., Andersen, P.M., Weishaupt, J.H., Brown, R.H., Jr., Al-Chalabi, A., Silani, V., Shaw, C.E., Van Den Berg, L.H., Veldink, J.H., and Landers, J.E. (2016). NEK1 variants confer susceptibility to amyotrophic lateral sclerosis. *Nat Genet* 48**,** 1037-1042.

Kennel, P.F., Finiels, F., Revah, F., and Mallet, J. (1996). Neuromuscular function impairment is not caused by motor neurone loss in FALS mice: an electromyographic study. *Neuroreport* 7**,** 1427-1431.

Ketschek, A., Jones, S., Spillane, M., Korobova, F., Svitkina, T., and Gallo, G. (2015a). Nerve growth factor promotes reorganization of the axonal microtubule array at sites of axon collateral branching. *Dev Neurobiol* 75**,** 1441-1461.

Ketschek, A., Jones, S., Spillane, M., Korobova, F., Svitkina, T., and Gallo, G. (2015b). Nerve growth factor promotes reorganization of the axonal microtubule array at sites of axon collateral branching. *Dev Neurobiol*.

Kevenaar, J.T., and Hoogenraad, C.C. (2015). The axonal cytoskeleton: from organization to function. *Front Mol Neurosci* 8**,** 44.

Kieran, D., Hafezparast, M., Bohnert, S., Dick, J.R., Martin, J., Schiavo, G., Fisher, E.M., and Greensmith, L. (2005). A mutation in dynein rescues axonal transport defects and extends the life span of ALS mice. *J Cell Biol* 169**,** 561-567.

Kihlmark, M., Imreh, G., and Hallberg, E. (2001). Sequential degradation of proteins from the nuclear envelope during apoptosis. *J Cell Sci* 114**,** 3643-3653.

Kim, N., and Burden, S.J. (2008). MuSK controls where motor axons grow and form synapses. *Nat Neurosci* 11**,** 19-27.

Kim, N., Stiegler, A.L., Cameron, T.O., Hallock, P.T., Gomez, A.M., Huang, J.H., Hubbard, S.R., Dustin, M.L., and Burden, S.J. (2008). Lrp4 is a receptor for Agrin and forms a complex with MuSK. *Cell* 135**,** 334-342.

King, A.E., Dickson, T.C., Blizzard, C.A., Woodhouse, A., Foster, S.S., Chung, R.S., and Vickers, J.C. (2011). Neuron-glia interactions underlie ALS-like axonal cytoskeletal pathology. *Neurobiology of aging* 32**,** 459-469.

King, A.E., Southam, K.A., Dittmann, J., and Vickers, J.C. (2013). Excitotoxin-induced caspase-3 activation and microtubule disintegration in axons is inhibited by taxol. *Acta Neuropathol Commun* 1**,** 59.

Kitaoka, Y., Hayashi, Y., Kumai, T., Takeda, H., Munemasa, Y., Fujino, H., Kitaoka, Y., Ueno, S., Sadun, A.A., and Lam, T.T. (2009). Axonal and cell body protection by nicotinamide adenine dinucleotide in tumor necrosis factor-induced optic neuropathy. *J Neuropathol Exp Neurol* 68**,** 915-927.

Kleele, T., Marinkovic, P., Williams, P.R., Stern, S., Weigand, E.E., Engerer, P., Naumann, R., Hartmann, J., Karl, R.M., Bradke, F., Bishop, D., Herms, J., Konnerth, A., Kerschensteiner, M., Godinho, L., and Misgeld, T. (2014). An assay to image neuronal microtubule dynamics in mice. *Nat Commun* 5**,** 4827.

Kleinberger, G., Yamanishi, Y., Suarez-Calvet, M., Czirr, E., Lohmann, E., Cuyvers, E., Struyfs, H., Pettkus, N., Wenninger-Weinzierl, A., Mazaheri, F., Tahirovic, S., Lleo, A., Alcolea, D., Fortea, J., Willem, M., Lammich, S., Molinuevo, J.L., Sanchez-Valle, R., Antonell, A., Ramirez, A., Heneka, M.T., Sleegers, K., Van Der Zee, J., Martin, J.J., Engelborghs, S., Demirtas-Tatlidede, A., Zetterberg, H., Van Broeckhoven, C., Gurvit, H., Wyss-Coray, T., Hardy, J., Colonna, M., and Haass, C. (2014). TREM2 mutations implicated in neurodegeneration impair cell surface transport and phagocytosis. *Sci Transl Med* 6**,** 243ra286.

Knight, D., Tolley, L.K., Kim, D.K., Lavidis, N.A., and Noakes, P.G. (2003). Functional analysis of neurotransmission at beta2-laminin deficient terminals. *J Physiol* 546**,** 789-800.

Knuesel, I., Mastrocola, M., Zuellig, R.A., Bornhauser, B., Schaub, M.C., and Fritschy, J.M. (1999). Short communication: altered synaptic clustering of GABAA receptors in mice lacking dystrophin (mdx mice). *Eur J Neurosci* 11**,** 4457-4462.

Kondo, T., Funayama, M., Tsukita, K., Hotta, A., Yasuda, A., Nori, S., Kaneko, S., Nakamura, M., Takahashi, R., Okano, H., Yamanaka, S., and Inoue, H. (2014). Focal transplantation of human iPSC-derived glial-rich neural progenitors improves lifespan of ALS mice. *Stem Cell Reports* 3**,** 242-249.

Konner, J., Grisham, R.N., Park, J., O'connor, O.A., Cropp, G., Johnson, R., Hannah, A.L., Hensley, M.L., Sabbatini, P., Mironov, S., Danishefsky, S., Hyman, D., Spriggs, D.R., Dupont, J., and Aghajanian, C. (2012). Phase I clinical, pharmacokinetic, and pharmacodynamic study of KOS-862 (Epothilone D) in patients with advanced solid tumors and lymphoma. *Invest New Drugs* 30**,** 2294-2302.

Krakora, D., Macrander, C., and Suzuki, M. (2012). Neuromuscular junction protection for the potential treatment of amyotrophic lateral sclerosis. *Neurol Res Int* 2012**,** 379657.

Kriz, J., Nguyen, M.D., and Julien, J.P. (2002). Minocycline slows disease progression in a mouse model of amyotrophic lateral sclerosis. *Neurobiol Dis* 10**,** 268-278.

Ku, N.O., and Omary, M.B. (2000). Keratins turn over by ubiquitination in a phosphorylation-modulated fashion. *J Cell Biol* 149**,** 547-552.

Kunita, R., Otomo, A., Mizumura, H., Suzuki-Utsunomiya, K., Hadano, S., and Ikeda, J.E. (2007). The Rab5 activator ALS2/alsin acts as a novel Rac1 effector through Rac1-activated endocytosis. *J Biol Chem* 282**,** 16599-16611.

Kwiatkowski, T.J., Jr., Bosco, D.A., Leclerc, A.L., Tamrazian, E., Vanderburg, C.R., Russ, C., Davis, A., Gilchrist, J., Kasarskis, E.J., Munsat, T., Valdmanis, P., Rouleau, G.A., Hosler, B.A., Cortelli, P., De Jong, P.J., Yoshinaga, Y., Haines, J.L., Pericak-Vance, M.A., Yan, J., Ticozzi, N., Siddique, T., Mckenna-Yasek, D., Sapp, P.C., Horvitz, H.R., Landers, J.E., and Brown, R.H., Jr. (2009). Mutations in the FUS/TLS gene on chromosome 16 cause familial amyotrophic lateral sclerosis. *Science* 323**,** 1205-1208.

Lagier-Tourenne, C., Polymenidou, M., and Cleveland, D.W. (2010). TDP-43 and FUS/TLS: emerging roles in RNA processing and neurodegeneration. *Hum Mol Genet* 19**,** R46-64.

Lagier-Tourenne, C., Polymenidou, M., Hutt, K.R., Vu, A.Q., Baughn, M., Huelga, S.C., Clutario, K.M., Ling, S.C., Liang, T.Y., Mazur, C., Wancewicz, E., Kim, A.S., Watt, A., Freier, S., Hicks, G.G., Donohue, J.P., Shiue, L., Bennett, C.F., Ravits, J., Cleveland, D.W., and Yeo, G.W. (2012). Divergent roles of ALS-linked proteins FUS/TLS and TDP-43 intersect in processing long pre-mRNAs. *Nat Neurosci* 15**,** 1488-1497.

Lai, C., Xie, C., Mccormack, S.G., Chiang, H.C., Michalak, M.K., Lin, X., Chandran, J., Shim, H., Shimoji, M., Cookson, M.R., Huganir, R.L., Rothstein, J.D., Price, D.L., Wong, P.C., Martin, L.J., Zhu, J.J., and Cai, H. (2006). Amyotrophic lateral sclerosis 2-deficiency leads to neuronal degeneration in amyotrophic lateral sclerosis through altered AMPA receptor trafficking. *J Neurosci* 26**,** 11798-11806.

Laird, F.M., Farah, M.H., Ackerley, S., Hoke, A., Maragakis, N., Rothstein, J.D., Griffin, J., Price, D.L., Martin, L.J., and Wong, P.C. (2008). Motor neuron disease occurring in a mutant dynactin mouse model is characterized by defects in vesicular trafficking. *J Neurosci* 28**,** 1997-2005.

Landen, J.W., Hau, V., Wang, M., Davis, T., Ciliax, B., Wainer, B.H., Van Meir, E.G., Glass, J.D., Joshi, H.C., and Archer, D.R. (2004). Noscapine crosses the blood-brain barrier and inhibits glioblastoma growth. *Clin Cancer Res* 10**,** 5187-5201.

Landen, J.W., Lang, R., Mcmahon, S.J., Rusan, N.M., Yvon, A.M., Adams, A.W., Sorcinelli, M.D., Campbell, R., Bonaccorsi, P., Ansel, J.C., Archer, D.R., Wadsworth, P., Armstrong, C.A., and Joshi, H.C. (2002). Noscapine alters microtubule dynamics in living cells and inhibits the progression of melanoma. *Cancer Res* 62**,** 4109-4114.

Landers, J.E., Melki, J., Meininger, V., Glass, J.D., Van Den Berg, L.H., Van Es, M.A., Sapp, P.C., Van Vught, P.W., Mckenna-Yasek, D.M., Blauw, H.M., Cho, T.J., Polak, M., Shi,

L., Wills, A.M., Broom, W.J., Ticozzi, N., Silani, V., Ozoguz, A., Rodriguez-Leyva, I., Veldink, J.H., Ivinson, A.J., Saris, C.G., Hosler, B.A., Barnes-Nessa, A., Couture, N., Wokke, J.H., Kwiatkowski, T.J., Jr., Ophoff, R.A., Cronin, S., Hardiman, O., Diekstra, F.P., Leigh, P.N., Shaw, C.E., Simpson, C.L., Hansen, V.K., Powell, J.F., Corcia, P., Salachas, F., Heath, S., Galan, P., Georges, F., Horvitz, H.R., Lathrop, M., Purcell, S., Al-Chalabi, A., and Brown, R.H., Jr. (2009). Reduced expression of the Kinesin-Associated Protein 3 (KIFAP3) gene increases survival in sporadic amyotrophic lateral sclerosis. *Proc Natl Acad Sci U S A* 106**,** 9004-9009.

Landino, L.M., Koumas, M.T., Mason, C.E., and Alston, J.A. (2007). Modification of tubulin cysteines by nitric oxide and nitroxyl donors alters tubulin polymerization activity. *Chem Res Toxicol* 20**,** 1693-1700.

Landino, L.M., Robinson, S.H., Skreslet, T.E., and Cabral, D.M. (2004). Redox modulation of tau and microtubule-associated protein-2 by the glutathione/glutaredoxin reductase system. *Biochem Biophys Res Commun* 323**,** 112-117.

Latvanlehto, A., Fox, M.A., Sormunen, R., Tu, H., Oikarainen, T., Koski, A., Naumenko, N., Shakirzyanova, A., Kallio, M., Ilves, M., Giniatullin, R., Sanes, J.R., and Pihlajaniemi, T. (2010). Muscle-derived collagen XIII regulates maturation of the skeletal neuromuscular junction. *J Neurosci* 30**,** 12230-12241.

Lee, J.C., Jin, Y., Jin, J., Kang, B.G., Nam, D.H., Joo, K.M., and Cha, C.I. (2011). Functional neural stem cell isolation from brains of adult mutant SOD1 (SOD1(G93A)) transgenic amyotrophic lateral sclerosis (ALS) mice. *Neurol Res* 33**,** 33-37.

Lee, J.D., Kamaruzaman, N.A., Fung, J.N., Taylor, S.M., Turner, B.J., Atkin, J.D., Woodruff, T.M., and Noakes, P.G. (2013a). Dysregulation of the complement cascade in the hSOD1G93A transgenic mouse model of amyotrophic lateral sclerosis. *J Neuroinflammation* 10**,** 119.

Lee, J.D., Kumar, V., Fung, J.N., Ruitenberg, M.J., Noakes, P.G., and Woodruff, T.M. (2017a). Pharmacological inhibition of complement C5a-C5a1 receptor signalling ameliorates disease pathology in the hSOD1G93A mouse model of amyotrophic lateral sclerosis. *Br J Pharmacol* 174**,** 689-699.

Lee, J.J., and Swain, S.M. (2006). Peripheral neuropathy induced by microtubule-stabilizing agents. *J Clin Oncol* 24**,** 1633-1642.

Lee, K.M., Chand, K.K., Hammond, L.A., Lavidis, N.A., and Noakes, P.G. (2017b). Functional decline at the aging neuromuscular junction is associated with altered laminin-alpha4 expression. *Aging (Albany NY)* 9**,** 880-899.

Lee, L. (2013). Riding the wave of ependymal cilia: genetic susceptibility to hydrocephalus in primary ciliary dyskinesia. *J Neurosci Res* 91**,** 1117-1132.

Lee, Y.B., Chen, H.J., Peres, J.N., Gomez-Deza, J., Attig, J., Stalekar, M., Troakes, C., Nishimura, A.L., Scotter, E.L., Vance, C., Adachi, Y., Sardone, V., Miller, J.W., Smith, B.N., Gallo, J.M., Ule, J., Hirth, F., Rogelj, B., Houart, C., and Shaw, C.E. (2013b). Hexanucleotide repeats in ALS/FTD form length-dependent RNA foci, sequester RNA binding proteins, and are neurotoxic. *Cell Rep* 5**,** 1178-1186.

Lefevre, J., Savarin, P., Gans, P., Hamon, L., Clement, M.J., David, M.O., Bosc, C., Andrieux, A., and Curmi, P.A. (2013). Structural basis for the association of MAP6 protein with microtubules and its regulation by calmodulin. *J Biol Chem* 288**,** 24910-24922.

Leigh, P.N., Anderton, B.H., Dodson, A., Gallo, J.M., Swash, M., and Power, D.M. (1988). Ubiquitin deposits in anterior horn cells in motor neurone disease. *Neurosci Lett* 93**,** 197-203.

Leitner, M., Menzies, S., and Lutz, C. (2009). "Working with ALS Mice: Guidelines for preclinical testing & colony management". The Jackson Laboritory).

Lendahl, U., Zimmerman, L.B., and Mckay, R.D. (1990). CNS stem cells express a new class of intermediate filament protein. *Cell* 60**,** 585-595.
Lesuisse, C., and Martin, L.J. (2002). Long-term culture of mouse cortical neurons as a model for neuronal development, aging, and death. *J Neurobiol* 51**,** 9-23.
Letourneau, P.C., and Ressler, A.H. (1984). Inhibition of neurite initiation and growth by taxol. *J Cell Biol* 98**,** 1355-1362.
Letourneau, P.C., Shattuck, T.A., and Ressler, A.H. (1986). Branching of Sensory and Sympathetic Neurites Invitro Is Inhibited by Treatment with Taxol. *Journal of Neuroscience* 6**,** 1912-1917.
Levine, T.P., Daniels, R.D., Gatta, A.T., Wong, L.H., and Hayes, M.J. (2013). The product of C9orf72, a gene strongly implicated in neurodegeneration, is structurally related to DENN Rab-GEFs. *Bioinformatics* 29**,** 499-503.
Levy, J.R., Sumner, C.J., Caviston, J.P., Tokito, M.K., Ranganathan, S., Ligon, L.A., Wallace, K.E., Lamonte, B.H., Harmison, G.G., Puls, I., Fischbeck, K.H., and Holzbaur, E.L. (2006). A motor neuron disease-associated mutation in p150Glued perturbs dynactin function and induces protein aggregation. *J Cell Biol* 172**,** 733-745.
Lewis, T.L., Jr., Courchet, J., and Polleux, F. (2013). Cell biology in neuroscience: Cellular and molecular mechanisms underlying axon formation, growth, and branching. *J Cell Biol* 202**,** 837-848.
Li, Y., Lee, Y.I., Thompson, W.J.J., Il Lee, Y., and Others (2011). Changes in Aging Mouse Neuromuscular Junctions Are Explained by Degeneration and Regeneration of Muscle Fiber Segments at the Synapse. *J Neurosci* 31**,** 14910-14919.
Li, Y., Pawlik, B., Elcioglu, N., Aglan, M., Kayserili, H., Yigit, G., Percin, F., Goodman, F., Nurnberg, G., Cenani, A., Urquhart, J., Chung, B.D., Ismail, S., Amr, K., Aslanger, A.D., Becker, C., Netzer, C., Scambler, P., Eyaid, W., Hamamy, H., Clayton-Smith, J., Hennekam, R., Nurnberg, P., Herz, J., Temtamy, S.A., and Wollnik, B. (2010). LRP4 mutations alter Wnt/beta-catenin signaling and cause limb and kidney malformations in Cenani-Lenz syndrome. *Am J Hum Genet* 86**,** 696-706.
Li, Y., and Thompson, W.J. (2011). Nerve terminal growth remodels neuromuscular synapses in mice following regeneration of the postsynaptic muscle fiber. *J Neurosci* 31**,** 13191-13203.
Ligon, L.A., Lamonte, B.H., Wallace, K.E., Weber, N., Kalb, R.G., and Holzbaur, E.L. (2005). Mutant superoxide dismutase disrupts cytoplasmic dynein in motor neurons. *Neuroreport* 16**,** 533-536.
Lim, S.S., Sammak, P.J., and Borisy, G.G. (1989). Progressive and spatially differentiated stability of microtubules in developing neuronal cells. *J Cell Biol* 109**,** 253-263.
Lin, W., Burgess, R.W., Dominguez, B., Pfaff, S.L., Sanes, J.R., and Lee, K.F. (2001). Distinct roles of nerve and muscle in postsynaptic differentiation of the neuromuscular synapse. *Nature* 410**,** 1057-1064.
Ling, S.C., Polymenidou, M., and Cleveland, D.W. (2013). Converging mechanisms in ALS and FTD: disrupted RNA and protein homeostasis. *Neuron* 79**,** 416-438.
Liu, J.S., Schubert, C.R., Fu, X., Fourniol, F.J., Jaiswal, J.K., Houdusse, A., Stultz, C.M., Moores, C.A., and Walsh, C.A. (2012). Molecular basis for specific regulation of neuronal kinesin-3 motors by doublecortin family proteins. *Mol Cell* 47**,** 707-721.
Liu, Y., Pattamatta, A., Zu, T., Reid, T., Bardhi, O., Borchelt, D.R., Yachnis, A.T., and Ranum, L.P. (2016). C9orf72 BAC Mouse Model with Motor Deficits and Neurodegenerative Features of ALS/FTD. *Neuron* 90**,** 521-534.
Liu, Y.C., Chiang, P.M., and Tsai, K.J. (2013). Disease animal models of TDP-43 proteinopathy and their pre-clinical applications. *Int J Mol Sci* 14**,** 20079-20111.

Logroscino, G., Traynor, B.J., Hardiman, O., Chio, A., Mitchell, D., Swingler, R.J., Millul, A., Benn, E., Beghi, E., and Eurals (2010). Incidence of amyotrophic lateral sclerosis in Europe. *J Neurol Neurosurg Psychiatry* 81**,** 385-390.

Lopez-Fanarraga, M., Carranza, G., Bellido, J., Kortazar, D., Villegas, J.C., and Zabala, J.C. (2007). Tubulin cofactor B plays a role in the neuronal growth cone. *J Neurochem* 100**,** 1680-1687.

Losen, M., Stassen, M.H., Martinez-Martinez, P., Machiels, B.M., Duimel, H., Frederik, P., Veldman, H., Wokke, J.H., Spaans, F., Vincent, A., and De Baets, M.H. (2005). Increased expression of rapsyn in muscles prevents acetylcholine receptor loss in experimental autoimmune myasthenia gravis. *Brain* 128**,** 2327-2337.

Luo, L., and O'leary, D.D. (2005). Axon retraction and degeneration in development and disease. *Annu Rev Neurosci* 28**,** 127-156.

Lyons, P.R., and Slater, C.R. (1991). Structure and function of the neuromuscular junction in young adult mdx mice. *J Neurocytol* 20**,** 969-981.

Ma, M. (2013). Role of calpains in the injury-induced dysfunction and degeneration of the mammalian axon. *Neurobiol Dis* 60**,** 61-79.

Maday, S., Twelvetrees, A.E., Moughamian, A.J., and Holzbaur, E.L. (2014). Axonal transport: cargo-specific mechanisms of motility and regulation. *Neuron* 84**,** 292-309.

Magiera, M.M., and Janke, C. (2014). Post-translational modifications of tubulin. *Curr Biol* 24**,** R351-354.

Marangi, G., and Traynor, B.J. (2015). Genetic causes of amyotrophic lateral sclerosis: new genetic analysis methodologies entailing new opportunities and challenges. *Brain Res* 1607**,** 75-93.

Martyn, J.A., Fagerlund, M.J., and Eriksson, L.I. (2009). Basic principles of neuromuscular transmission. *Anaesthesia* 64 Suppl 1**,** 1-9.

Maselli, R.A., Wollman, R.L., Leung, C., Distad, B., Palombi, S., Richman, D.P., Salazar-Grueso, E.F., and Roos, R.P. (1993). Neuromuscular transmission in amyotrophic lateral sclerosis. *Muscle Nerve* 16**,** 1193-1203.

Masocha, W. (2015). Astrocyte activation in the anterior cingulate cortex and altered glutamatergic gene expression during paclitaxel-induced neuropathic pain in mice. *PeerJ* 3**,** e1350.

Mathewson, M.A., Chapman, M.A., Hentzen, E.R., Friden, J., and Lieber, R.L. (2012). Anatomical, architectural, and biochemical diversity of the murine forelimb muscles. *J Anat* 221**,** 443-451.

Matsuyama, S.S., and Jarvik, L.F. (1989). Hypothesis: microtubules, a key to Alzheimer disease. *Proc Natl Acad Sci U S A* 86**,** 8152-8156.

Maximino, J.R., De Oliveira, G.P., Alves, C.J., and Chadi, G. (2014). Deregulated expression of cytoskeleton related genes in the spinal cord and sciatic nerve of presymptomatic SOD1(G93A) Amyotrophic Lateral Sclerosis mouse model. *Front Cell Neurosci* 8**,** 148.

Mccann, C.M., Nguyen, Q.T., Santo Neto, H., and Lichtman, J.W. (2007). Rapid synapse elimination after postsynaptic protein synthesis inhibition in vivo. *J Neurosci* 27**,** 6064-6067.

Mccord, J.M., and Fridovich, I. (1969). The utility of superoxide dismutase in studying free radical reactions. I. Radicals generated by the interaction of sulfite, dimethyl sulfoxide, and oxygen. *J Biol Chem* 244**,** 6056-6063.

Mcgee Lab (2016). *Tactile and motor learning* [Online]. Available: http://mcgeelab.com/research/tactile-and-motor-learning [Accessed 17 Dec 2016].

Mcmurray, C.T. (2000). Neurodegeneration: diseases of the cytoskeleton? *Cell Death Differ* 7**,** 861-865.

Menon, P., Kiernan, M.C., and Vucic, S. (2015). Cortical hyperexcitability precedes lower motor neuron dysfunction in ALS. *Clin Neurophysiol* 126**,** 803-809.

Meyer, K., Ferraiuolo, L., Miranda, C.J., Likhite, S., Mcelroy, S., Renusch, S., Ditsworth, D., Lagier-Tourenne, C., Smith, R.A., Ravits, J., Burghes, A.H., Shaw, P.J., Cleveland, D.W., Kolb, S.J., and Kaspar, B.K. (2014). Direct conversion of patient fibroblasts demonstrates non-cell autonomous toxicity of astrocytes to motor neurons in familial and sporadic ALS. *Proc Natl Acad Sci U S A* 111**,** 829-832.

Mezzapesa, D.M., D'errico, E., Tortelli, R., Distaso, E., Cortese, R., Tursi, M., Federico, F., Zoccolella, S., Logroscino, G., Dicuonzo, F., and Simone, I.L. (2013). Cortical thinning and clinical heterogeneity in amyotrophic lateral sclerosis. *PLoS One* 8**,** e80748.

Michaelis, M.L., Georg, G., Telikepalli, H., Mcintosh, M., and Rajewski, R.A. (2006). Ongoing in vivo studies with cytoskeletal drugs in tau transgenic mice. *Curr Alzheimer Res* 3**,** 215-219.

Millecamps, S., and Julien, J.P. (2013). Axonal transport deficits and neurodegenerative diseases. *Nat Rev Neurosci* 14**,** 161-176.

Miller, T.M., Kim, S.H., Yamanaka, K., Hester, M., Umapathi, P., Arnson, H., Rizo, L., Mendell, J.R., Gage, F.H., Cleveland, D.W., and Kaspar, B.K. (2006). Gene transfer demonstrates that muscle is not a primary target for non-cell-autonomous toxicity in familial amyotrophic lateral sclerosis. *Proc Natl Acad Sci U S A* 103**,** 19546-19551.

Miner, J.H., and Sanes, J.R. (1994). Collagen IV alpha 3, alpha 4, and alpha 5 chains in rodent basal laminae: sequence, distribution, association with laminins, and developmental switches. *J Cell Biol* 127**,** 879-891.

Misgeld, T., Kummer, T.T., Lichtman, J.W., and Sanes, J.R. (2005). Agrin promotes synaptic differentiation by counteracting an inhibitory effect of neurotransmitter. *Proc Natl Acad Sci U S A* 102**,** 11088-11093.

Mitchison, T., and Kirschner, M. (1984). Dynamic instability of microtubule growth. *Nature* 312**,** 237-242.

Mitsumoto, H., Brooks, B.R., and Silani, V. (2014). Clinical trials in amyotrophic lateral sclerosis: why so many negative trials and how can trials be improved? *Lancet Neurol* 13**,** 1127-1138.

Mohan, R., and John, A. (2015). Microtubule-associated proteins as direct crosslinkers of actin filaments and microtubules. *IUBMB Life* 67**,** 395-403.

Mohan, R., Tosolini, A.P., and Morris, R. (2014). Targeting the motor end plates in the mouse hindlimb gives access to a greater number of spinal cord motor neurons: an approach to maximize retrograde transport. *Neuroscience* 274**,** 318-330.

Mohseni, P., Sung, H.-K., Murphy, A.J., Laliberte, C.L., Pallari, H.-M., Henkelman, M., Georgiou, J., Xie, G., Quaggin, S.E., Thorner, P.S., Eriksson, J.E., and Nagy, A. (2011). Nestin Is Not Essential for Development of the CNS But Required for Dispersion of Acetylcholine Receptor Clusters at the Area of Neuromuscular Junctions. *The Journal of Neuroscience* 31**,** 11547-11552.

Moloney, E.B., De Winter, F., and Verhaagen, J. (2014). ALS as a distal axonopathy: molecular mechanisms affecting neuromuscular junction stability in the presymptomatic stages of the disease. *Front Neurosci* 8**,** 252.

Mori, K., Weng, S.M., Arzberger, T., May, S., Rentzsch, K., Kremmer, E., Schmid, B., Kretzschmar, H.A., Cruts, M., Van Broeckhoven, C., Haass, C., and Edbauer, D. (2013). The C9orf72 GGGGCC repeat is translated into aggregating dipeptide-repeat proteins in FTLD/ALS. *Science* 339**,** 1335-1338.

Morohoshi, F., Ootsuka, Y., Arai, K., Ichikawa, H., Mitani, S., Munakata, N., and Ohki, M. (1998). Genomic structure of the human RBP56/hTAFII68 and FUS/TLS genes. *Gene* 221**,** 191-198.

Morris, J.A., Kandpal, G., Ma, L., and Austin, C.P. (2003). DISC1 (Disrupted-In-Schizophrenia 1) is a centrosome-associated protein that interacts with MAP1A, MIPT3, ATF4/5 and NUDEL: regulation and loss of interaction with mutation. *Hum Mol Genet* 12**,** 1591-1608.

Morsch, M., Reddel, S.W., Ghazanfari, N., Toyka, K.V., and Phillips, W.D. (2013). Pyridostigmine but not 3,4-diaminopyridine exacerbates ACh receptor loss and myasthenia induced in mice by muscle-specific kinase autoantibody. *J Physiol* 591**,** 2747-2762.

Mozaffar, T., Strandberg, E., Abe, K., Hilgenberg, L.G., Smith, M.A., and Gupta, R. (2009). Neuromuscular junction integrity after chronic nerve compression injury. *J Orthop Res* 27**,** 114-119.

Muggeo, V.M. (2003). Estimating regression models with unknown break-points. *Statistics in medicine* 22**,** 3055-3071.

Mulder, D.W., Kurland, L.T., Offord, K.P., and Beard, C.M. (1986). Familial adult motor neuron disease: amyotrophic lateral sclerosis. *Neurology* 36**,** 511-517.

Munch, C., Rosenbohm, A., Sperfeld, A.D., Uttner, I., Reske, S., Krause, B.J., Sedlmeier, R., Meyer, T., Hanemann, C.O., Stumm, G., and Ludolph, A.C. (2005). Heterozygous R1101K mutation of the DCTN1 gene in a family with ALS and FTD. *Ann Neurol* 58**,** 777-780.

Munch, C., Sedlmeier, R., Meyer, T., Homberg, V., Sperfeld, A.D., Kurt, A., Prudlo, J., Peraus, G., Hanemann, C.O., Stumm, G., and Ludolph, A.C. (2004). Point mutations of the p150 subunit of dynactin (DCTN1) gene in ALS. *Neurology* 63**,** 724-726.

Munnamalai, V., and Suter, D.M. (2009). Reactive oxygen species regulate F-actin dynamics in neuronal growth cones and neurite outgrowth. *J Neurochem* 108**,** 644-661.

Musaro, A. (2013). Understanding ALS: new therapeutic approaches. *FEBS J* 280**,** 4315-4322.

Mutihac, R., Alegre-Abarrategui, J., Gordon, D., Farrimond, L., Yamasaki-Mann, M., Talbot, K., and Wade-Martins, R. (2015). TARDBP pathogenic mutations increase cytoplasmic translocation of TDP-43 and cause reduction of endoplasmic reticulum Ca(2)(+) signaling in motor neurons. *Neurobiol Dis* 75**,** 64-77.

Narayanan, R.K., Mangelsdorf, M., Panwar, A., Butler, T.J., Noakes, P.G., and Wallace, R.H. (2013). Identification of RNA bound to the TDP-43 ribonucleoprotein complex in the adult mouse brain. *Amyotroph Lateral Scler Frontotemporal Degener* 14**,** 252-260.

Naumova, E.N., Must, A., and Laird, N.M. (2001). Tutorial in Biostatistics: Evaluating the impact of 'critical periods' in longitudinal studies of growth using piecewise mixed effects models. *Int J Epidemiol* 30**,** 1332-1341.

Neumann, M., Sampathu, D.M., Kwong, L.K., Truax, A.C., Micsenyi, M.C., Chou, T.T., Bruce, J., Schuck, T., Grossman, M., Clark, C.M., Mccluskey, L.F., Miller, B.L., Masliah, E., Mackenzie, I.R., Feldman, H., Feiden, W., Kretzschmar, H.A., Trojanowski, J.Q., and Lee, V.M. (2006). Ubiquitinated TDP-43 in frontotemporal lobar degeneration and amyotrophic lateral sclerosis. *Science* 314**,** 130-133.

Ngo, S.T., Baumann, F., Ridall, P.G., Pettitt, A.N., Henderson, R.D., Bellingham, M.C., and Mccombe, P.A. (2012). The relationship between Bayesian motor unit number estimation and histological measurements of motor neurons in wild-type and SOD1(G93A) mice. *Clin Neurophysiol* 123**,** 2080-2091.

Nguyen, K.T., Zhang, Z., Barrett, E.F., and David, G. (2012). Morphological and functional changes in innervation of a fast forelimb muscle in SOD1-G85R mice. *Neurobiology of disease* 48**,** 399-408.
Nguyen, M.D., Lariviere, R.C., and Julien, J.P. (2001). Deregulation of Cdk5 in a mouse model of ALS: toxicity alleviated by perikaryal neurofilament inclusions. *Neuron* 30**,** 135-147.
Niebroj-Dobosz, I., Rafalowska, J., Fidzianska, A., Gadamski, R., and Grieb, P. (2007). Myelin composition of spinal cord in a model of amyotrophic lateral sclerosis (ALS) in SOD1G93A transgenic rats. *Folia Neuropathol* 45**,** 236-241.
Nikolic, M., Dudek, H., Kwon, Y.T., Ramos, Y.F., and Tsai, L.H. (1996). The cdk5/p35 kinase is essential for neurite outgrowth during neuronal differentiation. *Genes Dev* 10**,** 816-825.
Nishimune, H., Sanes, J.R., and Carlson, S.S. (2004). A synaptic laminin-calcium channel interaction organizes active zones in motor nerve terminals. *Nature* 432**,** 580-587.
Nogales, E., and Wang, H.W. (2006). Structural mechanisms underlying nucleotide-dependent self-assembly of tubulin and its relatives. *Curr Opin Struct Biol* 16**,** 221-229.
Nolan, M., Talbot, K., and Ansorge, O. (2016). Pathogenesis of FUS-associated ALS and FTD: insights from rodent models. *Acta Neuropathol Commun* 4**,** 99.
Nonneman, A., Robberecht, W., and Van Den Bosch, L. (2014). The role of oligodendroglial dysfunction in amyotrophic lateral sclerosis. *Neurodegener Dis Manag* 4**,** 223-239.
Northcutt, R.G. (1989). Body and Brain. A Trophic Theory of Neural Connections. Dale Purves. Harvard University Press, Cambridge, MA, 1988. viii, 231 pp., illus. $35. *Science* 244**,** 993.
O'brien, E.T., Salmon, E.D., and Erickson, H.P. (1997). How calcium causes microtubule depolymerization. *Cell Motil Cytoskeleton* 36**,** 125-135.
O'hanlon, G.M., Humphreys, P.D., Goldman, R.S., Halstead, S.K., Bullens, R.W., Plomp, J.J., Ushkaryov, Y., and Willison, H.J. (2003). Calpain inhibitors protect against axonal degeneration in a model of anti-ganglioside antibody-mediated motor nerve terminal injury. *Brain* 126**,** 2497-2509.
O'malley, J.P., Waran, M.T., and Balice-Gordon, R.J. (1999). In vivo observations of terminal Schwann cells at normal, denervated, and reinnervated mouse neuromuscular junctions. *J Neurobiol* 38**,** 270-286.
Ohkawara, B., Cabrera-Serrano, M., Nakata, T., Milone, M., Asai, N., Ito, K., Ito, M., Masuda, A., Ito, Y., Engel, A.G., and Ohno, K. (2014). LRP4 third beta-propeller domain mutations cause novel congenital myasthenia by compromising agrin-mediated MuSK signaling in a position-specific manner. *Hum Mol Genet* 23**,** 1856-1868.
Ohno, K., Engel, A.G., Shen, X.M., Selcen, D., Brengman, J., Harper, C.M., Tsujino, A., and Milone, M. (2002). Rapsyn mutations in humans cause endplate acetylcholine-receptor deficiency and myasthenic syndrome. *Am J Hum Genet* 70**,** 875-885.
Oosthuyse, B., Moons, L., Storkebaum, E., Beck, H., Nuyens, D., Brusselmans, K., Van Dorpe, J., Hellings, P., Gorselink, M., Heymans, S., Theilmeier, G., Dewerchin, M., Laudenbach, V., Vermylen, P., Raat, H., Acker, T., Vleminckx, V., Van Den Bosch, L., Cashman, N., Fujisawa, H., Drost, M.R., Sciot, R., Bruyninckx, F., Hicklin, D.J., Ince, C., Gressens, P., Lupu, F., Plate, K.H., Robberecht, W., Herbert, J.M., Collen, D., and Carmeliet, P. (2001). Deletion of the hypoxia-response element in the vascular endothelial growth factor promoter causes motor neuron degeneration. *Nat Genet* 28**,** 131-138.
Ou, S.H., Wu, F., Harrich, D., Garcia-Martinez, L.F., and Gaynor, R.B. (1995). Cloning and characterization of a novel cellular protein, TDP-43, that binds to human immunodeficiency virus type 1 TAR DNA sequence motifs. *J Virol* 69**,** 3584-3596.
Palazzo, A.F., Cook, T.A., Alberts, A.S., and Gundersen, G.G. (2001). mDia mediates Rho-regulated formation and orientation of stable microtubules. *Nat Cell Biol* 3**,** 723-729.

Pandya, R.S., Mao, L.L., Zhou, E.W., Bowser, R., Zhu, Z., Zhu, Y., and Wang, X. (2012). Neuroprotection for amyotrophic lateral sclerosis: role of stem cells, growth factors, and gene therapy. *Cent Nerv Syst Agents Med Chem* 12**,** 15-27.

Panzeri, C., De Palma, C., Martinuzzi, A., Daga, A., De Polo, G., Bresolin, N., Miller, C.C., Tudor, E.L., Clementi, E., and Bassi, M.T. (2006). The first ALS2 missense mutation associated with JPLS reveals new aspects of alsin biological function. *Brain* 129**,** 1710-1719.

Paolicelli, R.C., Bolasco, G., Pagani, F., Maggi, L., Scianni, M., Panzanelli, P., Giustetto, M., Ferreira, T.A., Guiducci, E., Dumas, L., Ragozzino, D., and Gross, C.T. (2011). Synaptic pruning by microglia is necessary for normal brain development. *Science* 333**,** 1456-1458.

Park, J.Y., Jang, S.Y., Shin, Y.K., Koh, H., Suh, D.J., Shinji, T., Araki, T., and Park, H.T. (2013). Mitochondrial swelling and microtubule depolymerization are associated with energy depletion in axon degeneration. *Neuroscience* 238**,** 258-269.

Patton, B.L., Cunningham, J.M., Thyboll, J., Kortesmaa, J., Westerblad, H., Edstrom, L., Tryggvason, K., and Sanes, J.R. (2001). Properly formed but improperly localized synaptic specializations in the absence of laminin alpha4. *Nat Neurosci* 4**,** 597-604.

Patzke, H., and Tsai, L.H. (2002). Cdk5 sinks into ALS. *Trends Neurosci* 25**,** 8-10.

Perez-Garcia, M.J., and Burden, S.J. (2012). Increasing MuSK activity delays denervation and improves motor function in ALS mice. *Cell Rep* 2**,** 497-502.

Perry, G.M., Tallaksen-Greene, S., Kumar, A., Heng, M.Y., Kneynsberg, A., Van Groen, T., Detloff, P.J., Albin, R.L., and Lesort, M. (2010). Mitochondrial calcium uptake capacity as a therapeutic target in the R6/2 mouse model of Huntington's disease. *Hum Mol Genet* 19**,** 3354-3371.

Pesiridis, G.S., Lee, V.M., and Trojanowski, J.Q. (2009). Mutations in TDP-43 link glycine-rich domain functions to amyotrophic lateral sclerosis. *Hum Mol Genet* 18**,** R156-162.

Peters, O.M., Ghasemi, M., and Brown, R.H., Jr. (2015). Emerging mechanisms of molecular pathology in ALS. *J Clin Invest* 125**,** 1767-1779.

Petkau, T.L., and Leavitt, B.R. (2014). Progranulin in neurodegenerative disease. *Trends Neurosci* 37**,** 388-398.

Pevzner, A., Schoser, B., Peters, K., Cosma, N.C., Karakatsani, A., Schalke, B., Melms, A., and Kroger, S. (2012). Anti-LRP4 autoantibodies in AChR- and MuSK-antibody-negative myasthenia gravis. *J Neurol* 259**,** 427-435.

Pfohl-Leszkowicz, A., Hadjeba-Medjdoub, K., Ballet, N., Schrickx, J., and Fink-Gremmels, J. (2015). Assessment and characterisation of yeast-based products intended to mitigate ochratoxin exposure using in vitro and in vivo models. *Food Additives and Contaminants Part a-Chemistry Analysis Control Exposure & Risk Assessment* 32**,** 604-616.

Philips, T., and Rothstein, J.D. (2015). Rodent Models of Amyotrophic Lateral Sclerosis. *Curr Protoc Pharmacol* 69**,** 5 67 61-21.

Picher-Martel, V., Valdmanis, P.N., Gould, P.V., Julien, J.P., and Dupre, N. (2016). From animal models to human disease: a genetic approach for personalized medicine in ALS. *Acta Neuropathol Commun* 4**,** 70.

Pilgram, G.S., Potikanond, S., Baines, R.A., Fradkin, L.G., and Noordermeer, J.N. (2010). The roles of the dystrophin-associated glycoprotein complex at the synapse. *Mol Neurobiol* 41**,** 1-21.

Pirog, K.A., Jaka, O., Katakura, Y., Meadows, R.S., Kadler, K.E., Boot-Handford, R.P., and Briggs, M.D. (2010). A mouse model offers novel insights into the myopathy and tendinopathy often associated with pseudoachondroplasia and multiple epiphyseal dysplasia. *Hum Mol Genet* 19**,** 52-64.

Pokrishevsky, E., Grad, L.I., Yousefi, M., Wang, J., Mackenzie, I.R., and Cashman, N.R. (2012). Aberrant localization of FUS and TDP43 is associated with misfolding of SOD1 in amyotrophic lateral sclerosis. *PLoS One* 7**,** e35050.

Polymenidou, M., Lagier-Tourenne, C., Hutt, K.R., Huelga, S.C., Moran, J., Liang, T.Y., Ling, S.C., Sun, E., Wancewicz, E., Mazur, C., Kordasiewicz, H., Sedaghat, Y., Donohue, J.P., Shiue, L., Bennett, C.F., Yeo, G.W., and Cleveland, D.W. (2011). Long pre-mRNA depletion and RNA missplicing contribute to neuronal vulnerability from loss of TDP-43. *Nat Neurosci* 14**,** 459-468.

Puls, I., Jonnakuty, C., Lamonte, B.H., Holzbaur, E.L., Tokito, M., Mann, E., Floeter, M.K., Bidus, K., Drayna, D., Oh, S.J., Brown, R.H., Jr., Ludlow, C.L., and Fischbeck, K.H. (2003). Mutant dynactin in motor neuron disease. *Nat Genet* 33**,** 455-456.

Pun, S., Santos, A.a.F., Saxena, S., Xu, L., Caroni, P., and S, S. (2006). Selective vulnerability and pruning of phasic motoneuron axons in motoneuron disease alleviated by CNTF. *Nat Neurosci* 9**,** 408-419.

Radford, R.A., Morsch, M., Rayner, S.L., Cole, N.J., Pountney, D.L., and Chung, R.S. (2015). The established and emerging roles of astrocytes and microglia in amyotrophic lateral sclerosis and frontotemporal dementia. *Front Cell Neurosci* 9**,** 414.

Radunovic, A., Shaw, C.E., Akman-Demir, G., Idrisoglu, H., and Leigh, P.N. (1997). CuZnSOD-associated amyotrophic lateral sclerosis. *Ann Neurol* 42**,** 273-274.

Raff, M.C., Whitmore, A.V., and Finn, J.T. (2002). Axonal self-destruction and neurodegeneration. *Science* 296**,** 868-871.

Ragonese, P., Cellura, E., Aridon, P., D'amelio, M., Spataro, R., Taiello, A.C., Maimone, D., La Bella, V., and Savettieri, G. (2012). Incidence of amyotrophic lateral sclerosis in Sicily: A population based study. *Amyotroph Lateral Scler*.

Rando, T.A. (2001). The dystrophin-glycoprotein complex, cellular signaling, and the regulation of cell survival in the muscular dystrophies. *Muscle Nerve* 24**,** 1575-1594.

Re, D.B., Le Verche, V., Yu, C., Amoroso, M.W., Politi, K.A., Phani, S., Ikiz, B., Hoffmann, L., Koolen, M., Nagata, T., Papadimitriou, D., Nagy, P., Mitsumoto, H., Kariya, S., Wichterle, H., Henderson, C.E., and Przedborski, S. (2014). Necroptosis drives motor neuron death in models of both sporadic and familial ALS. *Neuron* 81**,** 1001-1008.

Redler, R.L., and Dokholyan, N.V. (2012). The complex molecular biology of amyotrophic lateral sclerosis (ALS). *Prog Mol Biol Transl Sci* 107**,** 215-262.

Redler, R.L., Fee, L., Fay, J.M., Caplow, M., and Dokholyan, N.V. (2014). Non-native soluble oligomers of Cu/Zn superoxide dismutase (SOD1) contain a conformational epitope linked to cytotoxicity in amyotrophic lateral sclerosis (ALS). *Biochemistry* 53**,** 2423-2432.

Ren, Y., Liu, W., Jiang, H., Jiang, Q., and Feng, J. (2005). Selective vulnerability of dopaminergic neurons to microtubule depolymerization. *J Biol Chem* 280**,** 34105-34112.

Ren, Y., Zhao, J., and Feng, J. (2003). Parkin binds to alpha/beta tubulin and increases their ubiquitination and degradation. *J Neurosci* 23**,** 3316-3324.

Renton, A.E., Majounie, E., Waite, A., Simon-Sanchez, J., Rollinson, S., Gibbs, J.R., Schymick, J.C., Laaksovirta, H., Van Swieten, J.C., Myllykangas, L., Kalimo, H., Paetau, A., Abramzon, Y., Remes, A.M., Kaganovich, A., Scholz, S.W., Duckworth, J., Ding, J., Harmer, D.W., Hernandez, D.G., Johnson, J.O., Mok, K., Ryten, M., Trabzuni, D., Guerreiro, R.J., Orrell, R.W., Neal, J., Murray, A., Pearson, J., Jansen, I.E., Sondervan, D., Seelaar, H., Blake, D., Young, K., Halliwell, N., Callister, J.B., Toulson, G., Richardson, A., Gerhard, A., Snowden, J., Mann, D., Neary, D., Nalls, M.A., Peuralinna, T., Jansson, L., Isoviita, V.M., Kaivorinne, A.L., Holtta-Vuori, M., Ikonen, E., Sulkava, R., Benatar, M., Wuu, J., Chio, A., Restagno, G., Borghero, G., Sabatelli, M.,

Consortium, I., Heckerman, D., Rogaeva, E., Zinman, L., Rothstein, J.D., Sendtner, M., Drepper, C., Eichler, E.E., Alkan, C., Abdullaev, Z., Pack, S.D., Dutra, A., Pak, E., Hardy, J., Singleton, A., Williams, N.M., Heutink, P., Pickering-Brown, S., Morris, H.R., Tienari, P.J., and Traynor, B.J. (2011). A hexanucleotide repeat expansion in C9ORF72 is the cause of chromosome 9p21-linked ALS-FTD. *Neuron* 72**,** 257-268.

Reyes-Gibby, C.C., Morrow, P.K., Buzdar, A., and Shete, S. (2009). Chemotherapy-induced peripheral neuropathy as a predictor of neuropathic pain in breast cancer patients previously treated with paclitaxel. *J Pain* 10**,** 1146-1150.

Rimer, M., Cohen, I., Lomo, T., Burden, S.J., and Mcmahan, U.J. (1998). Neuregulins and erbB receptors at neuromuscular junctions and at agrin-induced postsynaptic-like apparatus in skeletal muscle. *Mol Cell Neurosci* 12**,** 1-15.

Rizzuto, E., Pisu, S., Musaro, A., and Del Prete, Z. (2015). Measuring Neuromuscular Junction Functionality in the SOD1(G93A) Animal Model of Amyotrophic Lateral Sclerosis. *Ann Biomed Eng* 43**,** 2196-2206.

Robberecht, W., and Philips, T. (2013). The changing scene of amyotrophic lateral sclerosis. *Nat Rev Neurosci* 14**,** 248-264.

Rocha, M.C., Pousinha, P.A., Correia, A.M., Sebastiao, A.M., and Ribeiro, J.A. (2013). Early changes of neuromuscular transmission in the SOD1(G93A) mice model of ALS start long before motor symptoms onset. *PLoS One* 8**,** e73846.

Rosen, D.R., Siddique, T., Patterson, D., Figlewicz, D.A., Sapp, P., Hentati, A., Donaldson, D., Goto, J., O'regan, J.P., Deng, H.X., and Et Al. (1993). Mutations in Cu/Zn superoxide dismutase gene are associated with familial amyotrophic lateral sclerosis. *Nature* 362**,** 59-62.

Rothstein, J.D. (2009). Current hypotheses for the underlying biology of amyotrophic lateral sclerosis. *Ann Neurol* 65 Suppl 1**,** S3-9.

Ruschel, J., Hellal, F., Flynn, K.C., Dupraz, S., Elliott, D.A., Tedeschi, A., Bates, M., Sliwinski, C., Brook, G., Dobrindt, K., Peitz, M., Brustle, O., Norenberg, M.D., Blesch, A., Weidner, N., Bunge, M.B., Bixby, J.L., and Bradke, F. (2015). Axonal regeneration. Systemic administration of epothilone B promotes axon regeneration after spinal cord injury. *Science* 348**,** 347-352.

Rustici, G., Kolesnikov, N., Brandizi, M., Burdett, T., Dylag, M., Emam, I., Farne, A., Hastings, E., Ison, J., Keays, M., Kurbatova, N., Malone, J., Mani, R., Mupo, A., Pedro Pereira, R., Pilicheva, E., Rung, J., Sharma, A., Tang, Y.A., Ternent, T., Tikhonov, A., Welter, D., Williams, E., Brazma, A., Parkinson, H., and Sarkans, U. (2013). ArrayExpress update--trends in database growth and links to data analysis tools. *Nucleic Acids Res* 41**,** D987-990.

Sahlgren, C.M., Mikhailov, A., Vaittinen, S., Pallari, H.M., Kalimo, H., Pant, H.C., and Eriksson, J.E. (2003). Cdk5 regulates the organization of Nestin and its association with p35. *Mol Cell Biol* 23**,** 5090-5106.

Sakakibara, A., Ando, R., Sapir, T., and Tanaka, T. (2013). Microtubule dynamics in neuronal morphogenesis. *Open Biol* 3**,** 130061.

Sakuma, K., and Yamaguchi, A. (2011). The recent understanding of the neurotrophin's role in skeletal muscle adaptation. *J Biomed Biotechnol* 2011**,** 201696.

Sandrock, A.W., Jr., Dryer, S.E., Rosen, K.M., Gozani, S.N., Kramer, R., Theill, L.E., and Fischbach, G.D. (1997). Maintenance of acetylcholine receptor number by neuregulins at the neuromuscular junction in vivo. *Science* 276**,** 599-603.

Sanes, J.R., and Lichtman, J.W. (1999). Development of the vertebrate neuromuscular junction. *Ann Rev Neurosci* 22**,** 389-442.

Sanes, J.R., Marshall, L.M., and Mcmahan, U.J. (1978). Reinnervation of muscle fiber basal lamina after removal of myofibers. Differentiation of regenerating axons at original synaptic sites. *J Cell Biol* 78**,** 176-198.

Santos, A.F., and Caroni, P. (2003). Assembly, plasticity and selective vulnerability to disease of mouse neuromuscular junctions. *J Neurocytol* 32**,** 849-862.

Sasaki, S., and Iwata, M. (1996). Impairment of fast axonal transport in the proximal axons of anterior horn neurons in amyotrophic lateral sclerosis. *Neurology* 47**,** 535-540.

Sasaki, S., Warita, H., Abe, K., and Iwata, M. (2004). Slow component of axonal transport is impaired in the proximal axon of transgenic mice with a G93A mutant SOD1 gene. *Acta Neuropathol* 107**,** 452-460.

Saxena, S., and Caroni, P. (2007). Mechanisms of axon degeneration: from development to disease. *Prog Neurobiol* 83**,** 174-191.

Sayas, C.L., Tortosa, E., Bollati, F., Ramirez-Rios, S., Arnal, I., and Avila, J. (2015). Tau regulates the localization and function of End-binding proteins 1 and 3 in developing neuronal cells. *J Neurochem* 133**,** 653-667.

Schaefer, A.M., Sanes, J.R., and Lichtman, J.W. (2005). A compensatory subpopulation of motor neurons in a mouse model of amyotrophic lateral sclerosis. *J Comp Neurol* 490**,** 209-219.

Schafer, D.P., Lehrman, E.K., Kautzman, A.G., Koyama, R., Mardinly, A.R., Yamasaki, R., Ransohoff, R.M., Greenberg, M.E., Barres, B.A., and Stevens, B. (2012). Microglia sculpt postnatal neural circuits in an activity and complement-dependent manner. *Neuron* 74**,** 691-705.

Schafer, D.P., and Stevens, B. (2013). Phagocytic glial cells: sculpting synaptic circuits in the developing nervous system. *Curr Opin Neurobiol* 23**,** 1034-1040.

Schafer, S., and Hermans, E. (2011). Reassessment of motor-behavioural test analyses enables the detection of early disease-onset in a transgenic mouse model of amyotrophic lateral sclerosis. *Behavioural brain research* 225**,** 7-14.

Schiff, P.B., Fant, J., and Horwitz, S.B. (1979). Promotion of microtubule assembly in vitro by taxol. *Nature* 277**,** 665-667.

Schneider, C.A., Rasband, W.S., and Eliceiri, K.W. (2012). NIH Image to ImageJ: 25 years of image analysis. *Nat Methods* 9**,** 671-675.

Scott, S., Kranz, J.E., Cole, J., Lincecum, J.M., Thompson, K., Kelly, N., Bostrom, A., Theodoss, J., Al-Nakhala, B.M., Vieira, F.G., Ramasubbu, J., and Heywood, J.A. (2008). Design, power, and interpretation of studies in the standard murine model of ALS. *Amyotroph Lateral Scler* 9**,** 4-15.

Seilhean, D., Cazeneuve, C., Thuries, V., Russaouen, O., Millecamps, S., Salachas, F., Meininger, V., Leguern, E., and Duyckaerts, C. (2009). Accumulation of TDP-43 and alpha-actin in an amyotrophic lateral sclerosis patient with the K17I ANG mutation. *Acta Neuropathol* 118**,** 561-573.

Shalom, O., Shalva, N., Altschuler, Y., and Motro, B. (2008). The mammalian Nek1 kinase is involved in primary cilium formation. *FEBS Lett* 582**,** 1465-1470.

Shemesh, O.A., and Spira, M.E. (2010). Paclitaxel induces axonal microtubules polar reconfiguration and impaired organelle transport: implications for the pathogenesis of paclitaxel-induced polyneuropathy. *Acta Neuropathol* 119**,** 235-248.

Shemesh, O.A., and Spira, M.E. (2011). Rescue of neurons from undergoing hallmark tau-induced Alzheimer's disease cell pathologies by the antimitotic drug paclitaxel. *Neurobiol Dis* 43**,** 163-175.

Shepheard, S.R., Chataway, T., Schultz, D.W., Rush, R.A., and Rogers, M.L. (2014). The extracellular domain of neurotrophin receptor p75 as a candidate biomarker for amyotrophic lateral sclerosis. *PLoS One* 9**,** e87398.

Shi, L., Fu, A.K., and Ip, N.Y. (2012). Molecular mechanisms underlying maturation and maintenance of the vertebrate neuromuscular junction. *Trends Neurosci* 35**,** 441-453.

Shi, Y., Ivannikov, M.V., Walsh, M.E., Liu, Y., Zhang, Y., Jaramillo, C.A., Macleod, G.T., and Van Remmen, H. (2014). The lack of CuZnSOD leads to impaired neurotransmitter release, neuromuscular junction destabilization and reduced muscle strength in mice. *PLoS One* 9**,** e100834.

Shiao, T., Fond, A., Deng, B., Wehling-Henricks, M., Adams, M.E., Froehner, S.C., and Tidball, J.G. (2004). Defects in neuromuscular junction structure in dystrophic muscle are corrected by expression of a NOS transgene in dystrophin-deficient muscles, but not in muscles lacking alpha- and beta1-syntrophins. *Hum Mol Genet* 13**,** 1873-1884.

Shibata, N., Hirano, A., Kobayashi, M., Sasaki, S., Kato, T., Matsumoto, S., Shiozawa, Z., Komori, T., Ikemoto, A., Umahara, T., and Et Al. (1994). Cu/Zn superoxide dismutase-like immunoreactivity in Lewy body-like inclusions of sporadic amyotrophic lateral sclerosis. *Neurosci Lett* 179**,** 149-152.

Shibata, N., Hirano, A., Kobayashi, M., Siddique, T., Deng, H.X., Hung, W.Y., Kato, T., and Asayama, K. (1996). Intense superoxide dismutase-1 immunoreactivity in intracytoplasmic hyaline inclusions of familial amyotrophic lateral sclerosis with posterior column involvement. *J Neuropathol Exp Neurol* 55**,** 481-490.

Slaughter, T., and Black, M.M. (2003). STOP (stable-tubule-only-polypeptide) is preferentially associated with the stable domain of axonal microtubules. *J Neurocytol* 32**,** 399-413.

Smith, B.N., Ticozzi, N., Fallini, C., Gkazi, A.S., Topp, S., Kenna, K.P., Scotter, E.L., Kost, J., Keagle, P., Miller, J.W., Calini, D., Vance, C., Danielson, E.W., Troakes, C., Tiloca, C., Al-Sarraj, S., Lewis, E.A., King, A., Colombrita, C., Pensato, V., Castellotti, B., De Belleroche, J., Baas, F., Ten Asbroek, A.L., Sapp, P.C., Mckenna-Yasek, D., Mclaughlin, R.L., Polak, M., Asress, S., Esteban-Perez, J., Munoz-Blanco, J.L., Simpson, M., Consortium, S., Van Rheenen, W., Diekstra, F.P., Lauria, G., Duga, S., Corti, S., Cereda, C., Corrado, L., Soraru, G., Morrison, K.E., Williams, K.L., Nicholson, G.A., Blair, I.P., Dion, P.A., Leblond, C.S., Rouleau, G.A., Hardiman, O., Veldink, J.H., Van Den Berg, L.H., Al-Chalabi, A., Pall, H., Shaw, P.J., Turner, M.R., Talbot, K., Taroni, F., Garcia-Redondo, A., Wu, Z., Glass, J.D., Gellera, C., Ratti, A., Brown, R.H., Jr., Silani, V., Shaw, C.E., and Landers, J.E. (2014). Exome-wide rare variant analysis identifies TUBA4A mutations associated with familial ALS. *Neuron* 84**,** 324-331.

Snider, N.T., and Omary, M.B. (2014). Post-translational modifications of intermediate filament proteins: mechanisms and functions. *Nat Rev Mol Cell Biol* 15**,** 163-177.

Sofola, O.A., Jin, P., Qin, Y., Duan, R., Liu, H., De Haro, M., Nelson, D.L., and Botas, J. (2007). RNA-binding proteins hnRNP A2/B1 and CUGBP1 suppress fragile X CGG premutation repeat-induced neurodegeneration in a Drosophila model of FXTAS. *Neuron* 55**,** 565-571.

Sotelo-Silveira, J.R., Lepanto, P., Elizondo, V., Horjales, S., Palacios, F., Martinez-Palma, L., Marin, M., Beckman, J.S., and Barbeito, L. (2009). Axonal mitochondrial clusters containing mutant SOD1 in transgenic models of ALS. *Antioxid Redox Signal* 11**,** 1535-1545.

Sreedharan, J., Blair, I.P., Tripathi, V.B., Hu, X., Vance, C., Rogelj, B., Ackerley, S., Durnall, J.C., Williams, K.L., Buratti, E., Baralle, F., De Belleroche, J., Mitchell, J.D., Leigh, P.N., Al-Chalabi, A., Miller, C.C., Nicholson, G., and Shaw, C.E. (2008). TDP-43 mutations in familial and sporadic amyotrophic lateral sclerosis. *Science* 319**,** 1668-1672.

St John, P.A., and Gordon, H. (2001). Agonists cause endocytosis of nicotinic acetylcholine receptors on cultured myotubes. *J Neurobiol* 49**,** 212-223.

Stallings, N.R., Puttaparthi, K., Luther, C.M., Burns, D.K., and Elliott, J.L. (2010). Progressive motor weakness in transgenic mice expressing human TDP-43. *Neurobiol Dis* 40**,** 404-414.

Stancu, I.C., Vasconcelos, B., Terwel, D., and Dewachter, I. (2014). Models of beta-amyloid induced Tau-pathology: the long and "folded" road to understand the mechanism. *Mol Neurodegener* 9**,** 51.

Strom, A.L., Gal, J., Shi, P., Kasarskis, E.J., Hayward, L.J., and Zhu, H. (2008). Retrograde axonal transport and motor neuron disease. *J Neurochem* 106**,** 495-505.

Strong, M.J. (2010). The evidence for altered RNA metabolism in amyotrophic lateral sclerosis (ALS). *J Neurol Sci* 288**,** 1-12.

Swinnen, B., and Robberecht, W. (2014). The phenotypic variability of amyotrophic lateral sclerosis. *Nat Rev Neurol* 10**,** 661-670.

Taes, I., Timmers, M., Hersmus, N., Bento-Abreu, A., Van Den Bosch, L., Van Damme, P., Auwerx, J., and Robberecht, W. (2013). Hdac6 deletion delays disease progression in the SOD1G93A mouse model of ALS. *Hum Mol Genet* 22**,** 1783-1790.

Taetzsch, T., Tenga, M.J., and Valdez, G. (2017). Muscle Fibers Secrete FGFBP1 to Slow Degeneration of Neuromuscular Synapses during Aging and Progression of ALS. *J Neurosci* 37**,** 70-82.

Tahara, E.B., Navarete, F.D., and Kowaltowski, A.J. (2009). Tissue-, substrate-, and site-specific characteristics of mitochondrial reactive oxygen species generation. *Free Radic Biol Med* 46**,** 1283-1297.

Takahashi, K., Rochford, C.D., and Neumann, H. (2005). Clearance of apoptotic neurons without inflammation by microglial triggering receptor expressed on myeloid cells-2. *J Exp Med* 201**,** 647-657.

Takalo, M., Salminen, A., Soininen, H., Hiltunen, M., and Haapasalo, A. (2013). Protein aggregation and degradation mechanisms in neurodegenerative diseases. *Am J Neurodegener Dis* 2**,** 1-14.

Tallon, C., Russell, K.A., Sakhalkar, S., Andrapallayal, N., and Farah, M.H. (2016). Length-dependent axo-terminal degeneration at the neuromuscular synapses of type II muscle in SOD1 mice. *Neuroscience* 312**,** 179-189.

Tateno, M., Kato, S., Sakurai, T., Nukina, N., Takahashi, R., and Araki, T. (2009). Mutant SOD1 impairs axonal transport of choline acetyltransferase and acetylcholine release by sequestering KAP3. *Hum Mol Genet* 18**,** 942-955.

Teng, F.Y., and Tang, B.L. (2008). Nogo-A and Nogo-66 receptor in amyotrophic lateral sclerosis. *J Cell Mol Med* 12**,** 1199-1204.

Tessier-Lavigne, M., and Goodman, C.S. (1996). The molecular biology of axon guidance. *Science* 274**,** 1123-1133.

Thompson, A.G., Gray, E., Heman-Ackah, S.M., Mager, I., Talbot, K., Andaloussi, S.E., Wood, M.J., and Turner, M.R. (2016). Extracellular vesicles in neurodegenerative disease - pathogenesis to biomarkers. *Nat Rev Neurol* 12**,** 346-357.

Thrash, J.C., Torbett, B.E., and Carson, M.J. (2009). Developmental regulation of TREM2 and DAP12 expression in the murine CNS: implications for Nasu-Hakola disease. *Neurochem Res* 34**,** 38-45.

Ticozzi, N., Ratti, A., and Silani, V. (2010). Protein aggregation and defective RNA metabolism as mechanisms for motor neuron damage. *CNS Neurol Disord Drug Targets* 9**,** 285-296.

Ticozzi, N., Tiloca, C., Morelli, C., Colombrita, C., Poletti, B., Doretti, A., Maderna, L., Messina, S., Ratti, A., and Silani, V. (2011). Genetics of familial Amyotrophic lateral sclerosis. *Arch Ital Biol* 149**,** 65-82.

Tischfield, M.A., Cederquist, G.Y., Gupta, M.L., Jr., and Engle, E.C. (2011). Phenotypic spectrum of the tubulin-related disorders and functional implications of disease-causing mutations. *Curr Opin Genet Dev* 21**,** 286-294.

Tischfield, M.A., and Engle, E.C. (2010). Distinct alpha- and beta-tubulin isotypes are required for the positioning, differentiation and survival of neurons: new support for the 'multi-tubulin' hypothesis. *Biosci Rep* 30**,** 319-330.

Todd, T.W., and Petrucelli, L. (2016). Insights into the pathogenic mechanisms of Chromosome 9 open reading frame 72 (C9orf72) repeat expansions. *J Neurochem*.

Tollervey, J.R., Curk, T., Rogelj, B., Briese, M., Cereda, M., Kayikci, M., Konig, J., Hortobagyi, T., Nishimura, A.L., Zupunski, V., Patani, R., Chandran, S., Rot, G., Zupan, B., Shaw, C.E., and Ule, J. (2011). Characterizing the RNA targets and position-dependent splicing regulation by TDP-43. *Nat Neurosci* 14**,** 452-458.

Tong, J., Huang, C., Bi, F., Wu, Q., Huang, B., Liu, X., Li, F., Zhou, H., and Xia, X.G. (2013). Expression of ALS-linked TDP-43 mutant in astrocytes causes non-cell-autonomous motor neuron death in rats. *EMBO J* 32**,** 1917-1926.

Tortosa, E., Galjart, N., Avila, J., and Sayas, C.L. (2013). MAP1B regulates microtubule dynamics by sequestering EB1/3 in the cytosol of developing neuronal cells. *EMBO J* 32**,** 1293-1306.

Towne, C., Raoul, C., Schneider, B.L., and Aebischer, P. (2008). Systemic AAV6 delivery mediating RNA interference against SOD1: neuromuscular transduction does not alter disease progression in fALS mice. *Mol Ther* 16**,** 1018-1025.

Trinczek, B., Ebneth, A., Mandelkow, E.M., and Mandelkow, E. (1999). Tau regulates the attachment/detachment but not the speed of motors in microtubule-dependent transport of single vesicles and organelles. *J Cell Sci* 112 (Pt 14)**,** 2355-2367.

Tsang, Y.M., Chiong, F., Kuznetsov, D., Kasarskis, E., and Geula, C. (2000). Motor neurons are rich in non-phosphorylated neurofilaments: cross-species comparison and alterations in ALS. *Brain Res* 861**,** 45-58.

Tudor, E.L., Perkinton, M.S., Schmidt, A., Ackerley, S., Brownlees, J., Jacobsen, N.J., Byers, H.L., Ward, M., Hall, A., Leigh, P.N., Shaw, C.E., Mcloughlin, D.M., and Miller, C.C. (2005). ALS2/Alsin regulates Rac-PAK signaling and neurite outgrowth. *J Biol Chem* 280**,** 34735-34740.

Turner, B.J., and Talbot, K. (2008). Transgenics, toxicity and therapeutics in rodent models of mutant SOD1-mediated familial ALS. *Prog Neurobiol* 85**,** 94-134.

Turner, M.R., Hardiman, O., Benatar, M., Brooks, B.R., Chio, A., De Carvalho, M., Ince, P.G., Lin, C., Miller, R.G., Mitsumoto, H., Nicholson, G., Ravits, J., Shaw, P.J., Swash, M., Talbot, K., Traynor, B.J., Van Den Berg, L.H., Veldink, J.H., Vucic, S., and Kiernan, M.C. (2013). Controversies and priorities in amyotrophic lateral sclerosis. *Lancet Neurol* 12**,** 310-322.

Turner, M.R., and Swash, M. (2015). The expanding syndrome of amyotrophic lateral sclerosis: a clinical and molecular odyssey. *J Neurol Neurosurg Psychiatry* 86**,** 667-673.

Umemori, H., and Sanes, J.R. (2008). Signal regulatory proteins (SIRPS) are secreted presynaptic organizing molecules. *J Biol Chem* 283**,** 34053-34061.

Vadlamudi, R.K., Barnes, C.J., Rayala, S., Li, F., Balasenthil, S., Marcus, S., Goodson, H.V., Sahin, A.A., and Kumar, R. (2005). p21-activated kinase 1 regulates microtubule dynamics by phosphorylating tubulin cofactor B. *Mol Cell Biol* 25**,** 3726-3736.

Vaittinen, S., Lukka, R., Sahlgren, C., Rantanen, J., Hurme, T., Lendahl, U., Eriksson, J.E., and Kalimo, H. (1999). Specific and innervation-regulated expression of the intermediate filament protein nestin at neuromuscular and myotendinous junctions in skeletal muscle. *Am J Path* 154**,** 591.

Valdez, G., Tapia, J.C., Kang, H., Clemenson, G.D., Jr., Gage, F.H., Lichtman, J.W., and Sanes, J.R. (2010). Attenuation of age-related changes in mouse neuromuscular synapses by caloric restriction and exercise. *Proc Natl Acad Sci U S A* 107**,** 14863-14868.

Van Beuningen, S.F., Will, L., Harterink, M., Chazeau, A., Van Battum, E.Y., Frias, C.P., Franker, M.A., Katrukha, E.A., Stucchi, R., Vocking, K., Antunes, A.T., Slenders, L., Doulkeridou, S., Sillevis Smitt, P., Altelaar, A.F., Post, J.A., Akhmanova, A., Pasterkamp, R.J., Kapitein, L.C., De Graaff, E., and Hoogenraad, C.C. (2015). TRIM46 Controls Neuronal Polarity and Axon Specification by Driving the Formation of Parallel Microtubule Arrays. *Neuron* 88**,** 1208-1226.

Van Damme, P., Bogaert, E., Dewil, M., Hersmus, N., Kiraly, D., Scheveneels, W., Bockx, I., Braeken, D., Verpoorten, N., Verhoeven, K., Timmerman, V., Herijgers, P., Callewaert, G., Carmeliet, P., Van Den Bosch, L., and Robberecht, W. (2007). Astrocytes regulate GluR2 expression in motor neurons and their vulnerability to excitotoxicity. *Proc Natl Acad Sci U S A* 104**,** 14825-14830.

Van Damme, P., Dewil, M., Robberecht, W., and Van Den Bosch, L. (2005). Excitotoxicity and amyotrophic lateral sclerosis. *Neurodegener Dis* 2**,** 147-159.

Vance, C., Rogelj, B., Hortobagyi, T., De Vos, K.J., Nishimura, A.L., Sreedharan, J., Hu, X., Smith, B., Ruddy, D., Wright, P., Ganesalingam, J., Williams, K.L., Tripathi, V., Al-Saraj, S., Al-Chalabi, A., Leigh, P.N., Blair, I.P., Nicholson, G., De Belleroche, J., Gallo, J.M., Miller, C.C., and Shaw, C.E. (2009). Mutations in FUS, an RNA processing protein, cause familial amyotrophic lateral sclerosis type 6. *Science* 323**,** 1208-1211.

Veldink, J.H., Bar, P.R., Joosten, E.A., Otten, M., Wokke, J.H., and Van Den Berg, L.H. (2003). Sexual differences in onset of disease and response to exercise in a transgenic model of ALS. *Neuromuscul Disord* 13**,** 737-743.

Vickers, J.C., King, A.E., Woodhouse, A., Kirkcaldie, M.T., Staal, J.A., Mccormack, G.H., Blizzard, C.A., Musgrove, R.E., Mitew, S., Liu, Y., Chuckowree, J.A., Bibari, O., and Dickson, T.C. (2009). Axonopathy and cytoskeletal disruption in degenerative diseases of the central nervous system. *Brain Res Bull* 80**,** 217-223.

Volle, J., Brocard, J., Saoud, M., Gory-Faure, S., Brunelin, J., Andrieux, A., and Suaud-Chagny, M.F. (2013). Reduced expression of STOP/MAP6 in mice leads to cognitive deficits. *Schizophr Bull* 39**,** 969-978.

Vucic, S., Lin, C.S., Cheah, B.C., Murray, J., Menon, P., Krishnan, A.V., and Kiernan, M.C. (2013). Riluzole exerts central and peripheral modulating effects in amyotrophic lateral sclerosis. *Brain* 136**,** 1361-1370.

Vucic, S., Nicholson, G.A., and Kiernan, M.C. (2008). Cortical hyperexcitability may precede the onset of familial amyotrophic lateral sclerosis. *Brain* 131**,** 1540-1550.

Waibel, S., Reuter, A., Malessa, S., Blaugrund, E., and Ludolph, A.C. (2004). Rasagiline alone and in combination with riluzole prolongs survival in an ALS mouse model. *J Neurol* 251**,** 1080-1084.

Wang, J.T., Medress, Z.A., and Barres, B.A. (2012). Axon degeneration: molecular mechanisms of a self-destruction pathway. *J Cell Biol* 196**,** 7-18.

Wang, W., Jin, K., Mao, X.O., Close, N., Greenberg, D.A., and Xiong, Z.G. (2008). Electrophysiological properties of mouse cortical neuron progenitors differentiated in vitro and in vivo. *Int J Clin Exp Med* 1**,** 145-153.

Wang, X., and Schwarz, T.L. (2009). The mechanism of Ca2+ -dependent regulation of kinesin-mediated mitochondrial motility. *Cell* 136**,** 163-174.

Warita, H., Itoyama, Y., and Abe, K. (1999). Selective impairment of fast anterograde axonal transport in the peripheral nerves of asymptomatic transgenic mice with a G93A mutant SOD1 gene. *Brain research* 819**,** 120-131.

Watson, C., Paxinos, G., and Kayalioglu, G. (2009). *The Spinal Cord: A Christopher and Dana Reeve Foundation Text and Atlas*. Netherlands: Elsevier/Academic Press.

Watts, R.J., Hoopfer, E.D., and Luo, L. (2003). Axon pruning during Drosophila metamorphosis: evidence for local degeneration and requirement of the ubiquitin-proteasome system. *Neuron* 38**,** 871-885.

Weber, U.J., Bock, T., Buschard, K., and Pakkenberg, B. (1997). Total number and size distribution of motor neurons in the spinal cord of normal and EMC-virus infected mice--a stereological study. *J Anat* 191 (Pt 3)**,** 347-353.

Wen, Y., Eng, C.H., Schmoranzer, J., Cabrera-Poch, N., Morris, E.J., Chen, M., Wallar, B.J., Alberts, A.S., and Gundersen, G.G. (2004). EB1 and APC bind to mDia to stabilize microtubules downstream of Rho and promote cell migration. *Nat Cell Biol* 6**,** 820-830.

Weydt, P., Hong, S.Y., Kliot, M., and Moller, T. (2003). Assessing disease onset and progression in the SOD1 mouse model of ALS. *Neuroreport* 14**,** 1051-1054.

Williams, A.H., Valdez, G., Moresi, V., Qi, X., Mcanally, J., Elliott, J.L., Bassel-Duby, R., Sanes, J.R., and Olson, E.N. (2009). MicroRNA-206 delays ALS progression and promotes regeneration of neuromuscular synapses in mice. *Science* 326**,** 1549-1554.

Williamson, T.L., and Cleveland, D.W. (1999). Slowing of axonal transport is a very early event in the toxicity of ALS-linked SOD1 mutants to motor neurons. *Nat Neurosci* 2**,** 50-56.

Wilson, C., and Gonzalez-Billault, C. (2015). Regulation of cytoskeletal dynamics by redox signaling and oxidative stress: implications for neuronal development and trafficking. *Front Cell Neurosci* 9**,** 381.

Wishart, T.M., Parson, S.H., and Gillingwater, T.H. (2006). Synaptic vulnerability in neurodegenerative disease. *J Neuropathol Exp Neurol* 65**,** 733-739.

Wojnacki, J., Quassollo, G., Marzolo, M.P., and Caceres, A. (2014). Rho GTPases at the crossroad of signaling networks in mammals: impact of Rho-GTPases on microtubule organization and dynamics. *Small GTPases* 5**,** e28430.

Wong, F., Fan, L., Wells, S., Hartley, R., Mackenzie, F.E., Oyebode, O., Brown, R., Thomson, D., Coleman, M.P., Blanco, G., and Ribchester, R.R. (2009). Axonal and neuromuscular synaptic phenotypes in Wld(S), SOD1(G93A) and ostes mutant mice identified by fiber-optic confocal microendoscopy. *Mol Cell Neurosci* 42**,** 296-307.

Wong, M., and Martin, L.J. (2010). Skeletal muscle-restricted expression of human SOD1 causes motor neuron degeneration in transgenic mice. *Human Molecular Genetics* 19**,** 2284-2302.

Wong, N.K., He, B.P., and Strong, M.J. (2000). Characterization of neuronal intermediate filament protein expression in cervical spinal motor neurons in sporadic amyotrophic lateral sclerosis (ALS). *Journal of neuropathology and experimental neurology* 59**,** 972-982.

Wood-Allum, C., and Shaw, P.J. (2010). Motor neurone disease: a practical update on diagnosis and management. *Clin Med* 10**,** 252-258.

Wooley, C.M., Sher, R.B., Kale, A., Frankel, W.N., Cox, G.A., and Seburn, K.L. (2005). Gait analysis detects early changes in transgenic SOD1(G93A) mice. *Muscle Nerve* 32**,** 43-50.

Wu, C.H., Fallini, C., Ticozzi, N., Keagle, P.J., Sapp, P.C., Piotrowska, K., Lowe, P., Koppers, M., Mckenna-Yasek, D., Baron, D.M., Kost, J.E., Gonzalez-Perez, P., Fox, A.D., Adams, J., Taroni, F., Tiloca, C., Leclerc, A.L., Chafe, S.C., Mangroo, D., Moore, M.J., Zitzewitz, J.A., Xu, Z.S., Van Den Berg, L.H., Glass, J.D., Siciliano, G., Cirulli, E.T., Goldstein, D.B., Salachas, F., Meininger, V., Rossoll, W., Ratti, A., Gellera, C., Bosco, D.A., Bassell, G.J., Silani, V., Drory, V.E., Brown, R.H., Jr., and Landers, J.E. (2012). Mutations in the profilin 1 gene cause familial amyotrophic lateral sclerosis. *Nature* 488**,** 499-503.

Wyatt, R.M., and Balice-Gordon, R.J. (2003). Activity-dependent elimination of neuromuscular synapses. *J Neurocytol* 32**,** 777-794.
Yadav, P., Selvaraj, B.T., Bender, F.L., Behringer, M., Moradi, M., Sivadasan, R., Dombert, B., Blum, R., Asan, E., Sauer, M., Julien, J.P., and Sendtner, M. (2016). Neurofilament depletion improves microtubule dynamics via modulation of Stat3/stathmin signaling. *Acta Neuropathol* 132**,** 93-110.
Yamanaka, K., Chun, S.J., Boillee, S., Fujimori-Tonou, N., Yamashita, H., Gutmann, D.H., Takahashi, R., Misawa, H., and Cleveland, D.W. (2008). Astrocytes as determinants of disease progression in inherited amyotrophic lateral sclerosis. *Nat Neurosci* 11**,** 251-253.
Yamanaka, K., Miller, T.M., Mcalonis-Downes, M., Chun, S.J., and Cleveland, D.W. (2006). Progressive spinal axonal degeneration and slowness in ALS2-deficient mice. *Ann Neurol* 60**,** 95-104.
Yan, J., Deng, H.X., Siddique, N., Fecto, F., Chen, W., Yang, Y., Liu, E., Donkervoort, S., Zheng, J.G., Shi, Y., Ahmeti, K.B., Brooks, B., Engel, W.K., and Siddique, T. (2010). Frameshift and novel mutations in FUS in familial amyotrophic lateral sclerosis and ALS/dementia. *Neurology* 75**,** 807-814.
Yan, Y., and Broadie, K. (2007). In vivo assay of presynaptic microtubule cytoskeleton dynamics in Drosophila. *J Neurosci Methods* 162**,** 198-205.
Yang, F., Jiang, Q., Zhao, J., Ren, Y., Sutton, M.D., and Feng, J. (2005). Parkin stabilizes microtubules through strong binding mediated by three independent domains. *J Biol Chem* 280**,** 17154-17162.
Yang, J., Dominguez, B., De Winter, F., Gould, T.W., Eriksson, J.E., and Lee, K.-F. (2011). Nestin negatively regulates postsynaptic differentiation of the neuromuscular synapse. *Nature neuroscience* 14**,** 1-8.
Yang, X., Arber, S., William, C., Li, L., Tanabe, Y., Jessell, T.M., Birchmeier, C., and Burden, S.J. (2001). Patterning of muscle acetylcholine receptor gene expression in the absence of motor innervation. *Neuron* 30**,** 399-410.
Yang, Y., Gozen, O., Watkins, A., Lorenzini, I., Lepore, A., Gao, Y., Vidensky, S., Brennan, J., Poulsen, D., Won Park, J., Li Jeon, N., Robinson, M.B., and Rothstein, J.D. (2009). Presynaptic regulation of astroglial excitatory neurotransmitter transporter GLT1. *Neuron* 61**,** 880-894.
Yaron, A., and Schuldiner, O. (2016). Common and Divergent Mechanisms in Developmental Neuronal Remodeling and Dying Back Neurodegeneration. *Curr Biol* 26**,** R628-639.
Yau, K.W., Schatzle, P., Tortosa, E., Pages, S., Holtmaat, A., Kapitein, L.C., and Hoogenraad, C.C. (2016). Dendrites In Vitro and In Vivo Contain Microtubules of Opposite Polarity and Axon Formation Correlates with Uniform Plus-End-Out Microtubule Orientation. *J Neurosci* 36**,** 1071-1085.
Ye, K., Ke, Y., Keshava, N., Shanks, J., Kapp, J.A., Tekmal, R.R., Petros, J., and Joshi, H.C. (1998). Opium alkaloid noscapine is an antitumor agent that arrests metaphase and induces apoptosis in dividing cells. *Proc Natl Acad Sci U S A* 95**,** 1601-1606.
Yrjanheikki, J., Tikka, T., Keinanen, R., Goldsteins, G., Chan, P.H., and Koistinaho, J. (1999). A tetracycline derivative, minocycline, reduces inflammation and protects against focal cerebral ischemia with a wide therapeutic window. *Proc Natl Acad Sci U S A* 96**,** 13496-13500.
Yumoto, N., Kim, N., and Burden, S.J. (2012). Lrp4 is a retrograde signal for presynaptic differentiation at neuromuscular synapses. *Nature* 489**,** 438-442.
Zagami, C.J., Beart, P.M., Wallis, N., Nagley, P., and O'shea, R.D. (2009). Oxidative and excitotoxic insults exert differential effects on spinal motoneurons and astrocytic

glutamate transporters: Implications for the role of astrogliosis in amyotrophic lateral sclerosis. *Glia* 57**,** 119-135.

Zagouri, F., Sergentanis, T.N., Chrysikos, D., Dimopoulos, M.A., and Bamias, A. (2015). Epothilones in epithelial ovarian, fallopian tube, or primary peritoneal cancer: a systematic review. *Onco Targets Ther* 8**,** 2187-2198.

Zakaryan, R.P., and Gehring, H. (2006). Identification and characterization of the nuclear localization/retention signal in the EWS proto-oncoprotein. *J Mol Biol* 363**,** 27-38.

Zhai, Q., Wang, J., Kim, A., Liu, Q., Watts, R., Hoopfer, E., Mitchison, T., Luo, L., and He, Z. (2003). Involvement of the ubiquitin-proteasome system in the early stages of wallerian degeneration. *Neuron* 39**,** 217-225.

Zhang, B., Carroll, J., Trojanowski, J.Q., Yao, Y., Iba, M., Potuzak, J.S., Hogan, A.M., Xie, S.X., Ballatore, C., Smith, A.B., 3rd, Lee, V.M., and Brunden, K.R. (2012). The microtubule-stabilizing agent, epothilone D, reduces axonal dysfunction, neurotoxicity, cognitive deficits, and Alzheimer-like pathology in an interventional study with aged tau transgenic mice. *J Neurosci* 32**,** 3601-3611.

Zhang, B., Luo, S., Dong, X.P., Zhang, X., Liu, C., Luo, Z., Xiong, W.C., and Mei, L. (2007a). Beta-catenin regulates acetylcholine receptor clustering in muscle cells through interaction with rapsyn. *J Neurosci* 27**,** 3968-3973.

Zhang, B., Luo, S., Wang, Q., Suzuki, T., Xiong, W.C., and Mei, L. (2008a). LRP4 serves as a coreceptor of agrin. *Neuron* 60**,** 285-297.

Zhang, B., Maiti, A., Shively, S., Lakhani, F., Mcdonald-Jones, G., Bruce, J., Lee, E.B., Xie, S.X., Joyce, S., Li, C., Toleikis, P.M., Lee, V.M., and Trojanowski, J.Q. (2005). Microtubule-binding drugs offset tau sequestration by stabilizing microtubules and reversing fast axonal transport deficits in a tauopathy model. *Proc Natl Acad Sci U S A* 102**,** 227-231.

Zhang, F., Strom, A.L., Fukada, K., Lee, S., Hayward, L.J., and Zhu, H. (2007b). Interaction between familial amyotrophic lateral sclerosis (ALS)-linked SOD1 mutants and the dynein complex. *J Biol Chem* 282**,** 16691-16699.

Zhang, H., Tan, C.F., Mori, F., Tanji, K., Kakita, A., Takahashi, H., and Wakabayashi, K. (2008b). TDP-43-immunoreactive neuronal and glial inclusions in the neostriatum in amyotrophic lateral sclerosis with and without dementia. *Acta Neuropathol* 115**,** 115-122.

Zhang, Y.J., Xu, Y.F., Cook, C., Gendron, T.F., Roettges, P., Link, C.D., Lin, W.L., Tong, J., Castanedes-Casey, M., Ash, P., Gass, J., Rangachari, V., Buratti, E., Baralle, F., Golde, T.E., Dickson, D.W., and Petrucelli, L. (2009). Aberrant cleavage of TDP-43 enhances aggregation and cellular toxicity. *Proc Natl Acad Sci U S A* 106**,** 7607-7612.

Zhou, J., and Giannakakou, P. (2005). Targeting microtubules for cancer chemotherapy. *Curr Med Chem Anticancer Agents* 5**,** 65-71.

Zhou, J., Panda, D., Landen, J.W., Wilson, L., and Joshi, H.C. (2002). Minor alteration of microtubule dynamics causes loss of tension across kinetochore pairs and activates the spindle checkpoint. *J Biol Chem* 277**,** 17200-17208.

Zhu, H., Bhattacharyya, B.J., Lin, H., and Gomez, C.M. (2011). Skeletal muscle IP3R1 receptors amplify physiological and pathological synaptic calcium signals. *J Neurosci* 31**,** 15269-15283.

Zhu, S., Stavrovskaya, I.G., Drozda, M., Kim, B.Y., Ona, V., Li, M., Sarang, S., Liu, A.S., Hartley, D.M., Wu, D.C., Gullans, S., Ferrante, R.J., Przedborski, S., Kristal, B.S., and Friedlander, R.M. (2002). Minocycline inhibits cytochrome c release and delays progression of amyotrophic lateral sclerosis in mice. *Nature* 417**,** 74-78.

Zuber, B., and Unwin, N. (2013). Structure and superorganization of acetylcholine receptor-rapsyn complexes. *Proc Natl Acad Sci U S A* 110**,** 10622-10627.

Zwiegers, P., Lee, G., and Shaw, C.A. (2014). Reduction in hSOD1 copy number significantly impacts ALS phenotype presentation in G37R (line 29) mice: implications for the assessment of putative therapeutic agents. *J Negat Results Biomed* 13**,** 14.
Zyss, D., Ebrahimi, H., and Gergely, F. (2011). Casein kinase I delta controls centrosome positioning during T cell activation. *J Cell Biol* 195**,** 781-797.

8 Appendix

8.1 Commonly used Solutions

0.01 M Phostohate buffered saline (PBS), pH 7.4 – makes 1L

- 2mM $NaH_2PO_4.2H_2O$ (Ajax)
- 8mM Na_2HPO (BDH)
- 154mM NaCl (BDA)
- Made to 1L in milli-Q® water

4% Paraformaldehyde (PFA) – makes 100mL

- 1.33M paraformaldehyde (Sigma)
- 20mM Na_2HPO
- 80mM $NaH_2PO_4.2H_2O$ stock solution
- Made to 100mL in milli-Q® water

30% Sucrose Cryo-Protection Solution – makes 1L

- 876mM Sucrose (Sigma)
- 1000mL 0.01M PBS

0.02% Tissue Storage Solution – makes 1L

- 3.1mM Sodium azide (Sigma)
- 1000mL PBS

0.3% Triton/PBS diluent

- 600µL 100% Triton-X100 (Sigma)
- 200mL 0.01M PBS

1% Triton/PBS diluent blocking diluent

- 2mL 100% Triton-X100 (Sigma)
- 5% (w/v) BSA
- 200mL 0.01M PBS

50x TAE Buffer for Gel electrophoresis – makes 1L

- 2M Tris base (Sigma)
- 57.1mL Glacial acid (Millipore)
- 50mM EDTA (Sigma)
- Made to 1L in milli-Q® water

4x Sample buffer

- 900µL 4% Laemelli protein sample buffer (Bio-Rad)
- 100µL β-Mercaptoethanol (Bio-Rad)

Lell lysis buffer (RIPA)

- 50mM Tris-HCL
- 150mM NaCl
- 1% (v/v) NP-40 (Sigma)
- 1% (w/v) Sodium Deoxycholate (Sigma)
- 0.1% SDS (v/v)
- Protease inhibitor tablet (1 per 10mL) (Roche)

Running buffer

- 25mM Tris base
- 192mM Glycine (Sigma)
- 0.1% SDS
- Made to 1L in milli-Q® water

Transfer buffer

- 25mM Tris base
- 192mM Glycine
- 20% (v/v) Ethanol (Sigma)
- Made to 1L in milli-Q® water

Tris buffered saline solution with tween (TBS-T) pH 7.5

- 25mM Tris base (Sigma)
- 150mM NaCl
- 0.2% Tween-20
- Made to 2L in milli-Q® water

- Adjust pH to 7.4 with 10M HCL

TBS-T/5% skim milk powder

- 100mL TBS-T
- 5g (w/v) skim milk powder